



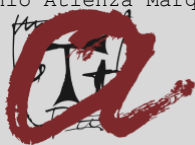
EXERGY RECOVERY FROM LNG-REGASIFICATION FOR POLYGENERATION OF ENERGY

Antonio Atienza Márquez

ADVERTIMENT. L'accés als continguts d'aquesta tesi doctoral i la seva utilització ha de respectar els drets de la persona autora. Pot ser utilitzada per a consulta o estudi personal, així com en activitats o materials d'investigació i docència en els termes establerts a l'art. 32 del Text Refós de la Llei de Propietat Intel·lectual (RDL 1/1996). Per altres utilitzacions es requereix l'autorització prèvia i expressa de la persona autora. En qualsevol cas, en la utilització dels seus continguts caldrà indicar de forma clara el nom i cognoms de la persona autora i el títol de la tesi doctoral. No s'autoritza la seva reproducció o altres formes d'explotació efectuades amb finalitats de lucre ni la seva comunicació pública des d'un lloc aliè al servei TDX. Tampoc s'autoritza la presentació del seu contingut en una finestra o marc aliè a TDX (framing). Aquesta reserva de drets afecta tant als continguts de la tesi com als seus resums i índexs.

ADVERTENCIA. El acceso a los contenidos de esta tesis doctoral y su utilización debe respetar los derechos de la persona autora. Puede ser utilizada para consulta o estudio personal, así como en actividades o materiales de investigación y docencia en los términos establecidos en el art. 32 del Texto Refundido de la Ley de Propiedad Intelectual (RDL 1/1996). Para otros usos se requiere la autorización previa y expresa de la persona autora. En cualquier caso, en la utilización de sus contenidos se deberá indicar de forma clara el nombre y apellidos de la persona autora y el título de la tesis doctoral. No se autoriza su reproducción u otras formas de explotación efectuadas con fines lucrativos ni su comunicación pública desde un sitio ajeno al servicio TDR. Tampoco se autoriza la presentación de su contenido en una ventana o marco ajeno a TDR (framing). Esta reserva de derechos afecta tanto al contenido de la tesis como a sus resúmenes e índices.

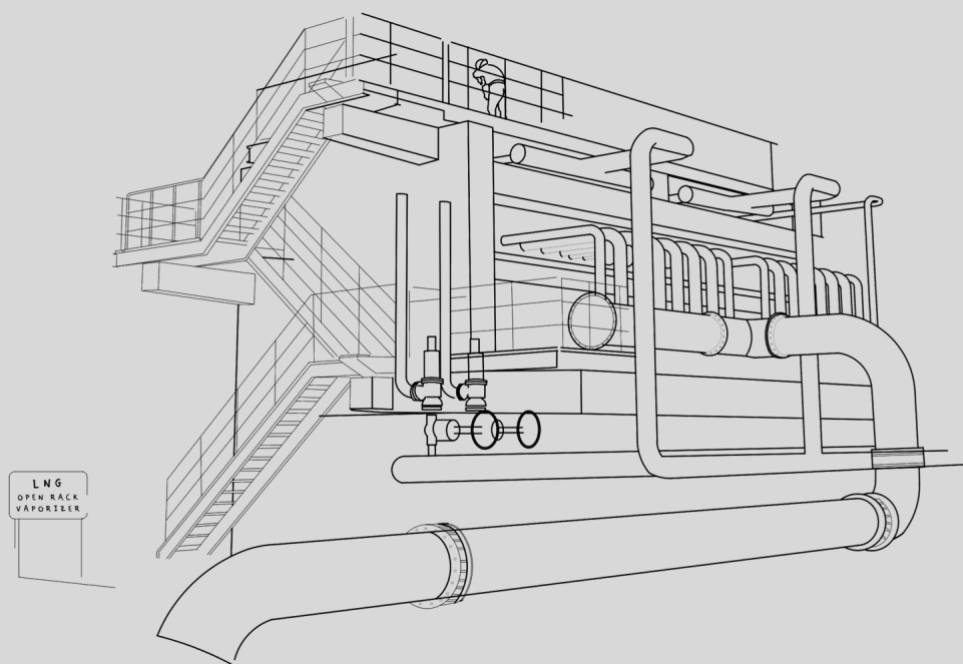
WARNING. Access to the contents of this doctoral thesis and its use must respect the rights of the author. It can be used for reference or private study, as well as research and learning activities or materials in the terms established by the 32nd article of the Spanish Consolidated Copyright Act (RDL 1/1996). Express and previous authorization of the author is required for any other uses. In any case, when using its content, full name of the author and title of the thesis must be clearly indicated. Reproduction or other forms of for profit use or public communication from outside TDX service is not allowed. Presentation of its content in a window or frame external to TDX (framing) is not authorized either. These rights affect both the content of the thesis and its abstracts and indexes.



UNIVERSITAT
ROVIRA I VIRGILI

Exergy recovery from LNG-regasification for polygeneration of energy

ANTONIO ATIENZA MÁRQUEZ



DOCTORAL THESIS
2020

UNIVERSITAT ROVIRA I VIRGILI
EXERGY RECOVERY FROM LNG-REGASIFICATION FOR POLYGENERATION OF ENERGY
Antonio Atienza Márquez

ANTONIO
ATIENZA-MÁRQUEZ

EXERGY RECOVERY FROM LNG-REGASIFICATION FOR POLYGENERATION OF ENERGY

DOCTORAL THESIS

Supervised by

Prof. Dr Alberto Coronas
Dr Joan Carles Bruno

Department of Mechanical Engineering



UNIVERSITAT ROVIRA I VIRGILI

Tarragona (Spain), November 2020

UNIVERSITAT ROVIRA I VIRGILI

EXERGY RECOVERY FROM LNG-REGASIFICATION FOR POLYGENERATION OF ENERGY

Antonio Atienza Márquez



UNIVERSITAT
ROVIRA I VIRGILI
DEPARTAMENT D'ENGINYERIA MECÀNICA
Escola Tècnica Superior d'Enginyeria Química (ETSEQ).
Avgda Paisos Catalans, 26; 43007 Tarragona (Spain)

Declaration

We STATE that the present study, entitled “Exergy recovery from LNG-regasification for polygeneration of energy”, presented by Antonio Atienza Márquez for the award of the degree of Doctor, has been carried out under my supervision at the Research Group CREVER in the Department of Mechanical Engineering of this university, and it fulfils all the requirements to be eligible for the International Doctorate Award.

Tarragona, November 5, 2020

Doctoral Thesis Supervisors



Prof. Dr Alberto Coronas



Dr Joan Carles Bruno

UNIVERSITAT ROVIRA I VIRGILI

EXERGY RECOVERY FROM LNG-REGASIFICATION FOR POLYGENERATION OF ENERGY

Antonio Atienza Márquez

*This doctoral thesis is dedicated to
my beloved grandparents,
M^a Carmen García and Blas Márquez.*

UNIVERSITAT ROVIRA I VIRGILI

EXERGY RECOVERY FROM LNG-REGASIFICATION FOR POLYGENERATION OF ENERGY

Antonio Atienza Márquez

Acknowledgements

First of all, I would like to express my deepest gratitude to my supervisors, Prof. Dr Alberto Coronas and Dr Joan Carles Bruno. I am very much thankful for their consistent support and patience during my doctoral thesis. Their knowledge and experience have encouraged me in my research, and I appreciate every constructive criticism they provided me, which helped me develop a broader perspective of my thesis.

I wholeheartedly thank Prof. Dr Atsushi Akisawa, from the Tokyo University of Agriculture and Technology in Japan, for his wise guidance as co-advisor during my research stay in his research laboratory. I extend my thankfulness and appreciation to every other student or staff member that made my stay quite pleasant: Dr Nakayama, Dr Erdenedavaa, Takada, Tanaka, and many others.

Many thanks to Dr Dereje S. Ayoub, Dr Daniel Salavera, Dr Juan Prieto and the rest of staff members of CREVER group, whose invaluable assistance was a milestone in the completion of my thesis. I would also like thanks to Dr Adriana Coca, Maycon, Paul, Ronny, Martín, Raul, Richard, Santi and many others of my previous and current colleagues. It has been a great delight to discuss with them about the findings of my thesis.

Thank you, all my fellow swimmers, for all the good times we had together *tant dins com fora de l'aigua*. Diego, Alberto, Sergi, Claustre, Uri, Jorge, Silvia, Mar, Ignacio, Sandra, Toni, Gemma, and many others, thanks for being a crucial part of my daily life in Tarragona. And I cannot forget my pals, Javi and Pedro, whom I warmly thank for their support and friendship over the many years.

My special heartfelt thanks go to my family, of which I am so proud. I deeply thank my parents, Ana and Antonio, for their infinite love, unconditional trust and for teaching to know and understand myself. Thanks to my sister, my uncles Juan and Pilar, my grandmother M^a Carmen, for the love and support they give me despite the distance. Thanks to my sweetheart, whose “*joie de vivre*” raised me again when I got weary. And thanks to my grandfather Blas, for the core values he taught me, and which explain the way I am.

Finally, I gratefully acknowledge the financial support received from the Ministerio de Ciencia, Innovación y Universidades (MICINN) of Spain for the pre-doctoral contract No. FPU15/04514 between the academic years 2016-17 and 2019-20. Also, I would like to acknowledge the CREVER group for funding my research stay in Japan.



UNIVERSITAT ROVIRA I VIRGILI

EXERGY RECOVERY FROM LNG-REGASIFICATION FOR POLYGENERATION OF ENERGY

Antonio Atienza Márquez

Abstract

In the context of the current climate emergency situation, Liquefied Natural Gas (LNG) emerges as a key transition primary energy source. Apart from the environmental benefits concerning other fossil fuels, LNG is a valuable physical exergy source because of its cryogenic temperature and usually high regasification pressure. To exploit that exergetic potential throughout the regasification process, multiple applications and technologies have been investigated. However, at present, their deployment in receiving terminals worldwide is scarce because of major drawbacks such as their limited techno-economic viability, among other bottlenecks.

The combination of different applications through cascaded polygeneration schemes is an attractive technical solution to achieve high efficiency. But the structural complexity and, therefore, the capital investment increase considerably concerning single-applications configurations. This doctoral thesis tackles the development of innovative and sustainable polygeneration systems to harness the physical exergy of LNG (and other cryogenics fluids such as bio-LNG) with a competitive efficiency-complexity ratio both in large-scale and satellite regasification facilities. The different configurations proposed consist of non-combustion systems that regasify LNG and produce electric power and/or refrigeration at different temperatures as by-products. Unlike more sophisticated applications based on immature technologies and which offer services to a very specific type of customers, electricity is a versatile energy carrier. Also, to find neighbouring industries and buildings with a certain refrigeration demand (e.g., for foodstuff or air-conditioning applications) consuming considerable quantities of power will be quite common. Moreover, both services can be generated by combining already developed technologies (e.g., heat exchangers, pumps and turbines) which would increase their implementation opportunities.

The first large-scale cascaded polygeneration plant proposed is integrated by three power generation modules (Rankine cycles) driven by seawater, low-grade waste and biomass, respectively, and a district cooling network that supplies refrigeration at -20°C , -10°C and 5°C . The plant is used as a case-study to preliminary estimate the exergy recovery potential and to address a major technical issue: the selection of the most suitable operating fluids. Despite the lack of an ideal candidate, a remarkable finding is the suitability of natural fluids even at different thermal boundary conditions. As for the simulation results, the plant reported an equivalent electricity production of 125 kWh/t-LNG regasified and an exergetic efficiency of 40%.

The next part of the thesis puts the spotlight on the techno-economic feasibility. The subsequent large-scale polygeneration configurations modelled consist of different combined cryogenic power and cooling units built upon the structure of a commercial 6 MW cryogenic power plant. The reference system is integrated by a propane Rankine cycle and a natural gas direct expansion unit, and has been in operation since long time

ago, providing a certain degree of technical reliability for the new configurations proposed derived from this power-only plant. It was gathered information regarding the operation and the equipment utilized by the reference unit to calibrate the modelling and estimate costs. The techno-economic analysis revealed that the combined production in cascade of electricity and refrigeration for both low-temperature (i.e., -50°C) and air-conditioning applications achieves a successful balance between efficiency and complexity. For the baseline scenario, the simulations reported a nameplate equivalent electricity production and an exergetic efficiency of 150 kWh/t-LNG and 42%, respectively, with an estimated payback period of five years. Despite a simpler structure with respect to the first polygeneration plant analysed in the thesis, the better performance of this plant is mainly due to the higher amount of refrigeration produced and also at a lower temperature.

The last part of the thesis deals with the recovery of the low-temperature exergy of LNG in satellite plants for foodstuff refrigeration applications. These facilities usually receive fossil LNG from large-scale harbour facilities, although they are also suitable for regasifying bio-LNG. Two strategies are evaluated to refrigerate the cold rooms. One aims to improve the efficiency of refrigeration machines by using LNG as a heat sink instead of the ambient whenever possible; the other option is to supply the LNG cold directly without conventional refrigeration devices. To model the energy demands, factors such as the application of the gas regasified, the activity schedules, the day of the week or the ambient conditions are considered. The results show that the techno-economic feasibility of the configurations developed is generally limited to temperate/warm climates and medium-large plant sizes (e.g., with nameplate regasification capacities above $\sim 1,500 \text{ Nm}^3/\text{h}$ in local satellite plants). Those plants with constant regasification rates encourage the direct utilization of the cold without back-up refrigeration machines. For the case of satellite facilities where the regasification rates fluctuate, hybrid configurations which keep the conventional refrigeration systems provided in place, turn to be a flexible solution to ensure refrigeration for cold rooms.

In conclusion, the cascaded polygeneration configurations developed in the thesis boost the competitiveness of the physical exergy recovery of cryogenic fluids. While their viability ultimately depends on factors such as electricity tariffs or the carbon prices, the production without combustion of electricity and multi-temperature refrigeration as regasification by-products contribute to the sustainability of the current energetic model and, particularly, to a cleaner refrigeration sector. Finally, in certain scenarios satellite plants are an attractive gateway to the integration of cryogenic biofuels in the energy mix for the recovery of the low-temperature heat from the regasification.

Keywords: Liquefied Natural Gas (LNG), Bio-LNG, Polygeneration, Physical exergy recovery, Modelling, Refrigeration, Cryogenic power.

Resumen

En el contexto actual de emergencia climática, el Gas Natural Licuado (GNL) se posiciona como una fuente de energía primaria de transición clave. Además de sus beneficios medioambientales con respecto a otros combustibles fósiles, el GNL es una valiosa fuente de exergía física debido a su temperatura criogénica y elevada presión a la que generalmente se regasifica. Para explotar este potencial exérgico en su proceso de regasificación se han investigado múltiples aplicaciones y tecnologías. Sin embargo, su grado de implementación actual en terminales receptoras de todo el mundo es escaso, debido a problemas como una limitada viabilidad tecno-económica, entre otros.

La combinación de diferentes aplicaciones en sistemas de poligeneración en cascada es una solución técnica atractiva para conseguir eficiencias altas. Pero la complejidad y, por tanto, las inversiones requeridas aumentan considerablemente con respecto a configuraciones de una sola aplicación. Esta tesis doctoral aborda el desarrollo de nuevos sistemas de poligeneración sostenibles para el aprovechamiento de la exergía física del GNL (y otros combustibles criogénicos como el bio-GNL) con un equilibrio competitivo entre eficiencia y complejidad, tanto en terminales a gran escala como en plantas de regasificación satélite. Las diferentes configuraciones propuestas se basan en sistemas sin combustión que regasifican el GNL y producen como subproductos electricidad y/o refrigeración a distintas temperaturas. A diferencia de otras aplicaciones más sofisticadas basadas en tecnologías en desarrollo y que ofrecen servicios a industrias muy específicas, la electricidad es un vector energético versátil. También es frecuente encontrar industrias y edificios adyacentes a las plantas de regasificación con demanda de frío (por ejemplo, para aplicaciones agroalimentarias o aire acondicionado) y que consumen grandes cantidades de energía. Además, ambos servicios se pueden producir combinando tecnologías ya desarrolladas (intercambiadores de calor, turbinas, bombas, etc.), lo que aumenta sus oportunidades de implementación.

La primera planta de poligeneración propuesta para terminales a gran escala está integrada por tres bloques de producción de potencia (ciclos Rankine) que usan como fuente de calor agua de mar, calor residual, y biomasa, respectivamente, y una red de frío de distrito que suministra refrigeración a -20°C , -10°C y 5°C . Esta planta se utiliza como caso de estudio para una evaluación preliminar del potencial de recuperación de exergía y abordar una cuestión técnica esencial: la selección de los fluidos de servicio más adecuados. Aunque no hay candidatos ideales, una conclusión importante es que los fluidos naturales son apropiados incluso para distintas condiciones térmicas. De las simulaciones se obtuvo una producción de electricidad equivalente de la planta de 125 kWh/t-GNL y una eficiencia exérgica del 40%.

La siguiente parte de la tesis se centra en la viabilidad tecno-económica. Los siguientes sistemas de poligeneración que se modelan consisten en configuraciones de producción combinada de potencia y frío desarrolladas a partir de la estructura de una planta de

potencia criogénica comercial de 6 MW. Este sistema de referencia está integrado por un ciclo Rankine con propano y una unidad de expansión directa de gas natural, y está en operación desde hace años, lo que confiere cierta viabilidad técnica a los nuevos sistemas desarrollados a partir de éste. Para calibrar modelos y estimar costes, se ha recopilado información sobre la operación y los equipos utilizados por el sistema de referencia. El análisis tecno-económico determina que con la producción combinada en cascada de electricidad y refrigeración para aplicaciones de baja temperatura (-50°C) y aire acondicionado se logra un equilibrio satisfactorio entre eficiencia y complejidad. De las simulaciones para un caso base, se obtuvo una producción equivalente de electricidad de 150 kWh/t-GNL y una eficiencia exergética del 42%. A pesar de su estructura más simple con respecto a la primera configuración de poligeneración analizada en la tesis, los mejores indicadores obtenidos por esta planta se deben principalmente a la mayor cantidad de refrigeración producida y su menor temperatura.

La última parte de la tesis trata sobre el uso de la baja temperatura del GNL en plantas de regasificación satélite para refrigeración en industrias agroalimentarias. Estas plantas habitualmente reciben GNL desde terminales a gran escala, aunque también son adecuadas para regasificar bio-GNL. Se han considerado dos estrategias para refrigerar cámaras frigoríficas. Una busca mejorar la eficiencia de las máquinas de refrigeración usando en la medida de lo posible el GNL en lugar del aire ambiente como foco frío. La otra estrategia consiste en refrigerar las cámaras usando directamente el frío del GNL sin equipos de refrigeración convencionales. Para modelizar las demandas energéticas se han tenido en cuenta factores como el uso del gas regasificado, perfiles de actividad, el día de la semana o las condiciones ambientales. Los resultados muestran que la viabilidad tecno-económica de las configuraciones desarrolladas generalmente se limita a climas templados/cálidos y a plantas medianas/grandes (por ejemplo, con capacidad de regasificación nominal por encima de $\sim 1,500 \text{ Nm}^3/\text{h}$ en plantas satélite locales). Los escenarios con perfiles de regasificación constantes favorecen el uso directo del frío sin equipos de refrigeración auxiliares. En plantas satélite donde el perfil de regasificación fluctúa, la configuración híbrida que utiliza sistemas de refrigeración convencionales proporciona una solución flexible para garantizar la refrigeración de las cámaras.

En conclusión, los sistemas de poligeneración en cascada desarrollados en esta tesis mejoran la competitividad de la recuperación de exergía física de combustibles criogénicos. Aunque la viabilidad está sujeta en última instancia a factores como el precio de la electricidad o del carbono, la producción de electricidad y refrigeración a distintas temperaturas como subproductos de la regasificación contribuyen a la sostenibilidad del sistema energético actual y, particularmente, a un sector de refrigeración menos contaminante. Finalmente, en ciertos casos, las plantas satélites constituyen una atractiva vía para integrar biocombustibles criogénicos en el mix energético y para la recuperación de frío en su proceso de regasificación.

Palabras clave: Gas Natural Licuado (GNL), Bio-GNL, Poligeneración, Recuperación de exergía física, Modelización, Refrigeración, Potencia criogénica.

Contributions by the Author

Articles in Peer Reviewed Academic Journals



ISSN: 1359-4311

A. Atienza-Márquez, J.C. Bruno, A. Coronas. Cold recovery from LNG-regasification for polygeneration applications. *Applied Thermal Engineering* 132 (2018), 463-478.

DOI: <https://doi.org/10.1016/j.applthermaleng.2017.12.073>



ISSN: 0360-5442

A. Atienza-Márquez, J.C. Bruno, A. Akisawa, M. Nakayama, A. Coronas. Fluids selection and performance analysis of a polygeneration plant with exergy recovery from LNG-regasification. *Energy* 176 (2019), 1020-1036.

DOI: <https://doi.org/10.1016/j.energy.2019.04.060>



ISSN: 0360-5442

A. Atienza-Márquez, J.C. Bruno, A. Akisawa, A. Coronas. Performance analysis of a combined cold and power (CCP) system with exergy recovery from LNG-regasification. *Energy* 183 (2019), 448-461.

DOI: <https://doi.org/10.1016/j.energy.2019.06.153>



ISSN: 2451-9049

A. Atienza-Márquez, D.S Ayou, J.C. Bruno, A. Coronas. Energy polygeneration systems. Energy polygeneration systems based on LNG-regasification: Comprehensive overview and techno-economic feasibility. *Thermal Science and Engineering Progress* 20 (2020), 100677.

DOI: <https://doi.org/10.1016/j.tsep.2020.100677>

Manuscripts in preparation:

A. Atienza-Márquez, J.C. Bruno, A. Coronas. Thermal design and performance analysis of a double-bundle heat exchanger for low-temperature exergy recovery from-LNG regasification.

A. Atienza-Márquez, J.C. Bruno, A. Coronas. Cold recovery from LNG-regasification for refrigeration applications in satellite plants.

Papers in Congresses, Conferences and Workshops

- 2020**
- **Antonio Atienza-Márquez**, Joan Carles Bruno and Alberto Coronas. LNG-regasification in satellite plants: Cold recovery for refrigeration applications in agro-food industries. *X Congreso Ibérico y VIII Congreso Iberoamericano de Ciencias y Técnicas del Frío – CYTEF 2020*. Online Virtual Conference: 11st-12nd November 2020.
 - **Antonio Atienza-Márquez**, Joan Carles Bruno and Alberto Coronas, An LNG-based system for the combined production of power and cooling. *IIR Rankine 2020 Conference - Advances in Cooling, Heating and Power Generation*. Online Virtual Conference: 27th-31st July 2020. DOI: [10.18462/iir.rankine.2020.1202](https://doi.org/10.18462/iir.rankine.2020.1202)
- 2019**
- **Antonio Atienza-Márquez**, Joan Carles Bruno, Atsushi Akisawa and Alberto Coronas. Thermal design of a vaporizer for cold recovery from LNG-regasification using CO₂ as heat transfer media. *25th IIR International Congress of Refrigeration*, Montreal (Canada), 24th-30th August 2019. DOI: [10.18462/iir.icr.2019.1018](https://doi.org/10.18462/iir.icr.2019.1018)
 - **Antonio Atienza-Márquez**, Joan Carles Bruno and Alberto Coronas. A **Double-Bundle** Heat Exchanger for Cold Recovery from LNG-Regasification. *9th International Seminar on Thermodynamic Engineering of Fluids*, Tarragona (Spain) 25th-26th July 2019. ISBN: 978-84-09-11635-5
 - **Antonio Atienza-Márquez**, Joan Carles Bruno and Alberto Coronas. Vaporizers for low-temperature exergy recovery from LNG-regasification. *XI National and II International Engineering Thermodynamics Congress*, Albacete (Spain), 12nd-14th June 2019. ISBN: 978-84-09-14637-6
 - **Antonio Atienza-Márquez**, Joan Carles Bruno, Atsushi Akisawa and Alberto Coronas. Combined Cold, Heat and Power (CCHP) Systems with Exergy Recovery from LNG-regasification. *5th International Conference on Polygeneration*, Fukuoka (Japan), 15th-17th May 2019. ISBN: 978-4-944005-29-1
 - **Antonio Atienza-Márquez**, Joan Carles Bruno and Alberto Coronas. Waste Cold Recovery from LNG-Regasification in Satellite Plants. *5th International Conference on Polygeneration*, Fukuoka (Japan), 15th-17th May 2019.
- 2018**
- **Antonio Atienza-Márquez**, Joan Carles Bruno and Alberto Coronas. Performance analysis of a novel polygeneration plant for LNG cold recovery. *Heat Powered Cycles (HPC) Conference 2018*, Bayreuth (Germany), 16th-19th September 2018. ISBN: 978-0-9563329-7-4
 - **Antonio Atienza-Márquez**, Joan Carles Bruno and Alberto Coronas. Thermoacoustic systems as emerging technology for LNG exergy recovery. *8th International Seminar on Thermodynamics Engineering of Fluids*, Tarragona (Spain), 25th-26th July 2018. ISBN: 978-84-09-10539-7
 - **Antonio Atienza-Márquez**, Joan Carles Bruno, Alberto Coronas, and Atsushi Akisawa. Selection of fluids for a polygeneration plant with LNG cold recovery. *13th IIR Gustav Lorentzen Conference on natural refrigerants (GL2018)*, Valencia (Spain), 18th-20th June 2018. DOI: [10.18462/iir.gl.2018.1375](https://doi.org/10.18462/iir.gl.2018.1375)

- **Antonio Atienza-Márquez**, Joan Carles Bruno, Alberto Coronas, Masayuki Nakayama, Atsushi Akisawa, Integration of renewable energy sources in a polygeneration plant with LNG cold recover, *Grand Renewable Energy International Conference & Exhibition 2018 – GREC2018*, Yokohama (Japan), 17th-22nd June 2018.
- 2017** • **Antonio Atienza-Márquez**, Joan Carles Bruno and Alberto Coronas. Performance analysis of a polygeneration plant using the cold recovered from an LNG-regasification process. *10^o Nacional / I International Engineering Thermodynamics Congress–10CNIT*, Lleida (Spain), 28th-30th June 2017. ISBN: 978-84-9144-044-4
- **Antonio Atienza-Márquez**, Joan Carles Bruno and Alberto Coronas. Cold recovery from LNG regasification using a CO₂ based district cooling network. *International Conference on Polygeneration. Technologies and Perspectives – ICP 2017*, Cuernavaca (Mexico), 24th-26th May 2017. ISBN: 978-84-697-3376-9

Other contributions

Articles in Peer Reviewed Academic Journals

- **A. Atienza-Márquez**, J.C. Bruno, A. Coronas. Recovery and Transport of Industrial Waste Heat for Their Use in Urban District Heating and Cooling Networks Using Absorption Systems. *Applied Sciences* 291 (2019), 10, 291. DOI: <https://doi.org/10.3390/app10010291>

Papers in Congresses, Conferences and Workshops

- 2019** • Juan Prieto, **Antonio Atienza-Márquez** and Alberto Coronas. Modelling and dynamic simulation of a liquid desiccant system coupled to a heat pump for air conditioning. *25th IIR International Congress of Refrigeration*, Montreal (Canada), 24th-30th August 2019. DOI: [10.18462/iir.icr.2019.1102](https://doi.org/10.18462/iir.icr.2019.1102)
- 2017** • **Antonio Atienza-Márquez**, Joan Carles Bruno and Alberto Coronas. Thermodynamic analysis of absorption systems for heat transport in district networks. *International Conference on Materials and Energy (ICOME2017)*, Tianjin (China), 6th-7th July 2017.
- **Antonio Atienza-Márquez**, Ivan Korolija, Richard Greenouhg, Andy Wright, Joan Carles Bruno and Alberto Coronas. Photovoltaic-thermal (PV/T) solar collectors: Features and performance. *VII International Conference for Renewable Energy, Energy Saving and Energy Education (CIER2017)*. La Habana (Cuba), 31st – 2nd June 2017. ISBN: 978-959-7113-52-2

- Adriana Coca-Ortegón, **Antonio Atienza-Márquez**, Jorge Gontupil, Fernando Salazar, Gabriel Merino and Alberto Coronas. Energy and economic analysis of an On-grid PV-T system in a dairy farm in Chile. *VII International Conference for Renewable Energy, Energy Saving and Energy Education (CIER2017)*. La Habana (Cuba), 31st – 2nd June 2017.

Internships

- **Host institution:** Tokyo University of Agriculture and Technology (TUAT), Tokyo (Japan)
- **Supervisor at host institution:** Prof. Atsushi Akisawa.
- **Period:** 3rd April – 4th July 2018.
- **Topic:** Physical exergy recovery from LNG-regasification for the combined production of electric power and low-temperature refrigeration.

Table of Contents

Acknowledgements	v
Abstract	vii
Resumen	ix
Contributions by the Author	xi
Table of Contents	xv
List of Figures	xix
List of Tables	xxv
Nomenclature	xxix

Chapter 1. Introduction and thesis objectives **31**

1.1. The climate emergency and energy transition	32
1.2. Natural gas and LNG: Facts and figures	34
1.3. LNG versus pipeline gas	35
1.3.1. The problem of methane emissions	36
1.3.2. LNG's global market	38
1.4. The LNG supply chain	40
1.4.1. The regasification: An opportunity to recover physical exergy	42
1.4.2. The widespread wasting of LNG physical exergy	46
1.5. The value of low-temperature energy reservoirs	48
1.5.1. Improving the thermal efficiency of power cycles	48
1.5.2. Contributing to a sustainable refrigeration system	49
1.5.3. The opportunity afforded by bio-LNG regasification	50
1.6. Objectives of the thesis	52
1.7. Structure of the thesis	53

Chapter 2. LNG physical exergy utilization: Potential, applications and technologies **55**

2.1. Introduction	56
2.2. Exergetic potential	56
2.2.1. The exergy breakdown	57
2.2.2. The physical exergy potential	58
2.2.3. The exergetic efficiency definition	60
2.3. Applications and technologies	61
2.3.1. Electric power production	64
2.3.2. Air-separation	70
2.3.3. Boil-off gas management	71
2.3.4. Liquefaction of carbon dioxide	73
2.3.5. Refrigeration production	73
2.3.6. Seawater desalination	77
2.3.7. Hydrogen production	79
2.4. Global deployment and implemented projects	82
2.4.1. Japan: The outstanding leader	83
2.4.2. Other countries	89

2.5. Conclusions	90
Chapter 3. LNG-based polygeneration applications and fluids selection	93
3.1. Introduction	94
3.2. LNG-based polygeneration systems	95
3.3. A polygeneration plant case-study	98
3.3.1. Description	98
3.3.2. Operation	100
3.3.3. Modelling and performance indicators	101
3.4. Preliminary screening of candidate fluids	106
3.5. Results and discussion	109
3.5.1. Power cycle RC-1	109
3.5.2. DC network and the power cycle RC-2	111
3.5.3. Power cycle RC-3	114
3.5.4. Performance analysis of the whole plant	117
3.6. Conclusions	120
Chapter 4. Development and techno-economic assessment of cryogenic power and cooling plants	123
4.1. Introduction	124
4.2. Configurations based on an existing plant	124
4.2.1. The benchmark cryogenic power unit	125
4.2.2. Combined Cold and Power (CCP) unit: Type (i)	127
4.2.3. Combined Cold and Power (CCP) unit: Type (ii)	131
4.2.4. Polygeneration plant	133
4.3. Modelling and performance indicators	135
4.3.1. Thermodynamic modelling	135
4.3.2. Economic analysis	140
4.4. Results and discussion	145
4.4.1. Thermodynamic and environmental performance	145
4.4.2. Economic performance	155
4.5. Conclusions	162
Chapter 5. LNG low-temperature exergy utilization in satellite plants	165
5.1. Introduction	166
5.2. Satellite plants: Description and operation	167
5.3. Opportunities and challenges	172
5.4. Configurations	173
5.4.1. Direct configuration	174
5.4.2. Indirect configuration	176
5.4.3. The heat transfer fluids	177
5.5. Scenarios analysed	179
5.5.1. Scenario (1): Satellite plant for a single consumer (on-site LNG Terminal)	180
5.5.2. Scenario (2): Satellite plant for electric power generation (on-site LNG Terminal)	182
5.5.3. Scenario (3): Satellite terminal of a local community (off-site LNG terminal)	182

5.6. Modelling	182
5.6.1. Mathematical modelling and indicators	182
5.6.2. Energy demands	188
5.6.3. Control system	192
5.6.4. Economic analysis	194
5.7. Results and discussion	195
5.7.1. Plant owned by a single user	195
5.7.2. Satellite plant for electric power production	196
5.7.3. Local satellite plant	201
5.7.4. The integration of PV technology	206
5.8. Conclusions	207
Chapter 6. General conclusions and future outlook	211
6.1. Conclusions	212
6.1.1. Large-scale regasification facilities	212
6.1.2. Satellite regasification facilities	214
6.2. Final remark and future outlook	215
References	217
Appendices	235
Appendix A. Natural gas and LNG composition, properties and conversion factors	237
Appendix B. Thermodynamic data of the polygeneration plant analysed in Chapter 3	239
Appendix C. Supplementary data of the Combined Cryogenic Power and Cooling configurations developed in Chapter 4	241
C.1. Convective heat transfer correlations	241
C.2. Temperature profiles in heat exchangers	245
C.3. Heat transfer coefficients	246
Appendix D. Supplementary material for Chapter 5	247
D.1. Freezing point and viscosity of aqueous ethylene glycol and propylene glycol solutions.	247
D.2. Modelling of the ammonia compressor	248
D.3. Modelling of the NH ₃ /CO ₂ VCR machine	252

UNIVERSITAT ROVIRA I VIRGILI

EXERGY RECOVERY FROM LNG-REGASIFICATION FOR POLYGENERATION OF ENERGY

Antonio Atienza Márquez

List of Figures

- Figure 1.1.** World primary energy supplied by source. Total renewables include hydro. Figure developed from data published by the International Energy Agency (IEA) [5] and BP Energy Outlook 2019 [6], considering an evolving energy transition. 33
- Figure 1.2.** Evolution and forecast of the share of natural gas trade between pipeline gas and LNG. Conversion factor utilized: 1 million tonnes (MT) = 0.743 billion cubic meters of natural gas (bcm). See Appendix A for more unit conversion factors. Figure prepared by Antonio Atienza-Márquez based on a compilation of data from the following sources: Cedigaz [27], BP Statistical Reviews of World Energy [28], IEA Natural Gas Information 2020 [12], International Gas Union (IGU) World LNG reports [29], GIIGNL Annual Reports [30]. 37
- Figure 1.3.** World map with: (a) Worldwide distribution of LNG regasification plants and major regasification capacities (in million tons per annum - MTPA) and (b) the most remarkable amounts of LNG in MTPA exported or imported in 2016 by the main countries in LNG market. Figure updated from [44]. Source of data: International Gas Union [25]. 39
- Figure 1.4.** A block diagram of the LNG supply chain. From Atienza-Márquez et al. [44]. 41
- Figure 1.5.** A block diagram of the LNG supply chain with the low-temperature energy (cold) opportunity throughout its regasification process [55]. 43
- Figure 1.6.** Conventional technologies of LNG vaporizers. (a) Open Rack Vaporizer – ORV (photo taken by the author with permission at Negishi LNG Terminal, Japan). (b) Submerged Combustion Vaporizer – SCV [62]. (c) Ambient Air Vaporizer – AAV. (d) Intermediate Fluid Vaporizer – IFV [63]. 44
- Figure 1.7.** LNG (assumed as pure methane) heat released curve. Assuming LNG as pure methane, a regasification pressure of 3,000 kPa, and initial and final temperatures of 111 K and a 273 K, respectively. 46
- Figure 1.8.** Schematic diagram of two thermal machines with the same Carnot’s efficiency but operating between two different temperature reservoirs. Redrawn from [44]. 49
- Figure 1.9.** Biogas consumption by end-use. Redrawn from IEA [9]. 51
- Figure 1.10.** Schematic layout of the bio-LNG supply chain and the cold recovery opportunity from its regasification process [55]. 52
- Figure 2.1.** Breakdown of LNG exergy content into chemical and physical exergy and conceptual flow diagram of the physical exergy utilization. 58
- Figure 2.2.** Specific physical exergy content of an LNG stream (assumed as pure methane) after pumping from storage tanks, divided into thermal and pressure exergy and considering regasification pressures up to 10 MPa. Exergy content calculated using Engineering Equation Solver (EES) [88]. Assumptions: Initial temperature and pressure -162°C and 0.12 MPa, respectively; Isentropic efficiency of cryogenic pumps: 75%. 59
- Figure 2.3.** Conceptual exergy flow diagram for an LNG physical exergy utilization system. 60
- Figure 2.4.** Number of publications per year related to cold/exergy recovery from LNG-regasification. Source of data: Scopus [89]. Figure adapted from Atienza-Márquez et al. [55]. 62
- Figure 2.5.** Applications of the low-temperature thermal energy of LNG at different temperature levels [44]. 63
- Figure 2.6.** LNG demand variation and available fraction for some applications. Redrawn from Kashiwama and Nakagawa [92] and Fujiwara et al. [131]. 65

Figure 2.7. Schematic diagram of the natural gas pressure regulation process using pressure reducing valves or an LNG direct expansion cycle to produce electricity by capturing the energy lost in the pressure reduction of natural gas. 66

Figure 2.8. (a) Turboexpander with power output up to 125 kW introduced by Calnetix Technologies [135]. (b) Turboexpander power up to Atlas Copco up to 50 MW [136]. (c) Image of an Atlas Copco's turboexpander operating in a natural gas pressure reduction station [136]. 66

Figure 2.9. Basic schematic diagram of some of the most studied configurations for power production and exploiting LNG low-temperature exergy. (a) Cryogenic Rankine cycle, (b) Turbine air cooling in an open Brayton cycle, and (c) Kalina cycle. 67

Figure 2.10. Typical power cycle configurations: (a) combined Rankine power cycle type I; (b) combined Rankine power cycle type II [44]. 67

Figure 2.11. Schematic diagram of a thermoacoustic Stirling engine with LNG low-temperature exergy utilization. 70

Figure 2.12. Simplified schematic diagram of the LNG low-temperature exergy utilization in a cryogenic air-separation unit. Adapted from [151]. 71

Figure 2.13. Different BOG management strategies. Redrawn from [155]. 72

Figure 2.14. Simplified schematic of a diagram of the LNG low-temperature exergy utilization in a liquid CO₂ manufacturing process. Figure made partially based on the information available at Osaka Gas Liquid Co., Ltd. website [159] and from Yamamoto and Fujiwara [160]. 73

Figure 2.15. Conceptual diagram of the low-temperature exergy recovery and utilization---Simplified schematic. Through a heat transfer loop. 74

Figure 2.16. System configuration proposed by TeraCool LLC to exploit the LNG low-temperature exergy for the combined production and supply of electric power and refrigeration to a data centre. Figure redrawn from [165]. 76

Figure 2.17. Schematic diagram of the utilization of the LNG low-temperature exergy in a self-refrigerated vehicle. Redrawn from [167]. 77

Figure 2.18. Use of the LNG low-temperature exergy for seawater desalination. Simplified schematics for (a) Freeze Desalination (FD) technique, and (b) Clathrate hydrate-based desalination (HyDesal) technique. 79

Figure 2.19. Conceptual diagram of the hydrogen production from LNG reforming by exploiting its low-temperature exergy content. Technologies for hydrogen purification: (a) Pressure Swing Adsorption technology (PSA), (b) LNG washing method. Figure developed from the information depicted in Ogawa et al. [179]. 81

Figure 2.20. Conceptual diagram of the hydrogen production from water electrolysis in a PEM electrolyzer driven by the electric power generated in power cycles that exploits LNG physical exergy. 82

Figure 2.21. Timeline with some relevant events and milestones regarding LNG physical exergy utilization. Source of data: [92,129,160,187]. Figure redrawn and completed [55]. 83

Figure 2.22. Pictures of power generation units utilizing LNG physical exergy in Japan. (a) Powerhouse of a 4 MW multi fluid RC built in Negishi LNG Terminal. Photograph property of the author of the thesis and taken with permission. Source of capacity data: [58,151]. (b) Unit No.2 (6 MW) Senboku II LNG Terminal managed by Osaka Gas Co., Ltd. Source: [191,193,194]. (c) Direct expansion unit installed in Himeji LNG Terminal. Source: Photographs (b) and (c) are property of Osaka Gas Co. Ltd., and are included with permission [151]. 85

Figure 2.23. Other utilization of LNG physical exergy in Senboku LNG Terminals (Osaka Gas Co. Ltd.). Air liquefaction facilities in Osaka Gas Senboku LNG Terminals: (a) Unit No. 1, Senboku II, (b) Unit No.

2, Senboku I. Source: [191]. (c) Boil-off gas re-liquefaction with a handling capacity of 15 t/h and cold storage. Source: [151,189]. *Note:* facility no longer operating. (d) Liquid CO₂ manufacturing facility. Source: [159,191]. Photographs property of Osaka Gas Co. Ltd. and are included with permission. 87

Figure 2.24. Cascade utilization of the LNG physical exergy in Senboku LNG Terminal. Figure redrawn from [160,191]. 88

Figure 2.25. External view of the gas turbine and the HRSG installed at the Himeji LNG Terminal. Photograph of the Gas turbine intake air cooling system (Source: [192,197]) property of Osaka Gas Co. Ltd. and are included with permission. Schematic diagram redrawn and simplified from Ikeda [192]. 88

Figure 2.26. Photographs of the cryogenic power generation plant (Rankine cycle) installed in Huelva LNG Terminal and schematic diagram. *Source:* Photographs property of Enagás (included with permission) and obtained from [200]. Schematic diagram drawn according with the description of the system provided in [200]. 89

Figure 2.27. Aerial view of the Barcelona LNG terminal (Spain) and neighbouring agro-food industry cluster with refrigeration demand that could utilize the LNG low-temperature exergy. 91

Figure 2.28. Aerial view of the place in the Huelva LNG Terminal (Spain) where the physical exergy of LNG will be used. Figure based on the information given by Solera Rico [205]. 91

Figure 3.1. Conceptual diagram of a polygeneration system. 94

Figure 3.2. Conceptual diagram of an LNG regasification-based polygeneration system. 95

Figure 3.3. A case-study polygeneration plant with LNG physical exergy utilization in cascade. Figure published in [82]. 99

Figure 3.4. Performance results for each candidate working fluid in the power cycle RC-1. (a) Specific energy and high pressure. (b) Required mass flow rate of working fluid to produce a unit of energy and seawater consumption. (c) Turbine size factor for the turbines T1 (HP) and T1 (LP). (d) Thermal and exergetic efficiencies. Shaded area represents the desired performance. Figure published in [82]. 110

Figure 3.5. Performance analysis of the DC network and the power cycle RC-2 for each candidate fluid: (a) Power produced and high pressure of the cycle. (b) Working fluid mass flow rate required per unit of energy produced. (c) Turbine T2 size indicator and waste heat (water) demand. (d) Thermal and exergetic efficiencies. Shaded area represents the desired performance. Figure published in [82]. 112

Figure 3.6. Performance analysis of the power cycle RC-3 for each candidate fluid: (a) Energy produced and high pressure of the cycle. (b) Working fluid mass flow rate required per unit of energy produced. (c) Turbine size factor for T3 (HP) and T3 (LP). (d) Thermal and exergetic efficiencies. Shaded area represents the desired performance. Figure published in [82]. 115

Figure 3.7. Temperature profile in the recuperator R-2 of the power cycle RC-3 for propane, ammonia and ammonia-water pair (ammonia mass fraction 90%) as working fluids. Figure published in [82]. 116

Figure 3.8. Detailed exergy flow chart of the LNG physical exergy utilization (temperature exergy + pressure exergy) in the proposed polygeneration plant. Nomenclature: PE – Pressure exergy; LTE – Low-temperature exergy. Figure published in [82]. 119

Figure 3.9. Exergy flow chart of natural gas supply chain with the integration of the proposed polygeneration plant with physical exergy recovery from LNG-regasification. The 100-base is assumed as the chemical exergy as fuel of 1 metric ton of natural gas. Figure published in Atienza-Márquez et al. [82]. 120

Figure 4.1. Cryogenic Power generation unit utilized as reference system. (a) Block diagram, (b) Detailed schematic layout. Redrawn from Atienza-Márquez et al. [211]. 126

Figure 4.2. A Combined Cold and Power (CCP) system Type (i) for the combined production of electric power and low-temperature refrigeration for the agro-food industry sector. Redrawn from [211]. 128

Figure 4.3. Double-bundle U-tube LNG vaporizer with low-temperature exergy recovery. Figure published in [211]. 129

Figure 4.4. Conceptual comparison between (a) a conventional CCP system and (b) a non-combustion CCP system based on LNG physical exergy recovery. Source: [211]. 131

Figure 4.5. A Combined Cold and Power (CCP) system Type (ii) for the combined production of electric power and refrigeration for air-conditioning applications. Figure redrawn from [93]. 132

Figure 4.6. A *Polygeneration plant* with physical exergy utilization for the simultaneous production of electric power and refrigeration at two temperature levels. (a) Block diagram. (b) Detailed schematic layout. Redrawn from [55]. 134

Figure 4.7. Variation of (a) the net power, (b) the Cold Recovery Ratio, (c) the Equivalent Electricity Production and (d) the exergetic efficiency, with the temperature of the heat source and for an LNG regasification rate of 150 t/h. 148

Figure 4.8. Exergy flow diagrams of (a) the CP plant and (b) the CCP system at design conditions. TE: Temperature component of LNG physical exergy, PE: Pressure component of LNG physical exergy. 150

Figure 4.9. Performance indicators obtained for the polygeneration plant and the reference CP unit for different heat source fluid temperatures and LNG flow rates: (a) Net electric power, (b) Cold Recovery Ratio *CRR*, (c) Equivalent Electricity Production *EEP*, and (d) Exergetic efficiency. 153

Figure 4.10. Effect of the variation of LNG regasification pressure on: (a) The low-temperature refrigeration produced by the CCP-(i) and the polygeneration systems, (b) the net power (total, propane RC and DE unit) of the CP plant, (c) the refrigeration for the conventional DC network, and (d) the *EEP* of the CP unit and the polygeneration plant. 154

Figure 4.11. Variation of the specific heat of LNG (assumed as pure methane) (a) for. Properties calculated using REFPROP [235]. 156

Figure 4.12. T-s diagram. Temperature of the gas stream leaving the DE unit in function of the inlet pressure (i.e., the regasification pressure). 156

Figure 4.13. Evolution of the Net Present Value for the base-case scenario and the different configurations considered. 159

Figure 4.14. Variation of the discounted payback time of the polygeneration plant and the reference cryogenic power system with the electricity and carbon prices, and the variation in the capital cost. Figure published in [55]. 161

Figure 5.1. LNG supply chain from harbour large-scale terminals to satellite plants. 166

Figure 5.2. Examples of operating satellite LNG plants: (a) *Sunddalsora, Norway*. Gas supplied to an aluminium foundry with 1,500 m³ (3×500 m³) storage, 4,200 Nm³/h vaporization capacity [293]. (b) *Jaen, Spain*. Gas supplied to an olive-pomace sludge drying industry, 8×120 m³ storage and 7,200 Nm³/h vaporization capacity, send-out pressure 36-37 bar(g) [294]. (c) *Gibraltar United Kingdom*. Gas supplied to an electric power plant with an installed electric capacity of 86 MW. (d) *Far North Quebec, Canada*. 6×303 m³ storage, regasified natural gas is used for seven 2.1. power generation sets at a diamond mine [295]. (e) *Falset, Spain*. 60 m³ total storage, vaporization capacity 600 Nm³/h. Gas is supplied through a local pipeline network of 4 km to 400 houses and commercial buildings [296]. (f) *Abarán, Spain*. Plant with a storage of 30 m³ and vaporization capacity of 1,000 Nm³/h. Natural Gas fed into a pipeline network that supplies gas to 13,000 people, 2,000 dwellings, shops and also small industries, send-out pressure 0.4 bar(g) [297]. 168

Figure 5.3. Schematic diagram of the conventional regasification process in an LNG satellite terminal without low-temperature exergy recovery. 169

Figure 5.4. LNG unloading at harbour large-scale plants, road transport towards a satellite facility, and regasification with low-temperature exergy utilization. 170

Figure 5.5. Pilot plant built in 2015 by *Eco Ice Kälte GmbH* in Borna, Germany. (a) Regasification site where LNG low-temperature exergy is exploited, and (b) heat exchanger utilized to recover the low-temperature thermal energy from LNG-regasification. Source: *Eco Ice Kälte GmbH website* [299]. 171

Figure 5.6. LNG (assumed as pure methane) cold energy recovery potential thorough its heating process from temperatures between -160°C to -135°C up to -70°C and considering different regasification pressures. 172

Figure 5.7. Conceptual example of the variation of a warehouse's refrigeration load and the cold available from LNG-regasification in a satellite plant. 174

Figure 5.8. Schematic layout of the (a) Direct and (b) Indirect cold utilization configurations in satellite LNG plants; and (c) utilization of the cold by multiple users connected to a low-temperature District Cooling network. 175

Figure 5.9. Schematic diagram of the different scenarios of satellite plants to recovery the low-temperature exergy of LNG for foodstuff refrigeration applications. 181

Figure 5.10. Schematic diagram of the NH_3/CO_2 refrigeration machine modelled. 186

Figure 5.11. EER curves for different heat sink temperatures and part load ratios for a given temperature of the refrigerated rooms of -18°C . 187

Figure 5.12. Natural demand pattern for household applications for typical weekdays and weekends. 191

Figure 5.13. Monthly average relative LNG and refrigeration demands and evolution of the annual dry temperature in a typical year in (a) Bangkok, Thailand; (b) Tarragona, Spain; and (c) Oslo, Norway. Weather data obtained from EnergyPlus database [334]. 192

Figure 5.14. Control system. (a) Modulation of the LNG flow rate entering the double-bundle heat exchanger both in the direct and the indirect cold use configurations, (b) Control of the pump P1 in the direct configuration and (c) Energy management in the indirect cold use configuration. 193

Figure 5.15. Annual results for a satellite LNG for power generation. (a) Cold Recovery Ratio, (b) Annual electricity-saving, (c) Energy Efficiency Ratio, *EER*, of the VCR machine, (d) Exergetic efficiency. 198

Figure 5.16. Levelized Cost of Refrigeration (*LCOR*) as a function of the size of satellite LNG plant (determined by the nameplate capacity electric power plant) for the direct, indirect and the conventional VCR system without LNG low-temperature exergy utilization in different locations. 201

Figure 5.17. Monthly results obtained for a *satellite LNG plant for base-load power production* in three different climate conditions analysed (Tarragona – TGN, Bangkok – BKK and Oslo – OSL). (a) Cold Recovery Ratio, (b) Electricity saving, (c) Energy Efficiency Ratio, *EER*, of the VCR machine and (d) Exergetic efficiency. 202

Figure 5.18. Levelized Cost of Refrigeration (*LCOR*) obtained for a **local satellite LNG plant** that supplies natural gas to a rural community in different locations, plant sizes (Small – $300 \text{ Nm}^3/\text{h}$; Medium – $1,500 \text{ Nm}^3/\text{h}$; and Large $5,000 \text{ Nm}^3/\text{h}$) and refrigeration capacity indexes. 205

Figure 5.19. Levelized Cost of Refrigeration (*LCOR*) as a function of the electricity tariff in a medium-size satellite LNG plant for the indirect cold utilization and for the conventional vapour-compression refrigeration system both with and without PV integration (coverage of 50% of the electricity consumption) and in different locations. A refrigeration capacity index (Eq. 5.19) equal to 1 is assumed. 207

Figure A.1. Thermodynamic properties of different types of natural gas for an LNG/NG pressure of 7.5 MPa. (a) Density, (b) Viscosity, (c) Thermal conductivity, (d) Specific Heat. 238

Figure C.1. Temperature profile in each heat exchanger of the polygeneration plant analysed in Chapter 4 of the thesis. 245

Figure D.1. Aqueous ethylene glycol and propylene glycol solutions. (a) Freezing point and (b) dynamic viscosity for a reference temperature of 273.15 K (0°C). Source of properties: Melinder [340].	247
Figure D.2. Two-stage refrigeration cycle used to obtain an expression of the isentropic efficiency.	248
Figure D.3. Assumed motor efficiency as a function of the load.	250
Figure D.4. Isentropic efficiencies of the two-stage ammonia compression calculated for the different compression ratios computed and the linear regression obtained.	251
Figure D.5. Comparison of the isentropic efficiency utilized for the two-stage ammonia compressor with others used in the literature [325,342,344].	251
Figure D.6. Comparison between the isentropic compression and the real case.	253
Figure D.7. Variation of the Energy Efficiency Ratio with the heat sink temperature and for different part-load ratios (PLRs).	254
Figure D.8. Polynomial adjustment of the coefficients given in Eq. D.11 for part load ratios ranging between 1 and 0.2.	255

List of Tables

Table 1.1. Some of the most significant natural gas liquefaction technologies classified by the number of refrigerant cycles and the type of refrigerant utilized. Source: Table prepared from information taken from Al-Mutaz et al. [50] and Mokhatab et al. [14].	42
Table 2.1. Definitions commonly utilized in the literature focused on LNG physical exergy utilization. Assuming fully preservation of the LNG chemical exergy (no combustion).	61
Table 2.2. Summary of applications and technologies for exploiting LNG physical exergy [93].	64
Table 2.3. Power generation plants based on LNG physical exergy utilization built in Japanese receiving terminals. Table prepared by using information gathered from different sources [131,151,186,195].	86
Table 2.4. Air separation plants with LNG low-temperature exergy utilization. Table prepared from sources: [94,108,129,160,191].	86
Table 3.1. Review of relevant cogeneration, trigeneration and polygeneration systems with LNG physical exergy recovery [55].	96
Table 3.2. Base-case operation parameters.	103
Table 3.3. Thermophysical properties, environmental data and safety group of the preselected candidate fluids. Table published in [82].	108
Table 3.4. Performance results of each candidate fluid for the DC network and power cycle RC-2: Pipe size, working pressures, pressure and temperature drop, latent heat of vaporization, density and dynamic viscosity. Table published in Atienza-Márquez et al. [82].	113
Table 3.5. Performance indicators of the LNG regasification process without exergy recovery and the obtained by the polygeneration plant proposed when operating with the selected working fluids and heat transfer fluids (Power cycle RC-1: Methane; DC + Power cycle RC-2: CO ₂ ; Power cycle RC-3: Propane) for an LNG regasification rate of 180 t/h.	117
Table 4.1. Energy outputs of the different configurations.	125
Table 4.2. Design parameters for the proposed cascaded configurations for exploiting the LNG physical exergy.	136
Table 4.3. Design criteria and constraints for the different heat exchangers integrated in the configurations developed in this chapter.	138
Table 4.4. Description and mathematical definition of the performance indicators utilized for the performance analysis of the different configurations proposed.	141
Table 4.5. Purchase cost functions for the different system components.	142
Table 4.6. Results for the power generation units in each configuration.	146
Table 4.7. Heat transfer area of heat exchangers for the different configurations considered.	146
Table 4.8. Results obtained for the different configurations and for an LNG regasification rate of 150 t/h.	147
Table 4.9. Thermodynamic data for each state point of the different configurations developed in this chapter at the design conditions.	149
Table 4.10. Irreversibilities (<i>I</i>) of each system component of both the different configurations studied for the base-case operation.	151

Table 4.11. Base-case scenario for the economic and environmental evaluation of the different types of configurations for an LNG regasification rate of 150 t/h. Values are given in million USD.	157
Table 4.12. Breakdown of Purchase Equipment Cost (reference year 2018) and share of each system component for the different configurations considered and using the cost functions listed in Table 4.5. Cost are given in thousand USD.	158
Table 5.1. Summary of features of the direct and the indirect configurations for the utilization of the LNG low-temperature exergy.	177
Table 5.2. Thermophysical properties, environmental and safety data of the candidate heat transfer fluids [88,236,237,313].	178
Table 5.3. Design parameters for each scenario of satellite LNG plant.	184
Table 5.4. Purchase cost functions (in USD) for the main system components.	195
Table 5.5. Results of design energy demands and LNG cold recovery potential in a satellite plant owned by a single user of two type of agro-food industries. Values referenced to total energy demand of 1 MW (Electricity + Heat).	197
Table 5.6. Annual energetic and economic results for an off-grid refrigerated warehouse with and without LNG cold energy utilization in different locations and for different total energy demands.	197
Table 5.7. Total capital investment (in thousand USD) estimated for the different configurations considered and refrigeration capacity indexes, and for a satellite LNG plant for baseload power generation.	200
Table 5.8. Capital investment estimated and annual electricity consumption calculated for the conventional refrigeration system without LNG cold energy utilization and the indirect LNG cold utilization configuration in local satellite plants with different sizes.	204
Table 5.9. Integration of PV technology in both a configuration for utilizing the LNG cold energy indirectly in a local medium-size satellite plant (Nameplate vaporization: 1,500 Nm ³ /h and peak refrigeration load assuming an $RCI = 1$ (Eq. 5.19): 175.7 kW) and in a conventional refrigeration system: Size of the PV generator, capital investment and GHGs emissions of during the whole systems' lifetime.	208
Table A.1. Different LNG compositions considered in the calculations. Source: REFPROP.	237
Table A.2. Approximate unit conversion factors for LNG. Values are approximated since depends on the composition of the natural gas.	237
Table B.1. Energy and exergy balance equations of all the components of the polygeneration plant.	239
Table B.2. Thermodynamic data of each state point of the polygeneration plant when operating with the selected working fluids and heat transfer fluids (Power cycle RC-1 – Methane; DC + power cycle RC-2 – CO ₂ ; Power cycle RC-3 – Propane).	240
Table C.1. Average convective and overall heat transfer coefficients calculated for each heat exchanger of the polygeneration plant analysed in Chapter 4 (see Figure 4.6).	246
Table D.1. Catalogue data of the ammonia two-stage screw compressor (commercial model iZN70W/TUW) manufactured by Kobe Steel, Ltd.	249
Table D.2. Mass and energy balances and assumptions in each component of the two-stage refrigeration cycle illustrated in Figure D.2.	250
Table D.3. Main mass and energy balances NH ₃ /CO ₂ refrigeration machine. Numeration of state points corresponds to the schematic layout shown in Figure 5.10.	252
Table D.4. Values of the coefficients of Eq. D.11 calculated for different part-load ratios.	253

Table D.5. Thermodynamic data obtained from the simulation of the NH_3/CO_2 refrigeration cycle modelled. Baseline case: Cold room temperature: -18°C , Heat sink temperature: 32°C , Full load operation (PLR = 1). Nameplate refrigeration capacity: 45 kW (based on Newton R-3000 by Mayekawa). The intermediate pressures are those which optimize the refrigeration efficiency.

255

UNIVERSITAT ROVIRA I VIRGILI

EXERGY RECOVERY FROM LNG-REGASIFICATION FOR POLYGENERATION OF ENERGY

Antonio Atienza Márquez

Nomenclature

Abbreviations

AEB	Annual economic benefit
bcm	Billion cubic meters
Bio-LNG	Bio Liquefied Natural Gas
CCP	Combined Cold and Power system
CDC	Conventional District Cooling
CF	Annual net cash flow
CI	Cost indices
CP	Cryogenic Power
CRR	Cold Recovery Ratio
CUF	Capacity utilization factor
DB	Double-bundle
DC	District cooling
DCS	District Cooling Service
DE	Natural gas direct expansion unit
EEP	Equivalent Electricity production
EER	Energy Efficiency Ratio
EF	GHGs Emission factor
EG	Ethylene glycol
FCI	Fixed capital investment
GHG	Greenhouse Gas
GT	Gas turbine
GWP	Global Warming Potential
HE	Heat exchanger
HTF	Heat transfer fluid
LHV	Lower Heating Value
LNG	Liquefied Natural Gas
LT-DC	Low-Temperature District Cooling
MTPA	Million tonnes per annum
ORC	Organic Rankine Cycle
ORV	Open Rack Vaporizer
PEC	Purchase equipment cost
PV	Photovoltaic
RC	Rankine cycle
SW	Seawater
TCI	Total capital investment

Variables

A	Heat transfer area, m^2
C_p	Specific heat, $\text{kJ}/(\text{kg} \cdot \text{K})$
D	Pipe diameter, m
$DBPT$	Discounted payback time, years
Ex	Specific exergy, kJ/kg
F	Correction factor to log-mean temperature difference
G	Mass flux, $\text{kg}/(\text{s} \cdot \text{m}^2)$
h	Specific enthalpy, kJ/kg
i	Annual discount rate, %
k	Thermal conductivity, $\text{W}/(\text{m} \cdot \text{K})$
IRR	Internal rate of return, %

XXX

L	Tube length / length of a DC network, m
$LMTD$	Log-mean temperature difference, K
\dot{m}	Flow rate, kg/s
n	Lifetime (in economic analysis)
NG	Natural gas
NPV	Net Present Value
Nu	Nusselt number
p	Pressure, kPa
PES	Primary energy saving, GWh
Pr	Prandtl number
\dot{Q}	Heat Flux, kW
R	Thermal resistance $m^2 \cdot K/W$
RCI	Refrigeration Capacity Index
Re	Reynolds number
s	Entropy, $kJ/(kg \cdot K)$
T	Temperature, K
TSF	Turbine size parameter, m
U	Overall heat transfer coefficient, $W/(m^2 \cdot K)$
V	Volume, m^3
\dot{W}	Power, kW

Greek letters

α	Convective heat transfer coefficient, $W/(m^2 \cdot K)$
Δ	Difference
η	Efficiency, %
ϕ	Latitude, °; Temperature factor
μ	Dynamic viscosity, Pa·s
ρ	Density, kg/m^3
σ	Surface tension, N/m
ξ	Activity factor

Subscripts

0	Reference environment
C	Compressor
eg	Electric generator
el	Electric
f	Fouling
gb	Gearbox
H	Heating
i	Inner
is	Isentropic
lm	Log-mean
m	Motor
np	Nameplate
o	Outer, outdoor (ambient)
P	Pressure (exergy component), pump
ph	Physical (exergy)
R	Refrigeration
shf	Shaft
T	Temperature (exergy component)
tot	Total

Chapter 1. Introduction and thesis objectives

1.1. The climate emergency and energy transition

The fight against climate change is one of the major challenges of today's society. The accelerated global warming of our planet is revealing the unsustainability of the current energetic model, whose effects are becoming increasingly evident. Some examples are extremely poor quality of air specially in urban areas, changes in precipitation patterns, and more frequent extreme weather events such as typhoons, heatwaves, the rising of global temperature or accelerated melting of polar ice caps that lead into a rising on the sea level [1]. Most of these effects may have irreversible consequences that threaten ecosystems, habitats, species and health. And although some theories point to a natural trend to explain climate change, it is unequivocal that human's behaviour and their activities (e.g., electricity generation, heating, cooling, transport, and so forth) blame for accelerating it.

The Industrial Revolution brought countless positive developments and a radical change in all the areas of society (economy, culture, technology, transport, and so forth). It also paved the way for the current productive and energetic models. However, it also marked the starting point of a massive burning of fossil fuels which speeded up the emission of Greenhouse Gases (GHGs) and other air pollutants (e.g., NO_x , SO_x) to the atmosphere. Today, the global energy demand continues growing, and oil and coal together account for more than half of the total primary energy share, as shown in Figure 1.1. But although recent energy outlooks forecast an upward trend of renewable energy sources (i.e., solar, wind, geothermal, biomass, and so on) and a decelerated growing rate of oil and coal, the reliance on these high pollutant fossil fuels will remain in the next decades.

To keep an ecologically sustainable welfare society, it is required a socially just and clean transition towards a decarbonized economy and a net-zero emissions energetic model based mainly on “green” energies. In this sense, energy policymakers should take coordinated actions to develop a common long-term regulatory framework (for instance, imposing carbon taxes) for tackling the climate emergency effectively and implementing a low-carbon productive model successfully. The climate summit celebrated in Kyoto (Japan) in 1997 led to adopt The *Kyoto Protocol* [2], the first climate agreement to reduce greenhouse gases in industrialized countries and lay the foundation for what is now known as carbon markets. Since then, many others Climate Summits have been celebrated and in 2015 was reached the *Paris Agreement* whose main objective is to limit the global temperature rise 2°C above pre-industrial levels [3]. The European Green Deal that aims to achieve zero-net emissions of GHGs 2050 is another example of institutional response to the climate emergency [4].

But in general, the actions of countries have been implemented at snail pace so far. Besides, the failed attempts of agreement and lack of coordinated efforts between the governments involved in the latest climate summits draw a gloomy picture and increase

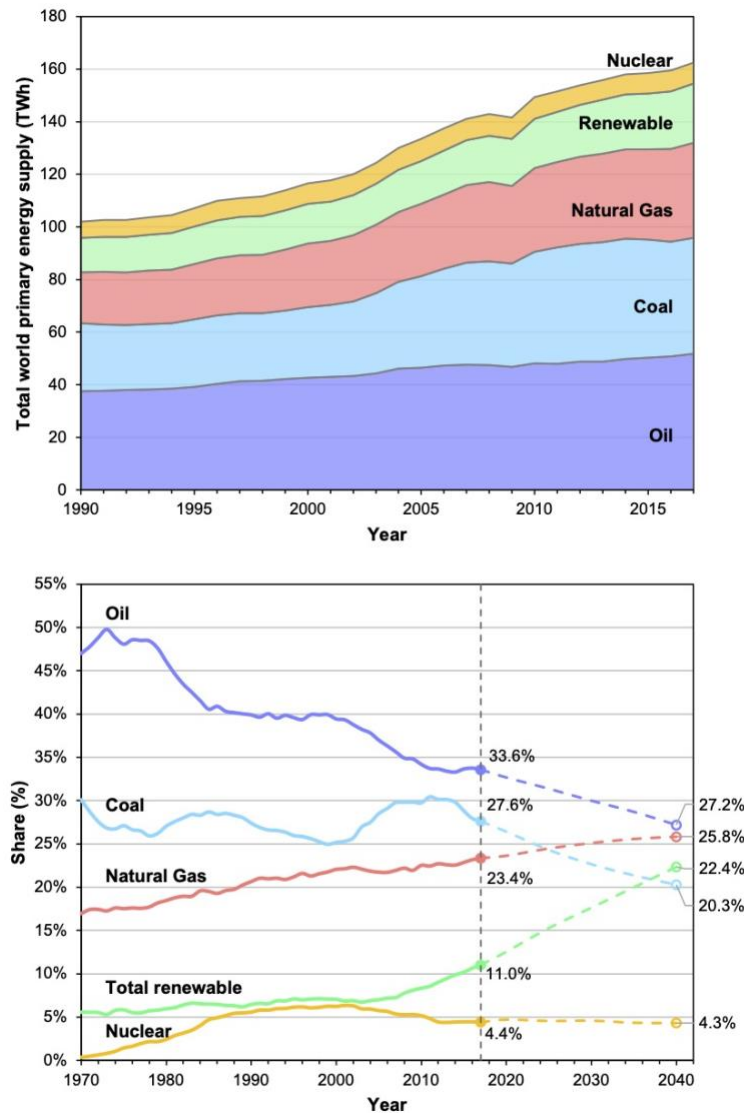


Figure 1.1. World primary energy supplied by source. Total renewables include hydro. Figure developed from data published by the International Energy Agency (IEA) [5] and BP Energy Outlook 2019 [6], considering an evolving energy transition.

the risk of missing the boat towards a sustainable future. For instance, the different parties involved in the Climate Summit celebrated in Madrid in 2019 were unable to reach an agreement on a global carbon market. Additionally, the energy transition is not a trivial issue that could be addressed overnight; fossil fuels are still required to mitigate the major weaknesses of renewable energies (e.g., intermittency and uncertainty). And the current crisis derived from the Covid-19 pandemic may threaten the priority to support

environmental policies in the upcoming years and may deaccelerate the deployment of clean technologies [7,8].

In this point, natural gas and, particularly, its cryogenic liquid form so-called Liquefied Natural Gas (LNG), can play the role of leader as a transition energy source. Natural gas has a lower both carbon footprint and air pollutants emissions than other fossil fuels and could facilitate a gradual deployment of green energies while technological solutions to overcome some of their above-mentioned limitations are developed. On the other hand, the utilization of renewable gases such as biogas or biomethane may give essential support to energy transition since allow dealing with the increasing amount of organic wastes and contributing to reducing the GHG emissions [9]. The rising interest in hydrogen is also remarkable.

But beyond the decarbonization towards a fossil fuels-free energy era, a sustainable energetic model requires more efficient utilization of the primary energy sources. The integration of different technologies through polygeneration systems allows minimizing energy wastes which boost the competitiveness of industries and decrease their carbon-intensity. It is in the focus of this doctoral thesis to develop sustainable and combustion-free polygeneration systems based on the utilization of the residual cryogenic energy content released in the regasification process of LNG as transition primary energy source as well as in the regasification of other cryogenic biofuels for the combined and simultaneous production of electric power and clean refrigeration.

This first chapter of the thesis showcases the current status and future perspectives mainly of LNG but also other cryogenic fuels as key primary energy sources. The cryogenic temperature of these fuels makes them a valuable physical exergetic source that could be exploited at a certain stage of their supply chain for multiple low-temperature industrial applications. Finally, the general and specific objectives of the thesis are described with a brief introduction of the topics discussed in the following chapters.

1.2. Natural gas and LNG: Facts and figures

Today, natural gas accounts for nearly a quarter of the world primary energy share, as shown above in [Figure 1.1](#). Its availability continues growing, and its demand will increase in the upcoming years with a pace which will depend on the policies scenario [10].

On the whole, the cleaner combustion concerning oil or coal is the key to understanding the growing interest in natural gas and is the motivation of fuel switching policies (coal-to-gas or oil-to-gas) [11]. According to the data published by the International Energy Agency (IEA) [12], in 2018 the global natural demand of natural gas increased by 4.6% accounting around 45% of the increase in the energy demand worldwide. Although in

2019 the natural gas demand kept growing (1.5% y-o-y, in line with the growing rate of the last decade), the data reflect a cool down with respect the two previous years (due to slower economic growth and mild temperatures) [13]. Regarding 2020, the Covid-19 crisis is going to cause an unprecedented fall not only in natural gas consumption but also in the global energy demand.

On the other hand, the unequal distribution of natural gas reserves makes its transport from extraction fields to final consumers a constraint. Natural gas is usually transported by pipeline. But when the distance between importer countries and gas suppliers is too long, the only feasible solution is the liquefaction of the natural gas to reduce its volume (achieved by a cryogenic cooling process of natural gas down to -162°C) and its shipping as Liquefied Natural Gas (LNG). Indeed, the growing demand for natural gas over the last years is boosted mainly due to the robust expansion of LNG [6,12].

LNG is a cryogenic liquid at normal atmospheric pressure [14]. It is odourless, colourless and non-corrosive. Although it is non-toxic, as occurs with any other gaseous materials, natural gas release from LNG can be hazardous in an enclosed and unventilated ambient due to lack of oxygen (causing asphyxiation) and ignition problems if mixed with the right concentration of air. LNG volume is approximately 600 times smaller than that gaseous phase at the burner tip and with a density between 400-500 kg/m^3 . Because it is lighter than water, if an accidental spill occurs during its maritime transport, LNG floats on top of the water surface and vaporizes rapidly without any environmental damage. Regarding its chemical composition, LNG is mostly methane plus a few per cent ethane, even less propane and butane, and trace amounts of nitrogen and CO_2 . Depending on the reservoir source of the original gas and its subsequent treatment process, the methane content of LNG is between 84-99 mol%. As a result, the amount of sulphur oxides in the combustion products is almost null, and the level of nitrogen oxides is very low. In [Appendix A](#) is given extra information regarding different LNG compositions with some of their thermophysical properties.

1.3. LNG versus pipeline gas

The transport as LNG entails several advantages concerning pipeline transport. The following are the most remarkable:

- **Fuel quality.** LNG has higher purity, higher methane and overall energy content, and a more stable composition than pipeline gas [15].
- **Access to distant markets.** LNG contributes to the gas market expansion and is more economically competitive than offshore pipelines for transport distances beyond 1,500-2,000 km in the case of long-distance routes crossing oceans or long stretches of water; or beyond 4,000-5,500 km in comparison with onshore pipelines [14,16].

- **Security and diversification of supply.** LNG provides significant flexibility to the gas market and contributes to avoiding the energy dependency from a specific country (since energy infrastructure is used as a diplomatic tool).
- **Speeding up agreements.** LNG shipments avoid lengthy negotiations on international pipeline routing, which sometimes is limited by geological and political constraints, particularly in the case of cross-border trade [17,18].

As a drawback, both the energy consumption and GHG emissions throughout the LNG supply chain (this issue is analysed in further detail in the following section) are generally higher than the pipeline, because of the extra processing steps [15]. However, the differences tend to wear off for very remote pipeline deliveries because the unavoidable fugitive emissions of methane increase as the length of pipelines do. The GHG emissions of the LNG delivery chain may be lower than pipeline routes for transport distances beyond 7,000 km.

Furthermore, the use of LNG as fuel for maritime transport (e.g., large container vessels, cruise ships, bulk carriers, ferries, and so on) rather than diesel or fuel oil theoretically represents significant environmental benefits because of a lower air pollutants emissions [19] and also with a competitive price. Particularly, the almost negligible quantity of SO_x in its combustion products allows complying with the International Maritime Organization (IMO) regulations [20]. Although few vessels are fuelled by LNG so far, its popularity is growing, as well as the bunkering infrastructure. Major shipping companies have already launched LNG powered commercial vessels, and top engine manufactures (e.g., Wärtsilä, Siemens, Man, Rolls-Royce, Caterpillar, MTU, among others) develop commercial LNG fuelled marine engines [21]. For similar reasons, LNG has also gained popularity as road transport fuel, specially, for heavy-duty vehicles (e.g., trucks [22], tractors, and so on) [23]. This is under consideration since the early '90s [24].

Because of the above-mentioned strengths, LNG is gaining ground with respect to pipelines in the gas market as illustrated in Figure 1.2, which depicts the evolution of the natural gas trade either as LNG or pipeline since the '80s until 2019. Global LNG trade continues growing sharply. For example, the growing rate of LNG trade in 2019 was 13% year-on-year (a six-year of consecutive growth), that equals to an increase of 41 million tonnes traded concerning 2018 [25]. By 2040, the natural gas trade could be shared almost equally between LNG and pipeline [6]. The continued expansion of LNG reinforces its role in the future energy mix.

1.3.1. The problem of methane emissions

The environmental advantages of natural gas and LNG mentioned above with respect to the other fossil fuels may be negatively outweighed by excessive methane emissions to the atmosphere over its whole supply chain. These emissions can have an intentional

nature (because of security issues), or unintentional either due to (1) small quantities of un-combusted methane in the flue gases once natural gas is burned as fuel or (2) fugitive leaks. The fugitive emissions are due to unintentionally leaks from equipment or components such as valves, pipeline damages, defects in sealing, and so forth [26]. Since methane is a potent greenhouse gas, any leakage throughout the gas supply chain represents not only an economic loss but also an environmental threat. This is one of the mean reasons why critics distrust of NG sustainability.

But, from a life-cycle perspective, *are the GHG emissions of LNG higher than those of other fuels?* This issue is hotly debated in the literature and specialized forums. Some

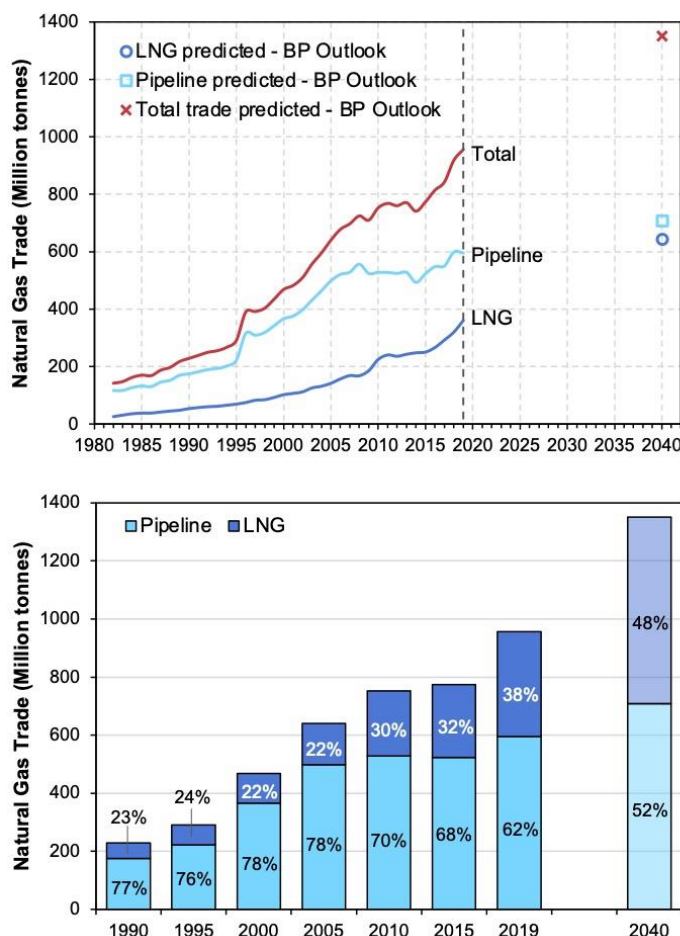


Figure 1.2. Evolution and forecast of the share of natural gas trade between pipeline gas and LNG. Conversion factor utilized: 1 million tonnes (MT) = 0.743 billion cubic meters of natural gas (bcm). See [Appendix A](#) for more unit conversion factors. Figure prepared by Antonio Atienza-Márquez based on a compilation of data from the following sources: Cedigaz [27], BP Statistical Reviews of World Energy [28], IEA Natural Gas Information 2020 [12], International Gas Union (IGU) World LNG reports [29], GIIGNL Annual Reports [30].

studies remark that is lower than other fossil fuels [31–33]. LNG may be even more environmentally friendly as transport fuel as other “*greener*” options from a life-cycle perspective depending on the production technologies utilized [34]. Authors such as Sun and Ertz [35] performed a statistical analysis concluding that the likelihood that LNG reduces the GHG emissions with respect to diesel is relatively high.

Nevertheless, other studies point out that the LNG life-cycle GHG footprint could be either comparable to that of conventional fuels or even worse [23,36,37]. Moreover, a recent study [38] has reported that some existing inventory methods underestimate methane emissions. To quantify accurately, the LNG life-cycle GHGs emissions and compare it with that of other fuels is challenging, and conclusive data are missing [26,39,40]. The values reported in the literature are subjected to the underlying uncertainty in the modelling data utilized [41]. Therefore, the dissemination and sharing existing information, data and knowledge are crucial to develop accurate inventory methods and perform a precise estimation of the methane emissions and help to understand the scale of the issue [40].

But anyway, it is undeniable the fact that methane leaks are a major contributor to the LNG GHGs emissions and also represent an economic loss for the gas industry. Therefore, there are crucial actions to undertake to mitigate and fix these emissions such as the following: the optimization of the natural gas extraction and liquefaction processes to reduce emissions, the investment on equipment for an exhaustive detection and tracking of methane seeping out, the improvement of the infrastructures across the entire gas value chain and a correct management of the BOG generated (e.g., in refuelling stations [42]). And last but not least, the suitable utilization of its cryogenic temperature for diverse refrigeration demanding applications is a further option to reduce the life-cycle methane emissions [31].

1.3.2. LNG’s global market

Figure 1.3 shows a world map with the major LNG exporter and importer countries. On the one hand, in 2019 there were a total of 20 LNG exporter countries. Qatar and Australia are the two main LNG exporter worldwide, followed by the USA and Russia. Since 2016, the USA is a net exporter of LNG, and has led LNG growth during the last years. On the other hand, according to the International Gas Union (IGU) [25] there are 130 large-scale regasification terminals spread over 37 different importer countries (including those which consume domestically-produced LNG). At the beginning of 2019, the global nominal regasification capacity was 821 million tonnes per annum. The LNG trade is dominated by countries of the Asia Pacific region. Japan leads the world in the LNG imports (22% of the market share in 2019), followed increasingly closer by China (17% of the market share in 2019) which has already surpassed the European importations and is expected to be the main driver of natural gas demand growth for the

near future [43]. The amount of LNG imported by India also grows vigorously, and its share to the global LNG imported in 2019 was 7%.

The increasing interest in LNG and its continued expansion reinforces its key role as transition primary energy source in the upcoming years. Furthermore, beyond the above-mentioned benefits as fuel with respect to pipeline gas and other fossil fuels, LNG is a *physical exergy gold mine* mainly because of its extremely low temperature. To understand better how this exergy content is introduced to natural gas and how it could be partially recovered and used it for different applications with the aim to enhance the competitiveness of industries, the LNG supply chain is analysed in the following section.

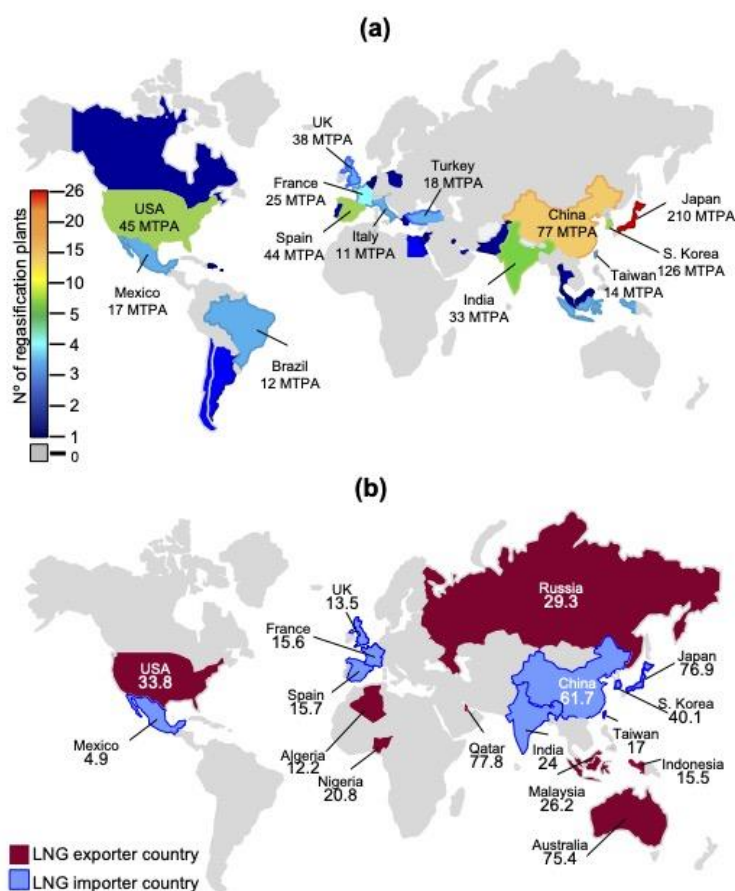


Figure 1.3. World map with: (a) Worldwide distribution of LNG regasification plants and major regasification capacities (in million tons per annum - MTPA) and (b) the most remarkable amounts of LNG in MTPA exported or imported in 2016 by the main countries in LNG market. Figure updated from [44]. Source of data: International Gas Union [25].

1.4. The LNG supply chain

The regasification is only one of the multiple stages of NG's supply chain, which is illustrated in [Figure 1.4](#). The fundamental steps of the LNG supply chain since the natural gas extraction till it is regasified and supplied to consumers are the following:

- 1) **Extraction** of raw natural gas.
- 2) **Pre-treatment** and **heavy hydrocarbons extraction**.
- 3) **Liquefaction** process, which is based on refrigeration cycles and is one of the most energy intensive stage of the LNG supply chain (i.e., between 5-15% of the natural gas income).
- 4) Maritime **transport** by ship.
- 5) **Regasification**, before being supplied to consumers (e.g., buildings, industries, power plants, and so forth). This is the stage with is in the focus of this doctoral thesis.
- 6) **Regulation**, which basically consists of tuning the send-out pressure of the regasified natural gas and also adjusting its heating value (by LPG, e.g., propane or butane injection) to meet the standards and transmission pipeline requirements.
- 7) **Odorization**, that consist of injecting a chemical (typically tetrahydrothiophene – THT or mercaptan) to the regasified natural gas stream to make natural gas (originally odourless) detectable if leakages occur.
- 8) Pipeline **transmission, pressure reduction** and local **distribution**.

Before being liquefied at the liquefaction plant, the raw gas extracted has to be submitted to several treatment processes to meet with its chemical composition limits [\[45\]](#). Solids, mercury, water, acid gas, heavy hydrocarbons and non-hydrocarbons such as nitrogen or helium have to be removed. The natural gas liquefaction is a process that requires a significant amount of energy (300-850 kWh/ton-LNG depending on the liquefaction technology used [\[46–48\]](#); between 5-15% of the natural gas income [\[48\]](#)). The liquefaction process technologies differ from each other depending on the type of refrigerants used, the number of refrigerant cycles, cascade or parallel arrangement of the refrigeration cycle, and so on [\[14,49\]](#). [Table 1.1](#) depicts some features of the most used liquefaction technologies [\[50\]](#). At the end of the liquefaction process, the temperature of the LNG is approximately 111 K (-162°C) and its physical volume is around 1/600 the volume of natural gas at its gaseous phase [\[51\]](#).

LNG is transported to importer countries over long distances in carriers of auto-refrigerated LNG tankers with a storage capacity up to 266,000 m³ of LNG [\[52\]](#). Once the LNG tanker docks at the receiving terminal port, the LNG is unloaded from the carrier to the terminal tanks. For instance, the regasification plant of Barcelona (Spain)

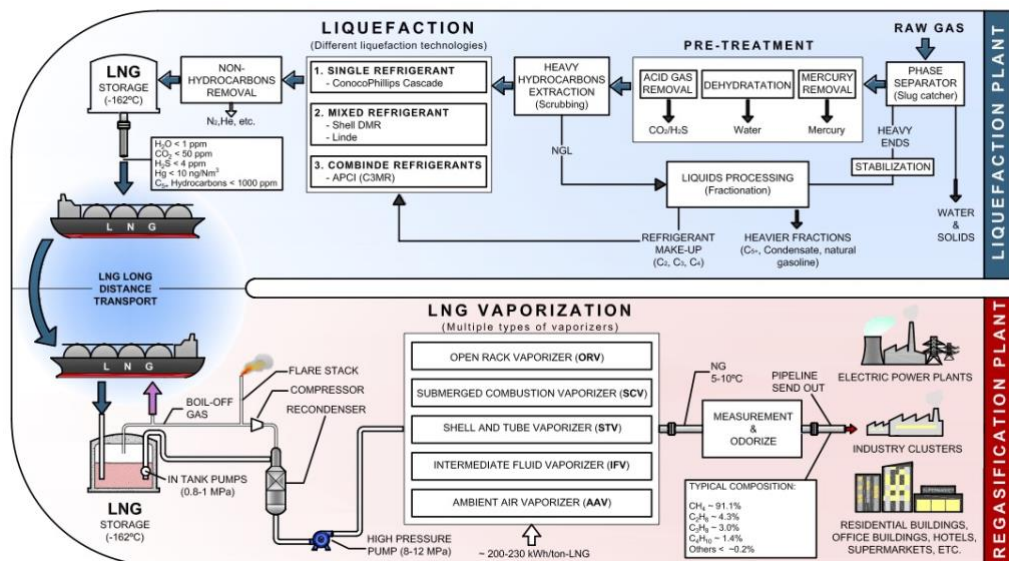


Figure 1.4. A block diagram of the LNG supply chain. From Atienza-Márquez et al. [44].

has a total storage capacity of 760,000 m³ of LNG (four tanks of 150,000 m³ and two of 80,000 m³) [53]. Inside LNG tanks, some boil-off gas (BOG) is produced. The management of the boil-off gas is an important task to control the pressure inside tanks between 110-250 mbar(g) [54]. The BOG is compressed and re-liquefied in the recondenser mixed with the LNG that is pumped from the tanks. Alternatively, the BOG may be introduced in the carriers of LNG tankers through a vapour line, or it may be burned in a torch.

Next, the LNG leaving the recondenser is pumped to the vaporizers where is regasified. Particularly in large-scale harbour terminals, where the regasification pressure is usually high, the high physical exergy content of LNG is not only due to its cryogenic temperature (temperature exergy) but also due to its pressure (or mechanical) exergy. Indeed, most of the polygeneration configurations developed in this thesis aim to exploit this physical exergy component as well. A detailed description of the physical exergy potential of LNG is given hereafter in this thesis.

The LNG regasification pressure relies upon the pressure requirements of the transmission and distribution pipelines. For example, in Spain, the natural gas pipeline transmission network is divided into two categories: primary network (distribution pressure > 60 bar) and secondary network (distribution pressure between 16 and 60 bar). On the other hand, the distribution pipelines that connect the core transmission networks with the end customers operate at the following relative pressures: between 4 and 16 bar (high-pressure distribution pipelines), between 0.4 and 4 bar (medium pressure A) or between 0.05 and 0.4 (medium pressure B). Nonetheless, distribution pressures higher

Table 1.1. Some of the most significant natural gas liquefaction technologies classified by the number of refrigerant cycles and the type of refrigerant utilized. Source: Table prepared from information taken from Al-Mutaz et al. [50] and Mokhatab et al. [14].

Liquefaction Process	Introducer	No. of refrigerant cycles	Type of refrigerant
Propane precooled mixed refrigerant (C3MR) ^a	Air Products and Chemicals Inc. (APCI)	2	Pure + Mixed
PRICO ^{®b}	Black & Veatch Pritchard	1	Mixed
AP-X [®]	Air Products and Chemicals Inc. (APCI)	3	Pure + Mixed
Dual Mixed Refrigerant (DMR)	Shell	2	Mixed
Mixed Fluid Cascade (MFC)	Linde	3	Mixed
Optimized cascade (OC)	Phillips	3	Pure

^a C3MR technology dominates around 75% of the natural gas liquefaction market.

^b Reserved for smaller-scale or peak shaving LNG plant applications.

than 40 bar are required to supply gas to, for example, combined power cycles and large industrial consumers. The final relative pressure of the gas supplied for household use is slightly above the atmospheric pressure (i.e., < 5 mbar). The pressure is adapted at the different connection points in regulation stations. As it will be explained in this thesis, the pressure regulation represents also an opportunity of harnessing the LNG physical exergy content.

1.4.1. The regasification: An opportunity to recover physical exergy

The regasification stage consists of the phase change process from liquid to gaseous phase by heating the LNG initially at around 111 K (-162°C) up to a temperature above 0°C using different vaporizer technologies and heat sources (e.g., seawater, process, ambient air or combustion heat). Almost the entire low-temperature exergy content of LNG (which was acquired at the liquefaction stage) is released throughout its regasification. Therefore, as illustrated in Figure 1.5, the cryogenic temperature of LNG could be exploited for useful low-temperature applications if the suitable technology and systems were utilized. Thus, part of the energy consumed in the liquefaction process would be recovered. **But what happens is that, with few exceptions that are described in the following chapters, LNG physical exergy is wasted in the vast majority of regasification terminals worldwide.**

To understand *how* that exergetic content is wasted, the following is a description of the most conventional technologies of vaporizers used in receiving terminals which are illustrated in Figure 1.6: Open Rack Vaporizers (ORVs), Submerged Combustion



Figure 1.5. A block diagram of the LNG supply chain with the low-temperature energy (cold) opportunity throughout its regasification process [55].

Vaporizers (SCVs), Ambient Air Vaporizers (AAVs) and Intermediate Fluid Vaporizers (IFVs). The following is a summary of the main features of each of them.

Open Rack Vaporizers (ORVs)

Figure 1.6 (a) shows a schematic diagram and a real picture of an Open Rack Vaporizer (ORV). The vaporizer is by far the most utilized in LNG regasification plants [56]. Around 70% of the vaporizers installed in base-load regasification terminals are based on this technology [14]. Typically, the maximum vaporization capacity of this type of unit is 300 t-LNG/h [57]. It consists of a set of tubes forming several tube-sheets where LNG flows through (generally, from bottom to the top). The seawater (preferably above 5°C) is sprayed outside LNG tubes (from top to bottom) and exchanging heat with LNG. According to some references, the energy consumed by seawater pumps is around 6-8 kWh/t-LNG [58,59]. Furthermore, Super-ORV is an evolved version of conventional ORVs units. This improved type of ORV vaporizer reduces the amount of seawater utilized in the LNG regasification process using a double tube structure so that the heat transferred is around three times higher than in conventional ORV [60].

Submerged Combustion Vaporizers (SCVs)

Figure 1.6 (b) shows a schematic diagram of a Submerged Combustion Vaporizer (SCV). This typology of vaporizer is the second most commonly used in LNG regasification facilities, accounting for around 20% of the vaporizers installed [14].

Usually, its duty is to cover the regasification demand in peak-shaving periods to give support to the ORVs which cover the baseload regasification rate in LNG facilities. It does not need clean or warm water nearby, and the typical vaporization capacity is 150/200 t-LNG/h [61]. The main drawback of this kind of vaporizer is that 1.5-2% of the natural gas regasified is consumed as fuel in the unit [59]. The heat released by the combustion of that fraction of natural gas is used to heat a bath that floods a set of tubes in which LNG flows through. In this way, LNG absorbs the required heat to be regasified.

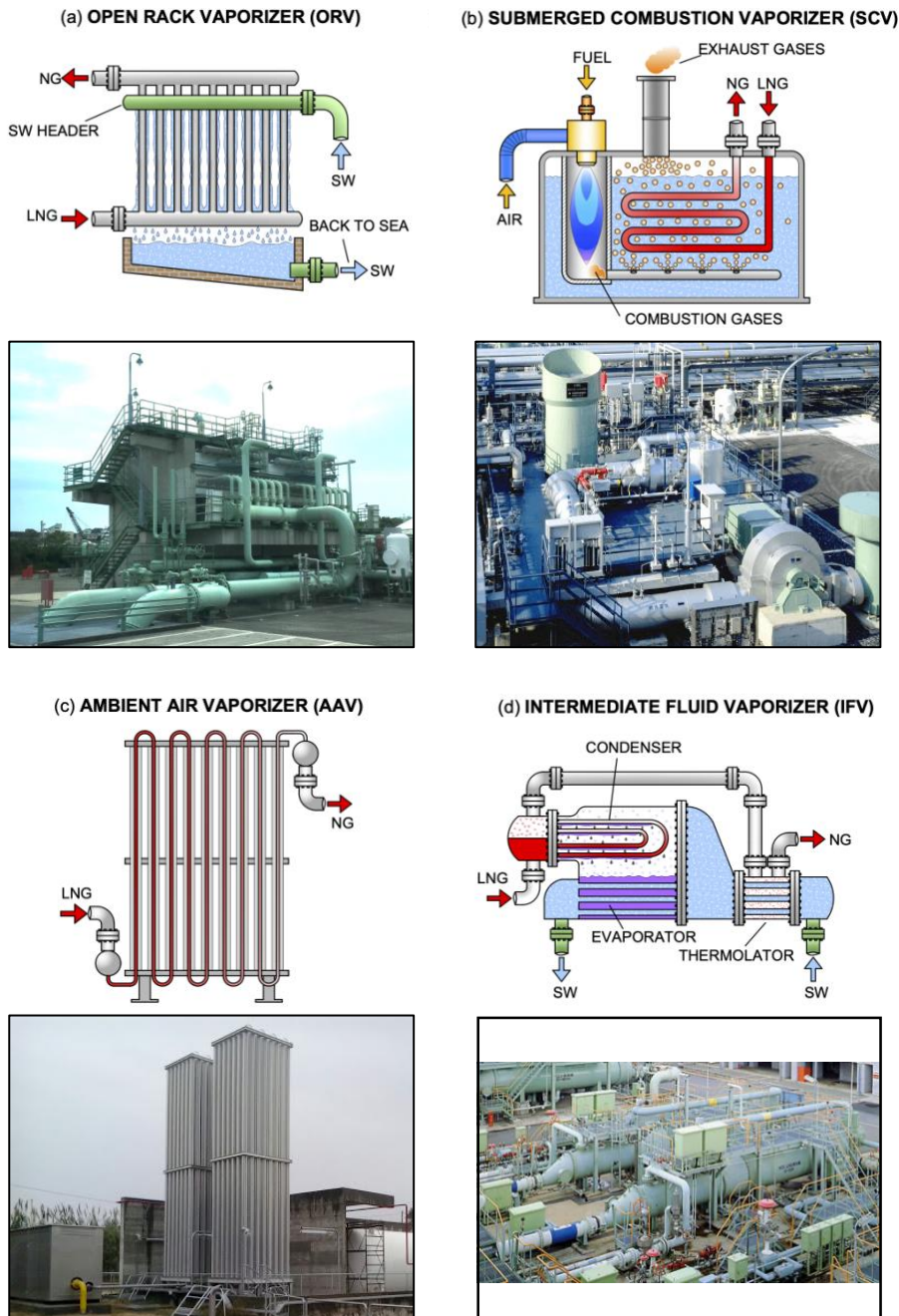


Figure 1.6. Conventional technologies of LNG vaporizers. (a) Open Rack Vaporizer – ORV (photo taken by the author with permission at Negishi LNG Terminal, Japan). (b) Submerged Combustion Vaporizer – SCV [62]. (c) Ambient Air Vaporizer – AAV. (d) Intermediate Fluid Vaporizer – IFV [63].

Ambient Air Vaporizers (AAVs)

Figure 1.6 (c) shows a schematic diagram and a picture of an Ambient Air Vaporizer (AAV). In this kind of unit, LNG flows through a set of finned and interconnected tubes arranged in parallel in such a way that the vaporizer has a rectangular-pyramid shape. In these vaporizers, the heat required to regasify LNG is taken from the ambient. As a consequence, the atmospheric conditions (temperature, humidity, etc.) affect a lot the performance of this type of unit.

Moreover, due to the low surface temperature reached in the unit, the moisture in the air condenses and freeze over the outer surface of the tubes, which damages the heat transfer [64]. Thus, it is quite common that at least a couple of AAVs operate alternatively to keep the LNG regasification process going while one of the units is in a defrosting shutdown. This type of unit is quite interesting for low LNG flow rates (< 5 t-LNG/h [57]). Therefore, they are the most common type of vaporizer in middle and small-medium size LNG facilities (also known as satellite LNG plants) because of its low operation cost and high environmental sustainability.

Intermediate Fluid Vaporizers (IFVs)

Figure 1.6 (d) shows a schematic diagram and a picture of an Intermediate Fluid Vaporizer (IFV). This typology of the unit consists of a sort of shell-and-tube heat exchanger with a double-bundle tube structure that uses an intermediate fluid (generally, propane) that plays the role of thermal buffer fluid and using seawater as the heat source to regasify LNG [65].

Regarding its structure, there are two tube bundles inside the shell. By one hand, the LNG/NG tube bundle is located in the upper part of the shell, and the intermediate fluid condenses in the outside surface of the tubes of this bundle. On the other hand, the seawater tube bundle is located in the bottoming part of the shell. This tube-bundle plays the role of the vaporizer of the thermal buffer fluid. Additionally, an extra heat exchanger (called thermolator) is integrated into the main shell to adjust the temperature of regasified LNG. The company Osaka Gas Co. Ltd. [63] originally developed this type of vaporizer, and the company Kobe Steel is an authorized manufacturer.

Some of the most remarkable advantages of IFVs are compact volume, environmentally friendly, the low quality required for the seawater utilized in the process and no ice formation [66]. Due to these features, this kind of unit is not only used in conventional land LNG facilities but also, they are used in Floating Regasification Units (FRSU). Although in a “conventional” IFV the exergetic potential of LNG because of its low-temperature is wasted via seawater, the structure of this typology of vaporizer makes it very attractive for addressing the low-temperature exergy recovery from LNG-regasification. Nevertheless, there is a hurdle regarding the lack of suitable fluids that could play the role of both heating media to regasify LNG and also the role of heat

transfer media to recover the low-temperature thermal energy from LNG for its subsequent use, for example, in refrigeration applications.

1.4.2. The widespread wasting of LNG physical exergy

The low-temperature thermal energy of LNG is wasted when using any of the technologies of vaporizers described above. Consequently, around 240 kWh of low-temperature thermal energy per metric tonne of LNG regasified is rejected to the ambient (e.g., through seawater or ambient air) without any useful application. Figure 1.7 shows the thermal energy input required to regasify a metric ton of LNG (assumed as pure methane) under different regasification pressures. And beyond an energy waste, the low-temperature thermal energy which is usually rejected via seawater has a negative impact on marine sea life (cold pollution).

The regasification entails an excellent opportunity to recover part of the energy supplied to liquefy natural gas. But the benefits of exploiting that “free” exergetic potential is not the result of recent research. The very first projects for using LNG physical exergy began in the early '70s in Japan. Also, currently, there are international energetic strategies that explicitly mentions LNG-regasification as a chance of waste cold recovery (e.g., the European Strategic Energy Technology Plan (SET) [67]). So why today the LNG physical exergy is rarely exploited in regasification plants? The reason is that there are

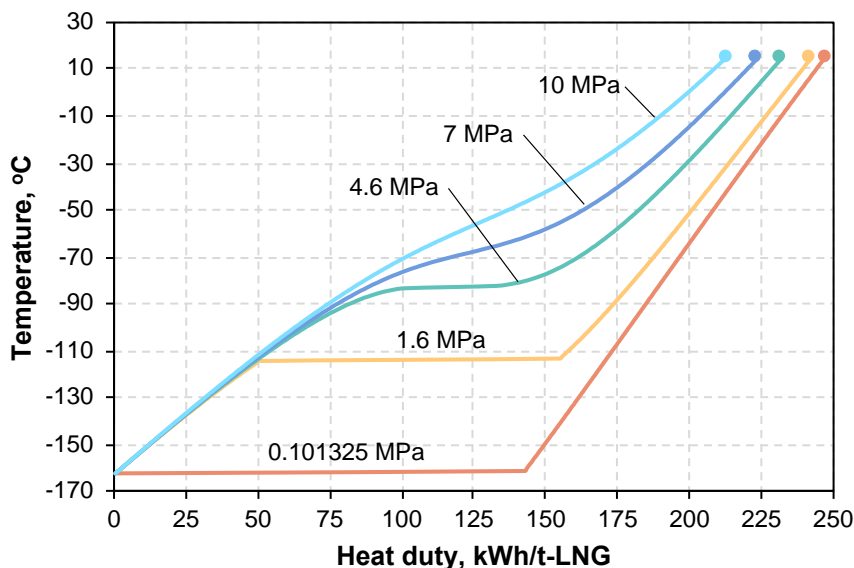


Figure 1.7. LNG (assumed as pure methane) heat released curve. Assuming LNG as pure methane, a regasification pressure of 3,000 kPa, and initial and final temperatures of 111 K and a 273 K, respectively.

technical as well as non-technical bottlenecks that still blocks a further development of LNG physical exergy utilization systems and their widespread implementation in regasification terminals worldwide. The following is a description of some of the most remarkable.

1.4.2.1. Non-technical bottlenecks

Some of the barriers which have non-technical nature are the following:

- **Mistrust of industry holders** about the reliability of LNG low-temperature exergy recovery systems to replace conventional refrigeration plants.
- **Limited interest of gas supplier companies** to exploit LNG physical exergy as additional cold supply is usually not considered as part of its business portfolio.
- **Legal and agreement bottlenecks** due to the high number of public administrations and private companies that have to participate in a final project implementation mainly governments, municipalities, gas companies, energy service providers and stakeholders.

1.4.2.2. Technical bottlenecks

Other barriers are purely *technical*:

- The possible **mismatch between the refrigeration demand and the low-temperature thermal energy available** from LNG-regasification.
- The **lack of an ideal heat transfer fluid** when the cold recovered has to be transported over distances in the order of kilometres. This implies that potential cold users should be located reasonably close to the LNG terminal. Although this is not a limiting issue when cold is delivered to a new industry hub installed specially to exploit LNG low-temperature exergy, it is of concern for the case of existing industries located far from the regasification site. Promoting the installation of new industrial facilities with a remarkable cooling demand to the surroundings of an LNG terminal would benefit the use of LNG physical exergy.
- The **low efficiencies** of the few existing LNG physical exergy utilization systems. Further details regarding this issue are provided in the following chapters of the thesis.
- The **low economic competitiveness** due to the expensive technologies and materials required, and also the high complexity of the proposed configurations to exploit LNG physical exergy.

This thesis will cover most of these technical barriers as will be explained later on.

1.5. The value of low-temperature energy reservoirs

Despite the barriers mentioned before, the widespread trend to wasting “free” low-temperature energy reservoirs such as LNG throughout its regasification process may be reversed in the immediate future. That change will be driven by climate and energy policies which pursues a more efficient utilization of primary energy sources and introduces carbon prices strategies. The new scenario *takes a fresh look* at the benefits of those systems that exploit low-temperature reservoirs and enhances their economic competitiveness, which may encourage the development and implementation of technologies for that aim in industrial areas.

The following is a detailed description of some remarkable and “reappraised” benefits derived by the utilization of low-temperature energy reservoirs for the multiple industrial applications which are detailed in the following chapters of this thesis. Furthermore, it is analysed the new horizon of opportunities opened by the emerging markets of clean cryogenic fluids like bio-LNG, which can also be considered low-temperature exergy reservoirs that could be exploited during its regasification stage.

1.5.1. Improving the thermal efficiency of power cycles

The temperature of the heat sink is crucial for the thermodynamic efficiency of any thermal cycle. In other words, the thermal efficiency improves as the temperature of the heat sink decreases. For example, [Figure 1.8](#) shows the schematic diagram of two thermal machines operating between different temperature reservoirs. The cycle shown on the left is representative of a conventional power cycle (e.g., Rankine) driven by, for example, combustion energy or solar energy and using the ambient as a heat sink. The right scheme corresponds to a thermal machine that uses LNG as a heat sink and ambient as a heat source (i.e., a cryogenic Organic Rankine Cycle).

Although both cycles have the same Carnot’s efficiency, the thermal machine that exploits the very low-temperature reservoir requires a much lower temperature difference with respect to the ambient temperature. Indeed, the variation of 1°C below the ambient affects much more the thermal efficiency than the variation of 1°C above the ambient. This phenomenon remarks the value of LNG as low-temperature exergy source and is a motivation to develop systems aiming to exploit it. Furthermore, the utilization of LNG low temperature can go towards non-combustion systems. But although systems and processes involving high temperatures are well studied, the same does not occur for low-temperature systems. This thesis aims to shed light on these kinds of processes.

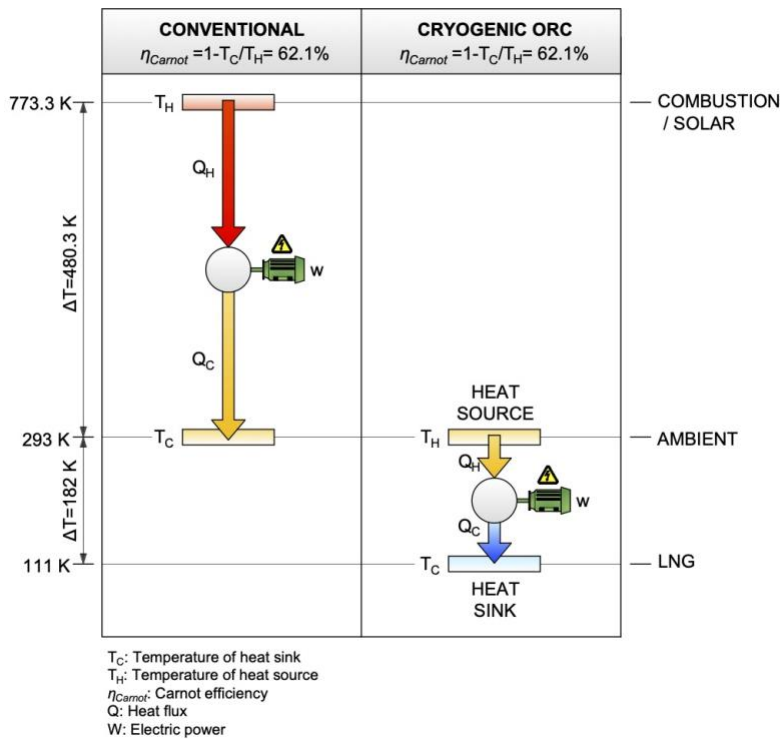


Figure 1.8. Schematic diagram of two thermal machines with the same Carnot's efficiency but operating between two different temperature reservoirs. Redrawn from [44].

1.5.2. Contributing to a sustainable refrigeration system

A *more sustainable refrigeration system* is essential to the achievement of carbon reduction targets. Refrigeration plays a crucial role in food, health or thermal comfort, and also in the economy [68] and its demand grows soaring worldwide [69]. For instance, the Energy Information Administration (EIA) of the United States forecast that energy use for air-conditioning will grow faster than any other use in buildings [70].

However, *cold* production (i.e., low-temperature thermal energy) is an energy-intensive activity and is a major contributor to carbon emissions [71]. The refrigeration sector (including air-conditioning) accounts for around 20% of the overall electricity consumption worldwide and 7.8% of the global GHG emissions, and these shares are steadily increasing [72]. Besides, the cold production through conventional system involves both direct and indirect emission of environmentally damaging substances [73]. The indirect emissions of pollutants are due to the generation of the energy required to drive the refrigeration systems. On the other hand, the direct emissions are due to the leakages or non-controlled disposals of man-made refrigerants (mainly,

chlorofluorocarbons – CFCs, hydrochlorofluorocarbons – HCFCs, hydrofluorocarbons – HFCs, perfluorocarbons – PFCs and sulphur hexafluoride – SF₆). CFCs and HCFCs with ozone depletion potential were regulated in the Montreal Protocol (1990) and generally replaced by HFCs, whose production and consumption have been also regulated in the Kigali Amendment to the Montreal Protocol (effective since January 2019). For example, the European Union “*F-Gas Regulation*” [74] (adopted in 2006 and updated in 2014) is legislation committed with the international climate agreements. Essentially, this regulation aims to phase-down fluorinated GHGs, prevent their leakages and banning their use in new types of equipment whenever other less harmful alternative refrigerants are available.

More sustainable refrigeration systems could be achieved, for example, by boosting the efficiency of refrigeration systems with a major utilization of natural refrigerants (e.g., water, ammonia or carbon dioxide), improving the design of buildings to minimize thermal loads, using renewably powered refrigeration systems or using distributed refrigeration networks [75]. Moreover, public authorities should pursue the implementation of policies and more rigorous efficiency standards and buildings codes. But harnessing low-temperature reservoirs such as LNG throughout its regasification process to produce “*free*” cold for multiple uses is also an excellent and promising way to contribute to a clean and sustainable refrigeration production. Indeed, **a key accomplishment of the systems and configurations developed in this thesis is to support the phasing-out of environmentally damaging refrigerants and to reduce the energy consumption of conventional refrigeration equipment.**

1.5.3. The opportunity afforded by bio-LNG regasification

Although the systems developed in this doctoral thesis mostly refers to the utilization of the physical exergy of *fossil* LNG, they also have an application to the regasification of other cryogenic fuels even more environmentally friendly. A clear example is liquid biomethane (LBM, or popularly known as *bio-LNG*) which is generally obtained from biogas [76].

Biogas is a mixture of methane (45-75% by volume), CO₂ and small fractions of other gases and can be used to produce heat and/or power and for household use as well, and which is produced from the anaerobic digestion of organic feedstocks in an oxygen-free environment. The increasing amount of organic residues and wastes produced due to daily human’s activities, livestock manure and other agro-food residues can be utilized to produce clean fuels and contribute to a circular economy and to provide a way to integrate rural communities and industries into the transformation of the energy sector [9]. However, the potential of these organic wastes has been underutilized so far. According to the International Energy Agency (IEA) [9], the vast availability of organic feedstocks (i.e., crop residues, animal manure, municipal solid waste, wastewater and forestry residues) reveals the technical potential for the production of biogas and

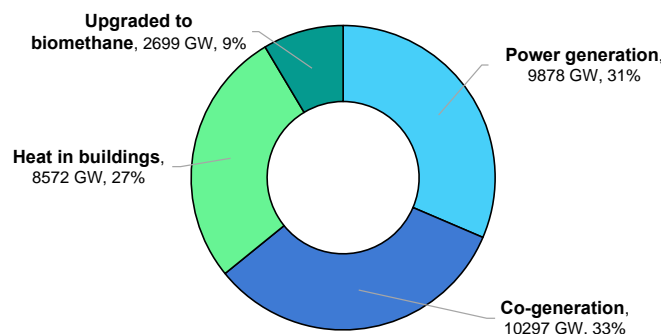


Figure 1.9. Biogas consumption by end-use. Redrawn from IEA [9].

biomethane is huge but largely untapped. For example, in 2018, the production of biogas and biomethane accounted only 1% of the whole estimated potential. But up to 20% of the world gas demand may be covered if that potential were fully exploited.

Today, the biogas sector is being shaped mainly because of policy support and feedstock availability. As shown in Figure 1.9, although most of the biogas produced is utilized as fuel for electric power generation and heat production, there is a fraction that is upgraded to biomethane and supplies into the gas network (as a substitute to conventional natural gas) or used as a fuel in the transport sector. Biomethane (also known as “renewable natural gas”) is usually obtained after a clean-up process that consists of removing CO₂ and other impurities from “raw” biogas. Around 90% of the biomethane produced worldwide is from biogas upgrading techniques [9,77]. Alternatively, biomethane can be obtained through the gasification of solid biomass followed by methanation. Because of the similarities with natural gas, biomethane can be transported and used wherever natural gas is consumed through the same transmission and transport pipeline networks.

As occurs in the conventional natural gas market, the transport of biomethane to regions without connections to the distribution pipelines is a problem; and a solution is its liquefaction [78] for onward transportation as a cryogenic liquid. Figure 1.10 shows the schematic diagram of the liquid biomethane (LBM) – hereafter called *bio-LNG* – supply chain [79,80]. Bio-LNG has the same advantages as the *fossil* LNG and almost the same chemical composition, but with a higher methane number and negligible emissions of NO_x, so can be considered a kind of *premium-quality* LNG [76]. The lower heating value (LHV) of bio-LNG is around 36 MJ/m³ which is slightly higher than a typical *fossil* LNG (~35.9 MJ/m³), and higher than that of biogas (16-28 MJ/m³). Besides, small-scale production of bio-LNG has a huge potential and also promotes local employment and economic development mainly in rural areas. Today the production and utilization of bio-LNG are in expansion with many corporate groups joining the business. As illustrated in Figure 1.10, as with the fossil LNG, the regasification of bio-LNG is an excellent opportunity to produce “free” low-temperature thermal energy for multiple applications.

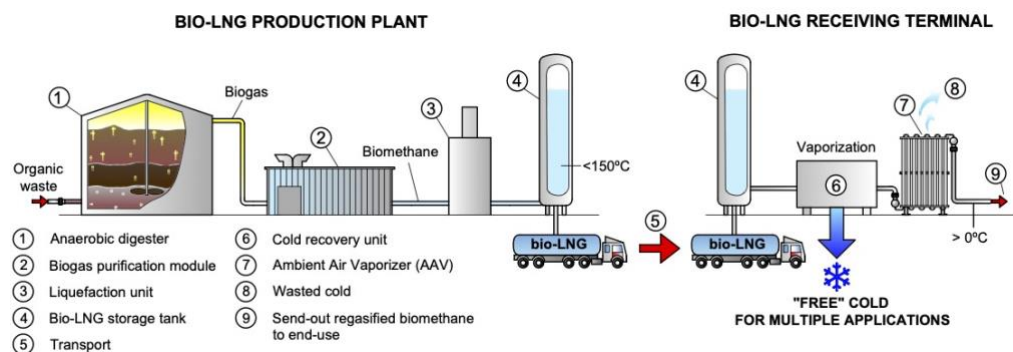


Figure 1.10. Schematic layout of the bio-LNG supply chain and the cold recovery opportunity from its regasification process [55].

1.6. Objectives of the thesis

The *main objective* of this doctoral thesis is **to develop techno-economically feasible, sustainable and reliable systems to harness the physical exergy content of LNG throughout its regasification process for polygeneration of energy**, particularly, cryogenic electric power generation and refrigeration production at different temperature levels. In this way, the findings of the thesis will contribute to overcome some of the barriers that hamper a widespread utilization of the LNG physical exergy and the implementation of systems for that purpose in receiving and regasification terminals worldwide. Besides, the systems proposed and analysed in the thesis would contribute to boost the efficiency and competitiveness of industries as well as reduce their environmental impact and also contribute to a more sustainable refrigeration model.

To accomplish the main objective of this thesis, the following *specific objectives* are set:

- **Evaluation of the LNG physical exergy potential and comprehensive review of applications and technologies** for its utilization. And also, analysis of the global deployment of the LNG physical exergy utilization in existing terminals.
- **Review of the polygeneration systems proposed in the literature** for the polygeneration of energy and analysis of the benefits obtained from these types of systems in terms of efficiency.
- Propose a **decision-making method for screening the most suitable working fluids and heat transfer fluids** under different operating conditions by using a new polygeneration plant as a case study. And also, develop specific performance indicators to evaluate the performance of this kind of polygeneration plants.

- **Develop different cascaded configurations - drawn from the structure of an existing cryogenic power generation unit** - for squeezing the LNG physical exergy content for more than a single application. Furthermore, **calibration** of the model of the benchmark cryogenic power unit by gathering operating data available in the literature. And also, evaluation of the thermodynamic, environmental and economic performance of the systems developed.
- **Simplified modelling of a double-bundle heat exchanger technology** suitable for the utilization of the LNG physical exergy for low-temperature refrigeration through indirect heat transfer using natural heat transfer fluids with relatively high freezing point. Then, the integration of the developed model in some of the systems and configurations developed.
- **Discussion** of the techno-economic feasibility of systems that exploits the fossil LNG / bio-LNG low-temperature exergy for refrigeration applications in **satellite regasification plants**. And also, analyse the feasibility of combining photovoltaic technology with the LNG exergy utilization system because of the current high interest in both systems.

1.7. Structure of the thesis

In the first chapter, it has been defined the context of climate change and energy transition in which this doctoral thesis is developed. Then, the role of natural gas and, specially, LNG as transition primary energy source has been examined according to significant global figures and future trends. The advantages of LNG with respect to pipeline gas trade have been identified to explain the increasing interest in that cryogenic liquid whose physical exergy content is intended to be exploited in this thesis for polygeneration of energy. The main stages of the LNG supply chain have been explained to identify both the most energy-consuming stages and the physical exergy recovery opportunities. The reasons why that physical exergy content is usually wasted in most of the LNG terminals worldwide are remarked. Afterwards, it has been highlighted the opportunities and thermodynamic benefits brought by the exploitation of “free” low-temperature thermal energy reservoirs such as either *fossil* LNG or bio-LNG. It is then followed by a description of the overall and specific objectives of the thesis. The remaining chapters of the thesis are organized as follows:

- **Chapter 2:** Evaluation of the LNG physical exergy potential as a function of its temperature and regasification pressure. Then, it is provided a description and a comprehensive literature review of the different application and technologies for the exploitation of that exergy. Also, it is analysed their current global deployment in existing regasification facilities.
- **Chapter 3:** Review of the systems proposed in the literature for utilization of the LNG physical exergy for polygeneration of energy. In this chapter is presented a

discussion of the most suitable working fluids and heat transfer fluids. It is developed the modelling of a polygeneration plant that is used as a case study to determine which are the most convenient fluids in function of the applications and the operating conditions. Some new performance indicators are defined to perform the decision-making process.

- **Chapter 4:** This chapter deals with the development, modelling and performance analysis of different non-combustion and cascaded configurations with different degree of complexity and energy outputs. The core structure of all these systems is built on that of an existing cryogenic power plant that exploits the physical exergy of LNG. The modelling of the basic cryogenic power cycle is calibrated using real operating data available in the open literature. Then, it is presented the simplified modelling of a double-bundle heat exchanger for the production of low-temperature refrigeration which is integrated into some of the configurations studied in this chapter. Finally, the economic feasibility of the proposed systems is evaluated under different scenarios.
- **Chapter 5:** This chapter is dedicated to the low-temperature exergy utilization of LNG (or bio-LNG) in satellite regasification plants. It is evaluated the techno-economic feasibility of different proposed configurations for the low-temperature exergy utilization in some common types of satellite facilities and in different climates. The feasibility of introducing photovoltaic technology in the system is also discussed.
- **Chapter 6:** This chapter gives the overall conclusions obtained in this doctoral thesis. Additionally, it is given a remark of the remaining research gaps that could be addressed in future studies and new research directions.

Chapter 2. LNG physical exergy utilization: Potential, applications and technologies

Major parts of this Chapter have been published in the following articles:

- **A. Atienza-Márquez**, J.C. Bruno, A. Coronas. *Applied Thermal Engineering* 132 (2018), 463-478, [10.1016/j.applthermaleng.2017.12.073](https://doi.org/10.1016/j.applthermaleng.2017.12.073)
- **A. Atienza-Márquez**, D.S Ayoub, J.C. Bruno, A. Coronas. *Thermal Science and Engineering Progress* 20 (2020), 100677, [10.1016/j.tsep.2020.100677](https://doi.org/10.1016/j.tsep.2020.100677)

2.1. Introduction

In this chapter, the LNG physical exergy potential is analysed in function of the temperature and regasification pressure. The various criteria utilized among engineers and researchers to evaluate the exergetic efficiency of the configurations proposed are explained. The criteria used in this thesis is explained and justified. Then the fundamentals of the different applications and technologies for exploiting the physical exergy content of LNG throughout its regasification process at different temperature levels are studied. Also, it is provided a comprehensive review of the most remarkable contributions in the literature focused on each of these applications. Finally, it is analysed the global deployment of LNG physical exergy utilization systems in regasification terminals worldwide. Future plants and active projects are also commented.

2.2. Exergetic potential

The terminology utilized in the literature dealing with the utilization of the cryogenic temperature of LNG and also its usually high regasification pressure is widely varied. While there is no agreement among authors and experts in this research area to use a unique term, some of the most frequently utilized are *cryogenic energy/exergy*, *cryogenic cold energy/exergy*, *low-temperature thermal energy*, *waste cold*, and so forth.

Among the terms mentioned above, talking about the *exergy* content of a cryogenic liquid such as LNG is particularly revealing since it provides a reference of the *potential* and *quality* as a thermal energy reservoir. Regarding the formal definition, *exergy* is a thermodynamic quantity that reveals the maximum amount of useful work that a system can perform as it approaches the thermodynamic equilibrium with its surroundings by reversible processes [81]. Accordingly, the exergy content of an energy stream (i.e., its potential and quality) increases as its thermodynamic state moves further away from the equilibria with the surroundings. Furthermore, exergy has also an interesting connection with economics. For example, the cost of producing a unit of refrigeration at -50°C is higher than at 6°C . Although from the energetic point of view the cold production is the same (e.g., 1 kW), the efficiency of a refrigeration machine decreases with the set-point temperature and its electricity consumption increases. In conclusion, the cost of producing an energy flow increases as its thermodynamic state moves further away from the ambient.

The wide temperature gap between an LNG stream (111 K, -162°C) and the ambient, and sometimes also its high pressure, endows LNG a huge *exergetic potential*. The suitable utilization of that potential for different applications could lead to important

energy and economic savings. But the installation of systems to exploit that exergetic potential requires a capital investment, so the economic feasibility depends ultimately on the economic value of the energy products obtained. In other words, how the initial exergy content of LNG is preserved in the energy products determines the economic performance of any exergy utilization system. Since any loss or exergy destruction represents an economic loss, exergetic analysis is a useful tool to gather information upon the components whose operation could be improved and optimized [82]. The exergetic analysis is usually incorporated in the specific literature dealing with the utilization of the cryogenic temperature and pressure of LNG [83].

2.2.1. The exergy breakdown

By neglecting the potential, kinetic and electric exergies, the total exergy content of a cryogenic fluid stream such as LNG is the sum of its chemical ($\dot{E}x_{ch}$) and physical ($\dot{E}x_{ph}$) parts [84]:

$$\dot{E}x_{tot} = \dot{E}x_{ch} + \dot{E}x_{ph} \quad (2.1)$$

By one hand, the chemical exergy of natural gas can be calculated as follows [85]:

$$\dot{E}x_{ch} = \xi \times LHV \quad (2.2)$$

where the chemical exergy to energy ratio (ξ) of LNG (assumed as pure methane) is 1.06 [86], and the lower heating value (LHV) of LNG is approximately 13.4 kWh/kg-LNG. Therefore, the chemical exergy of an LNG stream is ~14,200 kWh/t-LNG. **Since in the systems and configurations developed in this doctoral thesis are non-combustion systems designed to exploit only the physical exergy, the chemical exergy of any LNG stream is fully preserved.** Figure 2.1 illustrates the breakdown of the LNG exergy content and a generic exergy flow diagram of the physical exergy utilization systems developed in this doctoral thesis. The *quality* of the energy products in relation to the exergy losses and the remaining physical exergy in the regasified natural gas depends mainly on the application and the process followed to exploit the LNG physical exergy inflow.

On the other hand, the physical exergy content of an LNG stream splits into two components with different utilizations: low-temperature exergy ($\dot{E}x_T$) and pressure component ($\dot{E}x_p$), also known as thermal and mechanical exergy, respectively [87]. For a material stream, these exergy components are calculated as follows:

$$\dot{E}x_{ph} = \dot{E}x_T + \dot{E}x_p = \dot{m}[(h - h_0) - T_0(s - s_0)] \quad (2.3)$$

$$Ex_T = Ex(T, p) - Ex(T_0, p) = h_{T,p} - h_{T_0,p} - T_0(s_{T,p} - s_{T_0,p}) \quad (2.4)$$

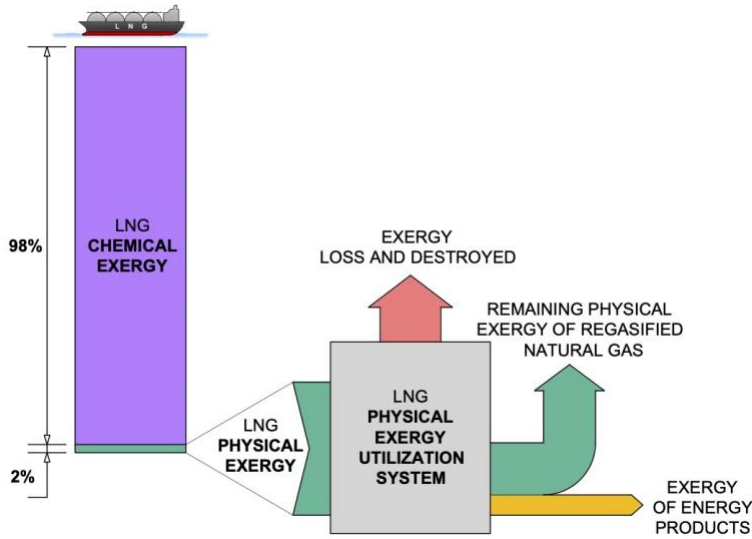


Figure 2.1. Breakdown of LNG exergy content into chemical and physical exergy and conceptual flow diagram of the physical exergy utilization.

$$Ex_p = Ex(T_0, p) - Ex(T_0, p_0) = h_{T_0, p} - h_{T_0, p_0} - T_0(s_{T_0, p} - s_{T_0, p_0}) \quad (2.5)$$

Notice that other types of physical exergy such as the kinetic and the potential are not considered since are smaller than the thermal and the mechanical exergies [81]. As stated before, the thermal exergy content of LNG is due to its cryogenic temperature, whilst the mechanical exergy content varies depending on the regasification pressure. For instance, the regasification pressure in small regasification plants located in areas without access to transmission pipelines is usually low because the regasified gas is supplied directly to consumers or through short distribution pipelines. In such cases, the mechanical exergy of LNG is low. Instead, in large-scale harbour regasification terminals, the regasified LNG is injected into long-distance transmission pipelines or is supplied to consumers which require of natural gas pressures, so the LNG regasification pressure is usually high; thus, the mechanical exergy content is also high to the total physical exergy content. As described below, that pressure exergy can be exploited for the production of shaft work.

2.2.2. The physical exergy potential

Figure 2.2 depicts the thermal and mechanical exergy content of an LNG stream for different regasification pressures. In this doctoral thesis, the reference-environment for the exergy calculations is set to 298.15 K and 101.325 kPa. Higher regasification pressures lead to an increase of the pressure exergy content but also into a lower low-

temperature exergy content and, therefore, a lower potential for its exploitation in low-temperature applications. The total physical exergy content of LNG (assumed as pure methane) is around 300 kWh/t-LNG.

As illustrated in Figure 2.1, this amount is significantly lower than the chemical exergy, so that *the physical exergy represents only ~2% of the total LNG exergy content*. This result is one of the reasons why the LNG physical is rarely exploited in regasification terminals. For example, instead of exploiting the low temperature of LNG directly for refrigeration directly through heat exchanger networks, sometimes is more economically advantageous to burn natural gas and produce the electric power required to drive conventional refrigeration equipment.

However, this value must not be misunderstood. Although it seems to be very low because of the high chemical exergy content of LNG as fuel, the physical exergy potential is not negligible, and it can be recovered in multiple industrial applications. For instance, assuming LNG as pure methane at -160°C and at atmospheric pressure, the physical exergy potential of a 150 t-LNG/h stream (amount consistent with a typical handling capacity of an ORV) is ~40 MW. The systems developed in this doctoral thesis target the enhancement of the efficiency and the simplification of configurations to make the utilization of the LNG physical exergy economically competitive.

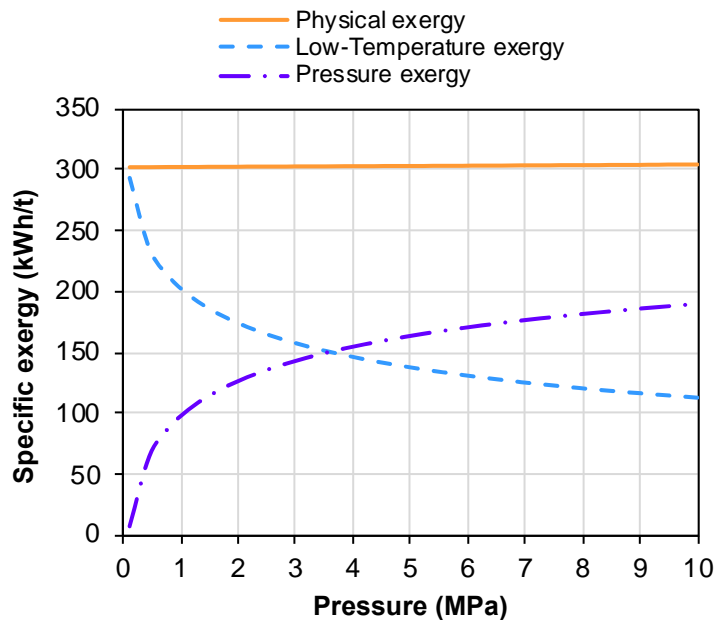


Figure 2.2. Specific physical exergy content of an LNG stream (assumed as pure methane) after pumping from storage tanks, divided into thermal and pressure exergy and considering regasification pressures up to 10 MPa. Exergy content calculated using Engineering Equation Solver (EES) [88]. Assumptions: Initial temperature and pressure -162°C and 0.12 MPa, respectively; Isentropic efficiency of cryogenic pumps: 75%.

2.2.3. The exergetic efficiency definition

The general definition of the exergetic efficiency of any energy system is formulated as follows:

$$\eta_{ex} = \frac{\sum \dot{Ex}_{us}}{\sum \dot{Ex}_{in}} = 1 - \frac{\dot{Ex}_{D\&L}}{\sum \dot{Ex}_{in}} \quad (2.6)$$

However, regarding LNG physical exergy utilization systems, there is a lack of agreement among authors to use a standard definition of exergetic efficiency. Figure 2.3 shows a conceptual exergy flow diagram, and Table 2.1 depicts definitions of that efficiency frequently utilized in the literature dealing with systems that exploit the LNG physical exergy.

The definition considered as the most consistent to evaluate the performance of an LNG physical exergy utilization system and, therefore, the utilized in this doctoral thesis is the (V) given by Eq. (2.11). The reasons are the following:

- The chemical exergy is fully preserved in the systems developed in this thesis (no combustion of the gas regasified). Therefore, the chemical exergy should be out of the definition of exergetic efficiency to assess only of the physical exergy utilization.
- The remaining physical exergy content of the regasified gas ($\dot{Ex}_{NG,ph}$) is neither a loss nor a useful output of the physical exergy utilization system because is fixed by the pipeline operating requirements.
- This definition allows to set the zero-efficiency reference for the typical LNG regasification process (i.e., without physical exergy recovery). This allow setting a common reference to compare the performance of different systems and configurations.

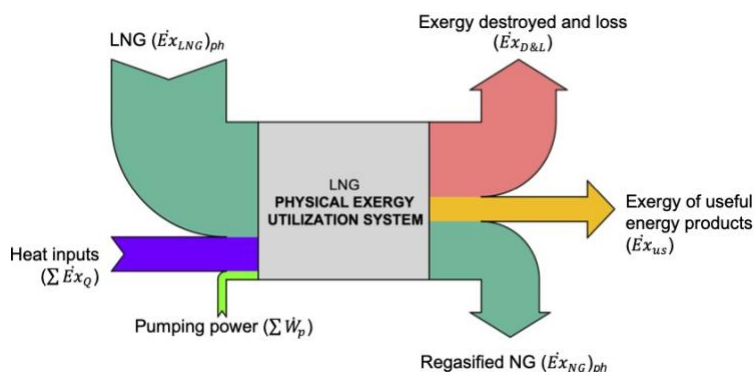


Figure 2.3. Conceptual exergy flow diagram for an LNG physical exergy utilization system.

Table 2.1. Definitions commonly utilized in the literature focused on LNG physical exergy utilization. Assuming fully preservation of the LNG chemical exergy (no combustion).

Type	Mathematical expression	Remark
(I)	$\eta_{ex} = 1 - \frac{\dot{E}x_{D\&L}}{(\dot{E}x_{LNG})_{ch+ph} + \sum \dot{E}x_Q} \quad (2.7)$	In non-combustion systems, this definition leads into very high efficiency since the chemical exergy of the regasified gas is fully preserved.
(II)	$\eta_{ex} = \frac{\sum \dot{E}x_{us} - \sum \dot{W}_p + (\dot{E}x_{NG})_{ph}}{(\dot{E}x_{LNG})_{ph} + \sum \dot{E}x_Q} \quad (2.8)$	The physical exergy of the regasified gas is considered a useful energy product of the system.
(IV)	$\eta_{ex} = \frac{\sum \dot{E}x_{us} - \sum \dot{W}_p}{(\dot{E}x_{LNG} - \dot{E}x_{NG})_{ph} + \sum \dot{E}x_Q} \quad (2.9)$	May cause an undefined mathematical expression (division by 0) in the case of the conventional regassification without exergy recovery; or generate a negative efficiency in a scenario without LNG exergy recovery because in such case there is no useful exergy output, but there can be an electricity consumption by seawater pumping if ORVs are used.
(III)	$\eta_{ex} = \frac{\sum \dot{E}x_{us} + (\dot{E}x_{NG})_{ph}}{(\dot{E}x_{LNG})_{ph} + \sum \dot{E}x_Q + \sum \dot{W}_p} \quad (2.10)$	Although this definition avoids mathematical inconsistencies, the exergetic efficiency of the conventional regasification without physical exergy recovery may be higher than 0 since the physical exergy of the regasified gas is considered a useful energy product.
(V)	$\eta_{ex} = \frac{\dot{E}x_{us}}{(\dot{E}x_{LNG} - \dot{E}x_{NG})_{ph} + \sum \dot{E}x_Q + \sum \dot{W}_p} \quad (2.11)$	This definition produces a zero-efficiency reference case for an LNG regasification plant without exergy recovery. Notice that this definition does not consider the physical exergy of a regasified gas stream as a useful output.

2.3. Applications and technologies

Currently, there is a growing interest among researchers and engineers in the topic of physical exergy recovery from LNG regasification. Figure 2.4 shows the number of publications since 1974. As can be seen, from 2009 – approximately – the number of publications registered in scientific databases has increased exponentially. In other words, there is a clear ongoing effort to harness the exergetic potential of LNG for multiple applications fields and to develop suitable technologies for this purpose. So far, the literature on this topic is focused on *fossil* LNG, although most of the systems and configurations proposed would be fully compatible with the regasification of bio-LNG as well.

From the physical exergy utilization point of view, the thermal and mechanical components are exploited for different applications. The mechanical exergy due to the excess pressure of LNG can be exploited only for shaft work production. On the other hand, the thermal exergy component can be exploited for practically any refrigeration demanding activity. Figure 2.5 shows multiple applications at different temperature levels that can use the low-temperature thermal energy recovered from LNG-regasification.

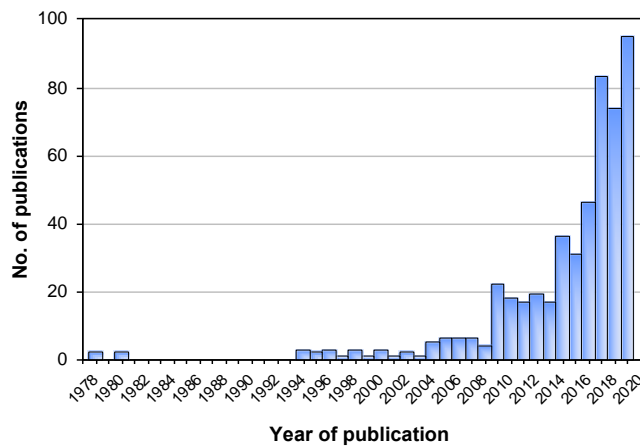


Figure 2.4. Number of publications per year related to cold/exergy recovery from LNG-regasification. Source of data: Scopus [89]. Figure adapted from Atienza-Márquez et al. [55].

On the other hand, [Table 2.2](#) depicts a summary of the different applications and technologies that can take advantage of the LNG physical exergy. Some of the most studied in the literature are the following [90,91]:

- Electric power production.
- Cryogenic air separation.
- Boil-off gas (BOG) re-liquefaction.
- Carbon dioxide capture and liquefaction.
- Refrigeration (e.g., agro-food industry, buildings, and so on).
- Hydrogen production.

An important fact that has to be considered carefully is the hourly fluctuation of the LNG send-out rate. The gas demand is fixed by the demand from consumers; therefore, the LNG regasification pattern is fluctuating so that the physical exergy content available varies. As illustrated in [Figure 2.6](#) there are applications (e.g., air-separation or CO₂ liquefaction) that could require a constant LNG flow rate (i.e., corresponding to the baseload regasification rate), whilst others such as cryogenic power cycles or BOG re-liquefaction are more flexible and can utilize un-constant portions of LNG flow [92]. Nonetheless, there are peaks of demand whose corresponding physical exergy hardly could be utilized.

The following is a literature survey on the most studied applications among the listed in [Table 2.2](#) and is an extension of the presented in Atienza-Márquez et al. [44,55]. This

review is focused mainly on research works tackling single-application configurations, whilst cascaded and polygeneration systems that combine different applications are reviewed in the next chapter of the thesis.

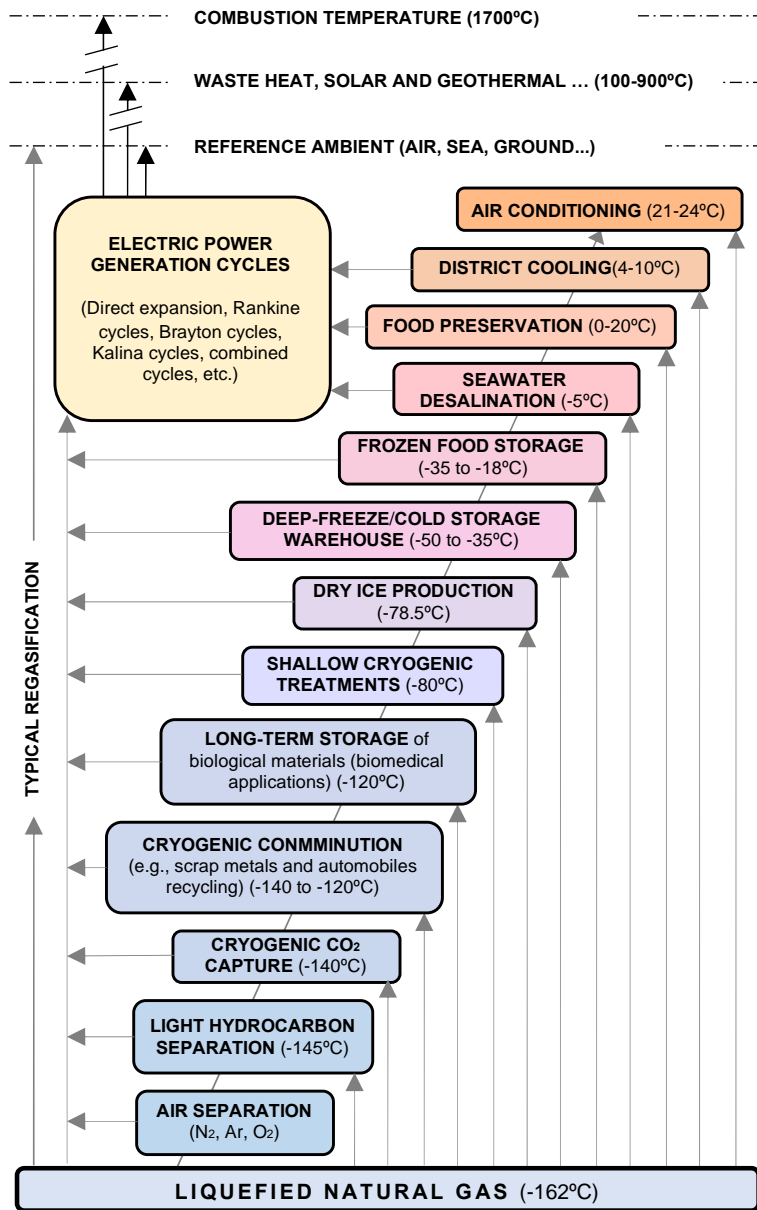


Figure 2.5. Applications of the low-temperature thermal energy of LNG at different temperature levels [44].

Table 2.2. Summary of applications and technologies for exploiting LNG physical exergy [93].

Application	Description and technologies
- Power production	<ul style="list-style-type: none"> LNG low-temperature exergy can be used as heat sink at a wide range of temperatures (-160 to -20°C [94]) in: cryogenic <i>Rankine Cycles</i> (RCs) [95], <i>Kalina cycles</i>, <i>supercritical CO₂</i> (S-CO₂) cycles [96], <i>transcritical CO₂</i> (T-CO₂) and <i>Stirling engines</i> [97]. Also, it can be used to pre-cool the air at the inlet of compressors or inter-cooling in <i>Brayton</i> (gas turbine – GT) cycles [83]. As emerging technologies, <i>thermoacoustic Stirling</i> [98,99] and <i>thermoelectric</i> generators [100] could be used. Beyond LNG's low-temperature, the high LNG regasification pressure in large-scale plants can be converted into electric power using <i>direct expansion units</i> (DEs) [101] (i.e., turboexpanders) instead of pressure reducing valves at regulation stations utilized to meet the pressure requirements of natural gas distribution pipelines. <p>Configurations that combine some of these technologies are widespread in the literature: for instance, RC + DE [102,103]; RC + GT + DE unit [104]; RC + Kalina cycle [105], and so on. <i>Solid oxy fuel cell</i> (SOFC) technology can be combined with some of the power production systems described above [106] and with <i>steam-injected gas turbines</i> (STIG) technology as well [107].</p>
- Air liquefaction	<ul style="list-style-type: none"> LNG low-temperature exergy can be used to reduce energy consumption of compressors in air liquefaction process, for example, in air separation units – ASUs [108–110]. Air liquefaction process requires very low temperatures (< -195°C). Thus, LNG low temperature is exploited with lower exergy destruction rates than in other applications.
- Boil-off gas re-liquefaction	<ul style="list-style-type: none"> LNG low-temperature exergy can be used to re-liquefy the boil-off gas (BOG) generated in LNG tanks [111], which is approximately 0.15% of the tank volume per day [48]. This application reduced the consumption of BOG compressors.
- Cold energy storage	<ul style="list-style-type: none"> Cryogenic energy storage (CES) systems [112] such as Liquid Air Energy Storages (LAES) [113] or Phase Change Materials (PCMs) [90] allow to store LNG cold when energy demand is low. This stored energy could be used later to produce power and cover peak shavings when energy demand increases.
- Seawater desalination	<ul style="list-style-type: none"> The low-temperature exergy of LNG can be utilized to reduce the energy consumption of freeze desalination process utilized to remove minerals from seawater producing fresh water [114,115]. Moreover, LNG could be used as source of cold in clathrate hydrate-based desalination [90].
- Cryogenic CO ₂ capture	<ul style="list-style-type: none"> LNG low-temperature can be utilized to reduce the energy consumption of cryogenic CO₂ capturing systems used to capture the CO₂ in the flue gas from combustion process by liquefying it [116]; The condensed CO₂ can be further cooled to produce dry ice.
- Refrigeration	<ul style="list-style-type: none"> Very low temperature of LNG can be used for refrigeration applications. For example, refrigeration in the agro-food industry sector (0 to -50°C) (deep-freeze/refrigerated warehouses [117], supermarkets [118–120], and so on), for refrigeration in data centres [90], or for district cooling applications [121].
- Hydrogen production	<ul style="list-style-type: none"> The electricity produced in any of the power cycles mentioned above can be utilized to drive proton exchange membrane (PEM) electrolyzers to produce hydrogen [122,123].
- Others	<ul style="list-style-type: none"> Low-temperature of LNG can be harnessed for many others applications: Cryogenic crushing/comminution/grinding (e.g., waste rubber, tires) [124,125], heavy and light hydrocarbon separation [126–128], freezing drying or high purity ozone production [129], ice cubes production, gasification (e.g., coal, biomass). It also has applications for leisure activities, for example, artificial snow production.

2.3.1. Electric power production

The use of LNG to produce electric power is the most studied application in the literature. It is also the most common application among the few LNG terminals exploiting the LNG physical exergy. Romero Gómez et al. [130] described in detail different types of power plants configurations to exploit LNG exergy.

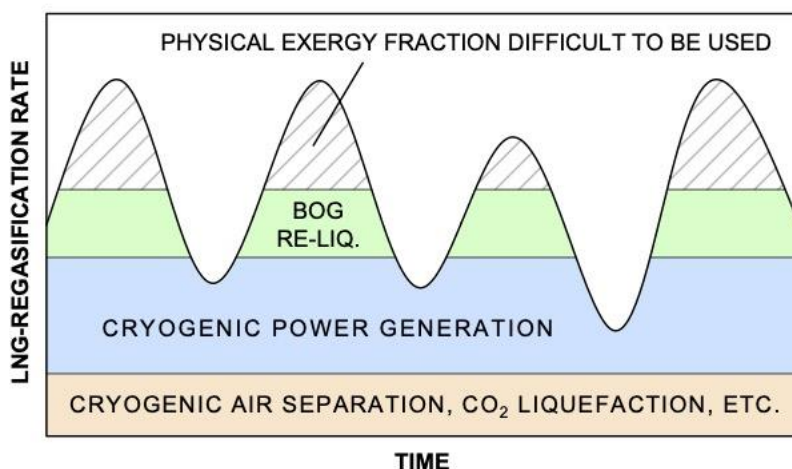


Figure 2.6. LNG demand variation and available fraction for some applications. Redrawn from Kashiwama and Nakagawa [92] and Fujiwara et al. [131].

One of the most direct, simple, cheap and compact option to produce electricity is the installation of direct expansion units (DEs) [101] (i.e., turbomachinery devices like turboexpanders) to exploits the LNG pressure exergy. Particularly in large-scale regasification plants, the operating pressure of a regasification line is sometimes higher than one or more of the send-out pressure levels of the regasification facility. As illustrated in Figure 2.7, turboexpanders convert the excess pressure into shaft work and are an alternative to conventional pressure reducing valves utilized at regulation stations to meet the pressure requirements of natural gas transport and distribution pipelines. Figure 2.8 shows pictures of turboexpanders introduced by representative manufactures.

Furthermore, the LNG low-temperature exergy can be used as a heat sink at a wide range of temperatures (-160 to -20°C [94]) in different power cycles. The following critical review of representative works dealing with the utilization of LNG physical exergy for power generation is an extension of the presented in Atienza-Márquez et al. [44].

Cryogenic **Rankine Cycles** (RCs) are suitable for a wide range of low-temperature heat sources (seawater, low-grade waste heat, solar energy, geothermal energy, etc.). Figure 2.9 (a) depicts the basic structure of a cryogenic RC and Figure 2.10 summarizes a combination of the most common cryogenic RCs. Ferreira et al. [132] compared the energy saving of the regasification plant of Sines (Portugal) when it is upgraded with (1) an LNG direct expansion unit, (2) a simple RC cycle and (3) the combination of both. They determined that the plant produces net power of 2 MW (13.6 kWh/t-LNG) when using LNG as the heat sink in a simple RC using propene as working fluid (operating between 842.03-95.99 kPa) and seawater as the heat source. The increase in the net power by adding an LNG direct expansion unit to the simple RC was negligible. Ahmadi

et al. [133] simulated a transcritical CO_2 basic RC using geothermal water at 140°C as the heat source in the base case. LNG was firstly used as the heat sink to condense the CO_2 . LNG was regasified using water at ambient temperature as the heat source and expanded in a turbine to produce extra power. For the base case (CO_2 entering the turbine at 12 MPa), the net power of the plant was around 540 kW (44 kWh/t-LNG) with an exergetic efficiency of around 12%. Furthermore, regenerative RCs are a modification of the basic RC to reduce heat rejection in the condenser [134].

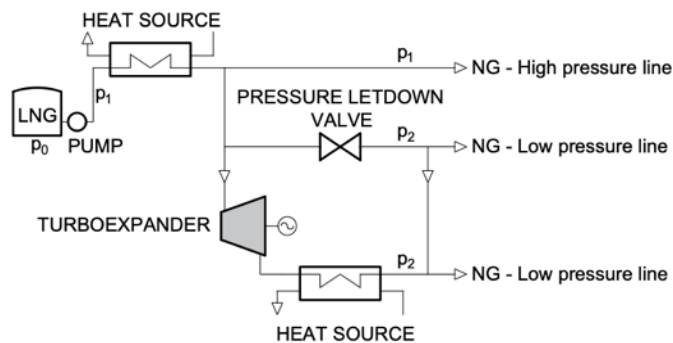


Figure 2.7. Schematic diagram of the natural gas pressure regulation process using pressure reducing valves or an LNG direct expansion cycle to produce electricity by capturing the energy lost in the pressure reduction of natural gas.

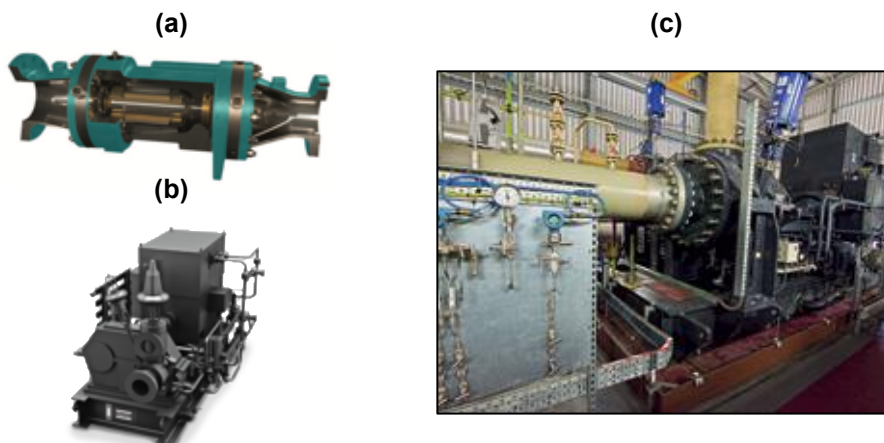


Figure 2.8. (a) Turboexpander with power output up to 125 kW introduced by Calnetix Technologies [135]. (b) Turboexpander power up to Atlas Copco up to 50 MW [136]. (c) Image of an Atlas Copco's turboexpander operating in a natural gas pressure reduction station [136].

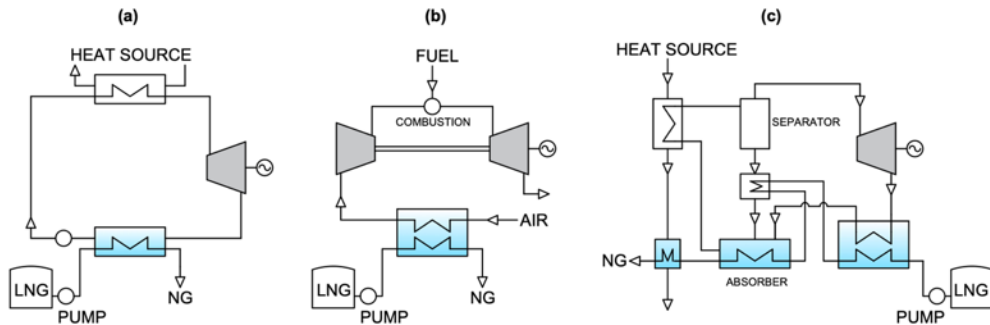


Figure 2.9. Basic schematic diagram of some of the most studied configurations for power production and exploiting LNG low-temperature exergy. (a) Cryogenic Rankine cycle, (b) Turbine air cooling in an open Brayton cycle, and (c) Kalina cycle.

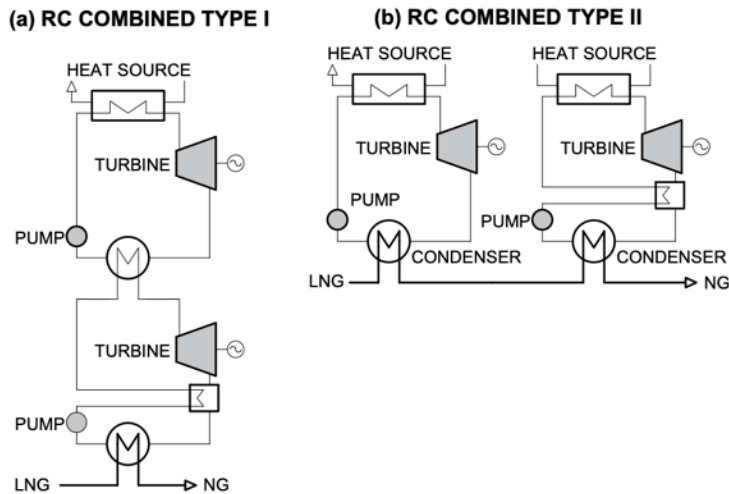


Figure 2.10. Typical power cycle configurations: (a) combined Rankine power cycle type I; (b) combined Rankine power cycle type II [44].

Combined RCs have also been studied. In Figure 2.10, we differentiate between combined Types I and II, depending on how the cycle is arranged. Oliveti et al. [137] studied two cascaded ORCs with LNG direct expansion. This combined cycle has a Type I structure (Figure 2.10 (a)) which is suitable for heat sources at high temperatures. The top cycle is a steam RC (vaporizing at 4 MPa and condensing at 0.013 MPa) driven by waste heat at 400°C from an incineration plant located close to the planned Gioia Tauro LNG regasification plant (Italy). The bottoming RC uses ammonia as working fluid (vaporizing at 0.4 MPa and condensing at 0.04 MPa) and it exploits the LNG cold in the condenser. The proposed plant produced 27.8 MW for an LNG flow rate of 97 kg/s (79.6

kWh/ton-LNG) with a thermal efficiency of 28.8%. Also, the seawater flow rate was reduced by 60% respect to the regasification plant without LNG cold recovery. As an example of combined RCs type II (Figure 2.10 (b)), Ferreiro García et al. [103] presented a regasification and power plant that consists of two cascade transcritical ORCs using argon (higher and lower pressures of 21.7 MPa and 3.91 MPa, respectively) and methane (higher and lower pressures of 19.1 MPa and 4.0 MPa, respectively) as working fluids and a multi-stage direct expansion unit. The heat source of both RCs is seawater. This plant has a net power of 65.3 kWh/t-LNG and a thermal and exergetic efficiencies of 24.1% and 42.7%, respectively.

Brayton cycles (BCs) are suitable for high-temperature heat sources (e.g., combustion heat) [130]. In open BCs, the most straightforward uses of LNG cold are focused on the reduction of the compression work: air cooling at the compressor inlet (as shown in Figure 2.9 (b)) or intercooling for multiple stage compression. Shi et al. [138] presented a power plant where both LNG cold uses were applied. The mirror gas-turbine technology is a solution to cool the exhaust gasses and increase the useful work [139]. On the other hand, LNG exergy can be exploited as a heat sink in closed BCs.

Dispenza et al. [140,141] presented a regasification and power plant that consists of an open BC and a closed BC. LNG was used as heat sink in the closed BC. The exhaust gases leaving the open BC are used as heat source of the closed BC (with Helium as working fluid). The higher and lower temperatures of He in the closed BC were 579°C and -129°C, respectively; and the higher and lower pressures were 2.27 MPa and 0.3 MPa, respectively. The power capacity of the plant 380 kWh/t-LNG and the thermal efficiency of the plant was 69% (considering the heat absorbed by LNG as a useful output of the plant), and the exergetic efficiency was 49% (considering the exergy of regasified NG supplied to the distribution pipeline as a useful exergy output of the plant). Morosuk and Tsatsaronis [83] discussed the convenience of installing a LNG direct expansion unit in a LNG regasification and power plant that combined an open and a closed BC. The closed BC (working with N₂ between 4,275 kPa and 285 kPa) was driven by the combustion gases leaving the open BC (435°C), and it used LNG as heat sink. The regasification capacity of the plant increased without an LNG direct expansion unit while the electric power output remains near the same. The power capacity of the plant was 144 MW (531 kWh/t-LNG) with a thermal efficiency of 78.1% (considering the heat absorbed by LNG as a useful output of the plant) and an exergetic efficiency of 52.1% (considering the difference in mechanical exergy between NG regasified and the LNG storage as a useful exergy output of the system).

The **combination of RCs with BCs** is a further option. Romero Gómez et al. [142] presented a combined power plant that consists of a closed BC and an RC in series. LNG exergy is exploited as cooling media in the compressor suction of the closed BC. The heat source of the closed BC is combustion heat at 1,300°C. Once the combustion gases have feed the closed BC, they are used as heat source in the RC. The most advantageous working fluids were He and CO₂ for the BC and the RC, respectively. The electric output

of the plant was plant 684.7 kWh/t-LNG with a thermal efficiency of 67.6%. Lu and Wang [143] studied a regasification and power plant that combined an open BC, ammonia-water RC (optimal higher and lower pressures are 2.29 MPa and 0.04 MPa, respectively) and LNG direct expansion unit. LNG is also used as heat sink in the condenser of the RC. The maximum temperature in the plant was 993.2°C. The optimal net power of this plant was 48.3 MW (around 139 kWh/t-LNG).

Other thermal power cycles have been explored in the literature. For instance, as shown in Figure 2.9 (c), **Kalina cycles (KCs)** have a structure similar to ORCs but with a solution circuit but higher exergetic efficiencies [91]. KCs use a mixture with different boiling points as working fluid, such as ammonia-water mixture and binary mixtures of tetrafluoromethane and propane [144]. As an example of systems operating with mixtures as working fluids, Miyazaki et al. [145] modelled a plant that consists of an ammonia-water power cycle driven by heat from an incinerator and an LNG power cycle. The plant has a power production of 105 kWh/t-LNG with a thermal efficiency of 29% and an exergetic efficiency of 30% (considering the exergy of the regasified NG supplied to the distribution pipeline as an output).

Regarding emerging technologies for exploiting LNG physical exergy, **thermoacoustic engines** are one of the most promising. Wang et al. [99] proposed a thermoacoustic Stirling generator to produce electricity from LNG physical exergy. The general working principle of a thermoacoustic engine is as follows. When a gas-filled inside a tube is submitted to a temperature gradient, the gas begins to oscillate spontaneously, and an acoustic wave is excited [146]. The type of acoustic wave generated depends on the structure of the tube: standing acoustic wave in the case of straight pipe and travelling acoustic wave in the case of a looped tube. At present, researchers are more interested in devices with a looped tube because of the more efficient energy conversion of travelling acoustic waves. Furthermore, because a temperature gradient is required, these kinds of systems are a promising technology for exploiting the low-temperature of LNG [147]. However, this technology has still pending technical issues, for example, the need to handle too many design parameters, thermal expansion and fatigue stresses or the inefficient acoustic-to-electricity conversion.

Figure 2.11 shows a schematic diagram of a thermoacoustic engine with a looped tube structure. The main components of the engine are indicated in this figure: Cold heat exchanger, hot heat exchanger, regenerator (or stack), thermal buffer tube, feedback tube and the device for the energy conversion from acoustic power to electric power. The regenerator consists of a structure located inside the tube with many narrow channels that interact thermally with the excited acoustic wave [148].

The literature survey presented above confirms that the definitions of both the thermal and exergetic efficiencies are heterogeneous. The thermal efficiency is mainly defined as the ratio of the power produced by the system to the heat input from the heat sources [103,134,137,142,143,145]. However, some authors also consider the heat absorbed by

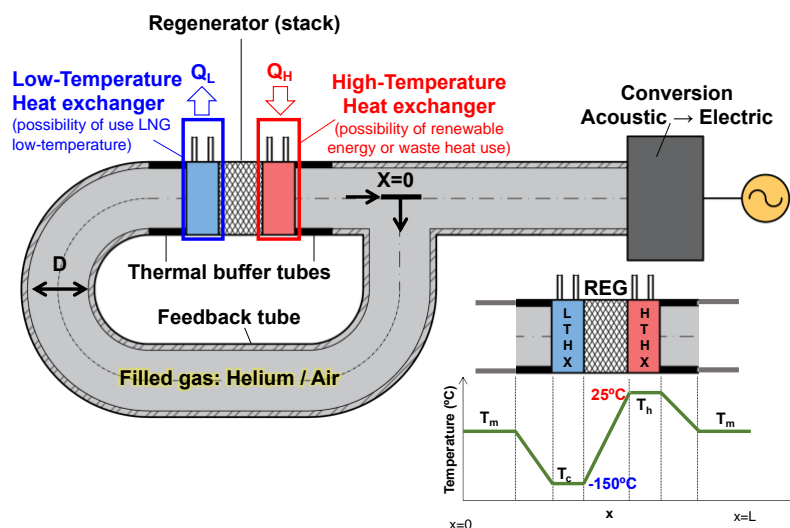


Figure 2.11. Schematic diagram of a thermoacoustic Stirling engine with LNG low-temperature exergy utilization.

the LNG during the regasification process as a useful output of the power plant [83,141]. With respect to the exergetic efficiency, as stated before, there are authors that only consider the electricity output of the system as a useful exergy output of the power plant [103,133,134], while others also consider the exergy of the regasified NG supplied to the distribution pipeline [141,145] or the difference in mechanical exergy between the NG regasified and the LNG storage in tanks [83].

2.3.2. Air-separation

Commercial air separation processes include three different processes: cryogenic air separation, pressure swing adsorption and membrane air separation [144]. The cryogenic air separation technique is based on different condensation temperature of the air components and is an appropriate technology when aiming to obtain high purity oxygen, argon and nitrogen from the air in distillation columns. This separation process is carried out in air separation units (ASUs) where very low temperatures are required (-173°C to -196°C) and consuming a significant amount of energy. As illustrated in Figure 2.12, LNG can be integrated in the air separation process by replacing an external refrigeration cycle to reduce the energy consumption of the refrigeration system [149]. As explained in greater details later in this Chapter, this integration has been implemented in some receiving terminals since the early 70's [150]. As the operating temperatures of cryogenic ASUs are lower than LNG temperature (-162°C), LNG cold can be recovered efficiently [109].

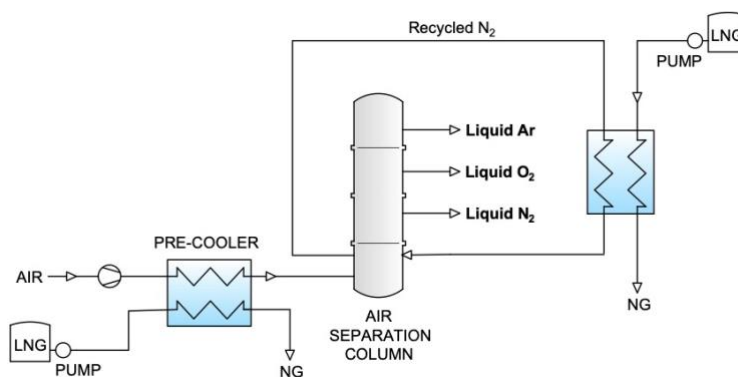


Figure 2.12. Simplified schematic diagram of the LNG low-temperature exergy utilization in a cryogenic air-separation unit. Adapted from [151].

Some representative studies published in the open literature are the following. Ebrahimi and Ziabasharhagh [152] studied a two columns cryogenic ASU where LNG cold was integrated and recovered. The LNG integration in the ASU contributed to an energy saving of 8.04%. The oxygen production rate of the plant was 68.5 t/h (~ 0.24 kg-O₂/kg-LNG). Mehrpooya et al. [153] proposed and analysed a cryogenic air separation unit to produce liquid nitrogen and oxygen and with the utilization of the LNG low-temperature thermal energy. The systems proposed reported an energy consumption 38.5% lower than a conventional cryogenic air separation unit.

Xu et al. [108] proposed a novel cryogenic air separation process by harnessing LNG low-temperature with an air handling capacity of 20 t/h. The plant operates at lower pressures, and the power consumption was reduced by 12.6% concerning the traditional process. The exergetic efficiency obtained by the novel system and the conventional were 66.4% and 38.2%, respectively. Also, Jieyu et al. [154] simulated a novel single-column cryogenic air separation process able to handle 20 t-air/h and exploiting LNG low-temperature exergy. The specific energy consumption of the proposed plant per unit mass of liquid products 218 kWh/t, which was 39% lower than the calculated for a traditional air separation unit. The exergetic efficiency obtained was 57.5%. On the other hand, Kim et al. [150] compared two different LNG cold utilization strategies in a single-column air separation unit; one based on the air pre-cooling and the other based on the integration with a liquid nitrogen production cycle. The authors concluded that the first option had a lower specific consumption (281 versus 310 kWh/t) and the higher exergetic efficiency.

2.3.3. Boil-off gas management

As explained in Chapter 1, inside tanks of receiving terminals, some LNG vaporization occurs producing some boil-off-gas (BOG) because of the heat transfer with the

environment. The management of that BOG inevitably produced is a technical problem, but handling it correctly is crucial to keep the methane emissions under desirable values. The daily maximum allowed generation of BOG is equivalent to 0.05% of the stored liquid and has to be removed to keep the storage pressure under acceptable limits [54].

Figure 2.13 illustrates different strategies for tackling with the BOG. Burning the BOG in a torch is the most straightforward handling method since that always is installed in an LNG terminal due to security reasons. However, that method represents fuel wasting and a direct economic loss. Another strategy to handle the BOG generated is the compression up to 30-90 bar(g) for later use as city gas or fuel for power generation [155]. Alternatively, the utilization of the LNG low-temperature exergy allows re-liquefy the BOG generated and reduce the energy consumption [111]. In this case, the BOG is compressed below ~ 10 bar(g), so a smaller compressor is required, and the compression power is reduced. Then, the BOG and the LNG stream pressurized by an in-tank low-pressure pump undergo contact heat exchange in the recondenser. The subsequent heat and mass transfer result in the absorption and condensation of BOG [111]. Afterwards, the liquid stream leaving the BOG condenser is pumped to the LNG vaporizers.

Regarding the management of the BOG generated in LNG carriers, a fraction of the BOG generated is usually consumed as fuel in the engines, whilst the excess BOG is just burned without any useful application. Arias Fernández et al. [156] proposed the production of hydrogen by the steam reforming of the excess BOG generated, but the LNG physical exergy remained unused. As an alternative, Yin and Ju [157] performed a theoretical study on the feasibility of using the subcooled LNG to re-liquefy the BOG, as an energy-saving alternative to the traditional technique which requires the utilization of cryogenic compressors.

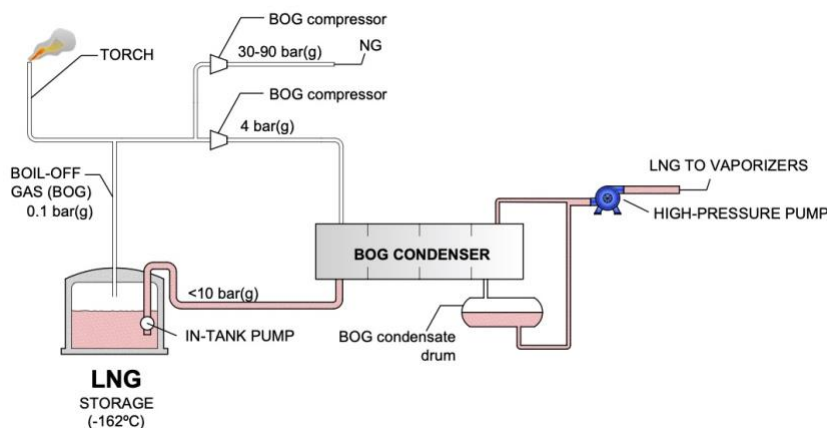


Figure 2.13. Different BOG management strategies. Redrawn from [155].

2.3.4. Liquefaction of carbon dioxide

The cryogenic capture of CO₂ is a method to liquefy and separate the CO₂ from flue gas or any other gaseous stream containing CO₂ as a subproduct of an industrial process (e.g., in hydrogen manufacturing plant, petrochemical facilities, fertilizer plants, beverage factories, and so on). A detailed review of the different strategies and technologies utilized in cryogenic CO₂ capturing processes is presented in Song et al. [158]. The method consists of cooling the stream to be treated (i.e., the raw CO₂ material) with the objective to liquefy the CO₂, so that is separated from the rest of the components. The liquefied CO₂ is utilized in industry, food and beverage, flower cultivation, and so on [144]. Figure 2.14 shows the conceptual schematic diagram of the cryogenic CO₂ capture process with utilization of the LNG low-temperature exergy. The conventional cryogenic capturing process is quite an energy demanding since the compression of the raw CO₂ materials, and an external refrigeration cycle is required. Therefore, the utilization of the LNG low-temperature exergy represents an energy-saving opportunity both to reduce the compression and the liquefaction energy consumptions. Once liquefied it is stored in tanks and distributed to final consumers or to dry ice manufacturing facilities.

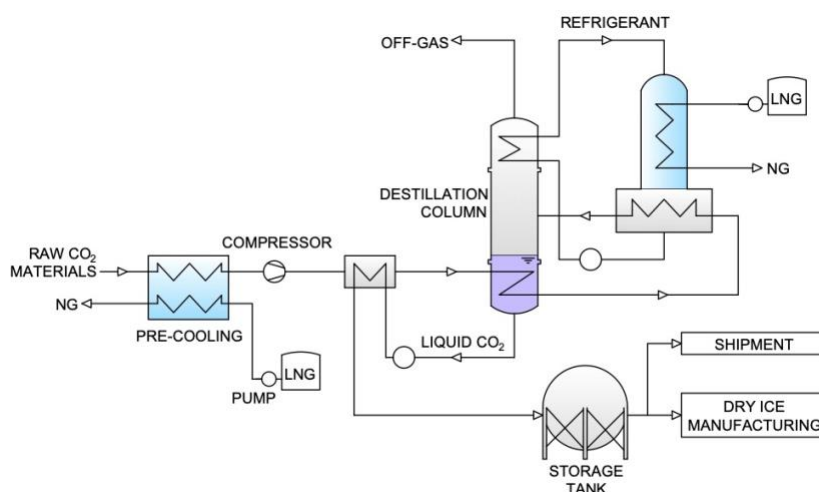


Figure 2.14. Simplified schematic of a diagram of the LNG low-temperature exergy utilization in a liquid CO₂ manufacturing process. Figure made partially based on the information available at Osaka Gas Liquid Co., Ltd. website [159] and from Yamamoto and Fujiwara [160].

2.3.5. Refrigeration production

Refrigeration is one of the most direct and attractive applications to exploit the LNG low-temperature exergy throughout its regasification process. As illustrated in Figure 2.15, this application consists of the installation of a heat transfer loop to distribute the

low-temperature thermal energy recovered from the LNG-regasification to buildings with refrigeration demand. As mentioned in the previous chapter, this application represents an excellent opportunity to shape a more sustainable refrigeration industry. But so far, its degree of deployment in regasification plants of cryogenic fluids as well as commercial solutions is scarce.

Occasionally there are buildings and/or industries located at the surroundings of regasification facilities with refrigeration demand at different temperatures depending on their activity sector. Since the “free” cold has to be transported from the regasification site to the cold consumer, the design of a suitable cold distribution system is required. Therefore, the selection of the most convenient heat transfer fluids and the technology of heat exchangers should be carefully addressed. However, this is not a trivial issue from the technical point of view because the multiple particularities of each specific case for exploiting the cold must be considered. For example, the temperature at which refrigeration is required, the distance to the regasification site, the hourly fluctuation of the refrigeration demand, the availability and shortages of the “free” cold (constrained by the LNG regasification pattern), and so forth. Besides, the utilization for refrigeration applications raises essential questions such as the following: *Are conventional mechanical refrigeration machines still required? Is the LNG low-temperature thermal energy enough to handle the whole thermal load? Are conventional refrigeration systems compatible with LNG low-temperature exergy utilization systems?* The conclusions presented at the end of this doctoral thesis intend to solve these questions.

In the specific literature, only a few authors have examined this application in depth. The few works dealing with the use of the LNG low-temperature exergy for refrigeration applications are focused in the **agro-food industry** or **commercial sector**. In many cases it is common to find an industry cluster at the vicinity of a regasification terminal with refrigeration demand. A clear example is the Barcelona LNG Terminal (Spain) which is located just beside one of the most important agro-food markets worldwide with a huge refrigeration demand.

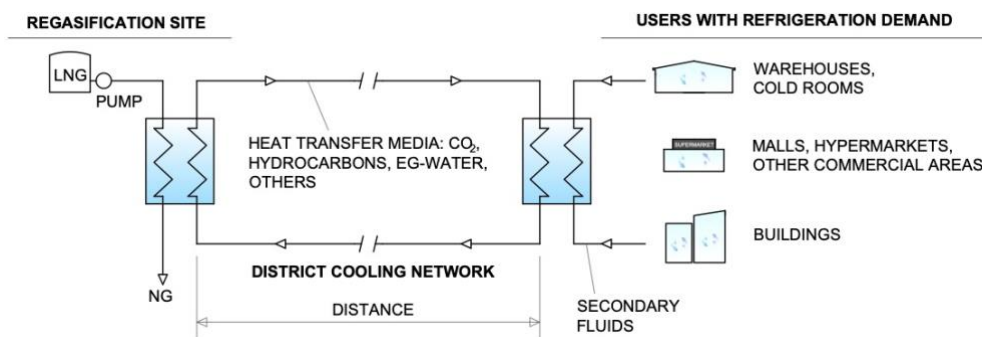


Figure 2.15. Conceptual diagram of the low-temperature exergy recovery and utilization--- Simplified schematic. Through a heat transfer loop.

Representative research works, La Rocca [119,120] analysed the cold recovering from LNG-regasification for deep-freezing in agro-food factories and refrigeration in supermarkets and hypermarkets using CO₂ as secondary fluid. For this purpose, the author uses a modular LNG regasification unit proposed by Dispenza et al. [161] with an LNG regasification capacity of 62.7 kg/h. The total cooling demand (at -43°C) from the agro-food cluster analysed was 9 MW, and the global energy and exergy efficiencies for the agro-food cluster were 95% and 79%, respectively. In the case of the analysed hypermarket, the cooling demand was 6 MW (0.5 MW at -35°C and 5.5 MW at -15°C) with a global energy and exergy efficiencies of 87% and 76%, respectively. Also, Messina and Panno [118] aimed to exploit the LNG cold in an agro-food industry near to the regasification site in Sicily (Italy) using CO₂ as heat transport fluid.

Li et al. [117] analysed the in-situ utilization of the LNG low-temperature exergy in a refrigerated warehouse at different temperature levels for different cold rooms and using a cascaded configuration. The authors studied the most feasible heat transfer fluids considering features such as specific volume, evaporation and condensing pressures, cost, environmental impact and availability. Among the different candidates, they concluded that R-23 was the most suitable (mainly due to lower operating pressure), despite its high environmental impact than, for example, CO₂. Others research works have considered the production of refrigeration together with other simultaneous applications but without a detailed study.

Beyond application in the agro-food industry, a further option is the utilization of the LNG cold for air-conditioning applications in new or retrofitted **residential/office buildings** or **data centres** [90]. By one hand, air-conditioning represents a significant energy demand in buildings. Although residential buildings are rarely located just beside an LNG receiving terminal, it is common to find office buildings (e.g., belonging to the gas company) with air-conditioning needs at the surroundings of the regasification site. An LNG-cooled heat transfer fluid could be distributed through a District Cooling (DC) network to different office buildings to cover their air-conditioning needs. DC networks are also required if the cooled heat transfer fluid has to an urban area located relatively far from the regasification site. For example, Ayoub and Eveloy [162] studied the production of chilled water for municipal district air-conditioning applications by exploiting the LNG low-temperature exergy through heat exchangers in combination with conventional chillers.

On the other hand, more and more data centres are built worldwide to store and process data. The hardware utilized in such buildings (so-called “*data centres*”) generates a huge amount of heat that is removed by highly power-consuming refrigeration systems. Therefore, the construction of data centres at the vicinity of regasification facilities (no more than 1-2 km far away) may enable the utilization of the LNG low-temperature exergy to reduce the energy consumption significantly due to air-conditioning and mitigate the environmental footprint of these type of buildings.

But the literature dealing with this particular application is scarce. For example, Ayachi et al. [163] proposed different configurations that exploit the LNG low-temperature exergy for handling the refrigeration demand in a data centre. In all the configurations proposed by the authors, the LNG low-temperature exergy was firstly utilized to pre-cool an air stream that is later liquefied. One of the solutions proposed by the authors was to use the liquid air to feed a cryo-cogenerator that produces and supplies electricity and refrigeration simultaneously to a data centre. The other solution proposed consists of providing a portion of the pre-cooled air directly to the data centre to handle only its refrigeration load. Also focused on providing “free” refrigeration to data centres but interested into the regasification of other cryogenic fluids, Ayachi et al. [164] proposed the utilization of the low-temperature exergy of liquid N₂. Regarding business initiatives, *TeraCool LLC* [165] developed the idea illustrated in Figure 2.16 which consists of supplying refrigeration and electricity to large data centres (i.e., 10-100 MW of continuous electricity demand) by exploiting the low-temperature of LNG. This novel idea was recognized with 2013 Green Enterprise IT Awards.

Lastly, innovative solutions have been proposed in the literature for LNG-fuelled to harness the low-temperature thermal energy released throughout the fuel regasification for refrigeration applications. For example, refrigeration in mobile applications [166]. Tan et al. [167] investigated experimentally the prototype of a self-refrigerating system (at -20°C) for recovering the low-temperature thermal energy of an LNG-fuelled vehicle, as illustrated in Figure 2.17. The authors concluded that the substitution of the original

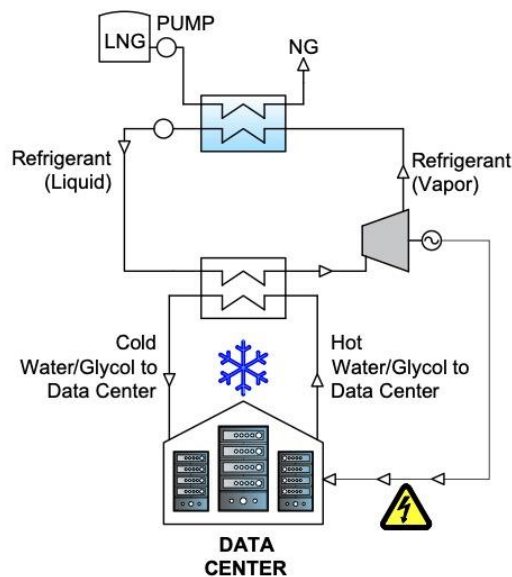


Figure 2.16. System configuration proposed by TeraCool LLC to exploit the LNG low-temperature exergy for the combined production and supply of electric power and refrigeration to a data centre. Figure redrawn from [165].

mechanical refrigeration unit is possible under certain conditions. Nevertheless, they highlighted the need of examining the influence of some parameters (e.g., environmental conditions, airflow patterns, storage pressure of LNG, and so forth) that affect the performance of the proposed system. Also focused on LNG-fuelled vehicles, Yan et al. [168] developed the modelling of a heat exchanger designed for recovering the low-temperature thermal energy and use for air-conditioning in the vehicle.

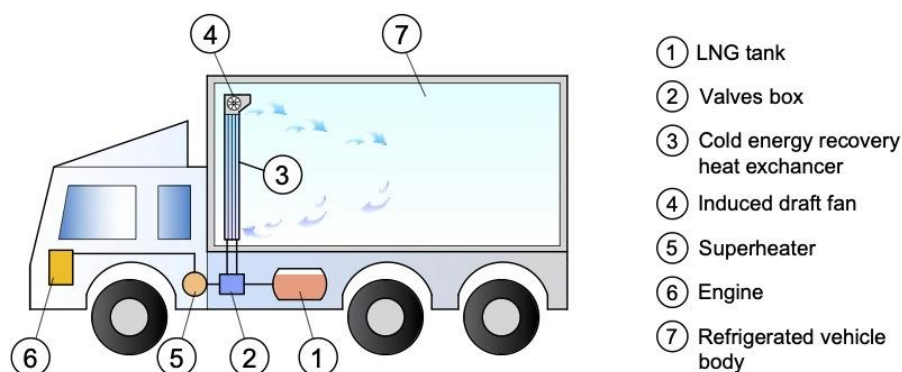


Figure 2.17. Schematic diagram of the utilization of the LNG low-temperature exergy in a self-refrigerated vehicle. Redrawn from [167].

As shown in Figure 2.5, air-conditioning is one of the highest temperature applications for exploiting the LNG low-temperature exergy. As a consequence, the exergetic value of producing air-conditioning (at around 3–6°C) as “*energy product*” is relatively low in comparison with the initial exergetic content of LNG. In certain cases, since the efficiencies of current vapor-compression refrigeration systems for air-conditioning applications are very competitive, the economic saving derived from the utilization of the LNG low-temperature exergy could be not enough to offset a high capital investment. Therefore, the economic feasibility of an investment for this application should be carefully evaluated in each specific case-study. As occurs with cryogenic power units, the economic feasibility depends mostly on the electricity prices, rather than on the positive environmental effect. But this scenario may change in the next years, and the imposition of carbon taxes would reappraise the environmental benefit of exploiting the LNG physical exergy even for applications with relatively high temperatures such as air-conditioning.

2.3.6. Seawater desalination

Seawater desalination is a technical solution to tackle the freshwater scarcity issue but requires considerable amounts of energy to separate salts from water. The commercial desalination plants are based on the multi-stage flash (MSF) distillation and reverse

osmosis (RO) processes. Both are reliable desalination methods, but also energy-intensive [169]. As alternative methods, processes based on freezing have been proposed. Their operation at low temperatures arises the interest in exploiting the LNG low-temperature exergy.

By one hand, **freeze desalination** (FD) consists basically of lowering the temperature of seawater to its crystallization point to produce ice crystals that, by nature, are mostly composed of pure water. As illustrated in Figure 2.18 (a), the utilization of the LNG low-temperature exergy is a solution to decrease the input of electrical energy required by the refrigeration systems used in FD. Although FD is an immature desalination technology, some authors are simulating and developing experimental prototypes to evaluate the performance for future implementation in industry. Cao et al. [170] simulated a flake ice-maker that uses an intermediate refrigerant to transfer the cold from LNG to seawater. The device produces two kg of ice melt water/kg-LNG with energy consumption near null. Lin et al. [171] built a seawater FD prototype that exploits LNG cold and using R410A as intermediate refrigerant between LNG and seawater in a flake-ice maker. The experiments carried out reported two kg-fresh water/kg-LNG and the desalination rate was 50%. Xie et al. [172] developed a direct contact ice generator prototype that allows to exploits LNG cold and to regasify LNG simultaneously using HFE-7100 as an intermediate refrigerant. The ice production efficiency was 0.92-1.15 kg-ice/kg-LNG, and the desalination rate was 83.5-80.1%. Then, Ong et al. [114] evaluated the techno-economic feasibility of that system. The authors concluded that, although the prospects are promising, the economic competitiveness of the system in a specific location depends mainly on both the household water price and the electricity tariff.

Another technology for seawater desalination that can take advantage of the LNG low-temperature is the **clathrate hydrate-based desalination** (HyDesal). This technology is similar to FD and allows operating at a temperature above the normal freezing point of water, so that is less energy-intensive [169]. Figure 2.18 (b) illustrates the conceptual diagram of this desalination method with utilization of the LNG low-temperature exergy. In the available literature, He et al. [173] presented a novel conceptual design for an HyDesal process by utilizing LNG low-temperature exergy. Based on an LNG regasification rate of 1 t/h, the specific energy consumption was 0.60 and 0.84 kWh/m³-pure water without and with hydrate recycling, respectively; whilst the specific energy consumption of the conventional HyDesal system was 65.13 and 65.29 kWh/m³ without and with hydrate recycling, respectively. Also, Chong et al. [174] studied the economic performance of an HyDesal system that produces 260 m³. The utilization of the low-temperature exergy of an LNG flow rate of 200 t/h allows reducing the levelized cost of water from 9.31 to 1.11 USD/m³. The authors confirmed the economic feasibility of the proposed technology for large-scale projects. And He et al. [175] studied an HyDesal system using LNG low-temperature and cyclopentane as hydrate former, reducing the specific energy consumption by 58% when compared with a gas such as propane as a hydrate forming guest.

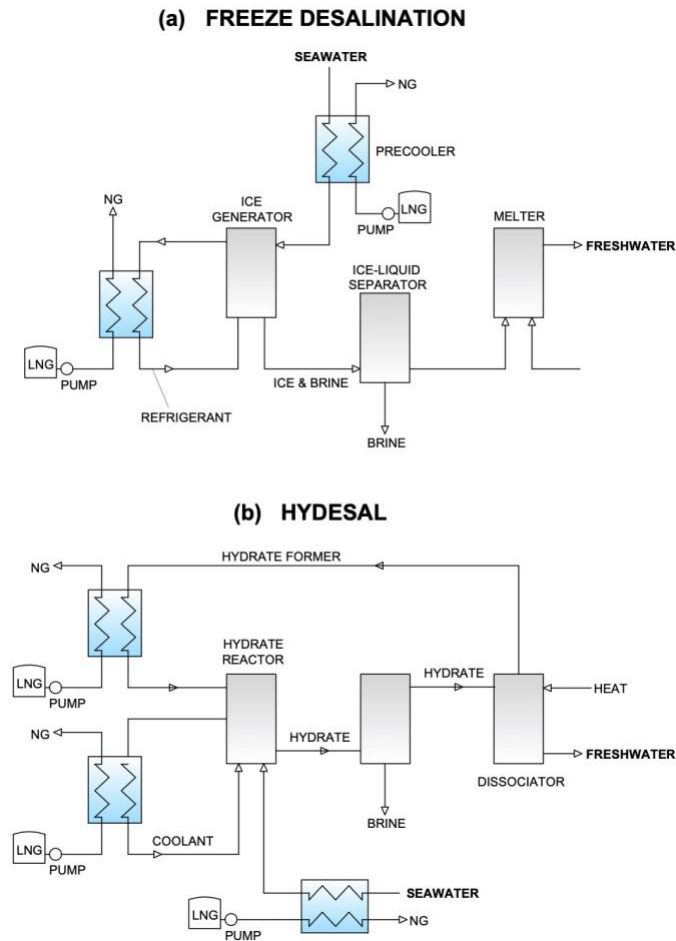


Figure 2.18. Use of the LNG low-temperature exergy for seawater desalination. Simplified schematics for (a) Freeze Desalination (FD) technique, and (b) Clathrate hydrate-based desalination (HyDesal) technique.

2.3.7. Hydrogen production

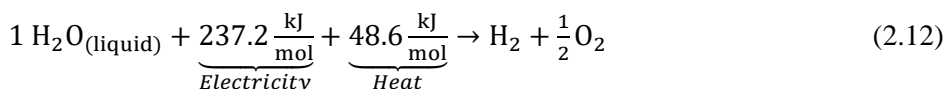
Hydrogen is a versatile energy carrier and will play a key role in a sustainable energy future [176]. Hydrogen is mostly used for the refining of oil and gas and the production of fertilizers, methanol, and other chemicals. But is also a zero-emissions fuel source for a wide range of applications (e.g., in transport, heating, steel production and electricity) or can be used as a feedstock for industrial production. Furthermore, it contributes to an integrated energy system and can be a flexible complement to other primary energy sources (e.g., fossil LNG, bio-LNG and other cryogenic fluids) throughout the energy transition.

Today hydrogen demand continues to rise and is directly supported by more and more policies and projects in all parts of the world. Nevertheless, hydrogen has seen other previous wave of interest in recent history that were not translated into its consolidation as a widespread energy source due to different reasons (e.g., lower prices of other energy sources, uncertainty regarding climate policies, availability of more economically competitive technologies and with simpler infrastructures, and so forth). Moreover, the hydrogen industry has pending challenges: a cost-effective and cleaner production is required, a robust infrastructure needs to be developed, storage complications, and regulatory barriers persists. But today the taking-off of the hydrogen industry could be definitive. The cost of technologies has fallen, and the energy transition is a top issue that cannot wait any longer. Also, not only public organisms but also relevant private-sectors players (e.g., automakers, oil and gas companies, major engineering firms) are committed to developing projects and markets based on hydrogen.

Hydrogen is one of the most abundant elements in the universe but rarely found pure. There is a number of ways to produce hydrogen such as hydrocarbon reforming/gasification, water electrolysis, renewable liquid hydrocarbon reforming, and fermentation of biomass feedstock [177]. Among them, two methods allow exploiting the physical exergy of cryogenic fluids such as LNG to improve the competitiveness of the hydrogen market: steam reforming and water electrolysis.

Nowadays, **steam reforming** is the major industrial process to produce hydrogen for fuel [17]. Natural gas contains methane (CH₄) that can be used to produce hydrogen with thermal processes, such as steam-methane reformation and partial oxidation [178]. Figure 2.19 illustrates a conceptual diagram of a steam reforming process with LNG low-temperature exergy utilization. Very high-temperature steam (i.e., 700 – 1,000°C) reacts with a methane source (e.g., natural gas) under a pressure of 3-25 bar in the presence of a catalyst to produce hydrogen, carbon monoxide and a minor quantity of carbon dioxide. Then, the reformed gas produced is cooled to ~500°C and introduced into a CO shift converter, and the carbon monoxide and the steam reacts using a catalyst to produce carbon dioxide and more hydrogen (so-called *water-gas shift reaction*). The use of LNG latent heat can be utilized to reduce the hydrogen production costs either using the Pressure Swing Adsorption (PSA) method or and LNG washing method [179]. As illustrated in Figure 2.19, LNG low-temperature can be utilized for (1) pre-cooling the raw hydrogen produced before compression, and (2) cooling the exhaust gas (that includes H₂, CO₂, CO and residual CH₄) and recover the CO₂ as a liquid.

On the other hand, **water electrolysis** is the second most common method of hydrogen production [180]. Electrolysis of water is the process of using electricity to split water molecules are into hydrogen and oxygen molecules. The following is the basic reaction with the thermodynamic energy values:



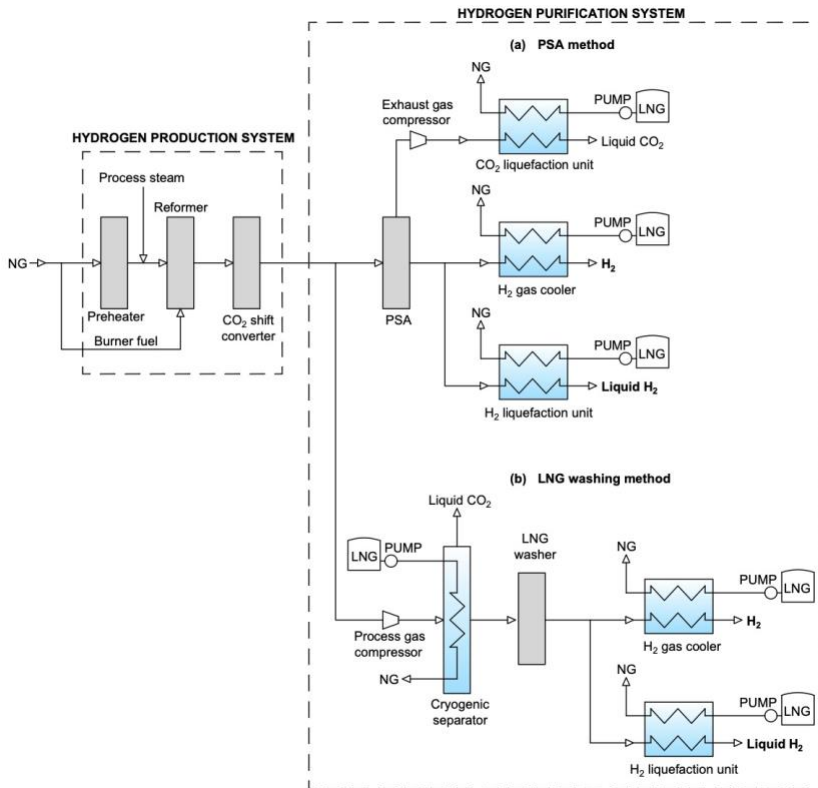


Figure 2.19. Conceptual diagram of the hydrogen production from LNG reforming by exploiting its low-temperature exergy content. Technologies for hydrogen purification: (a) Pressure Swing Adsorption technology (PSA), (b) LNG washing method. Figure developed from the information depicted in Ogawa et al. [179].

The water electrolysis technologies are classified into the following types: alkaline, solid oxide, microbial and PEM [181]. Although alkaline electrolysis is a mature technology and already marketed, the PEM (proton-exchange membrane or polymer electrolyte membrane [182]) technology is considered the most promising. Despite PEM systems are still designed for capacities below 1 MW and have a higher cost than alkaline, important companies have started to develop PEM systems encouraged by the decrease in the manufacturing cost and because of the advantages of PEM over alkaline electrolysis: higher current densities and efficiencies.

Most of the systems studied in the literature tackling hydrogen production by LNG physical exergy utilization are based on the PEM method. The basic idea is to utilize the LNG physical exergy through any of the technologies described in section 2.3.1 to generate the electric power required to drive a PEM electrolyzer to produce hydrogen. Figure 2.20 shows the conceptual diagram of hydrogen production by following this approach. In the open literature tackling the utilization of the LNG physical exergy, there

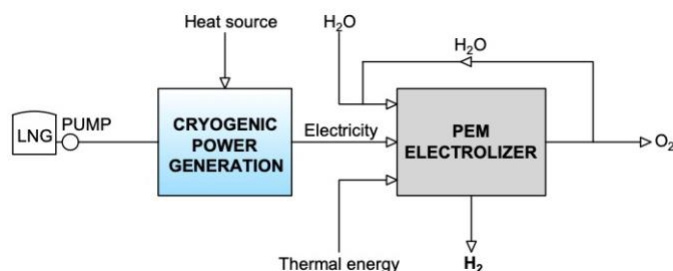


Figure 2.20. Conceptual diagram of the hydrogen production from water electrolysis in a PEM electrolyzer driven by the electric power generated in power cycles that exploits LNG physical exergy.

is more and more research than introduces the production of hydrogen in combination with other applications. For example, Emadi et al. [122] proposed to use LNG as a heat sink in a Stirling cycle which is combined with a Kalina cycle driven by geothermal energy and the electricity generated was utilized to produce hydrogen in a PEM electrolyzer. Also, the research of Taheri et al. [183] or Akrami et al. [184], among others, are representative works focused on this topic.

2.4. Global deployment and implemented projects

Despite the many industrial applications that could take advantage of LNG cryogenic temperature and the increasing interest in this topic, today only 1% of global LNG cryogenic potential is utilized, and only a few countries have terminals with that capability [56]. This means that only a few of the more than one hundred thirty large-scale regasification terminals worldwide bet on the use of LNG physical exergy recovery. Regarding bio-LNG regasification, we are unaware of operating plants utilizing its physical exergy content so far.

Figure 2.21 illustrates some remarkable milestones. The very first attempts to exploit LNG physical exergy started at the early 1970s, particularly in air-separation applications. A sort of cryogenic power “boom” was in the decade of ’80s. Since then, the implementation of new systems has been scarce, and few projects have been launched. But recently the trend is changing. The LNG physical exergy utilization is getting attention again, possibly, because of factors such as the growing interest on LNG as a transition energy source, the introduction of carbon taxes or the need of a more sustainable refrigeration system. Regarding countries, Japan not only concentrates most of the LNG regasification facilities worldwide [185] but also is the country that bets on the utilization of LNG physical exergy [186]. Nonetheless, during the last decade, some projects and initiatives have been developed in other countries like Spain, China, South Korea, among others.

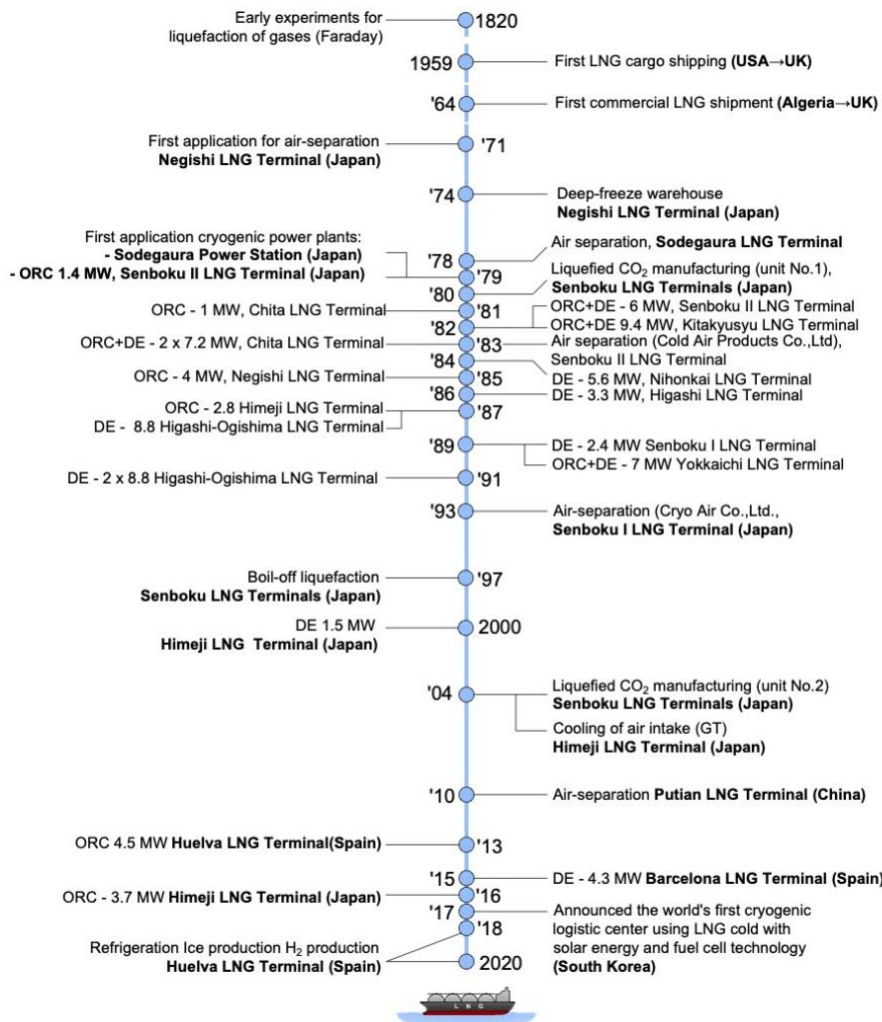


Figure 2.21. Timeline with some relevant events and milestones regarding LNG physical exergy utilization. Source of data: [92,129,160,187]. Figure redrawn and completed [55].

The following is an updated and extended version of the review presented in Atienza-Márquez et al. [55] regarding the global deployment of LNG physical exergy utilization in regasification terminals. Representative systems already built, projects developed and launched initiatives in operating regasification terminals worldwide are described.

2.4.1. Japan: The outstanding leader

In Japan, up to 20-30% of the total LNG physical exergy potential is utilized, mainly through cryogenic power cycles (ORCs and DE units, with installed capacities below 10

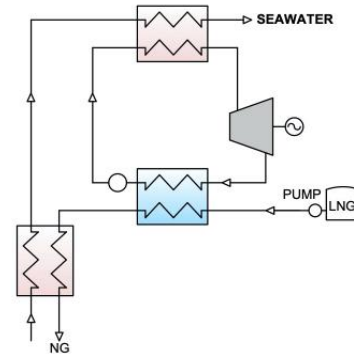
MW) and air-separation units [94]. Today, the total installed cryogenic power capacity is around 40 MW distributed in more than ten facilities [187].

Japan pioneered the development of LNG exergy utilization systems in the 1970s. Particularly, two Japanese companies have developed recognized know-how and experience in this field: *Tokyo Gas Co., Ltd.* and *Osaka Gas Co., Ltd.* In 1971 was built the first air separation system with LNG low-temperature exergy exploitation at Negishi LNG Terminal (Yokohama, Japan) managed by Tokyo Gas Co. Ltd. and the first LNG port of the country [129]. In that terminal LNG cryogenic energy is also used for refrigeration in an ultra-deep frozen warehouse at different temperature levels (tuna at -60°C; shrimp at -50°C; and salmon at -35°C), in a cryogenic power facility of ~4 MW [58] (multi-fluid RC that covers about 30% of the electricity demand in the Terminal, see Figure 2.22 (a)), for air-separation, production of dry-ice and liquid carbon acid.

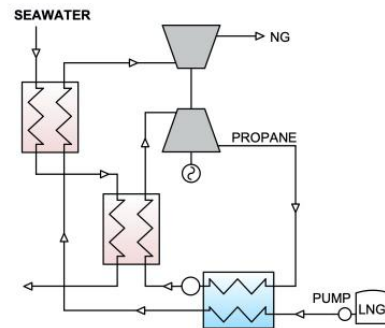
In 1979 entered in operation the world's first demonstration cryogenic power plant (DE + propane RC: 442 kW) at Sodegaura Power Station [188]. At the end of the same year, it was built the world's first commercial cryogenic power plant (ORC of 1.45 MW) [189] at Senboku LNG Terminals (Osaka, Japan) managed by Osaka Gas Co. Ltd. Afterwards, another cryogenic power generation unit of 6 MW (propane ORC + DE, see Figure 2.22 (b)) was installed in 1982 [190]. This facility remains a benchmark for new installations and research studies. Indeed, the core structure of some of the polygeneration systems developed in the following chapters of this thesis is based on that power plant. As shown in Figure 2.21, many other cryogenic power plants were installed in the 1980s. Table 2.3 shows a list of the cryogenic power plants and direct expansion units built in Japanese LNG regasification terminals. Most of them are based on Rankine cycles and their efficiencies are generally below 20% [187]. Generally, the poor efficiencies of this type of cryogenic power generation cycles often lead to long payback periods [94]. DE units such as the installed in Himeji LNG Terminal (Figure 2.22 (c)) are also one of the most utilized, but these units only utilized the mechanical exergy.

On the other hand, Table 2.4 shows some air-separation units with LNG low-temperature exergy utilization in Japan. Two representative units operating in Senboku LNG Terminals of Osaka Gas Co., Ltd. are shown in Figure 2.23 (a) and (b). The liquid nitrogen produced is later used for cryogenic crushing (i.e., cryogenic process for the disintegration of materials), among other applications. Many other applications for exploiting physical exergy have been implemented in Senboku LNG Terminals of Osaka Gas Co., Ltd. In fact, according to the Engineering Department of that company [191], the accomplishment of that exergy in Senboku Terminals I and II is 100% and 50%, respectively; also, in Himeji Terminal the electricity generated by exploiting the LNG physical exergy accounted for around 50% of the total energy consumed in the terminal [192]. In 1997 started the operation of a BOG re-liquefaction unit with cold storage and with a handling capacity of 15 t-BOG/h that achieves a power saving 900 kW [151] (see Figure 2.23 (c)) in Senboku II, although this unit is no longer in operation. Moreover, Figure 2.23 (d) is a photograph of one of the two liquid CO₂ manufacturing facility that

(a) Negishi Terminal (Tokyo Gas Co., Ltd.)
 Mixed fluid RC [100 t-LNG/h, Electric output: 4 MW]



(b) Unit No. 2 Senboku II LNG Terminal (Osaka Gas Co. Ltd.)
 RC + DE unit [150 t-LNG/h, Electric output: 6 MW, Seawater usage: 6,000 t/h]



(c) Himeji LNG Terminal (Osaka Gas Co., Ltd.)
 DE unit [80 t-LNG/h, 1.5 MW]

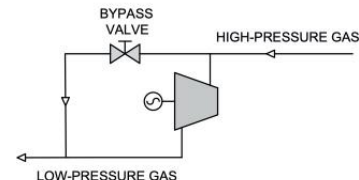


Figure 2.22. Pictures of power generation units utilizing LNG physical exergy in Japan. (a) Powerhouse of a 4 MW multi fluid RC built in Negishi LNG Terminal. Photograph property of the author of the thesis and taken with permission. Source of capacity data: [58,151]. (b) Unit No.2 (6 MW) Senboku II LNG Terminal managed by Osaka Gas Co., Ltd. Source: [191,193,194]. (c) Direct expansion unit installed in Himeji LNG Terminal. Source: Photographs (b) and (c) are property of Osaka Gas Co. Ltd., and are included with permission [151].

Table 2.3. Power generation plants based on LNG physical exergy utilization built in Japanese receiving terminals. Table prepared by using information gathered from different sources [131,151,186,195].

Terminal name	Managing Company	No. of units	Start of operation	Type	LNG usage, t/h	Gas send-out pressure, MPa(g)	Electric output	
							Total, MW	Specific, kWh/t-LNG
Senboku II	Osaka Gas	1	1979	RC	60	3.0	1.45	24.2
Chita-Kyodo	Toho Gas	1	1981	RC	40	1.4	1.00	25.0
Senboku II	Osaka Gas	1	1982	RC + DE	150	1.7	6.00	40.0
Kitakyushu	Kyushu Electric Power and Nippon Steel	1	1982	RC + DE	150	0.9	9.40	62.7
Chita LNG	Chobu Electric Power	2	1983	RC + DE	150	0.9	7.20	48.8
			1984	RC + DE	150	0.9	7.20	48.8
Nihonkai	Tohoku Electric Power	1	1984	DE	175	0.9	5.60	32.0
Negishi	Tokyo Gas	1	1985	RC (MF)	100	2.4	4.00	40.0
Higashi-Ogishima	Tokyo Electric Power	1	1986	DE	100	0.8	3.30	33.0
Himeji	Osaka Gas	1	1987	RC	120	4.0	2.80	23.3
Higashi-Ogishima	Tokyo Electric Power	2	1987	DE	170	0.4	8.80	51.8
			1991	DE	170	0.4	8.80	51.8
Senboku I	Osaka Gas	1	1989	DE	83	0.7	2.40	28.9
Yokkaichi	Chobu Electric Power	1	1989	RC + DE	150	0.9	7.00	46.7
Himeji	Osaka Gas	1	2000	DE	80	1.5	1.52	19.0
Himeji	Osaka Gas	1	2004	GT+HRSG	-	-	~50	-

Nomenclature: RC: Rankine Cycle type; DE: Direct Expansion unit; MR: Mixed-fluid type; GT: Gas turbine; HRSG: Heat recovery steam generator.

Table 2.4. Air separation plants with LNG low-temperature exergy utilization. Table prepared from sources: [94,108,129,160,191].

Terminal name	Start year	LNG usage, t/h	Specific power consumption, kWh/t-liquid products	Manufacturing capacity, Nm ³ /h			
				Liquid Oxygen	Liquid Nitrogen	Liquid Argon	Gaseous Oxygen
Negishi	1971	8	670	7,000	3,050	150	-
Sodegaura	1978	34	450	6,000	6,000	100	-
Senboku II ^a	1983	40	-	7,500	7,500	200	-
Senboku I ^b	1993	50	-	6,500	15,000	440	4,000

^a Plant No. 1. Cold Air Products Co., Ltd.

^b Plant No. 2. Cryo Air Co., Ltd.

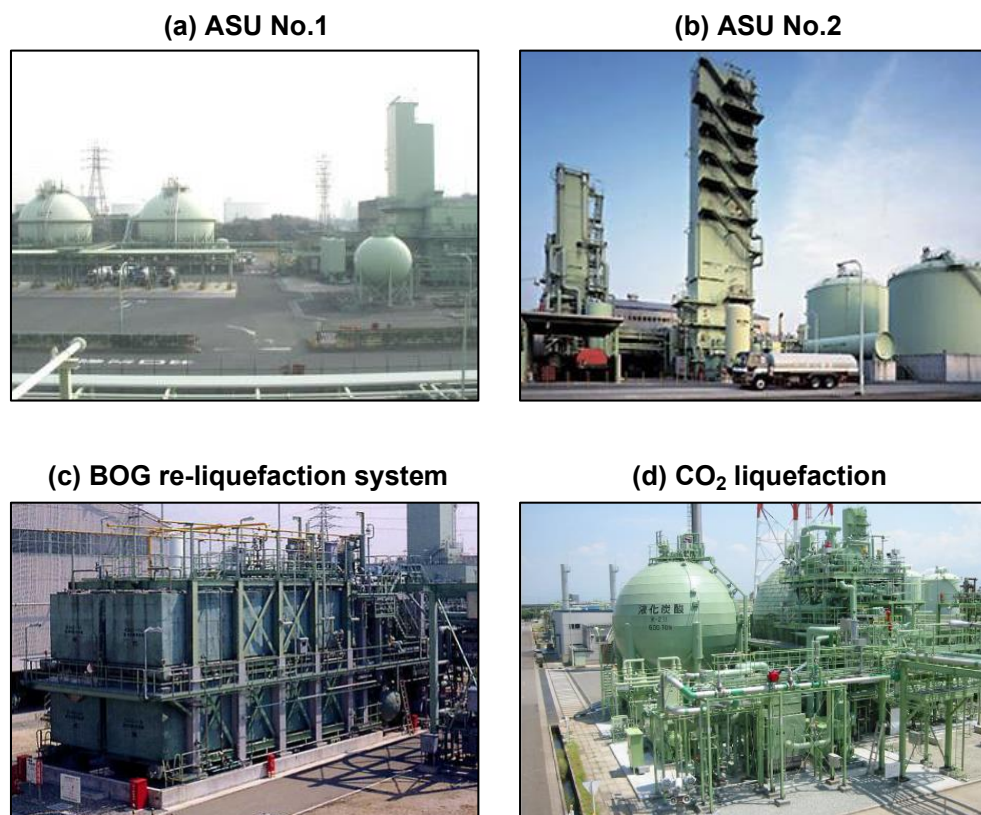


Figure 2.23. Other utilization of LNG physical exergy in Senboku LNG Terminals (Osaka Gas Co. Ltd.). Air liquefaction facilities in Osaka Gas Senboku LNG Terminals: (a) Unit No. 1, Senboku II, (b) Unit No. 2, Senboku I. Source: [191]. (c) Boil-off gas re-liquefaction with a handling capacity of 15 t/h and cold storage. Source: [151,189]. *Note:* facility no longer operating. (d) Liquid CO₂ manufacturing facility. Source: [159,191]. Photographs property of Osaka Gas Co. Ltd. and are included with permission.

exploits LNG cold in Senboku I Terminal [160]. The first of these plants started its operation in 1980 and has a production capacity of 125 t/day; the second started its operation in 2004 with a production capacity of 110 t/day. Part of the liquid CO₂ produced in the second plant is later used in a dry ice centre with a manufacturing capacity of 26 t/day [159]. The source of the CO₂ material is from a neighbouring petrochemical area. Then, LNG is also utilized as a low-temperature thermal energy source in neighbouring chemical plants (e.g., for butane cooling or, from 2010, to reduce the energy consumption of the refrigeration system utilized in an ethylene plant) [160].

On the other hand, the cascaded configuration illustrated in Figure 2.24 was proposed by Osaka Gas Co., Ltd., with the aim to utilize efficiently the LNG low-temperature thermal energy in a neighbouring oil refinery and chemical plants [160,191,196]. This

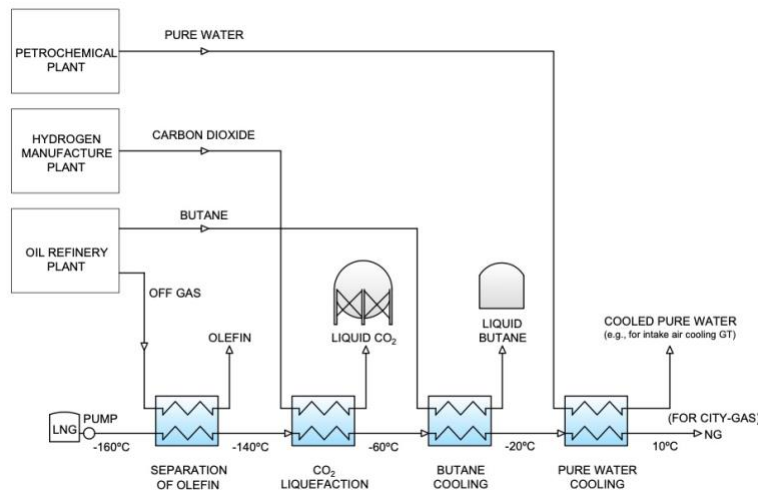


Figure 2.24. Cascade utilization of the LNG physical exergy in Senboku LNG Terminal. Figure redrawn from [160,191].

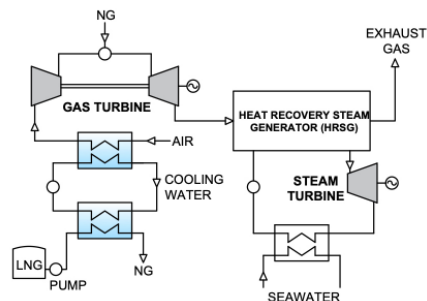


Figure 2.25. External view of the gas turbine and the HRSG installed at the Himeji LNG Terminal. Photograph of the Gas turbine intake air cooling system (Source: [192,197]) property of Osaka Gas Co. Ltd. and are included with permission. Schematic diagram redrawn and simplified from Ikeda [192].

sort of polygeneration scheme can improve significantly the performance of previous single-application and non-cascade configurations. Finally, it was installed in 2004 (Himeji LNG Terminal) the world's first inlet air cooling system that uses LNG cold energy for commercial power generation [192]. The facility is shown in Figure 2.25 and consists of a gas turbine combined cycle power generating unit (GTCC) with an efficiency of 50.2% [192]. The inlet air cooling system allows maximizing the performance of the GT.

2.4.2. Other countries

France, Australia and Asia-Pacific countries like **China** and **South Korea** use LNG low-temperature exergy for air-separation applications [108,144]. In **China**, the first air separation unit that integrates the use of the LNG low-temperature was installed in Putian [94]. In **South Korea**, which is third-largest LNG importer country, it has been evaluated the feasibility of using the LNG for applications such as cold power generation, air separation, cryogenic crushing, frozen food storage, and carbonic acid. Some projects were industrialized, such as a cryogenic air-separation plant (operated by Seoul Cold Air Products Co.) that uses 50 t-LNG/h from Pyungtaek regasification terminal and has rated production capacity of 9,400 Nm³/h of oxygen, 9,400 Nm³/h of nitrogen, and 387 Nm³/h of argon under rated operating conditions [198]. However, according to a study presented by Kim in the 23rd World Gas Conference (Amsterdam, 2006) [198], the economic benefits of that plant was below the expectations due to different technical problems. Also in South Korea, the group *Eugene Superfreeze Co. Ltd.*, announced in 2017 the construction of the world's first cryogenic logistic centre that combines the utilization of LNG low-temperature for refrigeration at different temperature levels with integration of solar energy and fuel cell power generation technology [199]. Companies such as *Tokyo Gas Engineering Solutions*, *KOGAS* and *Cryostar* are involved in that project.

Spain is quite active regarding LNG exergy use as well. In 2013 the first cryogenic power unit in Europe was installed in Enagás' Huelva LNG terminal [186]. The unit is based on a propane Rankine cycle with two turbines and two condensers (high and low pressure). The net power output is 4.5 MW at design conditions. According to Sánchez-Izquierdo and Pérez [200], the LNG and seawater flow rate utilized are 275 t/h and 8,000 m³/h, respectively. Photographs of this installation are shown in Figure 2.26. According to the description given in [200], the main components are a preheater, a vaporizer, two condensers (high and low pressure) and two turbines.



Figure 2.26. Photographs of the cryogenic power generation plant (Rankine cycle) installed in Huelva LNG Terminal and schematic diagram. *Source:* Photographs property of Enagás (included with permission) and obtained from [200]. Schematic diagram drawn according with the description of the system provided in [200].

Moreover, from 2015 a turbo-expander manufactured by Atlas Copco with a maximum generation capacity of 4.3 MW operates at Barcelona LNG Terminal [201], also managed by Enagás. This unit turns the pressure reduction of the regasified gas from 72 to 51 bar(g) (pressure drop necessary for the gas distribution to end-users) into electricity and covers around 20% of the total electricity consumption of this regasification plant [202,203]. In that terminal, the company *Ecoenergies* projected in 2014 a system to recover and supply an already existing industry cluster up to 24 MW of cold at -40°C using a CO_2 District Cooling network. Figure 2.27 shows an aerial view of the Barcelona LNG Terminal and the industry cluster (Mercabarna) where the cold recovered could be used for refrigeration applications.

Also in the Huelva LNG terminal, *Enagás* and the start-up “E4efficiency”, Ariema Enerxia and Grupo UniFood are powering a project called “*Shaky Project*” from the end of 2018 [204], co-financed by the Centre for the Development of Industrial Technology of Spain (CDTI) and the European Regional Development Fund (ERDF). This project seeks to harness LNG cryogenic temperature at the vicinity of regasification site for the following applications: refrigeration in deep-freeze warehouses, seawater desalination and later ice production, and hydrogen production by an electrolysis process driven by the electricity produced in a cryogenic ORC. Since this project is for a new industry hub and is the natural gas transmission company itself who aims to exploit LNG physical exergy, the chances of success may be higher than in the case of the project of Barcelona. The feasibility of the project and its positive environmental impact has been validated by well-known companies such as APPLUS or SGS TECNOS S.A. Figure 2.28 shows an aerial view of the place where the project will be implemented.

Regarding the global deployment of small-scale applications exploiting the LNG physical exergy, the degree of implementation is practically null. The few projects, initiatives and commercial solutions available are detailed analysed later in Chapter 5 of the thesis which tackles specifically the physical exergy recovery in satellite regasification facilities.

2.5. Conclusions

In this chapter of the potential of LNG as physical exergy source has been discussed and evaluated. Afterwards, it has been presented a detailed critical review of the different applications and technologies for exploiting that exergy and followed by an in-depth analysis of their global deployment in receiving terminals worldwide. The following conclusions can be drawn:

- 1) Despite the fact that the share of the physical exergy to the total exergy content of LNG is $\sim 2\%$, **vast amounts of low-temperature thermal energy can be recovered throughout the regasification process and utilized for multiple industrial applications**. Additionally, in large-scale terminals where regasification pressures

Barcelona LNG Terminal



Figure 2.27. Aerial view of the Barcelona LNG terminal (Spain) and neighbouring agro-food industry cluster with refrigeration demand that could utilize the LNG low-temperature exergy.



Figure 2.28. Aerial view of the place in the Huelva LNG Terminal (Spain) where the physical exergy of LNG will be used. Figure based on the information given by Solera Rico [205].

are usually high, the pressure exergy can be converted into shaft work using suitable technology. Although cryogenic power cycles are by far the most studied and implemented application, there are many others. For instance, air-separation, liquid CO₂ manufacturing, BOG re-liquefaction, refrigeration (e.g., in agro-food industry warehouses, residential/office buildings or data centres), seawater desalination, hydrogen production, among others.

- 2) The **degree of implementation and development is scarce**. Only a few systems for exploiting the physical exergy of LNG (or any other cryogenic fluid) have been built in receiving terminals worldwide, most of them in Japan. But, as demonstrated, the concept of LNG exergy recovery is not a novelty at all. However, the failed take-off

of LNG physical exergy utilization systems was because of factors such as the **poor efficiencies** reported and **high capital investments** required (i.e., expensive materials and technologies derived from the use of “*non-conventional*” fluids, the operation at cryogenic temperatures and high pressures). These drawbacks derived into the utilization of other more competitive technologies and systems to produce electricity or refrigeration for any application operating at temperatures below the ambient. But today, the use of the LNG physical exergy through its regasification is seeing **a new wave of interest**. There are many good reasons to explain this renewed attention, most of them mentioned in [Chapter 1](#) of this thesis. Some of the most remarkable are, new energy policies with ambitious climate targets that motivate the coal/oil to natural gas shifting, the imposition of carbon taxes or the extra taxes applied on damaging environmental refrigerants.

- 3) However, there are still research gaps and pending important technical issues that should be addressed to shape a hopeful prospect of LNG exergy utilization systems. For instance, **most of the literature already implemented projects are based on single applications**, which generally results in poor efficiencies and low economic competitiveness. In this sense, the systems and configurations developed in the following chapters of this thesis are based on the strategy “**polygeneration + cascade configuration**” seeking for **boosting the efficiency and enhancing the economic prospects**. Particularly, some of the systems developed are based on structures of real plants with a well-demonstrated reliable performance. And last but not least, most of the literature and implemented applications are focused on large-scale harbour LNG regasification terminals, whilst the **small-scale physical exergy recovery in satellite plants** remains almost unexplored. This will be dealt with also in a later chapter of the thesis.

Chapter 3. LNG-based polygeneration applications and fluids selection

Major parts of this Chapter have been published in the following articles:

- **A. Atienza-Márquez**, J.C. Bruno, A. Akisawa, A. Coronas. *Energy* 176 (2019), 1020-1036, [10.1016/j.energy.2019.04.060](https://doi.org/10.1016/j.energy.2019.04.060)
- **A. Atienza-Márquez**, D.S Ayoub, J.C. Bruno, A. Coronas. *Thermal Science and Engineering Progress* 20 (2020), 100677, [10.1016/j.tsep.2020.100677](https://doi.org/10.1016/j.tsep.2020.100677)

3.1. Introduction

This chapter of the thesis tackles the utilization of the LNG physical exergy through polygeneration systems. **Polygeneration** (also known as *multigeneration*) is defined as the simultaneous generation in an integrated process of more than two energy carriers or services by the use of one or multiple primary energy sources [55,206]. An “*integrated process*” consist of multiple successive processes, where the output or by-product of one process is the input of another process, so constituting an “energy supply system”. Besides, polygeneration is also a powerful weapon to face climate change since optimizes the use of primary energy sources.

Figure 3.1 illustrates the concept of polygeneration of energy. Different energy sources (e.g., fuels like oil, coal, natural gas - or LNG -, biofuels; renewable energies such as biomass, solar, geothermal, electricity) or material streams (e.g., water, air, and so on) can enter the system and be converted into different energy or material outputs (e.g., electricity, heat, refrigeration, freshwater, hydrogen, and so forth). Applying this concept to the LNG-regasification, energy polygeneration systems allow squeezing the physical exergy of LNG in cascade by the integration of different technologies and applications simultaneously, which boost the efficiency.

The chapter begins with a literature survey on relevant research works particularly focused on exploiting LNG physical exergy for polygeneration applications. Afterwards, it is presented a new polygeneration system that exploits LNG physical exergy in cascade for the combined production of electricity and refrigeration. Afterwards, the plant is utilized as a case-study to tackle a discussion about the most suitable working fluids and heat transfer fluids to be used in LNG physical exergy utilization systems, which is a major goal of the chapter. Diligent performance indicators are defined for that aim. Lastly, once the most suitable fluids are selected, it is evaluated the thermodynamic and environmental performance of the proposed polygeneration plant.

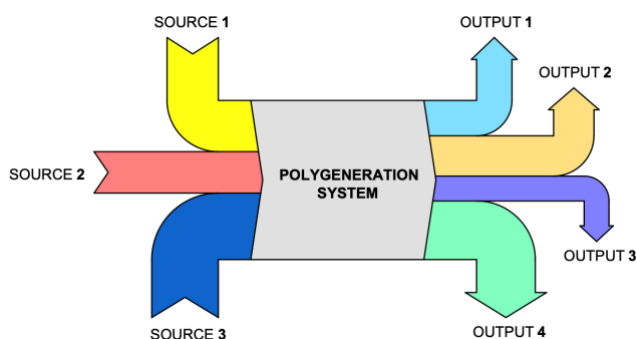


Figure 3.1. Conceptual diagram of a polygeneration system.

3.2. LNG-based polygeneration systems

As shown in the previous chapter of the thesis, there are large-scale receiving terminals that exploit the physical exergy of LNG for multiple applications. But, with few exceptions, each of those applications operates in an individual unit, rather than in an integrated structure, so a fraction of the exergetic potential is wasted. Likewise, early publications dealing with the physical exergy recovery from LNG-regasification were mostly focused on single-applications.

But in recent years, more and more authors have proposed different integrated configurations (i.e., cogeneration, trigeneration and other polygeneration systems) that combine more than one of the applications described in Chapter 2. Figure 3.2 shows a conceptual diagram of a polygeneration system that exploits the LNG physical exergy throughout its regasification process. As illustrated, the system is fully compatible with the integration of renewable energy sources (e.g., solar, biomass or geothermal). Also, it allows the recovery of low-grade heat sources (e.g., water from cooling towers) available in the process industries such as chemical, petroleum, pulp and power, food and drink, manufacturing, iron and steel, cement industries, and so on. The production of electricity and refrigeration are illustrated as possible energy outputs, but from the conceptual point of view, any other application could be integrated into these kinds of polygeneration systems.

Table 3.1 provides a critical review of recent LNG-based polygeneration configurations proposed in the literature. As a preliminary first remark, the use of the exergetic efficiency is frequently utilized as an indicator to evaluate the performance of LNG physical exergy based polygeneration systems. However, as discussed at the beginning of the previous chapter, the problem is the lack of agreement regarding its definition, which hampers the comparison between the different systems proposed in the literature.

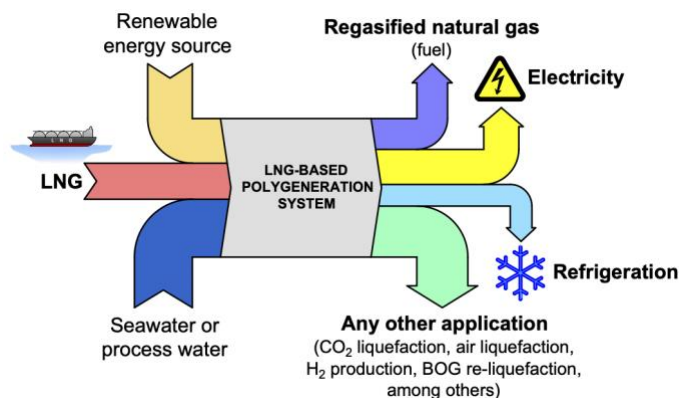


Figure 3.2. Conceptual diagram of an LNG regasification-based polygeneration system.

Table 3.1. Review of relevant cogeneration, trigeneration and polygeneration systems with LNG physical exergy recovery [55].

Year	Reference	LNG, t/h	Applications, technologies and production	η_{ex} , %
2009-11	Dispenza et al. [161]; La Rocca [119,120]	226	- Power (ORC): 3 MW (13.3 kWh/t-LNG); - Refrigeration : 9 MW at -43°C for an agro-food industry cluster + 7.5 MW for a hypermarket (7 MW for air-conditioning, 0.15 MW at -35, and 0.35 MW at -15°C).	64
2017	Mehrpooya and Sharifzadeh [207]	389	- Power (solar driven oxy-fuel T-CO ₂ cycle + CO ₂ RC): 43.5 MW (112 kWh/t-LNG); - CO₂ capture : 10.3 t/h.	60.7
2017	Mehrpooya et al. [208]	121	- Power (T-CO ₂ cycle): 11.5 MW (95 kWh/t-LNG); - Air separation : energy consumption of an ASU reduced in 2.3 MW; Coal gasification ; and CO ₂ capture: 28.5 t/h.	n/d
2017	Taheri et al. [183]	30.3	- Power (Biomass integrated gasifier-GT cycle + 2xORC + steam RC + DE): 25 MW; - Refrigeration : 2,355 kW (in a single-effect water-LiBr absorption system); - Hydrogen (PEM electrolyzer): 122 kg/h.	25.7
2017	Ghaebi et al. [209]	11.3	- Power (Kalina cycle + DE): 1,379 kW (122 kWh/t-LNG); - Refrigeration : 1,736 kW at 5°C.	22.51
2018	Esfilar et al. [210]	230.3	- Power (Steam RC + T-CO ₂): 12.8 MW (56 kWh/t-LNG); - Air separation : energy saving of 2.3 MW in an ASU for production of pure N ₂ and 99.99 mol.% O ₂ purity; - Coal and biomass co-gasification; - CO ₂ capture: 0.10 kWh/kg-CO ₂ to capture 99% of CO ₂ .	97
2018	Emadi et al. [122]	81.72	- Power (geothermally driven Kalina cycle + DE + Stirling): 10.69 MW (131 kWh/t-LNG) to produce 204.77 kg of Hydrogen (PEM electrolyzer); - Refrigeration : 6.09 MW for domestic use.	43.46
2019	Atienza-Márquez et al. [82]	180	- Power (3xORC + DE): 13.2 MW (73.3 kWh/t-LNG); - Refrigeration : 16.4 MW at -25°C, -10°C and 5°C. The equivalent electricity production was 125 kWh/t-LNG.	40.6
2019	Atienza-Márquez et al. [211]	150	- Power (ORC + DE): 3.3 MW (22.4 kWh/t-LNG); - Refrigeration : 21 MW at -50°C. The equivalent electricity production was 139 kWh/t-LNG.	40.3
2019	Emadi and Mahmudimehr [212]	115.2	- Power (2xORC + DE): 7.92 MW (69 kWh/t-LNG) to produce 151.85 kg/h of hydrogen (PEM electrolyzer); - Refrigeration : 14.47 MW (5.34 MW in a geothermally driven single-effect water-LiBr absorption system + 9.13 MW domestic cooling unit); - Heat : 10.48 MW. Values are given for the reference case.	23.44
2019	Liu et al. [213]	49.1	- Power (GT + RC): 357.6 MW; Refrigeration (mechanical vapor compression chiller electrically driven by 2xORC): 22.5-24 MW.	n/d
2019	Ebadollahi et al. [214]	18.9	- Power (Geothermally driven ORC+DE): 1,060 kW (56 kWh/t-LNG); - Refrigeration (ejector system): 1,020 kW; - Heating : 334.8 kW; - Hydrogen (PEM electrolyzer): 5.43 kg/h.	28.91
2019	Parikhani et al. [215]	4.5	- Power (Geothermally driven Kalina cycle + DE): 520 kW (116 kWh/t-LNG); - Heating (domestic water heater): 4,833 kW; - Refrigeration : 302.1 kW; Hydrogen (PEM electrolyzer): 2.28 kg/h.	33.82
2019	Bao et al. [123]	3.6	- Power (RC): around 115-205 kW (32-57 kWh/t-LNG); - Hydrogen (PEM electrolyzer): around 2.1-3.6 kg/h.	n/d
2019	Ning et al. [216]	3.6	- Power (3xORC + DE): 71.9 kW (20 kWh/t-LNG) net value; - Refrigeration : 1053 kW (228 kW for frozen food storage + 203 kW food cooling storage + 622 kW of chilled water for air-conditioning). Results for an LNG regasification and send-out pressure of 10 MPa and 0.6 MPa, respectively.	85.19
2019	She et al. [217]	2.8	- Power (GT + DE): 83 kWh/t-LNG; - LAES	57
2019	Yang and Zhao [107]	0.76	- Power (SOFC-STIG): 1,682.9 kW; - Heating : 288 kW; - Refrigeration : 175 kW; - CO₂ capture : 0.15 kg/s.	61.9
2019	Liu et al. [218]	0.51	- Power (SOFC + GT + ORC + T-CO ₂ + S-CO ₂): 319.7 kW; - Heat : 54.9 kW; - Refrigeration : 3.4 kW for air-conditioning; - Cold storage : 20.4 kW; - Ice storage: 8.7 kW; - CO₂ capture (dry ice): 79.2 kg/h.	62.29
2020	Liu et al. [219]	148.5	- Power (3xORC+DE): 12.0 MW (81 kWh/t-LNG); - Heat : 4.2 MW; - Refrigeration : 29.6 MW (total) at -25°C, -20°C, -10°C and 5°C; - CO₂ capture : 7.9 t/h.	38.39
2020	Ghorbani et al. [220]	12,100	- Power (Solar driven ORC): 460 MW + 1,978 kW to drive a multi-effect desalination system that produces 65.3 t/h of fresh water.	87.11
2020	Chitgar and Moghimi [221]	n/d	- Power (SOFC-GT+KC+ORC+DE): 5.7 MW; - Refrigeration : 482.9 kW; - Fresh water (reverse osmosis): 85.2 m ³ /h, Hydrogen (PEM): 10.2 kg/h.	54.7

On the other hand, a remarkably fact is that the generation of electric power is a common application among all of them. The different authors utilize a wide variety of technologies for that application. It owes its popularity to operational flexibility that allows exploiting un-constant portions of LNG flow rate and its capability to be installed almost anywhere inside the terminal. In other words, applications such as air-separation or CO₂ liquefaction can be installed if there are a demand for the products (i.e., liquid N₂, O₂, Ar or CO₂) nearby the regasification site. In contrast, the cryogenic power units or turboexpanders can both convert the LNG physical exergy content into a useful energy carrier in sites without special requirements and no matter whether there are neighbouring industries or buildings with low-temperature thermal energy demand [92]. But despite these strengths, the low efficiencies of LNG physical exergy recovery systems based *only* on the generation of electricity requires of its combination with other applications in cascade to improve the economic competitiveness.

The polygeneration systems proposed in the literature generally enhance the efficiencies with respect to single-application configurations. But often, the selection criteria of the different applications that integrate the polygeneration units do not rely on either the specific characteristics of an existing receiving terminal nor of the activity sector of industries and buildings located nearby and where the cold is supposed to be used. In this sense, **the polygeneration systems presented in this thesis are developed, taking into consideration the specific activity sector and operating temperatures required by the potential cold consumers.** Cold consumers can be understood as facilities (already existing or that could be built in the future) that require refrigeration for their daily activity such as warehouses or buildings and that are located either inside of the regasification area or at its surroundings. Moreover, some key parameters utilized in the systems analysed, such as the regasification pressures and flow rates are based on those of existing LNG terminals. The availability of energy resources or materials (e.g., biomass, seawater, process water, etc.) also justifies the structure of the different configurations developed.

All the polygeneration systems developed in this thesis **regasify the LNG and use its physical exergy content as a by-product for the production of electric power and/or refrigeration at different temperature levels** and *without combustion of the natural gas regasified*. Electric power production applications are included because of their above-mentioned strengths. Besides, there is technology and equipment commercially available for this application, and some cryogenic power units have demonstrated a reliable operation. On the other hand, though very low-temperature applications (e.g., cryogenic air separation, CO₂ liquefaction or hydrocarbon separation) are preferable to get the most from LNG's physical exergy, to find such kind of industries already installed at the vicinity of the LNG terminal is rather unusual. Industry holders could build new facilities next to regasification sites, but this is not a trivial matter. In contrast, it is relatively common to find neighbouring industrial areas and warehouses (e.g., of the agro-food industry sector) with refrigeration demand at different temperatures in function of their activity sector. Also, it is common the presence of buildings (e.g.,

offices, logistic centres, among others) with air-conditioning demand. The utilization of the LNG low-temperature exergy to handle - totally o partially - the refrigeration demand of these buildings and industries would make it possible to contribute to a more sustainable refrigeration system as explained in [Chapter 1](#).

In short, the polygeneration systems presented and analysed in this thesis are developed under a “*realistic*” approach and are focused on applications that could be suitable for a large number of receiving terminals. The objective is to improve the chances of success of systems for physical exergy recovery from the regasification process of cryogenic fluids such as LNG and promote their widespread implementation worldwide.

3.3. A polygeneration plant case-study

In this section, it is presented a new polygeneration plant to exploit the physical exergy of LNG, and that could be installed in an existing regasification facility. Beyond allowing to measure the exergy recovery potential, the plant is utilized as a case-study to addressing a critical technical issue: **the selection of the most suitable working fluids and heat transfer fluids**.

However, the most suitable fluids depend on the particular operating conditions (e.g., heat source temperature and pressures) and other factors such as the limits of technology and equipment available, or the safety and environmental regulations. **The decision-making process and the different fluids selection criteria followed in this chapter of the thesis could apply to any LNG physical exergy utilization system and serve as a sort of guideline for researchers and engineers**. Some performance indicators and parameters are specifically defined to evaluate the performance of these systems and allow to compare the performance of the system when operating with different candidate fluids. Notice that the following study is mostly based on the publication of Atienza-Márquez at al. [82].

3.3.1. Description

[Figure 3.3](#) shows the schematic diagram of the polygeneration plant for LNG physical exergy recovery utilized as case-study in this chapter of the doctoral thesis. This plant, which is an evolved version of the one presented previously in Atienza-Márquez et al. [30], regasifies the LNG and utilizes its physical exergy for the combined and simultaneous production of electric power and refrigeration at different temperature levels. This plant is engineered for operating as a substitute of a conventional ORV in regasification terminals with refrigeration demanding neighbouring industrial area. In this sense, the Spanish **LNG terminal of Barcelona** (41.33°N, 2.16°E) is a promising scenario. Nowadays, the Barcelona LNG terminal has an LNG regasification capacity of 1,950,000 Nm³/h and counts on a vast industrial and commercial area (agro-food

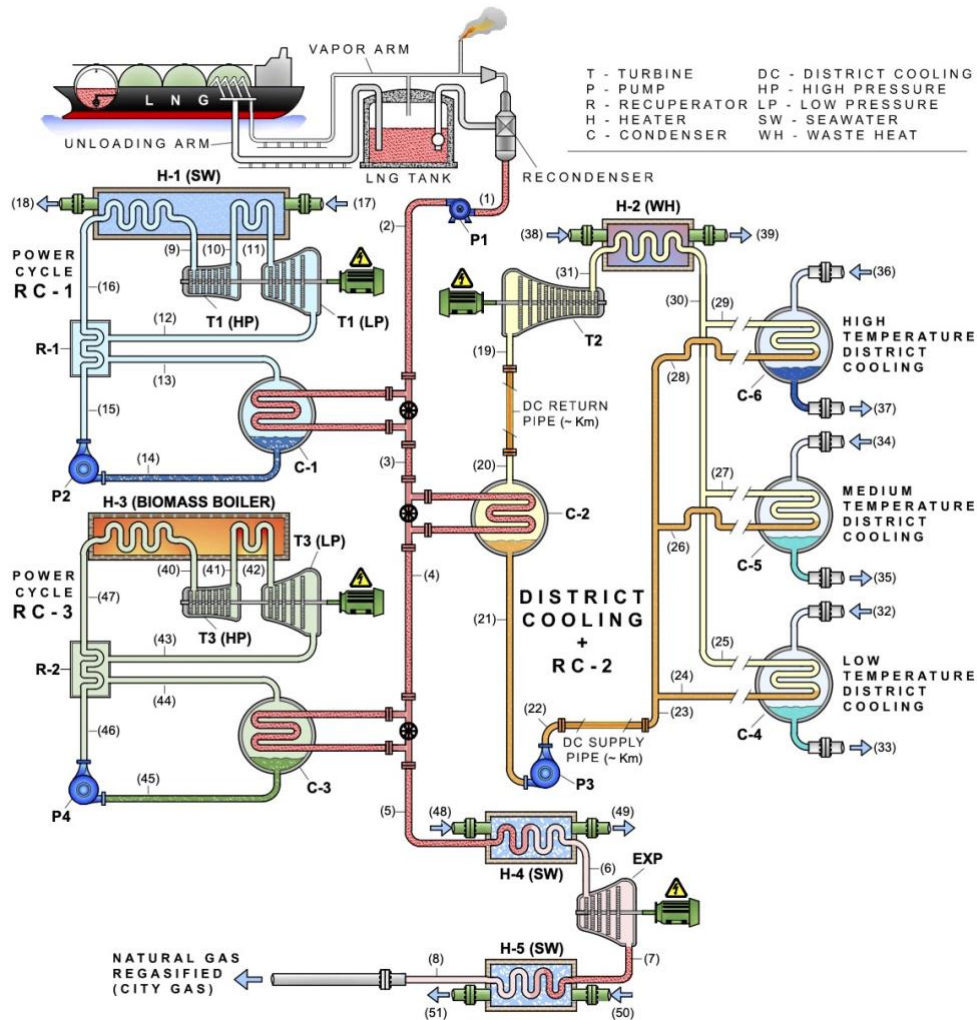


Figure 3.3. A case-study polygeneration plant with LNG physical exergy utilization in cascade. Figure published in [82].

sector) at its vicinity with high and constant refrigeration demand through the year (as illustrated in Figure 2.27).

The structure of the plant is divided into four subsystems. Following the LNG flow downstream (from the LNG tanks to the city gas distribution pipeline), these subsystems are a power unit (RC-1), a hybrid system that consists of a District Cooling (DC) network combined with a power unit (RC-2), another power unit (RC-3) and, finally, a natural gas direct expansion unit (EXP). These subsystems are arranged in series to recover the exergy from LNG-regasification in cascade. Moreover, this structure offers tremendous

operational flexibility and allows for an independent operation of each subsystem. Next is given a more detailed description of the subsystems that integrate the polygeneration plant:

- **Power cycle RC-1.** This power cycle exploits LNG exergy at its lowest temperature level. It consists of a regenerative Rankine cycle that uses seawater as a heat source and LNG as a heat sink. The cycle has intermediate reheating with two expansion-stages. It operates upstream of the DC network because, although the temperature required by the end-users connected to the DC network is relatively low in comparison with a conventional DC network, it is not so low as the LNG storage temperature. Thus, the power cycle RC-1 produces electricity from exploiting the low-temperature exergy gap between LNG storage temperature and the temperature required by the DC network.
- **DC network and power cycle RC-2.** This subsystem of the plant is designed for operating just downstream of the power cycle RC-1 and combines a DC network with a power cycle. The DC network provides refrigeration service at three temperature levels for a different type of end-users: The low-temperature DC (LT-DC) provides refrigeration service to, e.g., refrigerated warehouses; the medium-temperature DC (MT-DC) provides refrigeration service to commercial centres, supermarkets, etc.; and the high-temperature DC (HT-DC) that offers air-conditioning service for residential and office buildings, hotels, etc. Additionally, this subsystem of the plant operates also as a power cycle (RC-2) driven by low-grade waste heat.
- **Power cycle RC3.** This power cycle exploits the remaining low-temperature exergy of the LNG stream after going through the DC network and power cycle RC-2 since the temperature of the LNG stream at that point of the plant is still much lower than the ambient temperature. It consists of a regenerative Rankine cycle driven by the heat released from biomass combustion and using LNG as a heat sink. The cycle has intermediate reheating and two expansion-stages. At present, a biomass power plant is in operation near the Barcelona LNG terminal. In many cases, it is not uncommon to find availability of biomass from garden and park pruning, wood waste from construction debris and other solid waste close to urban environments.
- **Natural gas direct expansion unit (EXP).** The LNG operating pressure in the regasification terminal is higher than that required for the NG distribution pipeline. The NG direct expansion unit aims to harness the pressure exergy of NG to produce electrical power before NG is injected to the city gas distribution pipelines with the adapted pressure.

3.3.2. Operation

The operation of the polygeneration plant shown in [Figure 3.3](#) is as follows. The LNG at the exit of the boil-off-gas recondenser (stream 1) is pumped by the pump P1 up to

the high pressure of the plant (7.2 MPa, stream 2). Firstly, LNG low-temperature exergy is exploited in the condenser C-1 of the power cycle RC-1. The working fluid candidates for power cycle RC-1 must have a very low freezing point to avoid crystallization in condenser C-1. The pump P2 pressurizes the working fluid which is preheated in the recuperator R-1 and superheated in the seawater heat exchanger H-1. Next, the working fluid is first expanded down to the intermediate pressure in the high-pressure turbine (T1-HP), reheated in H-1, and it is expanded again in the low-pressure turbine (T1-LP).

Afterwards, low-temperature exergy of downstream LNG at point 3 is used as the heat sink of the heat transfer media of the DC network. Since power cycle RC-1 contributes to increasing the temperature of LNG, the risk of crystallization of the DC heat transfer media decreases in condenser C-2. In the DC network, the pump P3 raises the pressure of the condensed heat transfer media, which is also the working fluid of the power cycle RC-2. The cold distribution to the different type of end-users is made in parallel arrangement to facilitate the cold distribution and the control of the system. Therefore, all the end-users receive the cold at the same temperature (streams 24, 26, 28), regardless of their required temperature of use. The latent heat of vaporization of the heat transfer media is exploited in the end-users' substations (heat exchangers C-4, C-5 and C-6) and the secondary refrigerant used is ammonia for the facilities of the LT-DC and the MT-DC and water in the case of the HT-DC. The heat transfer media streams leaving all the end-users substations are joined in a single stream (stream 30) and superheated by low-grade waste heat (e.g., from auxiliary equipment) in the heat exchanger H-2. Next, it is expanded in the turbine T2 to produce mechanical power.

The LNG leaving condenser C-2 (stream 4) has low-temperature exergy enough to be exploited in the condenser C-3 of power cycle RC-3. The condensed working fluid (stream 45) is pumped by pump P4, preheated in the recuperator R-2 and superheated in the biomass boiler. The working fluid is first expanded in the high-pressure turbine (T3-HP). In a second expansion stage, the reheated working fluid (stream 42) is expanded in the low-pressure turbine (T3-LP). At the exit of the condenser C-3 (stream 5) and previously to exploit the NG pressure exergy, the NG is heated up to 5°C using seawater.

Finally, the pressure exergy of stream 6 is exploited by the NG direct expansion unit to produce mechanical power. The expansion takes place from the operating pressure of the LNG and NG in the plant (7.2 MPa) to the set-point pressure of the city gas distribution (3 MPa). The supply temperature of the regasified NG is adjusted to the pipeline requirements in the seawater heater H-5, just before to adjust the calorific value of NG, odorize NG and feed the city gas into the distribution pipeline.

3.3.3. Modelling and performance indicators

The polygeneration plant with LNG physical exergy exploitation is modelled with the software *Engineering Equation Solver* (EES) [88]. The simulation parameters, such as

temperatures, pressures or flow rates, are depicted in [Table 3.2](#). The following modelling assumptions are made:

- System operation under steady-state conditions.
- Thermal and pressure losses are neglected except in the distribution pipelines of the DC network.
- Kinetic and potential energies are not considered.
- The composition of LNG is assumed as pure methane, and seawater is assumed as regular water.
- Saturated liquid state is supposed for working fluids and heat transfer fluid streams leaving the condensers C-1, C-2 and C-3 (streams 14, 21 and 45).
- Streams of heat transfer media in the DC network leaving the heat exchangers C-4, C-5 and C-6 are at saturated vapour state (streams 25, 27 and 29).
- Streams of secondary refrigerants are at saturated vapour state at the inlet of heat exchangers C-4 and C-5 (streams 32 and 34) and saturated liquid state at the outlet (streams 33 and 35).
- Isentropic efficiency of turbines (including the DE unit) and pumps: 85% and 75%, respectively.
- Mechanical losses in reduction gears and electricity losses in generators are not considered.
- A pressure of 300 kPa is assumed for seawater in heat exchangers H-1, H-4 and H-5 (streams 17-18, 48-49 and 50-51, respectively) and also for the waste heat (stream 38-39) in heat exchanger H-2.

The heat transfer in the heat exchangers of the plant is calculated from energy balance equations:

$$\dot{Q} = \dot{m}_i(h_{i,in} - h_{i,out}) = \dot{m}_j(h_{j,out} - h_{j,in}) \quad (3.1)$$

On the other hand, the net power produced by each subsystem of the plant is calculated as:

$$\dot{W}_{net} = \sum \dot{W}_T - \sum \dot{W}_P \quad (3.2)$$

To compare the performance of each subsystem of the plant with the different candidate fluids, we define the specific energy produced per tonne of LNG regasified: $\dot{W}_{net}/\dot{m}_{LNG}$, given in kWh/t-LNG. Moreover, the mass flow rate is a good indicator of the size of the

Table 3.2. Base-case operation parameters.

Subsystem of the plant	Parameter	Value
LNG	LNG mass flow rate, (\dot{m}_{LNG})	180 t/h
	LNG storage pressure, (p_1)	0.13 MPa
	LNG storage temperature, (T_1)	-162°C
	Operating pressure of LNG in the plant	7.2 MPa
	Temperature at the exit of C-1, C-2 and C-3 (T_3, T_4, T_5)	-135/-65/-15°C
Power cycle RC-1	Minimum condensing temperature RC-1	-130°C
	Inlet temperature of turbine T1 (HP) and T1 (LP), (T_9, T_{11})	10°C
	Pinch temperature difference in recuperator R-1	10°C
	Seawater inlet/outlet temperature H-1	20/15°C
DC + power cycle RC-2	DC share of refrigeration demand LT/MT/HT	50/40/10%
	Temperature at the exit of C-4, C-5 and C-6 (T_{25}, T_{27}, T_{29})	-30°C
	DC supply temperature (main pipeline)	-50°C
	Length of DC supply (points 22→23) and return (points 19→20) pipelines	2 km
	Secondary fluid (water) supply/return temperature HT-DC	5/12°C
	Secondary refrigerant (ammonia) supply temperatures LT/MT	-25/-10°C
	Inlet temperature of turbine T2, (T_{31})	30°C
	Waste heat (water) stream inlet/outlet temperature, (T_{38}, T_{39})	40/35°C
Power cycle RC-3	Combustion temperature inside biomass boiler, (T_{bb})	850°C
	Condensing temperature RC-3	-10°C
	Pinch temperature difference in recuperator R-2	15°C
	Inlet temperature of turbine T3 (HP) and T3 (LP), (T_{40}, T_{42})	300°C
NG direct expansion unit	Inlet temperature of EXP, (T_6)	5°C
	Seawater inlet/outlet temperature H-4, H-5	20/15°C
	Temp. of NG supplied to distribution pipeline, (T_8)	5°C
	Pressure of NG supplied to distribution pipeline, (p_8)	3 MPa

system. Hence, we use another indicator defined as the ratio of the mass flow rate of working fluid required to produce a unit of energy: $\dot{m}_{WF}/\dot{W}_{net}$, given in kg/kWh.

On the other hand, the thermal efficiency of the power cycles of the plant is written as:

$$\eta_{th} = \frac{\dot{W}_{net}}{\dot{Q}_{in}} \quad (3.3)$$

Regarding the cold transport in the District Cooling network from the LNG regasification site to the end-user's location, the pressure loss along with the supply (state point 22→23) and return (19→20) distribution pipeline is calculated as follows:

$$\frac{\Delta P}{L} = f \frac{\rho v^2}{2D} \quad (3.4)$$

Where f is the friction factor that is calculated using the Colebrook's equation [222]:

$$\frac{1}{\sqrt{f}} = -2 \times \log_{10} \left(\frac{\varepsilon/D}{3.7} + \frac{2.51}{Re\sqrt{f}} \right) \quad (3.5)$$

A stainless-steel pipe ASTM-A333 grade 7 [223] for low-temperature service is assumed for the calculations. The temperature drops (ΔT) for both the supply and return DC pipeline is calculated from Eq. (3.6):

$$Q_{lim} = \frac{\Delta T}{R_{cv,i} + R_{cd,t} + R_{cd,ins} + R_{cd,soil}} \quad (3.6)$$

The insulation ($k=0.03 \text{ W/(m}\cdot\text{K)}$) thickness was determined to limit the heat gain (Q_{lim}) to 30 W/m and the thermal resistance of the soil is calculated according to ASHRAE [224] assuming a buried depth of 1.5 m and a ground temperature of 15°C .

Table B.1 in Appendix B shows both the energy and exergy balances for each component of the plant.

The exergetic efficiency of each subsystem of the plant ($\eta_{ex} = \sum \dot{Ex}_{us} / \sum \dot{Ex}_{in}$) is expressed as:

$$\eta_{ex,RC1} = \frac{\dot{W}_{T1-HP} + \dot{W}_{T1-LP}}{(\dot{Ex}_2 - \dot{Ex}_3) + \dot{W}_{P2}} \quad (3.7)$$

$$\eta_{ex,DC\&RC2} = \frac{\dot{W}_{T2} + (\dot{Ex}_{33} - \dot{Ex}_{32}) + (\dot{Ex}_{35} - \dot{Ex}_{34}) + (\dot{Ex}_{37} - \dot{Ex}_{36})}{(\dot{Ex}_3 - \dot{Ex}_4) + \dot{W}_{P3}} \quad (3.8)$$

$$\eta_{ex,RC3} = \frac{\dot{W}_{T3-HP} + \dot{W}_{T3-LP}}{(\dot{Ex}_4 - \dot{Ex}_5) + \dot{W}_{P4}} \quad (3.9)$$

$$\eta_{ex,EXP} = \frac{\dot{W}_{EXP}}{(\dot{Ex}_5 - \dot{Ex}_7) + \dot{W}_{P1}} \quad (3.10)$$

Finally, we use a *turbine size parameter* [225–227] to account the turbines sizes, but without pretending to perform a detailed design of the turbine. This parameter is proportional to the actual turbine size, and it is defined as:

$$TSF = \dot{V}_{out}^{1/2} \times \Delta h_{is}^{-1/4} \quad (3.11)$$

Where \dot{V}_{out} is the volumetric flow rate at the exit of the turbine (in m^3/s) and Δh_{is} is the isentropic specific enthalpy drop in the turbine (in J/kg). The turbine size parameter and the flow rates are indicators of the relative cost of the system.

Beyond the performance indicators defined previously to evaluate the performance of each subsystem individually, some other global indicators are defined to evaluate the

performance of the whole plant. These indicators are divided into two categories: (1) **Thermodynamic** performance indicators and (2) **energy and environmental** impact indicators. The *thermodynamic indicators* are:

- **Total net power of the plant ($\dot{W}_{net,tot}$)**. This indicator accounts for the total net power produced by each subsystem of the plant (RC-1, RC-2, RC-3 and the NG direct expansion unit):

$$\dot{W}_{net,tot} = \dot{W}_{net,RC1} + \dot{W}_{net,RC2} + \dot{W}_{net,RC3} + \dot{W}_{net,EXP} \quad (3.12)$$

- **District Cooling Service (DCS)**. This indicator accounts for the total refrigeration supplied by the DC network to the end-users:

$$DCS = \dot{Q}_{DC,LT} + \dot{Q}_{DC,MT} + \dot{Q}_{DC,HT} \quad (3.13)$$

Particularly, to compare the results obtained using the different candidate heat transfer fluids in [section 3.5.2](#), we use a specific *DCS* defined as the total refrigeration produced by the DC network per each tonne of LNG regasified by the plant: DCS/\dot{m}_{LNG} , given in kWh/t-LNG. Also, the mass flow rate of heat transfer fluid required to produce a unit of refrigeration is used as a relative indicator to compare all the candidates from a homogeneous basis: \dot{m}_{HTF}/DCS , given in kg/kWh.

- **Equivalent Electricity Production (EEP)**. This indicator accounts for the electrical power produced and the DCS converted into electric terms using the Energy Efficiency Ratios (*EER*):

$$EEP = \dot{m}_{LNG}^{-1} \left(\dot{W}_{net,tot} + \frac{\dot{Q}_{DC,LT}}{EER_{ref,LT}} + \frac{\dot{Q}_{DC,MT}}{EER_{ref,MT}} + \frac{\dot{Q}_{DC,HT}}{EER_{ref,HT}} \right) \quad (3.14)$$

For a refrigeration system, the *EER* is defined as the ratio of refrigeration capacity to the total rate of electric input. The lower the set-point temperature, the lower the *EER* [228]. The reference *EER* for each temperature level of the DC network were selected according to [228], and they are 1.3 for the LT-DC (refrigeration at -25 °C), 2.5 for the MT-DC (refrigeration at -10 °C) and 4.0 for the HT-DC (refrigeration at 5 °C).

- **Exergetic efficiency of the whole plant (η_{ex})**. It is defined as the total useful exergy output divided by the total exergy entering the polygeneration plant:

$$\eta_{ex} = \frac{\Sigma \dot{W}_T + \dot{W}_{EXP} + \dot{E}x_{us,DC}}{\dot{E}x_{in,LNG} + \dot{E}x_{in,WH} + \dot{Q}_{H-3}(1-T_0/T_{bb}) + \Sigma \dot{W}_P} \times 100\% \quad (3.15)$$

Notice that the above definition produces a zero-efficiency reference case for an LNG regasification plant without exergy recovery. The exergetic efficiencies of each subsystem of the plant are also formulated following this definition pattern.

On the other hand, the *energy and environmental indicators* are:

- **Primary Energy Saving (PES):**

$$PES = \eta_{ref}^{-1} \left(\dot{W}_{net,tot} + \frac{\dot{Q}_{DC,LT}}{EER_{ref,LT}} + \frac{\dot{Q}_{DC,MT}}{EER_{ref,MT}} + \frac{\dot{Q}_{DC,HT}}{EER_{ref,HT}} \right) \quad (3.16)$$

The thermal efficiency used as the reference is 52% (typical combined cycle).

- **Seawater Saving (SWS).** This indicator evaluates the seawater reduction with respect to the conventional LNG regasification process without LNG exergy recovery:

$$SWS = \left(1 - \frac{\Sigma \dot{m}_{SW}}{\dot{m}_{SW,ref}} \right) \times 100\% \quad (3.17)$$

- **Avoided GHGs emissions (GHGA):** This indicator estimates the amount of equivalent CO₂ emissions avoided by the polygeneration plant due to its equivalent electricity production.

$$GHGA = EF \left(\dot{W}_{net,tot} + \frac{\dot{Q}_{DC,LT}}{EER_{ref,LT}} + \frac{\dot{Q}_{DC,MT}}{EER_{ref,MT}} + \frac{\dot{Q}_{DC,HT}}{EER_{ref,HT}} \right) \quad (3.18)$$

The emissions factor (*EF*) represents the CO₂ emissions of a typical electricity mix integrated by diverse energy sources (e.g., natural gas, coal, nuclear energy, renewable energies, etc.). We chose an *EF* of 0.298 kg-CO₂/kWh as a representative value for Spain, but other values may be used depending on the reference electricity mix selected [229].

3.4. Preliminary screening of candidate fluids

A successful selection of the most suitable fluids in any energy system is essential for the appropriate performance of a system [230]. Also, the fluid selection criteria depend on the application, and the environmental legislation might be a constraint [231]. The basic and common properties of the ideal fluid that may be used in any energy system and also in the subsystems of the plant presented in this paper are [226,232,233]:

- The *normal boiling point* (NBP) of the fluid has to be lower than the condensing temperature to operate above the atmospheric pressure and avoid air infiltration risk.
- The *critical temperature* of the fluid has to be higher than the design condensing temperature.

- The *freezing point* has to be low enough to avoid crystallization problems when exchanging heat with LNG.
- Large *latent heat of vaporization* to reduce the mass flow rate, reduce the size of the installation and operating cost.
- *Low viscosity* to reduce the pressure drops and thermal losses.
- *Low specific volume* (or *high density*) to reduce the energy consumption by pumping and the installation cost that is related to the size of the equipment. The volume of the fluid leaving the expander determines the turbine size.
- *Chemical stability* at the operating temperatures.
- *Safe* (nontoxic, non-flammable, noncorrosive, etc.).
- *Environmentally friendly* (null ozone depletion potential – ODP and low global warming potential – GWP).
- *Good availability and low cost*.

Although the characteristic listed above are the most desirable, it is difficult to find a fluid that meets all of them. On the other hand, the subsystems of the polygeneration plant presented in this paper operate with lower condensing temperatures than the typical RCs [232] and with a lower temperature than common District Cooling networks [234]. Therefore, the characteristics of the working fluids and heat transfer fluids that operate in this kind of plant have some particularities. For example, the candidate fluids for this plant must have a much lower freezing point than most of the common fluids used in ORCs which condense at ambient temperature. Moreover, the NBP of the fluid has particular importance in cryogenic power systems. If the condensation temperature is lower than the NBP of the fluid, the condensing pressure is below the atmospheric pressure and air infiltration may occur. Thus, the freezing of air moisture might cause problems. Also, flammable mixtures can be generated if using flammable working fluids [130].

Table 3.3 shows the thermophysical properties [235], global warming potential (GWP) [236] and ASHRAE safety group (flammability and toxicity) [237] of the potential candidate fluids for the polygeneration plant. The traditional classification of fluids as ‘wet’, ‘dry’ or ‘isentropic’ is not so useful in this case. For certain fluids, this classification depends on the operating conditions [238], which are significantly different for each subsystem of the polygeneration plant. On the other hand, despite some CFCs such as R11, R12, R13 or R115, HCFCs such as R22, R123, and R502 (blend of R22/R115) may also be potential candidates due to their low freezing point, they are dismissed because all them are ozone depletion substances.

The particular operating constraints for the candidate fluids of each subsystem of the plant are the following (streams numbering are indicated in Figure 3.3):

Table 3.3. Thermophysical properties, environmental data and safety group of the preselected candidate fluids. Table published in [82].

Fluid	Type	T_{fr} , °C	NBP, °C	T_c , °C	P_c , kPa	T_{max}^a , °C	GWP ^b	Safety group ^c
R732 (Oxygen)	I.C.	-218.79	-182.96	-118.57	5,043	1726.85	-	n.d.
R740 (Argon)	I.C.	-189.34	-185.85	-122.46	4,863	1726.85	-	A1
R290 (Propane)	HC	-187.63	-42.114	96.74	4,251.2	376.85	~20	A3
R1270 (Propylene)	HC	-185.2	-47.619	91.061	4,555	301.85	<20	A3
R14	PFC	-183.61	-128.05	-45.64	3,750	349.85	7,390	A1
R170 (Ethane)	HC	-182.78	-88.581	32.172	4,872.2	401.85	~20	A3
R50 (Methane)	HC	-182.46	-161.48	-82.586	4,599.2	351.85	23	A3
R1150 (Ethylene)	HC	-169.16	-103.77	9.2	5,041.8	176.85	<20	A3
R600a (Isobutane)	HC	-159.42	-11.749	134.66	3,629	301.85	~20	A3
R23	HFC	-155.13	-82.018	26.143	4,832	201.85	14,200	A1
R218	PFC	-147.7	-36.79	71.87	2,640	166.85	8,830	A1
R41	HFC	-143.33	-78.31	44.13	5,897	151.85	107	n.d.
R600 (Butane)	HC	-138.26	-0.49	151.98	3,796	301.85	~20	A3
R32	HFC	-136.81	-51.651	78.105	5,782	161.85	716	A2L
R152a	HFC	-118.59	-24.023	113.26	4,516.8	226.85	133	A2
R143a	HFC	-111.81	-47.241	72.707	3,761	376.85	4,180	A2L
R1234ze(E)	HFO	-104.53	-18.973	109.36	3,634.9	146.85	6	A2L
R134a	HFC	-103.3	-26.074	101.06	4,059.3	181.85	1,370	A1
R125	HFC	-100.63	-48.09	66.023	3,617.7	226.85	3,420	A1
R116	PFC	-100.05	-78.09	19.88	3,048	151.85	12,200	A1
R717 (Ammonia)	I.C.	-77.655	-33.327	132.25	11,333	426.85	<1	B2L
R507A	HFC blend	-73.15 ^a	-46.74	70.615	3,704.9	226.85	3,800	A1
R404A	HFC blend	-73.15 ^a	-46.22	72.12	3,734.8	226.85	3,700	A1
R407C	HFC blend	-73.15 ^a	-43.63	86.195	4,631.7	226.85	1,700	A1
R410A	HFC blend	-73.15 ^a	-51.44	71.344	4,901.2	226.85	2,100	A1
R744 (Carbon dioxide)	I.C.	-56.558	-78.464	30.978	7,377.3	1726.85	1	A1
R1234yf	HFO	-53.15 ^a	-29.45	94.7	3,382.2	136.85	<4.4	A2L
R718 (Water)	I.C.	0.01	99.974	373.95	22,064	1726.85	<1	A1

^a Limit of EoS in NIST REFPROP [51] database; ^b GWP 100 years [52]; ^c ANSI/ASHRAE Standard 34 [53].

Nomenclature: I.C. – Inorganic compound; HC – Hydrocarbon; HFC – Hydrofluorocarbon; PFC – Perfluorocarbon; HFO – Hydrofluoro-Olefin.

- **Power cycle RC-1:** Condensing temperature (T_{14}) = max(-130°C, NBP+1°C) to ensure condensation above atmospheric pressure; Freezing point < min(-100°C, T_{14}) to prevent crystallization in the condenser; and critical temperature > than condensing temperature to allow condensation in heat exchanger C-1.
- **DC and power cycle RC-2:** NBP < DC supply temperature (T_{21} =-50°C) to ensure working above atmospheric pressure; Freezing point lower than the DC supply temperature to prevent crystallization in the condenser; and critical temperature > than the design temperature at the exit of heat exchanger C-4, C-5 and C-6 ($T_{25} = T_{27} = T_{29} = -30^\circ\text{C}$) to allow the condensation in heat exchanger C-2.
- **Power cycle RC-3:** NBP < than the condensing temperature (T_{45} =-10°C); Limit of EoS (T_{max} in Table 2) higher than the top temperature of the cycle (T_{40} and $T_{42} = 300^\circ\text{C}$). Critical temperature > than condensing temperature to allow condensation in heat exchanger C-3.

3.5. Results and discussion

A comparative assessment is performed between the different candidate working fluids and heat transfer fluids for each subsystem of the case-study polygeneration plant presented above. The discussion about the most suitable fluids is presented for each subsystem individually and in the following order: Power cycle RC-1 ([section 3.5.1](#)); District Cooling network and the power cycle RC-2 ([section 3.5.2](#)); and power cycle RC-3 ([section 3.5.3](#)). Finally, the performance of the whole polygeneration plant is evaluated when operating with the previously selected fluids ([section 3.5.4](#)).

3.5.1. Power cycle RC-1

To select the most suitable working fluid for the power cycle RC-1, we considered as indicators the power produced, the mass flow rate of the working fluid, the seawater consumption, the size of the turbine and both the thermal and the exergetic efficiencies. [Figure 3.4](#) shows the performance results for each preselected candidate fluid that fits the operating constraints established for the power cycle RC-1. Both the high pressure and the intermediate pressure are calculated to optimize the net power. The following observations can be made:

- [Figure 3.4 \(a\)](#) shows the energy production per metric tonne of LNG and the high pressure of the cycle for each candidate fluid. Since a low NBP entails a low condensation temperature (because of the condensing pressure has to be above the ambient pressure), the candidate working fluids with the lowest NBP report the highest energy production. In this sense, methane is the working fluid that reports the highest energy produced per metric tonne of LNG (10 kWh/t-LNG) followed by R14 (9.6 kWh/t-LNG). Oxygen and argon also report an acceptable net power produced, although their maximum pressures are much higher than that for the rest of candidate fluids, and this will imply a major installation cost. Thus, oxygen and argon are dismissed as working fluids for the power cycle RC-1. On the other hand, R152a and R134a give the lowest power production (< 2.5 kWh/t-LNG).
- As shown in [Figure 3.4 \(b\)](#), methane reports the lowest mass flow rate of working fluid and seawater demand (17 kg/kWh and 0.57 t/kWh, respectively), which is economically favourable. In comparison with R14, methane requires 72% lower mass flow rate, while the seawater consumption is similar. In the case of ethylene, it also reports a low mass flow rate (22 kg/kWh) and a low seawater consumption (0.68 t/kWh). However, ethylene produces 22.7% less energy per metric tonne of LNG than methane (see [Figure 3.4 \(a\)](#)) and also the size of the turbine required is larger, which implies higher costs (see [Figure 3.4 \(c\)](#)). On the other hand, R218 and R152a report the highest working fluid mass flow rate and seawater demand, respectively.

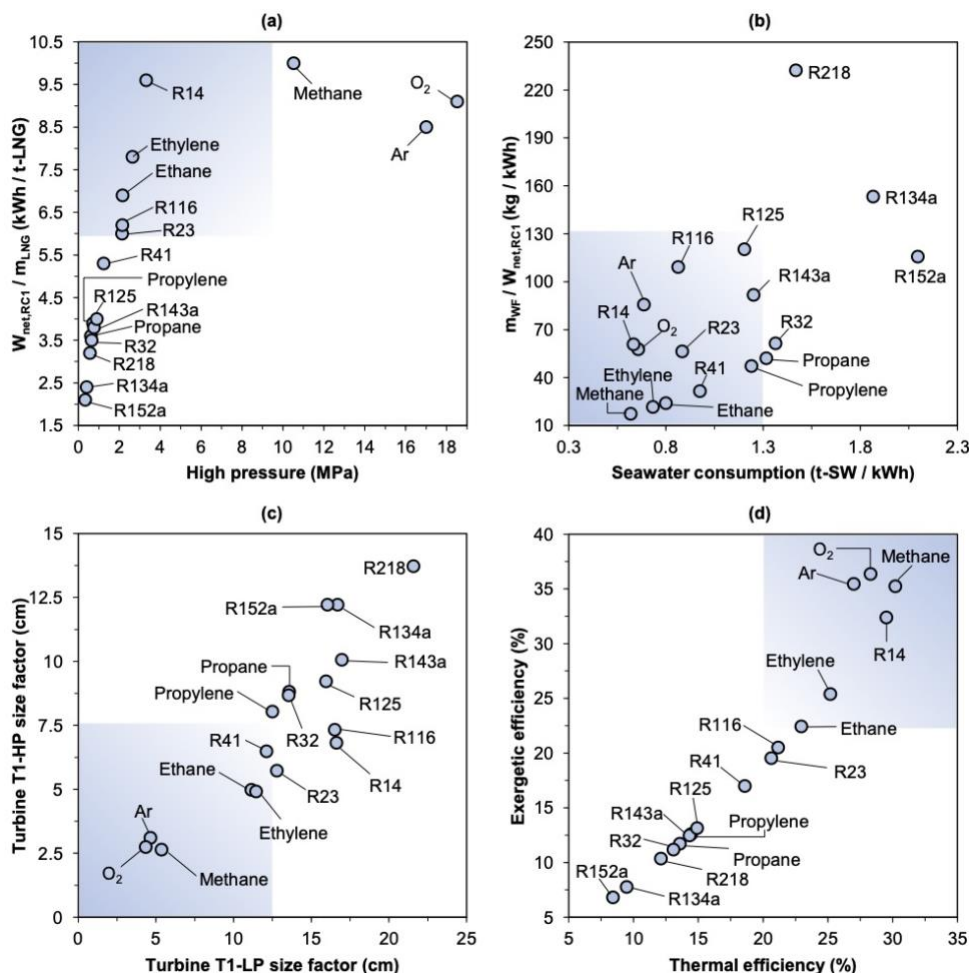


Figure 3.4. Performance results for each candidate working fluid in the power cycle RC-1. (a) Specific energy and high pressure. (b) Required mass flow rate of working fluid to produce a unit of energy and seawater consumption. (c) Turbine size factor for the turbines T1 (HP) and T1 (LP). (d) Thermal and exergetic efficiencies. Shaded area represents the desired performance. Figure published in [82].

- Regarding the thermal and exergetic efficiencies of the power cycle RC-1 shown in Figure 3.4 (d), methane reports one of the highest values (30.2% and 35.2%, respectively). In the case of R14, despite it has a thermal efficiency of 29.5% and an exergetic efficiency of 32.4%, it is dismissed as working fluid because of its environmental impact (high GWP) and its high turbine size factor in comparison with, e.g., methane, as shown in Figure 3.4 (c). Furthermore, the working fluids with relatively high NBP (propane, propylene, R32, R134a, R143a, etc.) report the lowest

both thermal and exergetic efficiencies, so they are not suitable for LNG exergy recovery in the power cycle RC-1.

According to the results, methane is selected as the working fluid for the power cycle RC-1. Despite its flammability risk, methane is a natural fluid, and it shows the best trade-off between all the performance indicators taken into account in the selection of working fluid for the power cycle RC-1.

3.5.2. DC network and the power cycle RC-2

The transport of the low-temperature thermal energy recovered from the LNG regasification site to the end-users is a critical constraint in the DC network and the power cycle RC-2. As shown in [Figure 3.3](#), unlike the other subsystems of the polygeneration plant that only produce mechanical power (power cycle RC-1, power cycle RC-3 and NG direct expansion unit), in the DC network and the power cycle RC-2 the length of pipelines is in the order of kilometres. Thus, depending on the heat transfer fluid selected, the pressure drop and heat loss due to transport affect the performance significantly. Although the priority of this subsystem of the plant is to provide refrigeration service, the power production is also analysed. Fluid flow rates, thermal and exergetic efficiencies, turbine size factors and pipeline characteristics are evaluated and compared.

[Figure 3.5](#) and [Table 3.4](#) show the performance results for each candidate fluid in the combined DC network and power cycle RC-2. The following observations can be made:

- [Figure 3.5 \(a\)](#) shows the refrigeration service provided to the end-users and the required mass flow rate of heat transfer fluid for each candidate fluid. R32 provides the highest DCS (95.1 kWh/t-LNG) followed by R41 (91.7 kWh/t-LNG). By the other side, R41 is the fluid which requires the lowest mass flow rate to provide a unit of cooling (8 kg/kWh). Although R410A reports an acceptable performance, it is dismissed because its high GWP and its lower refrigeration service compared with R32 (which is being used as a substitute of R410A in refrigeration systems [\[239\]](#)). Besides, CO₂ exhibits good performance, with a DCS of 90.8 kWh/t-LNG (higher than the obtained with ethane, ethylene and R23, but 4% lower than the given by R32) and a required mass flow rate of 10.5 kg/kWh. It is also remarkable that R116 reports both the lowest refrigeration service and the highest mass flow rate. This is mainly because of its low latent heat of vaporization (see [Table 3.4](#)).
- [Figure 3.5 \(b\)](#) shows the power produced by metric ton of LNG and the fluid mass flow rate required to produce a unit of power. R41 is the candidate with the highest energy production (6.8 kWh/t-LNG) and the lowest mass flow rate required to produce a unit of power (109 kg/kWh). The power production of R32 is 3 % lower than that for R41 and the required mass flow rate to produce a unit of power is 23.8% higher than that for R41. Although ethane achieves 3.6% higher power output than

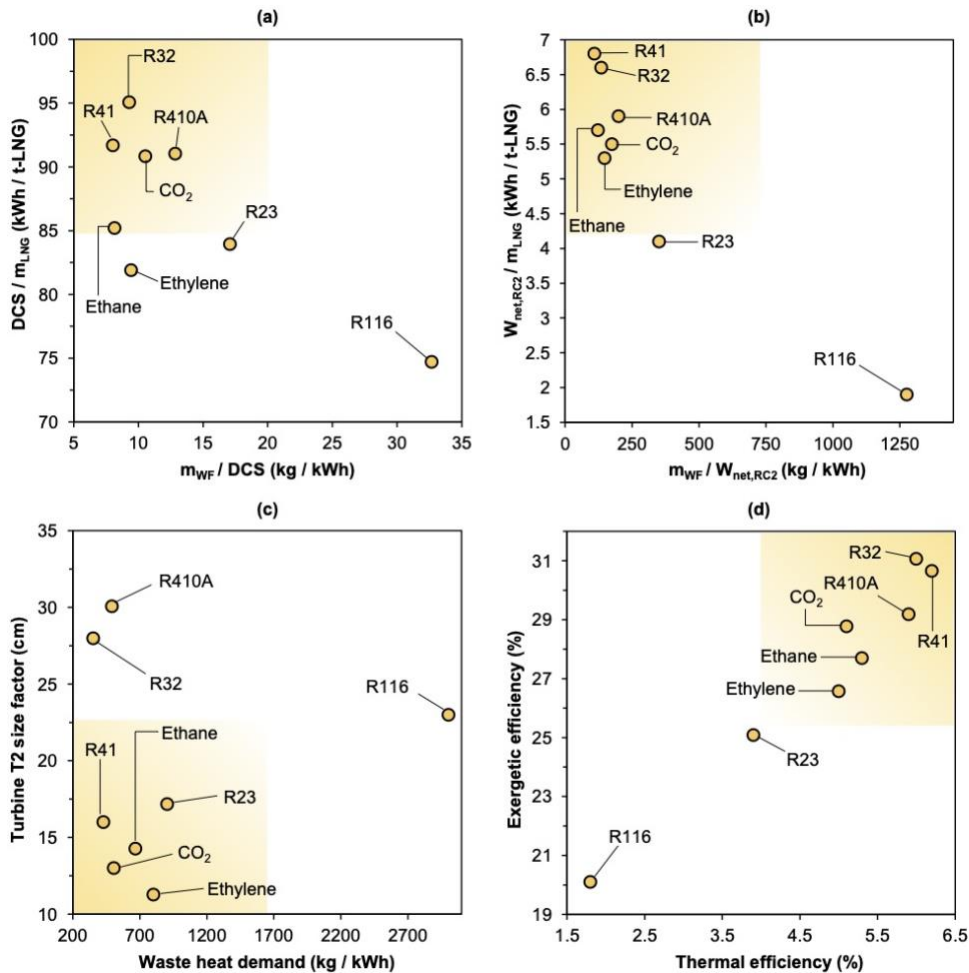


Figure 3.5. Performance analysis of the DC network and the power cycle RC-2 for each candidate fluid: (a) Power produced and high pressure of the cycle. (b) Working fluid mass flow rate required per unit of energy produced. (c) Turbine T2 size indicator and waste heat (water) demand. (d) Thermal and exergetic efficiencies. Shaded area represents the desired performance. Figure published in [82].

CO₂ and a lower mass flow rate than CO₂, these differences are not high enough to justify the higher both environmental impact and the safety risk of ethane with respect to CO₂. Also, Figure 3.5 (c) shows that the turbine size factor and the waste heat demand when using CO₂ are lower than that for ethane. Thus, ethane is dismissed as candidate fluid for the DC network and the power cycle RC-2. On the other hand, since ethylene and R23 both have a lacklustre performance not only in the power production, but also in the refrigeration service, they are dismissed as candidate fluids.

- **Figure 3.5 (d)** shows the thermal efficiency and the exergetic efficiency of the DC network and the power cycle RC-2 for the candidate working fluids. Altogether, the values of thermal efficiencies obtained are relatively poor (<6.2%). This is because the subsystem DC + RC-2 is not designed to produce power exclusively, but the priority is the refrigeration service. As a consequence, the pressures of the cycle are not optimized for power production but are constrained by the refrigeration set-point temperatures. While R41 has the highest thermal efficiency (6.2%), R32 has the highest exergetic efficiency (31.1%). Anyway, the differences in the thermal and exergetic efficiencies between R32 and R41 are very small. On the other hand, CO₂ has higher exergetic efficiency than ethane, but lower thermal efficiency.
- Because of its high liquid and vapour density CO₂ is one of the fluids with the smallest pipelines section for both the supply and return pipelines (see [Table 3.4](#)). This fact is positive from an economic point of view. In the case of R32, it has a low-section supply pipeline due to its high liquid density, but it has the largest section of the return pipeline because of it has the lowest vapour density among the candidate fluids. R41 requires pipelines with larger section than CO₂ but lower than R32. On the other hand, since R41 is one of the candidate fluids with the lowest viscosity, it reports a lower pressure drop in comparison with the rest of fluids and that means a lower pumping consumption to overcome the pressure losses. Furthermore, the price of the fluid has to be taken into account due to the large distance of the pipeline network, which implies a large volume of fluid. In this sense, CO₂ is very competitive because it is a naturally abundant fluid.

The following conclusions can be drawn: R32 achieves the highest refrigeration service and exergetic efficiency; R41 achieves the highest power production and thermal efficiency, and the lowest mass flow rate required to produce a unit of refrigeration and

Table 3.4. Performance results of each candidate fluid for the DC network and power cycle RC-2: Pipe size, working pressures, pressure and temperature drop, latent heat of vaporization, density and dynamic viscosity. Table published in Atienza-Márquez et al. [82].

Fluid	Pipe size (DN)		Pressure, kPa		$\Delta P/L$, (kPa/km)		ΔT , °C	
	S	R	P_{19}	P_{22}	S	R	S	R
CO ₂	150	450	854	1874	223	85.6	0.6	1.4
R23	200	500	677	1227	108	98.6	0.6	0.4
R32	150	900	131	648	187	10.6	0.9	1.6
R116	200	550	591	1311	274	112	0.5	-9
Ethane	200	500	650	1200	67.8	48.9	0.6	0.8
Ethylene	200	400	1273	2107	85.0	105	0.6	0.9
R41	200	600	439	1189	186	25.8	0.8	1.4
R410A	200	900	136	843	287	23.4	0.7	1.3

S: Supply pipeline (liquid) with a design velocity of 1.5 – 2.5 m/s.

R: Return pipeline (superheated vapor) with a design velocity of 20 – 25 m/s.

Table 3.4 (cont.).

Fluid	Δh_v , kJ/kg		ρ , kg/m ³		μ , $\mu\text{Pa}\cdot\text{s}$	
	-30°C	-50°C	ρ_{19}	ρ_{22}	μ_{19}	μ_{22}
CO ₂	303.5	339.7	17.6	1155	13.8	229
R23	184.9	208.4	21.3	1308	14.3	186
R32	356.8	380.1	3.2	1208	11.0	278
R116	89.9	102.5	35.2	1475	15.1	173
Ethane	388.9	429.8	8.9	492	8.9	105
Ethylene	327.7	383.6	17.0	481	17.0	94
R41	407.0	444.4	7.1	819	11.8	162
R410A	153.5	271.6	4.4	1345	11.4	311

a unit of power. However, CO₂ has a notable balance between all the criteria with a performance relative similar to R-32 and R-41. Moreover, CO₂ is a natural fluid with a lower environmental impact and a more competitive cost. Therefore, CO₂ is selected as working media for the DC network and power cycle RC-2.

3.5.3. Power cycle RC-3

The power cycle RC-3 operates with a high temperature similar to common ORCs driven by biomass combustion heat (300 °C) [232], but with a much lower condensation temperature (-10°C), so that typical working fluid used for ORCs in biomass power plants (e.g., toluene or ethylbenzene [240]) are out of selection. Also, the limited temperature range for the equation of state (EoS) of some potential candidate fluids it is a constraint for the working fluid selection process [235]. Apart from the candidates preselected from Table 3.3 that satisfy the constraint for power cycle RC-3, we also consider the binary zeotropic mixture ammonia-water (with ammonia mass fractions of 70% and 90%) as a candidate because it is widely investigated for LNG exergy recovery systems [134,145,241]. The high and intermediate pressures of the cycle are optimized from thermodynamic point of view to maximize the power produced. Therefore, the calculated pressures might establish a benchmark for a future engineering stage in which the expander will be selected. All the candidate fluids are compared with respect to the power produced, the working fluid mass flow rate required, the turbine size and the thermal and exergetic efficiencies. Figure 3.6 shows the performance results obtained by each candidate working fluid in the power cycle RC-3. The following observations can be made:

- Figure 3.6 (a) shows the energy production per metric tonne of LNG and the high pressure of the cycle for each candidate fluid. According to the results, propane is the candidate that can produce the highest specific energy (41.8 kWh/t-LNG) with one of the lowest top-pressure of the cycle. Also, propylene achieves a large energy

production (41.1 kWh/t-LNG), although with a slightly higher pressure than propane. On the other hand, the pair ammonia-water (90% NH_3) reports a 5% higher power production than pure ammonia, and 9.4% higher than the pair ammonia-water (70% NH_3). Besides, the optimal high-pressure for ammonia-water pair (90% NH_3) is the lowest among all the candidates, so that it may result in lower installation costs. On the contrary, CO_2 reports one of the lowest energy production (35 kWh/t-LNG), and it requires the highest pressure for optimizing the power produced, which has a negative impact on costs.

- Figure 3.6 (b) shows the mass flow rate of working fluid required to produce a unit of energy and the specific heat recovered in the recuperator R-2. The results show

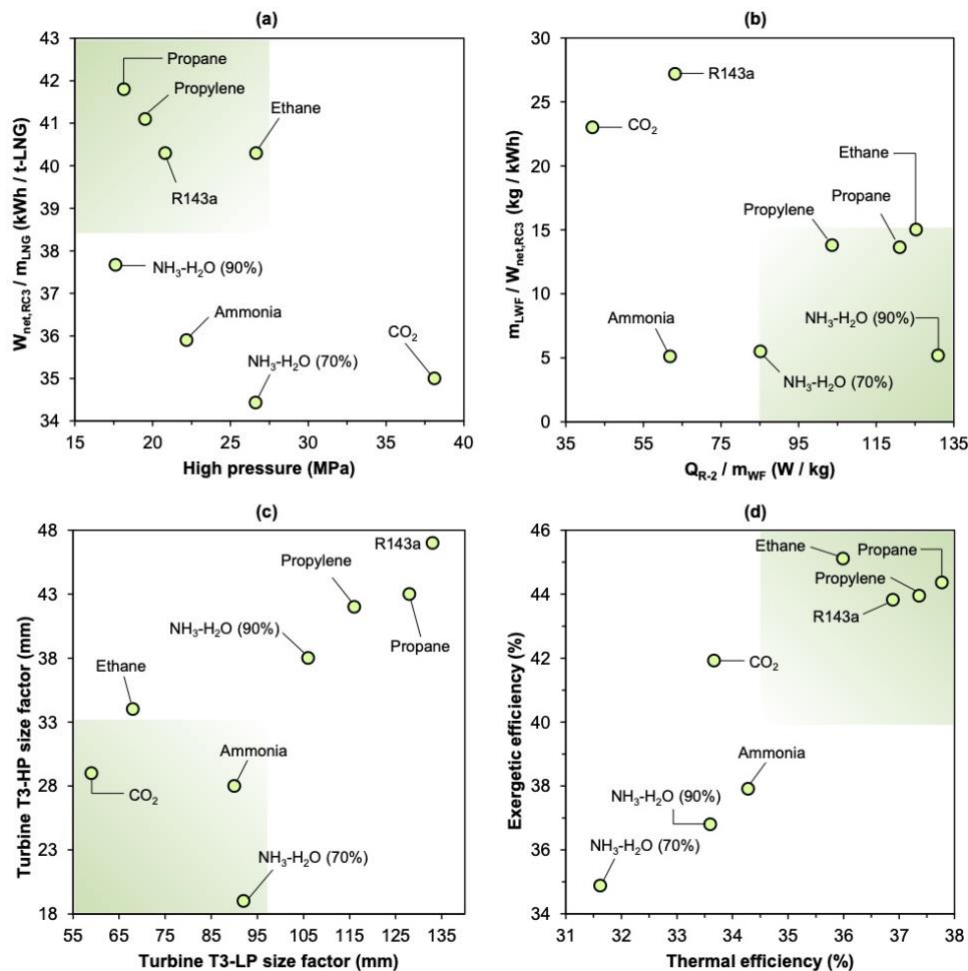


Figure 3.6. Performance analysis of the power cycle RC-3 for each candidate fluid: (a) Energy produced and high pressure of the cycle. (b) Working fluid mass flow rate required per unit of energy produced. (c) Turbine size factor for T3 (HP) and T3 (LP). (d) Thermal and exergetic efficiencies. Shaded area represents the desired performance. Figure published in [82].

that pure ammonia and ammonia-water pairs (70% and 90% NH_3) need the lowest mass flow rates to produce a unit of energy (around 5 kg/kWh), which has positive impact on costs. In contrast, CO_2 and R143a require the highest mass flow rates (23 and 27 kg/kWh, respectively), so both are dismissed as candidates. On the other hand, propane requires 13.6 kg/kWh, which is lower than that for propylene and ethane. Regarding the recuperator, ammonia-water pair (90% NH_3) has the best specific heat recovering (131 W/kg), followed by ethane and propane. Ammonia recovers only 62 W/kg. To understand these results, Figure 3.7 illustrates the profile of temperatures in the recuperator for propane, ammonia and ammonia-water (90% NH_3). As can be seen, the temperatures of the hot and cold stream for the ammonia-water (90% NH_3) approach better each other along the recuperator. This fact is also positive for the reduction of irreversibilities.

- Concerning the turbine size, Figure 3.6 (c) shows the turbine T3 size factor (both T3-HP and T3-LP). CO_2 , ethane, ammonia and ammonia-water pair (70% NH_3) require the lowest sizes, which may involve lower costs [225,242]. Propane, propylene and R134a require the larger sizes, mainly due to their larger specific volumes after the expansion. Figure 3.6 (d) shows the thermal and the exergetic efficiencies obtained. Ethane is the fluid that achieves the highest exergetic efficiency: 45.1%. However, this value is not higher enough than the given by propane (44.4%) to outweigh the lower power production and the higher pressure required by ethane.
- Moreover, propane is the fluid with the highest thermal efficiency: 37.8%. Despite propylene also shows high efficiencies, they are lower than that for propane and its environmental impact and security issues are unimproved, so propylene is dismissed as working fluid. Moreover, ammonia and ammonia-water pairs, together with CO_2 , show the poorest values of efficiencies.

According to the results and despite neither of the simulated fluids achieves all the desirable properties, propane is selected as working fluid for the power cycle RC-3

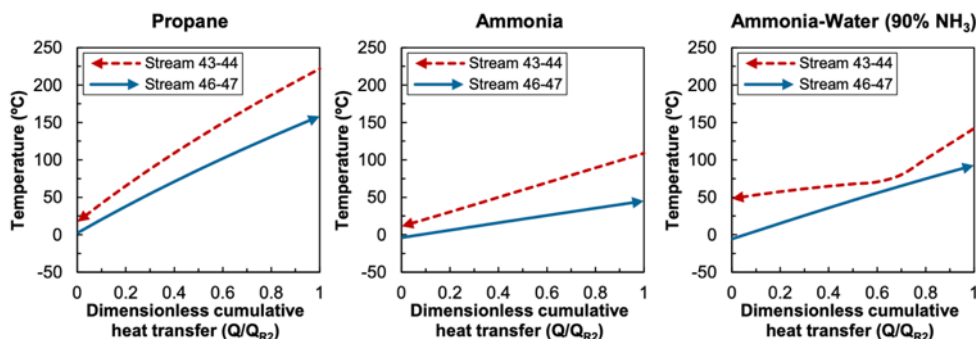


Figure 3.7. Temperature profile in the recuperator R-2 of the power cycle RC-3 for propane, ammonia and ammonia-water pair (ammonia mass fraction 90%) as working fluids. Figure published in [82].

because of it shows the best trade-off between all the selection criteria. Although propane is a natural fluid with a low GWP, its flammability risk must be considered, and precautions have to be taken in a further design of the plant.

3.5.4. Performance analysis of the whole plant

Once the fluid selection is completed for each subsystem of the polygeneration plant, we evaluate the performance of the whole plant. Table 3.5 shows a comparison of the performance of the typical LNG regasification process (that uses seawater as heat source without cold utilization) and the performance of the polygeneration plant proposed in this chapter of the thesis. Also, this table is a breakdown of the contribution of each subsystem of the total performance of the plant. According to the results, the following observations can be made:

- If the LNG physical exergy is wasted as in the typical LNG regasification process, the plant consumes 1.1 MW of electricity (by LNG pumping). Besides, no mechanical power is produced, and the LNG physical exergy is wasted. On the other hand, the proposed polygeneration plant with exergy recovery from LNG-regasification produces a mechanical power of 73.3 kWh/t-LNG (13.2 MW). For instance, this is 83% higher than the specific power produced by the cryogenic power plant No. 2 of Osaka Gas in Senboku II terminal (40 kWh/t-LNG) [194]. On the other hand, the power cycle RC-3 is the one which contributes the most to the total power production of the plant (57%), while the electric power given by the DC network and power cycle RC-2 is the lowest (7.6%).

Table 3.5. Performance indicators of the LNG regasification process without exergy recovery and the obtained by the polygeneration plant proposed when operating with the selected working fluids and heat transfer fluids (Power cycle RC-1: Methane; DC + Power cycle RC-2: CO₂; Power cycle RC-3: Propane) for an LNG regasification rate of 180 t/h.

Operation mode	Performance indicators						
	\dot{W}_{net} , MW	DCS, MW	EEP, kWh/t-LNG	PES ^a , GWh/y	SW, t-SW/t-LNG	GHGA ^b , t-CO _{2e} /y	η_{ex} , %
<i>LNG regasification without exergy recovery</i>	-1.1	0	-6.2	-19	38.7	+2,913	0
<i>Polygeneration plant with exergy recovery</i>	13.2	16.4	125.3	380	14.9	-58,877	40.6
- Power cycle RC-1	1.8	-	9.9	30	5.7	-4,652	35.2
- DC + power cycle RC-2	1.0	16.4	57.3	174	-	-26,924	28.8
- Power cycle RC-3	7.5	-	41.8	127	-	-19,641	44.4
- NG direct expansion unit	2.9	-	16.3	49	9.2	-7,659	62.7

^a Taking as a reference an efficiency of 52%.

^b Considering an emission factor of 0.298 kg-CO₂/kWh.

- The DC network provides 16.4 MW of refrigeration service (91.1 kWh/t-LNG) to the end-users, distributed for each temperature level as follows: 8.2 MW for the low-temperature network; 6.6 MW for the medium-temperature network; and 1.6 MW for the high-temperature network. To account for both the electricity production and the refrigeration service simultaneously in a single indicator, the Equivalent Electricity Production (Eq. (3.14)) is used. According to with this combined parameter, the polygeneration plant achieves an equivalent electricity production of 125.3 kWh from each metric ton of LNG regasified. Therefore, the plant can recover more than 15% of the electric energy consumed by the compressors of the refrigeration systems in a typical LNG liquefaction plant (using a reference value of 805 kWh per metric tonne of LNG produced [243]).
- Regarding the environmental impact, the proposed polygeneration plant reduces by 60% the amount of seawater utilized in a common LNG regasification plant. Also, it reports an annual primary energy saving of 380 GWh, and it ideally avoids the annual emission of 59 thousand tonnes of CO₂ to the atmosphere (34.7 kg-CO₂/t-LNG). Moreover, **all the selected fluids for the plant are natural fluids** (also denominated “*Not-In-Kind, NIK fluids*” [244]) with low GWP, so the environmental impact is negligible if leakage of fluids in the installation occurs.

The main thermodynamic data of each state point of the polygeneration plan illustrated in Figure 3.3 operating with the selected fluids are shown in Appendix B. Furthermore, to perform an exergy analysis is convenient and instructive in LNG exergy recovery systems.

Figure 3.8 depicts how each subsystem of the plant exploits LNG physical exergy. The two components of the LNG physical exergy (pressure exergy and low-temperature exergy) are identified in this diagram. A remarkable fact is that the maximum LNG physical exergy that can be exploited by the plant is limited to 53% of the total LNG physical exergy content at the exit of pump P-1. This is because the temperature and pressure of the regasified natural gas are constrained by the city gas distribution pipeline (set as 5°C and 3 MPa, respectively, for the polygeneration plant studied in this chapter). Thus, the remaining low-temperature and pressure components of LNG exergy at the exit of the heat exchanger H-5 cannot be exploited by the plant.

The power cycle RC-1, the DC network and the power cycle RC-2 and the power cycle RC-3 only exploit the low-temperature exergy of LNG. On the other hand, the NG direct expansion unit exploits the LNG pressure exergy available between 7.2 MPa and 3 MPa. Although most of the low-temperature exergy is exploited by the DC network and more than 90 kWh/t-LNG of refrigeration are supplied to the end-users, the useful exergy harnessed by the DC network is low: Only 9% of the total LNG physical exergy exploited by the plant. This is because of the relative high temperature (from the exergetic point of view) required by the end-users. By decreasing the supply temperature of the DC network, and also the temperature required by the end-users, the exergetic efficiency of the DC network will increase.

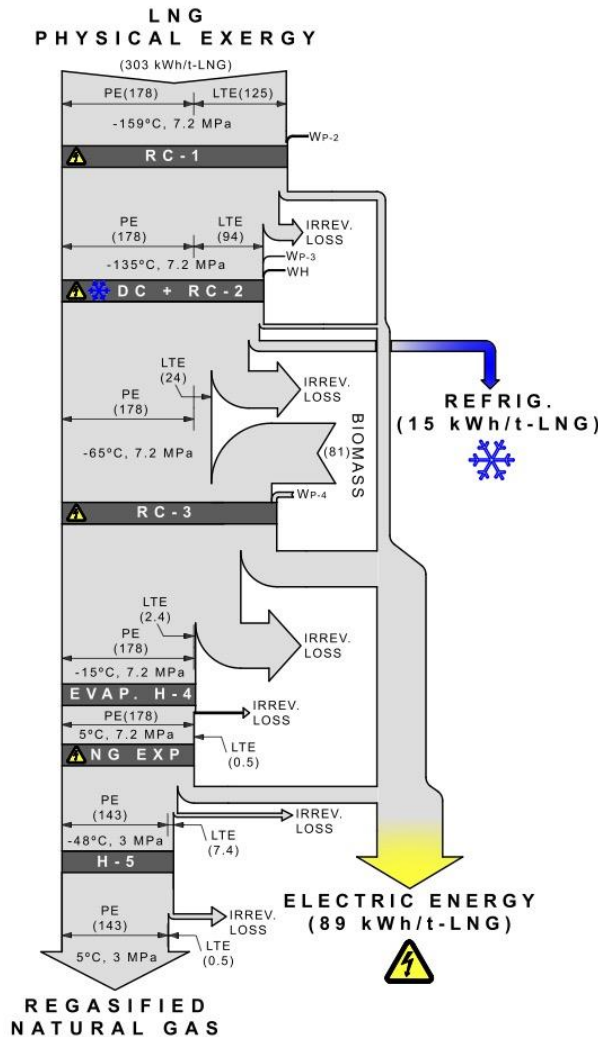


Figure 3.8. Detailed exergy flow chart of the LNG physical exergy utilization (temperature exergy + pressure exergy) in the proposed polygeneration plant. Nomenclature: PE – Pressure exergy; LTE – Low-temperature exergy. Figure published in [82].

Finally, [Figure 3.9](#) shows an exergy flow chart of the whole LNG supply chain. This figure aims to offer the reader a broad view about how the proposed polygeneration plant is integrated into the whole LNG value chain. The exergy path represented in this figure is described as follows. After extraction and before liquefaction, the raw gas has only chemical exergy. However, once liquefied (the liquefaction facility consumes approximately 10% of the total gas processed as fuel [245]) the LNG also gets physical exergy because of its low temperature. Afterwards, part of the LNG transported in LNG carriers is consumed as fuel. In the receiving terminals, the LNG from tanks is

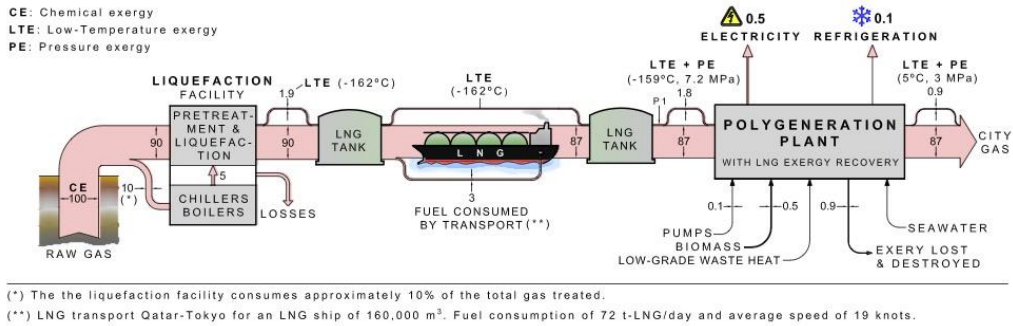


Figure 3.9. Exergy flow chart of natural gas supply chain with the integration of the proposed polygeneration plant with physical exergy recovery from LNG-regasification. The 100-base is assumed as the chemical exergy as fuel of 1 metric ton of natural gas. Figure published in Atienza-Márquez et al. [82].

pressurized before its regasification in the polygeneration plant, so the pressure exergy of LNG increases. The polygeneration system proposed in Figure 3.3 exploits only the physical exergy of LNG and the regasified natural gas supplied to the end-users (city gas) preserves all its chemical exergy as fuel. According to the results and the definition is given by Eq. (3.15), the exergetic efficiency of the proposed polygeneration plant is 40.6%, which is nearly double than the achieved by actual power units with LNG physical exergy utilization [187].

3.6. Conclusions

This chapter tackled some specific objectives of the thesis. By one hand, it is presented a literature review explicitly focused on polygeneration systems for exploiting the LNG physical exergy throughout its regasification process. On the other hand, the model of a cascaded polygeneration plant (for the combined and simultaneous production of electricity and refrigeration at different temperature levels) has been developed and utilized as a case study for addressing the selection of the most suitable working fluids and heat transfer fluids to operate in different subsystems and under different operating conditions. Moreover, the performance of the plant was evaluated. The following conclusions can be made:

- 1) Recently, a wide variety of LNG-based polygeneration systems have been studied in the literature. Despite the physical exergy recovery efficiency is generally enhanced with respect to single-application systems, these studies are rarely based on real scenarios of receiving terminals and their surroundings (i.e., the type of activity and demands of neighbouring industrial areas and buildings). Besides, the selection of the most suitable working fluids and heat transfer fluids for plants with several subsystems that operate at different conditions has not been addressed in depth.

- 2) Ultimately the selection of the most suitable fluids depends on the specific type of configurations and their operating conditions (e.g., temperature and pressure levels, flow rates, and so forth), as well as the degree of development and commercial availability of the technology compatible (e.g., turbines, pumps or heat exchanger), the environmental and security constraints, among other factors. Therefore, it is challenging to set a kind of rule of thumb for the fluid selection of LNG physical exergy recovery system. Thus, fluid selection has to be addressed carefully for each specific scenario. Nonetheless, the decision-making process for the selection of the most suitable fluid selection presented in this chapter and the performance indicators defined could be used as a guideline for future studies in this field.
- 3) All of the candidate fluids selected for operating in the different subsystems of the case-study polygeneration plant have some weaknesses. But those which reported the best trade-off between the different performance indicators were: Methane for the power cycle RC-1; Carbon dioxide for the DC network and the power cycle RC-2; and propane for the power cycle RC-3. Also, the secondary fluids of the DC network are natural fluids (ammonia and water). It is quite remarkable that **all the selected fluids are natural fluids, which reinforces the sustainability of LNG physical exergy recovery systems**. When operating with the selected fluids, the plant achieved an exergetic efficiency of 40.6%, and produces 73 and 91 kWh/t-LNG of net electrical energy and refrigeration, respectively. This represents an equivalent electricity production of 125.3 kWh/t-LNG and the avoided annual emissions of 59 thousand tonnes of GHGs to the atmosphere.

Last but not least, the plant modelled in this chapter could be implemented in any LNG receiving terminal with a neighbouring industrial area with refrigeration demand. Moreover, it allows integrating many energy and material inputs, including renewable sources such as biomass. However, the performance analysis presented is focused only on the energetic and environmental aspects, whilst no information is provided on the economic feasibility of cascaded polygeneration systems for the simultaneous production of electricity and refrigeration. An economic analysis requires of detailed information on, for example, the technology of the equipment and materials utilized. Additionally, it is required detailed modelling of those main components (e.g., heat exchangers) that integrates the plant, which is out of the scope of this chapter.

But the economic assessment of cascaded polygeneration systems is a major objective of this thesis, since the future chances of success of these systems depend largely on it. In the following chapter, some new configurations are developed on the basis of the basic structure of an existing LNG physical exergy utilization system. This strategy allows handling truthful and validated information on operating parameters (i.e., flow rates, pressures and temperature), and also on the technology and materials utilized in these types of facilities. This information enables developing detailed models of the main components. Therefore, reliable findings regarding the economic competitiveness of LNG physical exergy utilization systems could be obtained.

UNIVERSITAT ROVIRA I VIRGILI

EXERGY RECOVERY FROM LNG-REGASIFICATION FOR POLYGENERATION OF ENERGY

Antonio Atienza Márquez

Chapter 4. Development and technoeconomic assessment of cryogenic power and cooling plants

Major parts of this Chapter have been published in the following articles:

- **A. Atienza-Márquez**, J.C. Bruno, A. Akisawa, A. Coronas. *Energy* 183 (2019), 448-461, [10.1016/j.energy.2019.06.153](https://doi.org/10.1016/j.energy.2019.06.153)
- **A. Atienza-Márquez**, D.S Ayoub, J.C. Bruno, A. Coronas. *Thermal Science and Engineering Progress* 20 (2020), 100677, [10.1016/j.tsep.2020.100677](https://doi.org/10.1016/j.tsep.2020.100677)

4.1. Introduction

The polygeneration system for exploiting the LNG physical exergy in cascade presented in the previous chapter as well as other similar systems proposed in the literature offer attractive solutions to boost the efficiency with respect to single-application systems. However, these polygeneration configurations usually present highly complex structures which require many and sophisticated equipment. In several cases, this could result in a poor economic performance. In this sense, to find the best trade-off between simplicity and efficiency may be the key to boost a widespread implementation of LNG exergy recovery systems. Furthermore, although there are systems proposed that are built upon realistic scenarios, the vast majority are theoretical. In short, these configurations are not based on the layout, equipment or operating fluids utilized by already existing systems and with a reliable operation.

In this chapter, different configurations are developed for exploiting the LNG physical exergy in cascade for the simultaneous and combined production of electricity and refrigeration but **maintaining the core of an existing power generation unit with a well demonstrated operation and with a structure relatively simple**. The objective is to boost both the efficiency and the environmental performance through relatively simple and reliable polygeneration configurations; thereby the economic competitiveness would improve. Likewise, the chances of succeeding in future commercialization of these systems in regasification terminals would increase.

The chapter is arranged as follows. Firstly, the different configurations developed are described, and their operation is explained. Then, the modelling, the performance indicators and the formulation of the economic analysis are presented. Next, the model developed for the benchmark power generation unit is calibrated using operating data available in the open literature. Also, it is presented the discussion of the results obtained for the energetic and environmental performance of the different systems developed. The performance is evaluated both at design and off-design operating conditions through a sensitivity analysis. Finally, the economic viability of the systems studied is analysed under different scenarios.

4.2. Configurations based on an existing plant

Table 4.1 shows a comparison between the different configurations assessed in this chapter of the thesis, according to the energy outputs and the type of operating blocks that integrate the systems. The benchmark configuration is an already existing cryogenic power unit, and the other configurations presented are built from it by adding different components and modules in cascade to improve the LNG physical exergy utilization. A common feature among the different systems is that all the working fluids and heat

Table 4.1. Energy outputs of the different configurations.

Configuration	Designation	Electricity production		Refrigeration production	
		Propane RC	DE unit	Low temperature	Chilled water
Cryogenic power plant	CP	•	•		
CCP system Type (i)	CCP-(i)	•	•	•	
CCP system Type (ii)	CCP-(ii)	•	•		•
Polygeneration plant	Polygeneration	•	•	•	•

transfer fluids utilized are natural. A detailed description of the structure and operation of these configurations proposed are presented below.

4.2.1. The benchmark cryogenic power unit

Figure 4.1 shows the block diagram and the schematic layout of the cryogenic power (CP) plant used as a reference system to develop different configurations presented in this chapter and described below. The structure of this system is based on that of the cryogenic power unit No.2 operating in Senboku II LNG Terminal of Osaka Gas Co., Ltd. [189,193]. That power plant operates since 1982 [246], so its reliability and safety are well demonstrated, and it is a benchmark for later built cryogenic power units. It is assumed that this plant and the following configurations presented are baseload regasification units. Also, it is considered that the electricity generated by these configurations is for on-site consumption.

As shown in Figure 4.2, the structure of the power generation unit is divided into two subsystems:

1. **Rankine cycle (RC):** It consists of a Rankine power cycle with a single expansion stage that exploits the low-temperature component of LNG physical exergy as a heat sink. Seawater or warm water (e.g., from cooling towers, could be used as a heat source depending on its availability in the regasification site). The working fluid is propane because features as a very low-freezing point, moderate pressure at the operating temperatures, good heat transfer characteristics, high latent heat of vaporization, cost, and so forth [193].
2. **Natural Gas direct expansion (DE) unit:** It consists of an expander that converts the pressure component of LNG physical exergy into mechanical energy.

As a whole, the operation of the power unit is as follows. The LNG stored in tanks at around -162°C and 0.12 MPa (stream L1, 150 t/h) is pumped up to the high pressure of the plant (4.6 MPa) by the cryogenic pump (P1). Afterwards, the pressurized LNG stream (stream L2) is used as a heat sink in the propane RC. Afterwards, the stream

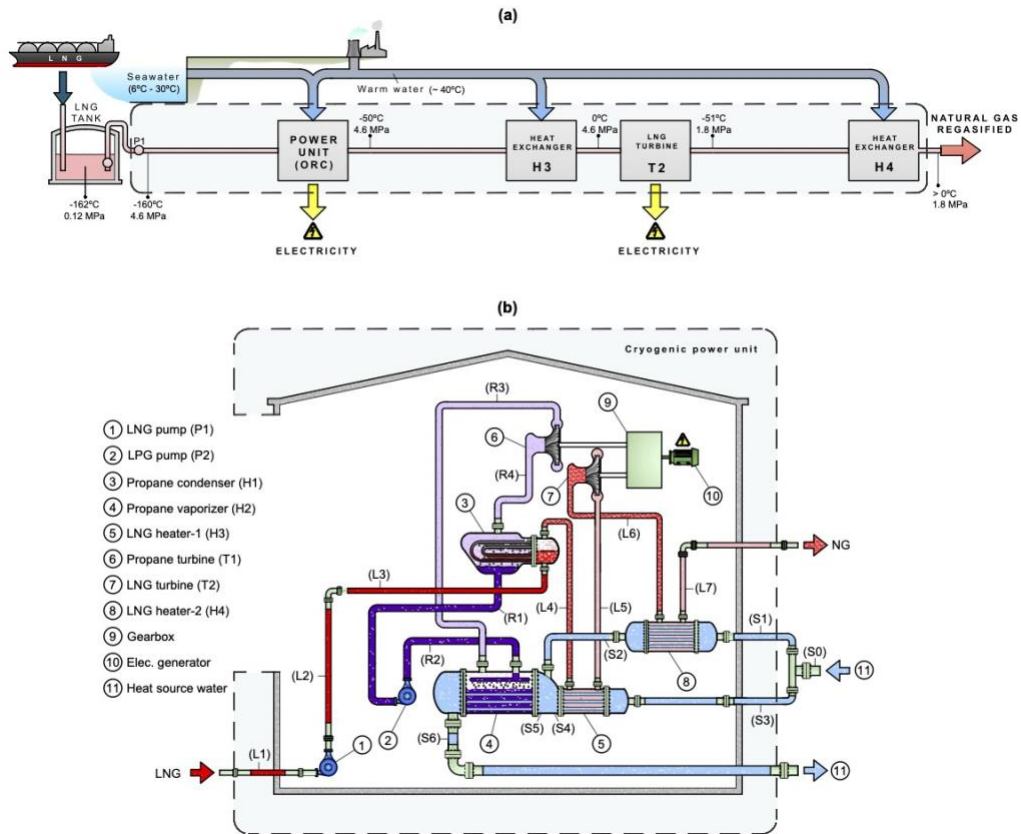


Figure 4.1. Cryogenic Power generation unit utilized as reference system. (a) Block diagram, (b) Detailed schematic layout. Redrawn from Atienza-Márquez et al. [211].

leaving the propane condenser (stream L4, -50°C) is superheated in a heat source water heat exchanger (H3) up to 0°C and expanded in the DE unit (T2) where the pressure exergy is converted into shaft work. The stream leaving expansion unit (stream L6, 1.8 MPa) has to heat up again in another heat source water heat exchanger (H4). In this way, the supply temperature of the regasified natural gas (stream L7, 5°C) is tuned before the calorific value adjustment and odorization stages. Both heat exchangers H3 and H4 are shell-and-tube type heat exchangers in which seawater flows through the tubes and NG flows in the shell side in cross-flow over the tubes.

The operation of the propane RC is the same for all the configurations analysed in this chapter. Once expanded, the propane leaving the turbine T1 (stream R4 at 130 kPa) condenses in a shell-and-tube type heat exchanger. Condensation occurs on the tubes in which LNG (used as the heat sink) flows through. Then, the condensed propane (stream R1, considered as saturated liquid) is pumped by the pump P2 (up to 620 kPa) and discharged in the propane vaporizer (heat exchanger H2). This heat exchanger consists

of a sort of shell-and-tube exchanger in which the heat source water flows through the tubes. The droplets of liquid propane are sprayed from a distributor and fall by gravity, forming a pool that floods the seawater tube bundle completely. Then, propane is vaporized by taking heat from the seawater or process water that was previously utilized in the heat exchangers H3 and H4 as a heat source for increasing the temperature of the natural gas. Once vaporized, the propane (stream R3, assumed saturated vapour) is expanded in the turbine T1 to produce mechanical power. Finally, the rotational speed of both turbine T1 and the turboexpander T2 is adapted by a gearbox, and the mechanical power is converted into electricity by means of an electric generator.

4.2.2. Combined Cold and Power (CCP) unit: Type (i)

The blocks diagram and the schematic layout of the CCP-(i) system are illustrated in [Figure 4.2](#). Beyond producing electric power, this configuration incorporates the production of low-temperature refrigeration. The structure of the CCP-(i) unit is divided into two different operational modules arranged in cascade. Following the LNG downstream (from the tanks to the city gas distribution pipeline), these modules are the refrigeration module where refrigeration at -50°C is produced from the recovery of the LNG low temperature, and the electric power generation module. Both modules operate simultaneously and using natural operating fluids exclusively.

The refrigeration module consists basically of a heat exchanger and a **low-temperature District Cooling network (LT-DC)**. The low-temperature thermal energy is distributed by the DC network at -50°C , which is a suitable temperature, for example, for refrigeration applications in the agro-food industry sector. The refrigeration service is delivered to warehouses located at the vicinity of the regasification site but not inside the terminal. Thus, cold has to be transported over distances of the order of a few kilometres. Once at the warehouses side, the cold energy is transferred to a secondary fluid (e.g., ammonia at -25°C) and supplied to freezing rooms using technologies of terminal units like some type of fan-coil. It should be noticed that end-users with refrigeration demands at different temperature levels for different agro-food applications could also join the DC network. Besides, inside an individual warehouse, the refrigeration could be yield at different temperatures depending on the type of product stored in each cold room. But in any case, the analysis of the cold utilization at warehouses side is out of the scope of this work which is limited to the utilization of the LNG physical exergy in the LNG physical exergy recovery plant.

As in the DC network included in the configuration presented in [Chapter 3](#), Carbon Dioxide (CO_2) is used as the heat transfer medium. CO_2 has been selected by some authors because of its several advantages with respect to the long-distance transport of the cold [\[119,120,223\]](#). Some of its advantages were mentioned in the previous chapter, for example, since liquid CO_2 has lower viscosities at very low temperatures and it requires lower flow rates than, e.g., water/glycol mixtures, the power consumption by

pumping can be reduced [247]. Moreover, CO₂ is an environmentally-friendly substance, secure and cheap so that it is a suitable heat transfer medium for a low-temperature District Cooling network. An additional benefit from using CO₂ instead of seawater as the heating medium is the mitigation of fouling phenomena in heat exchangers that may lead to minor maintenance tasks. Regarding the manufacturing materials, the cost could be reduced because CO₂ is a non-corrosive fluid and expensive materials (e.g., titanium) are not required.

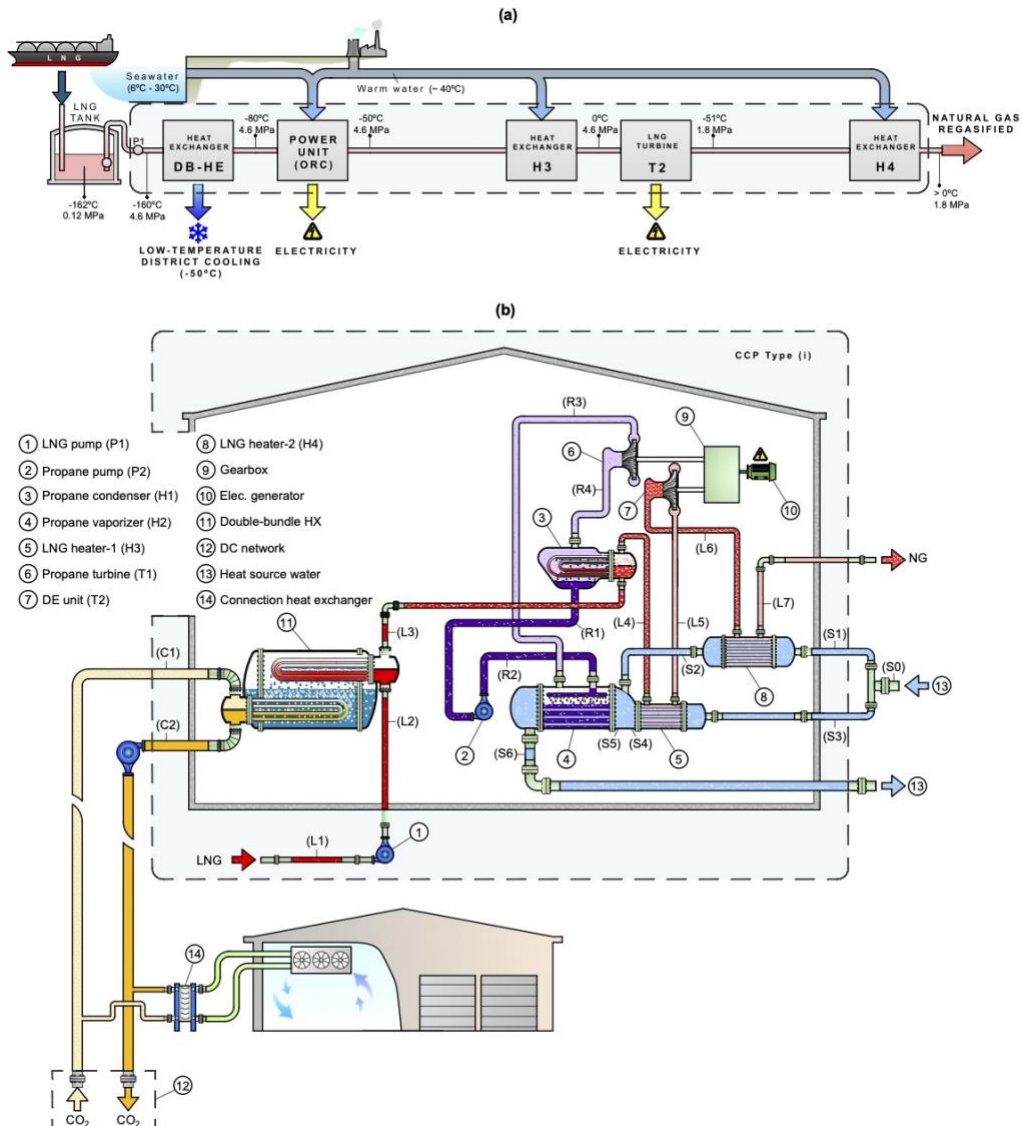


Figure 4.2. A Combined Cold and Power (CCP) system Type (i) for the combined production of electric power and low-temperature refrigeration for the agro-food industry sector. Redrawn from [211].

However, a major weakness of CO₂ is its freezing point (-55.6°C) which is relatively high with respect to LNG temperature. Thus, direct contact between LNG and CO₂ streams must be avoided in order to prevent the freezing of CO₂. Regarding this technical issue, Intermediate Fluid heat exchangers are a promising technology [223]. Figure 4.3 shows a schematic diagram of this type of heat exchanger, whose structure looks like those conventional Intermediate Fluid Vaporizers utilized for regasifying LNG using seawater as the heat source and without low-temperature exergy recovery [66,248,249], as explained in the Chapter 1. Hereafter, this technology of heat exchanger is referred to as *double-bundle* heat exchanger (DB-HE) as in Hewitt [250].

The proposed vaporizer consists basically of a sort of shell-and-tube type heat exchanger with two U-tube bundles both inside a single shared shell [251]. The shell is filled with a fluid (so-called *intermediate fluid* or *thermal buffer fluid* – TBF) which “pumps” the heat from the heating medium (CO₂) to the LNG and avoiding the direct contact between both streams. The LNG flows inside the upper tube bundle. On the other hand, the CO₂ stream that flows inside the bottoming tube bundle is used both as heating medium to regasify LNG and as heat transfer media to recover the low-temperature thermal energy from the LNG stream. CO₂ enters the tubes at saturated vapour conditions, and it leaves the tube bundle as saturated liquid. A similar vaporizer was proposed by Pineda Quijano et al. [223], although few details were given about the modelling, geometrical design parameters and the selection of the intermediate fluid. As for the most suitable TFB, ethane is selected because it is a not-in-kind fluid with a low freezing point (-182.8°C)

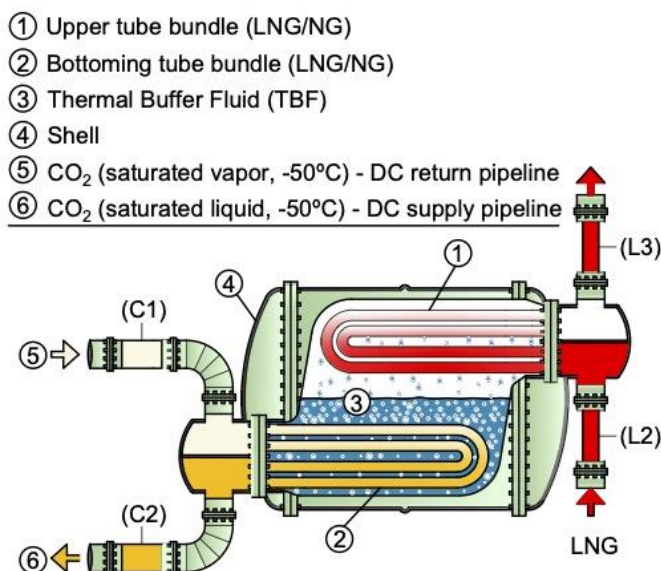


Figure 4.3. Double-bundle U-tube LNG vaporizer with low-temperature exergy recovery.
 Figure published in [211].

and a relatively low normal boiling point (-88.6°C) which avoids operating at vacuum conditions. Although ethylene is recommended as TBF in previous studies due to the heat transfer area estimated is somewhat lower [223,251], ethane is preferred in this chapter since it allows operating at a lower pressure.

The operation of the DB-HE is very alike that of a heat pipe. The TBF filling the shell is at saturated conditions, and it shifts continuously its phase between boiling and condensing. It condenses in the outside surface of the tubes of the upper tube bundle. The latent heat released from the TBF condensation is absorbed by the LNG stream so that it is heated-up and regasified. The TBF condensate drops flow downward by the influence of gravity, and they are accumulated in the bottoming part of the shell forming a pool that covers completely the tube bundle where the CO_2 flows through. Notice that the CO_2 tube bundle has to be fully submerged in the TBF pool to avoid local surface temperatures of tubes below CO_2 freezing point. Then, the TBF vaporizes by absorbing heat from the CO_2 stream in the bottoming tube bundle. Then, the vaporized fluid occupies the upper space of the shell where the LNG tube bundle is located, and the system remains working with a kind of closed-loop operation.

A remarkable difference between the CCP-(i) system and the CP plant is the temperature at which LNG is used as a heat sink in the RC (stream L3). While in the only-power system the pressurized LNG is used directly as a heat sink in the propane RC, the CCP system exploits the low-temperature exergy of LNG for refrigeration production before its use as a heat sink. As a result, the temperature of LNG at the inlet of the propane condenser (stream L3) shall be much lower for the reference system than that of the CCP system. As shown later, this fact has consequences on the electric power produced. Furthermore, the CCP-(i) system has significant differences with respect to a conventional CCP system. As shown in Figure 4.4 (a), a conventional CCP system requires the combustion of a fuel (e.g., natural gas, oil, coal) to produce the high-temperature thermal energy that is converted into mechanical energy by a prime mover (e.g., engines, steam or gas turbines). Afterwards, the rejected waste heat is used to drive a sorption chiller that produces the refrigeration effect [252].

On the other hand, Figure 4.4 (b) illustrates the general principle of a CCP system based on the physical exergy recovery from LNG-regasification. In this case, the refrigeration effect is produced directly through heat exchangers in which the low-temperature thermal energy (cold at -162°C) given off by the LNG-regasification is recovered. Therefore, it is not necessary to use sorption systems to produce refrigeration. The electric power is produced in a cryogenic power cycle (i.e., Rankine cycle) in which LNG is used as a heat sink or/and in a direct expansion unit to take advantage of the excess pressure. Regarding the heat source, seawater and warm water (for example, process water from cooling circuits of industrial processes) are considered in this work. A remarkable point of an LNG-based CCP system is that there is no combustion of the regasified natural gas in the plant, so its chemical exergy as fuel is fully preserved for later uses. Hence, the regasified natural gas is considered another useful output of the

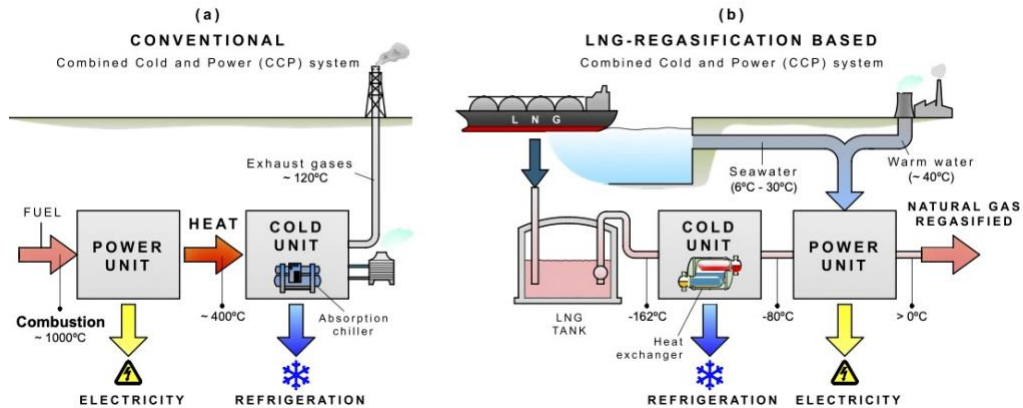


Figure 4.4. Conceptual comparison between (a) a conventional CCP system and (b) a non-combustion CCP system based on LNG physical exergy recovery. Source: [211].

system. As a result, an LNG based CCP system may operate upstream of a conventional CCP system.

4.2.3. Combined Cold and Power (CCP) unit: Type (ii)

Figure 4.5 shows the CCP-(ii) system. Although this configuration also produces electric power and refrigeration simultaneously, unlike the CCP-(i) unit presented above (see Figure 4.2), the refrigeration is produced at temperatures suitable for air-conditioning applications at buildings rather than for low-temperature refrigeration.

The power generation module is almost identical as for the cryogenic power unit illustrated in Figure 4.1. The LNG low-temperature exergy is fully preserved before being exploited as a heat sink by the propane RC, and the electric output of the CCP-(ii) system is almost identical to the produced by the benchmark cryogenic power unit. This configuration aims to harness the low-temperature exergy content remaining in the following gas streams:

- Stream leaving the propane condenser (stream L4, see Figure 4.5) at -50°C still has a temperature low enough to be further utilized to produce extra refrigeration.
- Stream leaving the DE unit (stream L6, see Figure 4.5). Notice that after the expansion, not only the pressure but also the temperature of the stream, leaving the DE unit (stream L7) has decreased.

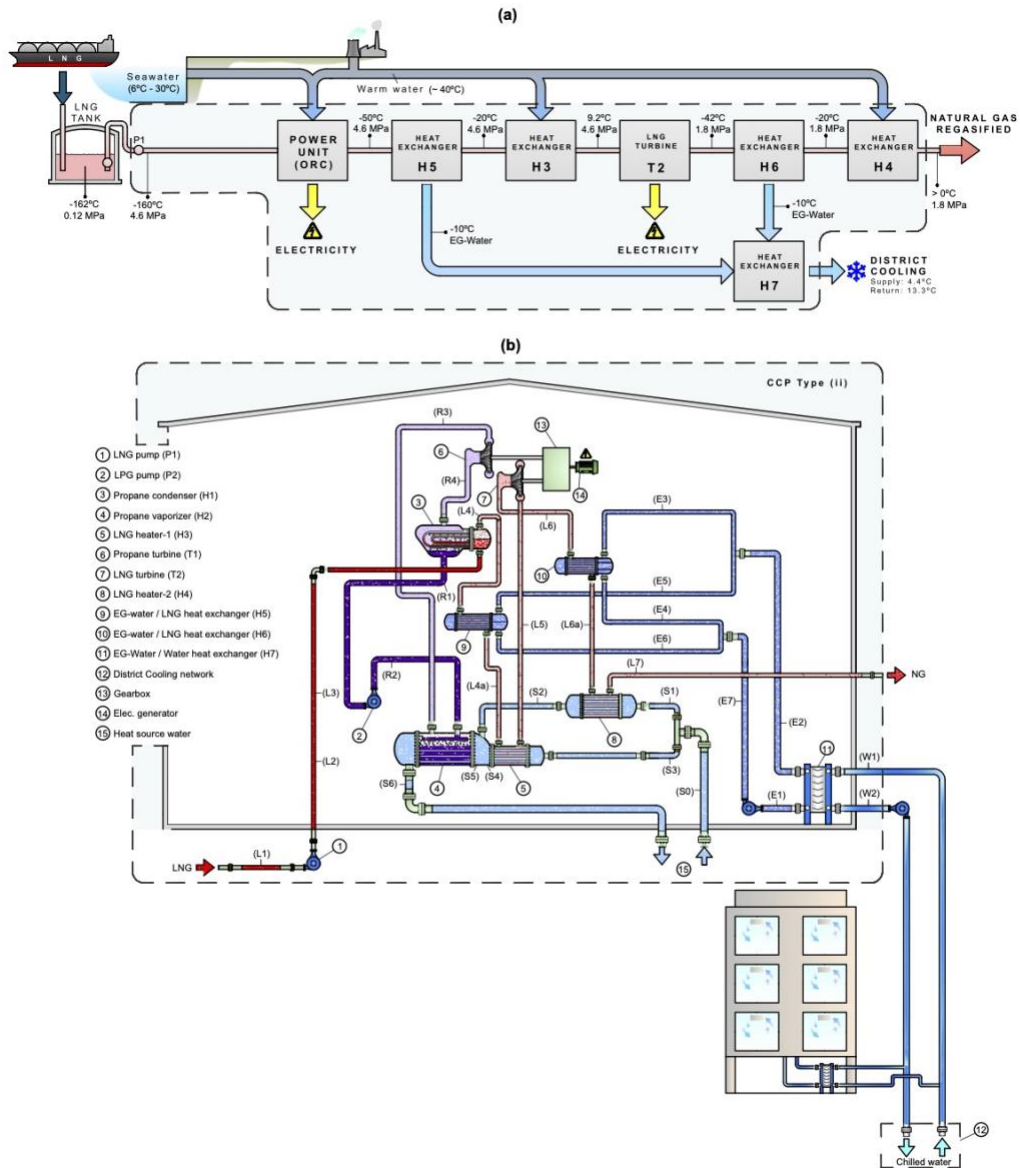


Figure 4.5. A Combined Cold and Power (CCP) system Type (ii) for the combined production of electric power and refrigeration for air-conditioning applications. Figure redrawn from [93].

Although the temperature of these streams is still well below the ambient, it is not low enough to be utilized in low-temperature refrigeration applications, but rather for air-conditioning applications. For this purpose, the shell-and-tube heat exchangers H5 and H6 are introduced downstream of streams L4 and L6, respectively. In each of these heat exchangers, the low-temperature thermal energy is transferred from LNG to an Ethylene

Glycol (EG) – water solution (35%) stream which is cooled from 0°C to –10°C. Then, as shown in Figure 4.5, the EG-water streams leaving the heat exchangers H5 and H6 (streams E4 and E6, respectively) join together in stream E7 which enters the plate-and-frame heat exchanger H7. In that heat exchanger, the low-temperature thermal energy is transferred to the chilled water of a **conventional DC network** (CDC) which distributes and yields the cold for air-conditioning use to buildings located inside the LNG terminal (control buildings, offices, and so forth). The design supply and return temperatures of this conventional DC network are set to 4.4°C and 13.3°C, respectively [253].

On the other hand, the LNG stream leaving H5 (stream L5) with a temperature of around –20°C is superheated up to a temperature above 0°C by taking the heat from the heat source water in the heat exchanger H3. Finally, the regasified natural gas (stream L8) is heated up to the set-point temperature of the distribution pipeline (> 5°C) in the heat source water of heat exchanger H4.

4.2.4. Polygeneration plant

Figure 4.6 shows a block diagram (Figure 4.6 (a)) and the schematic layout of the polygeneration plant (Figure 4.6 (b)) based on LNG-regasification studied in this chapter of the thesis. Concerning the polygeneration system developed in the previous chapter of the thesis, this configuration stands out by a more straightforward structure with fewer equipment and subsystems “squeezing” the LNG exergy content. That reduction in complexity may be positive from the techno-economic point of view and for the energy management, but at the expense of a less complete cascaded exploitation of LNG exergy.

The structure consists of hybridization between the CCP-(i) and the CCP-(ii) systems described in the sections above. As a summary, the polygeneration plant exploits the LNG physical exergy in cascade and provides the following services:

- 1) **LNG regasification** (assumed as a baseload regasification unit).
- 2) **Electricity production** for on-site consumption.
- 3) **Low-temperature refrigeration** to handle the thermal load of deep-freeze warehouses (foodstuff industry applications).
- 4) **Conventional refrigeration** service for in-situ air-conditioning applications (e.g., buildings of the polygeneration plant).

Notice that, although it is not addressed the transient performance analysis of this plant and the previous configurations presented in this chapter, the incorporation of cold thermal energy storage would allow collecting the LNG cold energy surplus at off-peak refrigeration load periods for use at peak load periods. This would provide operational flexibility and reliability to the DC networks (LT-DC and CDC), increase their effective refrigeration capacity and reduce the response time to refrigeration load variations.

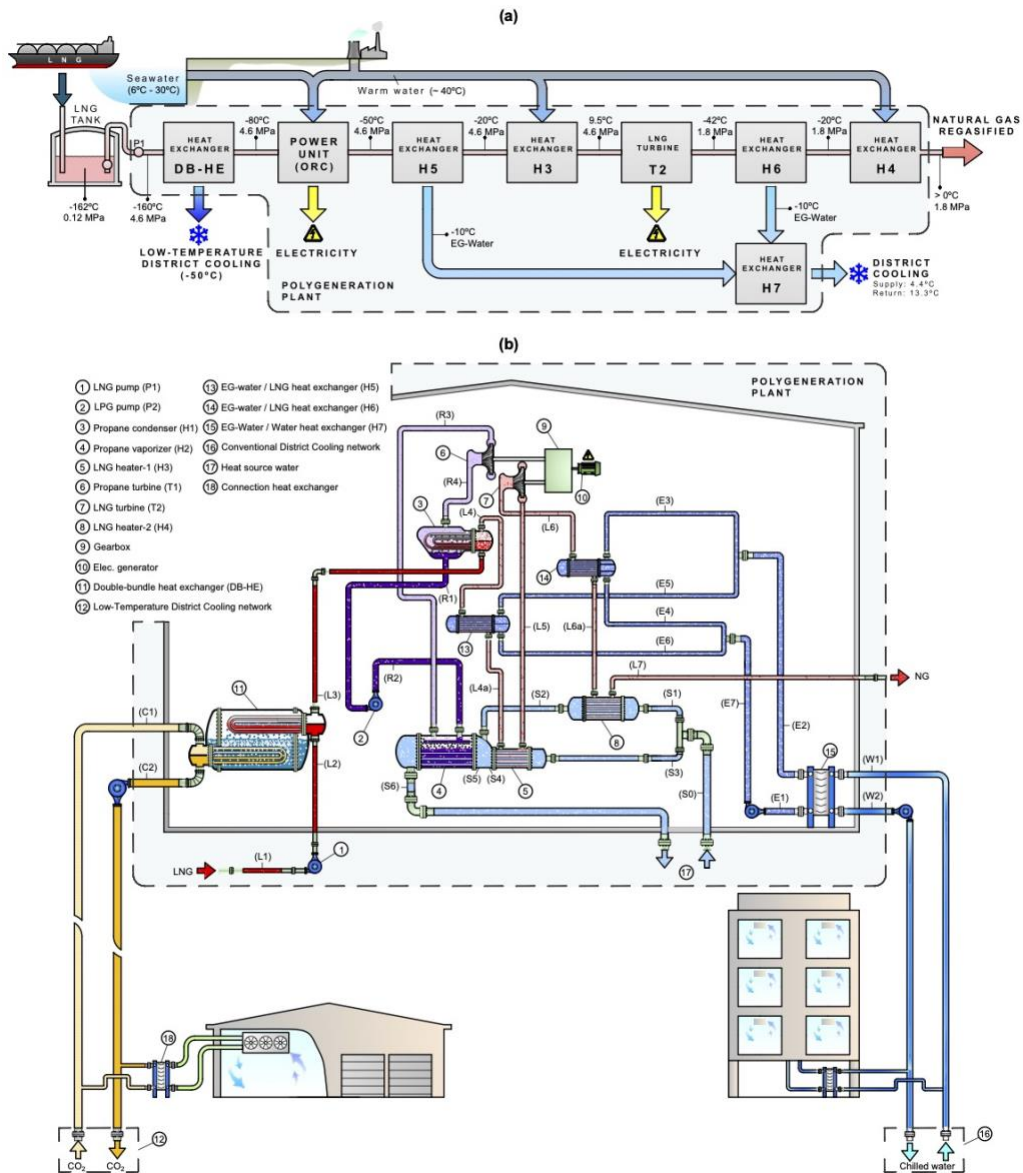


Figure 4.6. A Polygeneration plant with physical exergy utilization for the simultaneous production of electric power and refrigeration at two temperature levels. (a) Block diagram. (b) Detailed schematic layout. Redrawn from [55].

The operation polygeneration plant depicted in Figure 4.6 operates as follows. Firstly, the LNG stream pumped from the tanks enters the double-bundle heat exchanger (DB-HE) to produce low-temperature refrigeration. Afterwards, LNG at -80°C is utilized as the heat sink in the propane RC, and the stream leaving at -50°C is utilized to produce

refrigeration for air-conditioning applications in the heat exchanger H5. Once superheated (from -20°C to $>0^{\circ}\text{C}$) in the heat source water heat exchanger H3, the stream L5 is expanded in the DE unit. The temperature drop that occurs after the expansion is harnessed to produce extra refrigeration for air-conditioning applications. Finally, the natural gas is heated from -20°C up to a temperature $>0^{\circ}\text{C}$ in the heat exchanger H4.

4.3. Modelling and performance indicators

4.3.1. Thermodynamic modelling

The modelling of the different configurations presented in this chapter of the thesis is developed using the software Engineering Equation Solver [88]. On the other hand, Table 4.2 depicts the design parameters utilized. Many of these parameters are selected accordingly with those available in the literature for the actual cryogenic power unit used as a reference [92,193,246,254]. As other authors did [255], the aim is to use operation parameters as realistic as possible to confirm the reliability of the models developed. The main modelling assumptions are the following:

- System operation under steady-state conditions.
- Kinetic and gravitational energies are not considered.
- Fluids leakages are not considered.
- Pressure and thermal losses throughout heat exchangers and pipes are not considered.
- Natural gas and seawater are assumed as pure methane and regular water, respectively.
- Isentropic efficiencies of turbines and pumps are 80% and 75%, respectively.
- Efficiency of gearbox and electric generator are 95% and 97%, respectively.
- The condensing pressure of propane is a fixed parameter.
- The EG-water flow rate is adjusted to operate always at the design temperatures.
- Heat source water (Seawater/process water) discharge pressure is 300 kPa.
- The power consumption of EG-water and chilled water pumps are not considered.
- The polygeneration plant regasifies a constant LNG flow throughout the year (that is assumed to be lower than the baseload rate of the whole terminal).
- The electric power generated is self-consumed in the terminal, without surplus.

Table 4.2. Design parameters for the proposed cascaded configurations for exploiting the LNG physical exergy.

Subsystem	Design parameter	Configuration			
		CP	CCP-(i)	CCP-(ii)	Polygeneration
LNG/NG	LNG mass flow rate (\dot{m}_{LNG}), t/h	150	150	150	150
	LNG storage temperature (T_{L1}), °C	-162	-162	-162	-162
	LNG storage pressure (p_{L1}), kPa	120	120	120	120
	Regasification pressure ($p_{L2} \dots p_{L5}$), kPa	4,600	4,600	4,600	4,600
	Temperature at the inlet of H1 (T_{L3}), °C	-162	-80	-162	-80
	Temperature at the exit of H2 (T_{L4}), °C	-50	-50	-50	-50
	Temperature at the exit of H3 (T_{L5}), °C	0	0	0	0
	Temperature at the exit of H4 (T_{L7}), °C	5	5	5	5
	Temperature at the exit of H5 (T_{L7}), °C	-	-	-20	-20
	Temperature at the exit of H6 (T_{L7}), °C	-	-	-20	-20
	Regasified NG delivery pressure (p_{L6} , p_{L7}), kPa	1,800	1,800	1,800	1,800
Rankine Cycle	High pressure (p_{R2} , p_{R3}), kPa	620	620	620	620
	Low pressure (p_{R1} , p_{R4}), kPa	130	130	130	130
Low-temperature DC network	CO ₂ supply temperature (sat. liquid), °C	-	-50	-	-50
	CO ₂ return temperature (sat. vapor), °C	-	-50	-	-50
	Length, km	-	2	-	2
Conventional DC network	EG-water temp. at the inlet/outlet of H5 (T_{L7}/T_{L7}), °C	-	-	0 / -10	0 / -10
	EG-water temp. at the inlet/outlet of H6 (T_{L7}/T_{L7}), °C	-	-	0 / -10	0 / -10
	EG-water temp. at the inlet/outlet of H7 (T_{L7}/T_{L7}), °C	-	-	-10 / 0	-10 / 0
	Chilled water supply/return temperature	-	-	4.4 / 13.3	4.4 / 13.3
Heat source fluid	Total temperature drop ($T_{S0} - T_{S6}$), °C	6	6	6	6
	Discharging pressure, kPa	300	300	300	300
	Design heat source fluid temperature (T_{S1})	30°C	30°C	30°C	30°C

The heat transfer rate in each heat exchanger of the plant is calculated from energy balances and heat transfer equations as follows:

$$\dot{Q} = \dot{m}_i(h_{i,in} - h_{i,out}) = \dot{m}_j(h_{j,out} - h_{j,in}) \quad (4.1)$$

$$\dot{Q} = U_m \times A \times \Delta T_m \quad (4.2)$$

where, A is the heat transfer area, ΔT_m is the effective mean temperature difference between the fluids involved in each heat exchanger and U_m is the mean overall heat transfer coefficient.

Particularly, since the LNG regasification design pressure is above the critical value, the heat transfer for LNG/NG streams in the upper tube bundle of the DB heat exchanger or in the heat exchanger H1 is divided into two areas [66]: (1) temperature of LNG below the critical value, and (2) temperature of LNG above the critical value:

$$\dot{Q}_{LNG/NG} = \dot{Q}_{T < T_c} + \dot{Q}_{T > T_c} \quad (4.3)$$

$$\dot{Q}_{LNG/NG} = (U_m A \times \Delta T_m)_{T < T_c} + (U_m A \times \Delta T_m)_{T > T_c} \quad (4.4)$$

Unlike in the previous chapter, in this part of the thesis the calculation of the heat transfer area is necessary for the different sensitivity analysis performed and for the economic feasibility evaluation. The heat transfer area of the shell-and-tube type heat exchangers is calculated as follows:

$$A = N_t (\pi \times D_o \times L) \quad (4.5)$$

In the case of the plate-and-frame heat exchanger (H7), the heat transfer area is calculated as follows [256]:

$$A = N \times W \times H \times \phi \quad (4.6)$$

where, N , W and H are the number of plates, width, length of the heat exchanger, respectively, and ϕ represents the area increment factor owing to the corrugations of the plates.

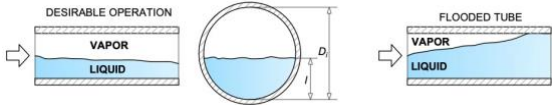
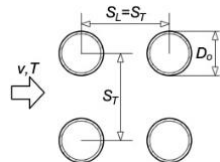
On the other hand, the overall heat transfer coefficient (U) based on the outside tube diameter is calculated from the following general expression:

$$\frac{1}{U} = \frac{1}{\alpha_i} \frac{A_o}{A_i} + R_{f_{o,i}} \frac{A_o}{A_i} + \frac{D_o}{2k} \ln \left(\frac{D_o}{D_i} \right) + R_{f_{o,o}} + \frac{1}{\alpha_o} \quad (4.7)$$

The thermal conductivity of the tubes (k) is set to 45 W/(m·K). The fouling factor (R_f) is set to 0.088 (m²·K)/kW [257] only in those heat exchangers in which the heat source fluid (either seawater or process water from cooling towers) is involved: heat exchangers H2, H3 and H4. Since the heat source fluid always flows through the tubes, the outer fouling factors ($R_{f_{o,o}}$) are not considered in any heat exchanger. The geometrical parameters of tubes (e.g., diameters and length of tubes) and the heat transfer areas of each heat exchangers are shown later in Section 4.4.1. Operating constraints such as fluids velocities, maximum allowable condensate loading in tubes, and so on, have been considered in the sizing of the heat exchangers and are depicted in Table 4.3. Notice that the velocity limits set for the fluid streams are consistent with their densities [258], allow operating with commercially available components (e.g., tube lengths and diameters), and allows avoiding operational problems such as freezing, erosion or vibrations.

The different convective heat transfer (or “*film*”) coefficients (α) are estimated from different well-known correlations available in the literature that best match the heat transfer mechanism, the fluids and the operating conditions (i.e., temperature, pressure and flow rate) of each heat exchanger that integrates the configurations presented in this chapter of the thesis. The selected correlations are the following: Correlation of Shah for

Table 4.3. Design criteria and constraints for the different heat exchangers integrated in the configurations developed in this chapter.

Heat exchanger	Design criteria/constraint	Remark
DB-HE	<ul style="list-style-type: none"> $\dot{m}_{CO_2} < 1,570 \times N_t \times \rho_L \times D_i^{2.56}$ N_t: number of tubes. ρ_L: density as liquid, kg/m³. D_i: inner tube diameter, m. $T_{w,t} > -54^\circ\text{C}$ $v_{CO_2,in} < 30 \text{ m/s}$ $L_t < 20 \text{ m}$ 	<p>Maximum allowable condensate loading (in kg/h) to avoid the flooding phenomena that will damage the heat transfer [259,260].</p>  <p>CO₂ tubes: Minimum inner wall temperature fixed to prevent freezing.</p> <p>Velocity of CO₂ streams at vapor state at the entry of the tubes is limited to avoid problems with erosion of the tube material and vibrations issues.</p> <p>Maximum straight length allowed for the U-tubes of both bundles due to constructional constraints.</p>
H1	<ul style="list-style-type: none"> $G_{LNG} = 300 \text{ kg}/(\text{s}\cdot\text{m}^2)$ 	Reference design value for the natural gas mass flux to keep the velocity of the inlet and outlet streams under desirable values (i.e., consistent with the density at each point). This mass flux is within the range found literature focused on LNG vaporizers (e.g., 600 kg/(s·m ²) [66], 210 kg/(s·m ²) [261]).
H2	<ul style="list-style-type: none"> $1 \text{ m/s} < v_{HSW} < 3 \text{ m/s}$ 	Too low velocities of heat source water streams (seawater or process water) may favour very low local temperatures and the formation of ice; whilst too high velocities may cause vibration and erosion problems. The tube lengths utilized should ensure operating within this velocity range.
H3	<ul style="list-style-type: none"> $v_{LNG,max,in} = 4 \text{ m/s}$ 	<p>Design maximum velocity of natural gas streams flowing across the banks of tubes (just at the inlet of the heat exchanger) and considering an aligned (square) tube layout pattern.</p> $v_{max} = v \times \frac{S_T}{S_T - D_o}$ <p>D_o: Outer tube diameter, m. S_T: Transverse pitch, m.</p> 
	<ul style="list-style-type: none"> $1 \text{ m/s} < v_{HSW} < 3 \text{ m/s}$ 	A similar tube length has been used for this heat exchanger in all the configurations analysed but ensuring an operating velocity within the range.
H4	<ul style="list-style-type: none"> $v_{LNG,max,in} = 8 \text{ m/s}$ $1 \text{ m/s} < v_{HSW} < 3 \text{ m/s}$ 	<p>Design maximum velocity of natural gas streams flowing across the banks of tubes (just at the inlet of the heat exchanger) and considering an aligned (square) tube layout pattern.</p> <p>Design velocity limits for the heat source water streams through tubes.</p>
H5	<ul style="list-style-type: none"> $v_{LNG,max,in} = 4 \text{ m/s}$ $1 \text{ m/s} < v_{EG/water} < 2 \text{ m/s}$ 	<p>Design maximum velocity of natural gas streams flowing across the banks of tubes (just at the inlet of the heat exchanger).</p> <p>Design velocity limits for the EG-water streams through tubes.</p>
H6	<ul style="list-style-type: none"> $v_{LNG,max,in} = 6 \text{ m/s}$ $1 \text{ m/s} < v_{EG/water} < 2 \text{ m/s}$ 	<p>Design maximum velocity of natural gas streams flowing across the banks of tubes (just at the inlet of the heat exchanger) and considering an aligned (square) tube layout pattern.</p> <p>Design velocity limits for the EG-water streams through tubes.</p>
H7	<ul style="list-style-type: none"> $v \sim 0.5 - 1 \text{ m/s}$ 	Design velocity limits for both the EG-water and chilled water streams through the cannels of the heat exchanger. Nonetheless, higher

Designation of heat exchangers: **DB-HE**: Double-bundle heat exchanger. **H1**: Propane condenser / LNG vaporizer. **H2**: Propane vaporizer. **H3**: Heat source water heater No. 1. **H4**: Heat source water heater No. 2. **H5**: EG-water heat exchanger No. 1. **H6**: EG-water heat exchanger No. 2. **H7**: EG-water / chilled water heat exchanger.

conventional tubes [262] for the condensation of CO₂ in the DB heat exchanger; the correlation of Jung et al. [263] is used for the boiling of the TBF in the DB heat exchanger and for propane in the vaporizer H2; for the condensation of propane in heat exchanger H1, the correlation of Jung et al. [264] is used; for the LNG/NG, the correlation of Bae and Kim [265] and that of Liang et al. [266] are used when the temperature is below and above the critical value, respectively. For the superheated NG flowing across the tube bank in heat exchangers H3 and H4, the correlation of Zukauskas for tubes arranged in-line is used [267]. Regarding the heat source fluid inside tubes in heat exchangers H2, H3 and H4, the Dittus-Boelter correlation is used. Finally, the correlation of Thonon [268] is utilized for the plate-and-frame heat exchanger (H7). The detailed description of these correlations and the film coefficients and temperature profiles in the heat exchangers are shown in [Appendix C](#).

On the other hand, the overall heat transfer coefficient is strongly dependent on the flow Reynolds number, heat transfer surface geometry, and fluids physical properties [257]. Therefore, in practical cases, the overall heat transfer coefficient varies throughout the heat exchanger, particularly, when the phase change occurs, or there are large temperature variations for the different streams which introduce variations in fluid properties and flow conditions. For the sake of modelling simplicity, it is assumed that U varies linearly with A throughout each of these two parts. Thus, U_m is approximated as the arithmetic value between the U values at the ends of the exchangers or between the ends of those sections in which the heat exchangers are divided (denoted by the subscripts a and b) [257,269]:

$$U_m \cong \frac{1}{2}(U_a + U_b) \quad (4.8)$$

Also, a linear variation with \dot{Q} is assumed for the temperature difference between the streams, so ΔT_m is approximated as the log-mean temperature difference (*LMTD*), which is calculated from the following mathematical expression:

$$LMTD = \frac{\Delta T_a - \Delta T_b}{\ln(\Delta T_a / \Delta T_b)} \times F \quad (4.9)$$

where, ΔT_a and ΔT_b represent the temperature difference between the hot and cold fluid streams on the ends of the heat exchanger. Particularly, for the bottoming tube bundle of the DB heat exchanger, both the CO₂ and the thermal buffer fluid (ethane) are pure fluids undergoing a phase change, so ΔT_m remains constant throughout.

The correction factor F gives a measure of the deviation of the LMTD from the corresponding values for the counter-flow case. Since heat exchangers with more than one tube pass can have some portions in concurrent flow or crossflow, the heat transfer is less effective than for the countercurrent flow case. Therefore, F is less than 1 for multitubepass and cross-flow exchangers, except for the particular case of isothermal boiling or condensing streams for which F is always 1 [270]. The value of this factor

depends on the geometry of the heat exchanger and the inlet and outlet temperatures of fluids streams. It can be calculated from analytical expressions or charts available in most heat transfer textbooks. Among all the heat exchangers integrated into the different configurations presented in this chapter of the thesis, the correction factor (F) to the $LMTD$ is applied only for EG-water heat exchangers H5 and H6 (included in the CCP-(ii) unit and the polygeneration plant) which have multiple tube passes (2 and 4, respectively). In the case of DB heat exchanger and heat exchangers H1 and H2, at least one of the fluids involved in the heat transfer undergoes a phase-change, so again no correction factor to the $LMTD$ is applied. The heat exchangers H3 and H4 have only one tube pass, and it is considered that the NG stream flowing in the shell side is fully mixed in any cross-section. Therefore, a uniform NG temperature is assumed in the entire cross-section of these heat exchangers and the $LMTD$ is defined as for a countercurrent configuration without applying any correction factor [271]. On the other hand, since the design of the polygeneration plant is drawn from the CCP-(i) system, these heat exchangers that are common for both configurations have the same heat transfer area. The same applies to heat exchangers that are common for the cryogenic power plant and the CCP-(ii) system.

A very detailed design and modelling of the heat exchanger is out of the scope of this chapter. The objective is to estimate an approximated heat transfer area that could be utilized later to get an estimation of the equipment cost. In this sense, the assumptions made for the U and ΔT_m described above allow estimating the heat transfer areas with a low computational cost and with an acceptable trade-off between accuracy and simplicity. However, it should be noticed that a more accurate estimation of the heat transfer area requires to divide the heat transfer domain by applying a finite-difference method to account the arbitrary variations of U through the heat exchanger, that especially occurs in the double-bundle heat exchanger or the propane condenser. But even if an exhaustive division of the area is considered, the correlations utilized to predict the film coefficients are major source uncertainty for the calculation of the heat transfer area. Thus, in future research particularly focused on a detailed study of the heat exchangers, it will be required the utilization of “*custom-made*” correlations for the specific fluids involved and their operating temperatures. Also, the real composition of LNG should be considered. Developing experimental setups would be necessary.

Finally, Table 4.4 depicts the description and mathematical definition of the performance indicators utilized to evaluate the different configurations presented.

4.3.2. Economic analysis

An economic analysis is desired to evaluate and compare the feasibility of the different configurations developed. This analysis is performed based on the results obtained from the steady-state simulation of the plant described in detail in section 4.4.1.1. The following assumptions are made for the economic analysis of each configuration:

Table 4.4. Description and mathematical definition of the performance indicators utilized for the performance analysis of the different configurations proposed.

Designation	Name and description	Mathematical definition	Eq.
\dot{W}_{net} , kW	Total net electric power produced by the system, calculated as the sum of the power produced by the propane RC and the NG DE unit.	$\dot{W}_{net} = \dot{W}_{net,ORC} + \dot{W}_{net,DE} = \eta_{eg}\eta_{gb}(\dot{W}_{T1} + \dot{W}_{T2}) - (\dot{W}_{P1} + \dot{W}_{P2})$	(4.10)
\dot{Q}_{LTDC} , MW	Low-Temperature refrigeration production: Accounts for the refrigeration demand covered by recovering the low-temperature exergy component of LNG in the double-bundle heat exchanger.	$\dot{Q}_{LTDC} = \dot{m}_{LNG}(h_{L3} - h_{L2}) = \dot{m}_{CO2}(h_{C1} - h_{C2})$	(4.11)
\dot{Q}_{CDC} , MW	Conventional refrigeration production: Accounts for the refrigeration produced for air-conditioning applications.	$\dot{Q}_{CDC} = \dot{m}_{LNG}[(h_{L5} - h_{L4}) + (h_{L8} - h_{L7})] \cong \dot{m}_E c_{pE}(T_{E2} - T_{E1}) = \dot{m}_W c_{pW}(T_{W1} - T_{W2})$	(4.12)
<i>CRR</i>	Cold Recovery Ratio: Evaluates the relative performance of the plant with respect to an ideal system which could convert into useful energy the whole cryogenic energy of LNG from the initial state (stream L1) and up to the reference environment condition (set to 298.15 K and 101.325 kPa).	$CRR = \frac{\dot{W}_{net} + \dot{Q}_{LTDC} + \dot{Q}_{CDC}}{\dot{m}_{LNG}(h_0 - h_{L1})} \times 100\%$	(4.13)
<i>EEP</i> , kWh/t-LNG	Equivalent Electricity Production: Accounts in a single parameter the electricity produced by the plant, and also the equivalent electricity saved due to the refrigeration produced that otherwise should be produced by conventional vapor-compression systems. The reference Energy Efficiency Ratios (EERs) of conventional vapor compression systems are taken as 1.2 (W/W) and 4.1 (W/W) for the low-temperature and conventional DC, respectively [228].	$EEP = \frac{1}{\dot{m}_{LNG}} \left(\dot{W}_{net,tot} + \frac{\dot{Q}_{LTDC}}{EER_{LTDC}} + \frac{\dot{Q}_{CDC}}{EER_{CDC}} \right)$	(4.14)
η_{ex} (%)	Exergetic efficiency of the whole system: This indicator provides a measure regarding how the initial “quality” of LNG (due to its temperature and pressure far away from the reference environment, set to 298.15 K and 101.325 kPa) is preserved in the energy products of the plant. Notice that the definition utilized sets a conventional regasification system without exergy recovery as the zero-efficiency reference.	$\eta_{ex} = \frac{\Sigma \dot{W}_T + (\dot{E}x_{C2} - \dot{E}x_{C1}) + (\dot{E}x_{W2} - \dot{E}x_{W1})}{\Sigma \dot{W}_P + (\dot{E}x_{L1} - \dot{E}x_{L9})} \times 100\%$	(4.15)
<i>GHGA</i> , kg-CO ₂ e/t-LNG	Specific Greenhouse House Gases emissions avoided , which are evaluated utilizing an emission factor (EF) of 0.298 kg-CO ₂ e/kWh as a value representative for an electricity mix involving several energy sources (e.g., Spain [229]).	$GHGA = EF \times EEP$	(4.16)

- The implementation of a new plant is considered.
- The system operates 8,040 hours per annum for 30 years (plant’s lifetime, denoted by “*n*”).
- The annual discount rate (*i*) is set to 10%.

- The annual plant expenditures are the following: operation and maintenance (*O&M*) cost, overhead cost (*OC*), and insurance and taxes (*I&T*), assumed as 6%, 1% and 1% of the fixed capital investment (*FCI*), respectively.
- A linear depreciation of the plant during its lifetime.
- The salvage value at the end of the plant's lifetime is null.
- The electricity consumption by seawater pumping in a conventional ORV system is 6 kWh/t-LNG [58].

To evaluate the economic viability of the systems, first, it is necessary to acquire the purchase equipment cost (*PEC*) of the plant components. The purchased costs of the main components of the polygeneration plant are estimated using the cost functions listed in Table 4.5. The *PEC* of the circulation pumps (for CO₂, EG-water, and water) is neglected since it is insignificant compared to the *PEC* of the rest of the plant components. All the cost data obtained using these cost functions are based on the value of the US dollar (USD) at the time of the cost functions were first obtained and published. Therefore, to incorporate the effect of inflation on the estimated plant components cost are brought to the reference year (2018 in this study) as follows:

Table 4.5. Purchase cost functions for the different system components.

System component	Purchase cost function (USD)	Source
- Pumps (P1, P2)	$1120 \times \dot{W}_{P,(kW)}^{0.8}$	[272,273]
- Turbines (T1, T2)	$4750 \times \dot{W}_{T,(kW)}^{0.75}$	[212]
- Electric generator	$10 \times 10^6 [\dot{W}_{g,(kW)} / (160 \times 10^3)]^{0.7}$	[274]
- Shell-and-tube HEs (DB, H1..6) ⁽¹⁾	$3.28 \times 10^4 (A_{o,(m^2)} / 80)^{0.68} \times f_m \times f_p$	[275]
- Plate-and-frame HE (H7)	$635.14 \times A_{(m^2)}^{0.778}$	[276]
- Pipelines of CO ₂ DC network ⁽²⁾	$[4700 \times D_{i,(m)}^{1.7}] \times L_{(m)}$	[277]

⁽¹⁾ Material: stainless steel high grade ($f_m = 3.4$); Operating pressure: 0.7-5 MPa ($f_p = 1.5$).

⁽²⁾ Material: 316 stainless steel; Pipe diameter: DN 200 (supply line); DN 500 (return line); Length = 2 km.

$$PEC_{2018} = PEC_y \times \left(\frac{CI_{2018}}{CI_y} \right) \quad (4.17)$$

where PEC_{2018} is the 2018 cost, PEC_y is the cost estimated using the cost function at year y , CI_{2018} and CI_y are the cost indices for 2018 (reference year) and year y in which the original cost was obtained. The Chemical Engineering Plant Cost Index (CEPCI) annual average composite values are used to update all the costs to the reference year.

The fixed capital investment (*FCI*) accounts the direct and indirect costs of the plant. The direct costs often include the *PEC* and costs associated with its installation, piping, instrumentation and control systems, materials and other costs (e.g., land and service facilities). Whereas the construction, engineering and supervision costs and contingencies are included in the indirect costs. The total capital investment (*TCI*) of the plant is then the sum of *FCI* and other expenditures such as working capital, start-up costs, R&D and licensing costs. According to Bejan [278], the *FCI* and *TCI* are estimated using the simplified relationship based on the total *PEC* of the plant, Eqs. (4.18) and (4.19) respectively, and used hereafter to estimate the *FCI* and *TCI* of the different configurations studied:

$$FCI = 4.30 \times PEC \quad (4.18)$$

$$TCI = 6.32 \times PEC \quad (4.19)$$

The implementation of the newly envisioned polygeneration plant allows the supply of 150 t/h of regasified LNG and provide cold at two-temperature levels (21 MW at -50°C and 5.8 MW at 4.4°C , see section 4.4) when the plant operates at full capacity (i.e., capacity utilization factor, *CUF*, of 100%). However, in practice, the polygeneration plant will not operate at full load throughout the year (i.e., 8,040 hours at *CUF* of 100%) due to a number of factors including refrigeration and air-conditioning demand variations. Therefore, in order to account for this, capacity utilization factor was assigned for each output of the polygeneration plant: 90% for electricity; 70% for low-temperature refrigeration; and 50% for air-conditioning applications. Accordingly, the capital costs and operational expenditure associated with the conventional LNG regasification plant (i.e., Open Rack Vaporizers – ORV) and cold production facilities (i.e., low-temperature chiller and conventional DC chiller plant) that can deliver the same number of services could be avoided.

The typical capital investment for the ORV and compression chillers at the reference year are used: total capital of 43,500 USD/(metric ton of LNG regasified/hour) [279]; fixed capital of 750 USD/kW for conventional DC chiller plant [253]; and total capital 1,936 USD/kW for low-temperature chiller plant (refrigeration load at -25°C) [280]. Notice that the capital investment of the conventional DC network is not considered since it is supposed to exist regardless of whether or not the polygeneration plant is built. However, the capital investment of the low-temperature DC network (i.e., CO_2 DC network) is taken into account according to the pipeline cost given in Table 4.5.

The discounted payback time (*DPBT*), net present value method (*NPV*), and internal rate of return (*IRR*) are applied to evaluate the economic viability of the polygeneration plant and other considered type of systems (i.e., cryogenic power plant, CCP-i plant, and CCP-ii plant) to capitalize and compare their economic and environmental benefits. The polygeneration plant gross annual economic benefits are obtained because of (1) net generated electricity, (2) electricity-saving related to avoided consumption for cold

production and LNG regasification (i.e. electricity consumption of seawater and LNG pumps), (3) economic benefit due to avoided GHG emissions during electricity generation, and (4) avoided expenditures associated to the conventional systems (*O&M*, *OC*, *I&T*, and plant depreciation cost (*PDC*) of ORV and vapour compression chillers). Thereby, the annual gross economic benefits (*AEB*) of the polygeneration plant is expressed as:

$$AEB = C_e \times \left[\left(\dot{W}_{net,tot} \times CUF + \frac{\dot{Q}_{LTDC} \times CUF}{EER_{LTDC}} + \frac{\dot{Q}_{CDC} \times CUF}{EER_{CDC}} + \nabla \dot{W}_{P,SW} \right) \times 8040 \right] + C_{CO_2}^{tax} \times GHGA + \sum (O\&M + I\&T + OC + PDC)_{avoided} \quad (4.20)$$

where C_e is industrial electricity price in USD/kWh, CUF the capacity utilization factor, $\nabla \dot{W}_{P,SW}$ the net electrical power consumed by seawater pumps and $C_{CO_2}^{tax}$ denotes the carbon tax in USD/t-CO₂e. It should be noted that, in the economic analysis, the selling price of NG (after regasified) and LNG price are not considered since the sole objective of the proposed plant is to utilize the LNG physical exergy during regasification.

Then, the annual net cash inflows (*CF*, Eq. (4.21)) is obtained from the calculated annual gross economic benefit (Eq. (4.20)) of the polygeneration plant reduced by the plant's annual expenditure (i.e., *O&M* cost, *OC*, *I&T*, and *PDC*).

$$CF = AEB - \sum (O\&M \text{ cost}, OC, I\&T, \text{ and } PDC)_{polygeneration \text{ plant}} \quad (4.21)$$

The *NPV* is calculated using the following expression:

$$NPV = \sum_{k=0}^n \frac{CF_k}{(1+i)^k} \quad (4.22)$$

where i is the discount rate (10%), k is the investment period, CF_k the net cash inflow during period k and n the plant lifetime. In the *NPV* calculation, the *TCI* is considered as the difference between the *TCI* of the polygeneration plant and the avoided conventional systems (i.e., the sum of the *TCI* of ORV, low-temperature chillers and conventional DC plant chillers).

The *DPBT* determines the profitability of the plant by giving the time period at which the plant investment is recovered taking into account the annual discount rate, and it is when the *NPV* of the plant becomes positive. Another economic parameter also used to analyse the economic feasibility of the plant is the *IRR*, and its mathematical expression is given in Eq. (4.23). The polygeneration plant could be economically feasible if the *IRR* is higher than the considered annual discount rate.

$$\sum_{k=0}^n \frac{CF_k}{(1+IRR)^k} = 0 \quad (4.23)$$

In Eq. (4.22) and Eq. (4.23), the total capital investment is considered as a negative cash inflow at the beginning of plant operation.

4.4. Results and discussion

This section presents the discussion of the results obtained from the modelling and simulation of the different configuration proposed and their techno-economic feasibility. Since operating parameters such as the heat source temperature, the LNG regasification rate or pressure may vary over a typical year of operation, these systems are not only analysed for the base case operation, but also the off-design performance.

4.4.1. Thermodynamic and environmental performance

4.4.1.1. Base-case

Table 4.6 shows the power capacity of pumps and turbines, and Table 4.7 depicts the heat transfer area with some geometrical details for each exchanger of the considered configuration. Afterwards, Table 4.8 and Figure 4.7 show the performance results obtained by each configuration at design conditions (base case) and producing the same amount of LNG regasified (150 t/h). The main thermodynamic data of each state point are depicted in Table 4.9.

To start with, a remarkable conclusion is that **the power output predicted by the model developed for the reference CP plant is in agreement with those published in the open literature** for the power generation unit No.2 in Senboku II Terminal of Osaka Gas [193,254,281]. This verifies the accuracy of the model. The following observations are made:

- The electric power production of the CCP-(ii) system (6.05 MW, 40.3 kWh/t-LNG) slightly enlarges the electric power generation of the reference cryogenic power plant by 3.5%, which produces 5.84 MW (39.0 kWh/t-LNG). The size and generation capacity of the propane RC unit is the same in both the CP and CCP-(ii) units, but the shaft power of the DE unit is slightly higher in the CCP-(ii). The improvement is because the NG stream leaving the propane condenser (heat exchanger H2) is preheated in the heat exchanger H6, which entails a higher degree of superheating before the expansion and a higher power produced by the DE unit. This small improvement is also observed in the polygeneration plant, which enlarges by 5.6% that produced by the CCP-(i) at design conditions (3.4 MW, 22.4 kWh/t-LNG). But in overall terms and regardless the heat source temperature, the power output of the polygeneration configuration (3.5 MW, 23.6 kWh/t-LNG) is much lower (~40%) than the generated by the CP and the CCP-(ii) system.
- The contribution of the RC to the total power in both the CP and CCP-(ii) configurations is ~53% where the LNG temperature remains at around -160°C before LNG stream is used as a heat sink in the propane condenser H1 (see Figure 4.1 and

Table 4.6. Results for the power generation units in each configuration.

Configuration	Power capacity, kW			
	Pumps		Turbines	
	P1	P2	T1	T2
Cryogenic power plant	586.5	73.6	3,542	3,515
CCP-(i) system	586.5	16.3	783.2	3,515
CCP-(ii) system	586.5	75.8	3,596	3,687
Polygeneration plant	586.5	17.4	810.8	3,693

Table 4.7. Heat transfer area of heat exchangers for the different configurations considered.

Heat exchanger	Heat transfer area, m ² and (Length of tubes, m)			
	CP	CCP-(i)	CCP-(ii)	Polygeneration
Double-bundle HE (DBHE) ^a	-	2,569 (14)	-	2,569 (14)
Propane condenser (H1) ^b	604 (15)	181 (5)	604 (15)	181 (5)
Propane vaporizer (H2) ^c	707 (8)	220 (6)	707 (8)	220 (6)
Heat source water heater No. 1 (H3) ^c	116 (2.5)	129 (3.5)	116 (2.5)	129 (3.5)
Heat source water heater No. 2 (H4) ^c	166 (4)	181 (5)	166 (4)	181 (5)
EG-water HE No. 1 (H5) ^b	-	-	207 (4.5)	207 (4.5)
EG-water HE No. 2 (H6) ^b	-	-	232 (4)	232 (4)
EG-water/chilled water HE (H7) ^d	-	-	104 (-)	104 (-)

^a Upper tube bundle: $D_o/D_i = 19.05/16.10$ mm; Bottoming tube bundle: $D_o/D_i = 25.40/22.90$ mm.

^b Tube diameters: $D_o/D_i = 19.05/16.10$ mm.

^c Tube diameters: $D_o/D_i = 31.75/28.45$ mm.

^d Plate-and-frame heat exchanger. Chevron corrugations angle = 45°, Channel depth and width = 5 mm, and 940 mm, respectively; Area increment factor = 1.14. No. of plates = 63. Notice that this design is not based on a particular commercial heat exchanger, but typical geometrical parameters are used.

Figure 4.5). In contrast, the contribution of the RC to the total electricity production in the polygeneration plant and the CCP-(i) system is only ~20% because the low-temperature exergy of LNG is partially exploited earlier to produce refrigeration at -50°C so that the LNG enters the propane condenser at -80°C. Besides, lower temperature gradients lead into a lower propane flow rate in the RC and, consequently, lower heat transfer areas and seawater flow rates required for both the propane condenser H1 and vaporizer H2 (see Table 4.7). Regarding a typical LNG regasification facility without LNG exergy recovery, electric power is not produced, but consumed (mainly for pumping) so that negative performance indicators are obtained (see Table 4.8).

Table 4.8. Results obtained for the different configurations and for an LNG regasification rate of 150 t/h.

System	Net power, kW			Refrigeration, kW		Cold Recovery Ratio, %	Equivalent Electricity Production ^{a, b} , kWh/t-LNG				
	RC	DE	Total	LTDC	CDC		RC	DE	LTDC	CDC	Total
-Typical regasification*	-	-	-600	-	-	-	-	-	-	-	-3.9
- CP	3,190	2,653	5,843	0	0	15	21.3	17.7	-	-	39.0
- CCP-(i)	706	2,652	3,358	21,001	0	64	4.7	17.7	116.7	-	139.1
- CCP-(ii)	3,238	2,811	6,049	0	5,864	31	21.6	18.7	-	9.5	49.9
- Polygeneration	730	2,817	3,546	21,001	5,842	80	4.9	18.8	116.7	9.5	149.8

* Using seawater as heat source fluid and without LNG physical exergy recovery.

^{a, b} Reference Energy Efficiency Ratios: ^a Low-Temperature refrigeration: 1.2 (W/W) and ^b Conventional refrigeration: 4.1 (W/W).

Table 4.8 (cont.). Results obtained for the different configurations and for an LNG regasification rate of 150 t/h.

System	Heat source flow rate, t/h	Exergetic efficiency, %					Avoided GHG emissions ^c , kg-CO ₂ e/t-LNG				
		RC	DE	LTDC	CDC	Total	RC	DE	LTDC	CDC	Total
- Typical regasification *	4,800	-	-	-	-	0	-	-	-	-	-
- CP	6,000	16.3	49.5	-	-	23.7	6.3	5.3	-	-	11.6
- CCP-(i)	2,600	26.5	49.5	41.1	-	40.3	1.4	5.3	34.8	-	41.5
- CCP-(ii)	6,000	16.6	50.0	-	23.2	25.7	6.4	5.6	-	2.8	14.9
- Polygeneration	2,600	27.4	50.0	41.1	23.2	42.1	1.5	5.6	34.8	2.8	44.6

* Using seawater as heat source fluid and without LNG physical exergy recovery.

^c GHGs emission factor: 0.298 t-CO₂e/kWh and for an ideal capacity factor of 100%.

- The polygeneration plant produces the same amount of refrigeration at -50°C (21 MW) than the CCP-(i) system; and the same amount of refrigeration at 4.4°C than the CCP-(ii) system. This fact offsets its lower electricity output in comparison with most of the other systems, showcasing the highest equivalent electricity production (*EEP*). According to the Cold Recovery Ratio (*CRR*) reported for the base-case operation, the polygeneration plant transforms up to 80% of the cryogenic energy of LNG into useful energy outputs, and the *EEP* is nearly 150 kWh/t-LNG. This value is 7.7% higher than the reported by the CCP-(i) system and almost four times higher than the reported by the cryogenic power plant. Likewise, the CCP-(ii) system enlarges by 28% the *EEP* of the cryogenic power plant, but this amount is well below the obtained by the polygeneration unit or the CCP-(i) system.
- The exergetic efficiency reported by the polygeneration plant (40-43%) slightly surpasses that obtained by the CCP-(i) system (38-41%). This small improvement is due to the low exergetic value of the refrigeration produced at 4.4°C. Anyway, the refrigeration production at -50°C has a *high quality* from the exergetic point of view; this explain the great improvement with respect to the cryogenic power plant and the CCP-(ii) system whose efficiencies are below 30%. Regarding the environmental

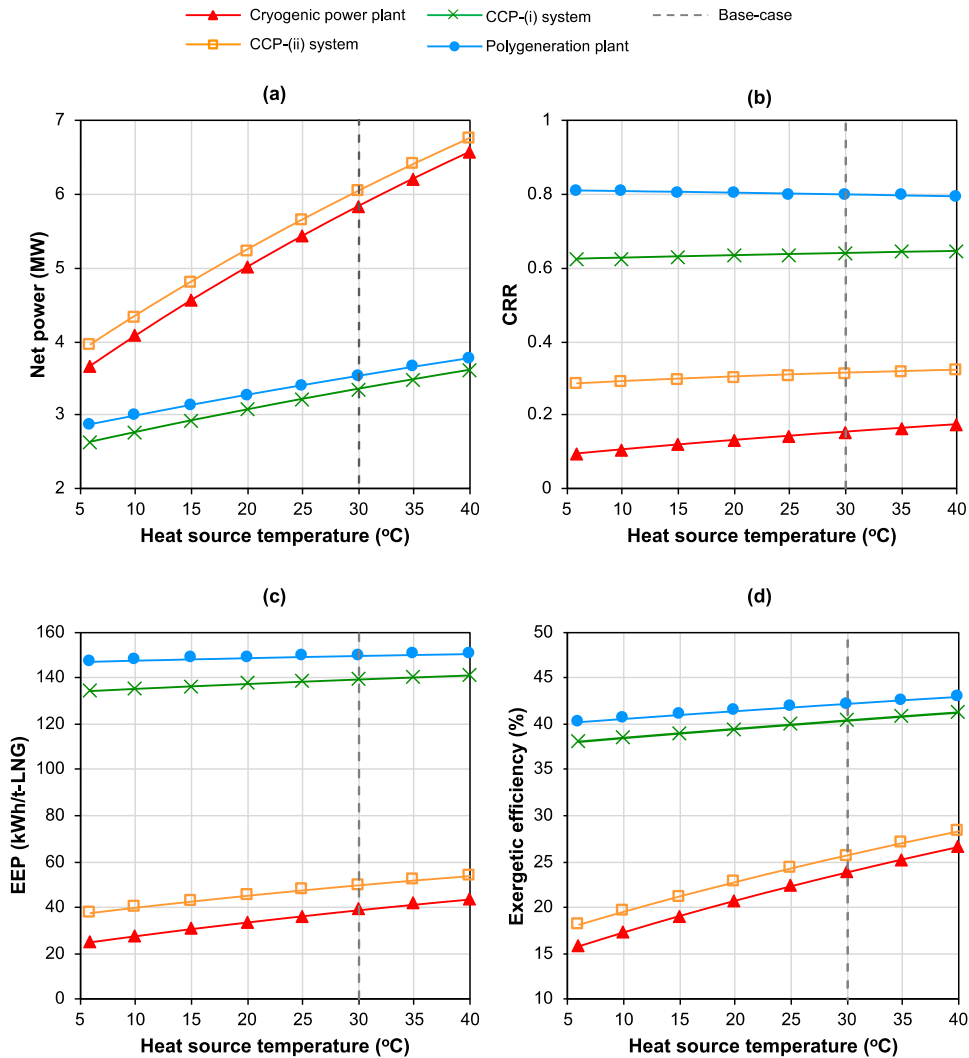


Figure 4.7. Variation of (a) the net power, (b) the Cold Recovery Ratio, (c) the Equivalent Electricity Production and (d) the exergetic efficiency, with the temperature of the heat source and for an LNG regasification rate of 150 t/h.

impact, the conventional regasification process has GHGs emissions associated with the pumping systems. On the contrary, the polygeneration plant could ideally avoid the annual emission of more than 50 thousand metric tons of GHG, which is the highest score among all the configurations considered. The refrigeration at -50°C is the energy output that contributes the most to the environmental benefit of the system.

Table 4.9. Thermodynamic data for each state point of the different configurations developed in this chapter at the design conditions.

No.	Fluid	CP			CCP-(i)			CCP-(ii)			Polygeneration		
		\dot{m} , t/h	T , °C	p , MPa	\dot{m} , t/h	T , °C	p , MPa	\dot{m} , t/h	T , °C	p , MPa	\dot{m} , t/h	T , °C	p , MPa
L1	LNG	150	-162.0	0.12	150	-162.0	0.12	150	-162.0	0.12	150	-162.0	0.12
L2	LNG	150	-159.8	4.6	150	-159.8	4.6	150	-159.8	4.6	150	-159.8	4.6
L3	NG	150	-159.8	4.6	150	-80.0	4.6	150	-80.0	4.6	150	-80.0	4.6
L4	NG	150	-50.0	4.6	150	-50.0	4.6	150	-50.0	4.6	150	-50.0	4.6
L4a	-	-	-	-	-	-	-	150	-20.0	4.6	150	-20.0	4.6
L5	NG	150	0.0	4.6	150	0.0	4.6	150	9.2	4.6	150	9.5	4.6
L6	NG	150	-50.9	1.8	150	-50.9	1.8	150	-42.6	1.8	150	-42.3	1.8
L6a	-	-	-	-	-	-	-	150	-20.0	1.8	150	-20.0	1.8
L7	NG	150	5.0	1.8	150	5.0	1.8	150	5.0	1.8	150	13.0	1.8
R1 ^a	Propane	233	-36.3	0.13	51.4	-36.3	0.13	233	-36.3	0.13	51.5	-36.3	0.13
R2	Propane	233	-36.0	0.62	51.4	-36.0	0.62	233	-36.0	0.63	51.5	-36.0	0.65
R3 ^b	Propane	233	9.1	0.62	51.4	9.1	0.62	233	9.9	0.63	51.5	11.0	0.65
R4 ^c	Propane	233	-36.3	0.13	51.4	-36.3	0.13	233	-36.3	0.13	51.5	-36.3	0.13
S0	Water	6,000	30.0	0.30	2,600	30.0	0.30	6,000	30.0	0.30	2,600	30.0	0.30
S1	Water	3,000	30.0	0.30	1,300	30.0	0.30	3,000	30.0	0.30	1,300	30.0	0.30
S2	Water	3,000	28.4	0.30	1,300	26.4	0.30	3,000	30.0	0.30	1,300	30.0	0.30
S3	Water	3,000	30.0	0.30	1,300	30.0	0.30	3,000	29.1	0.30	1,300	27.9	0.30
S4	Water	3,000	28.3	0.30	1,300	26.1	0.30	3,000	29.1	0.30	1,300	27.9	0.30
S5	Water	6,000	28.4	0.30	2,600	26.3	0.30	6,000	29.1	0.30	2,600	27.9	0.30
S6	Water	6,000	24.0	0.30	2,600	24.0	0.30	6,000	24.7	0.30	2,600	25.6	0.30
E1	EG-water 35%	-	-	-	-	-	-	597	-10.0	0.20	595	-10.0	0.20
E2	EG-water 35%	-	-	-	-	-	-	597	0.0	0.20	595	0.0	0.20
E3	EG-water 35%	-	-	-	-	-	-	223	0.0	0.20	221	0.0	0.20
E4	EG-water 35%	-	-	-	-	-	-	223	-10.0	0.20	221	-10.0	0.20
E5	EG-water 35%	-	-	-	-	-	-	374	0.0	0.20	374	0.0	0.20
E6	EG-water 35%	-	-	-	-	-	-	374	-10.0	0.20	374	-10.0	0.20
E7	EG-water 35%	-	-	-	-	-	-	597	-10.0	0.20	595	-10.0	0.20
W1	Chilled water	-	-	-	-	-	-	565	13.3	0.20	563	13.3	0.20
W2	Chilled water	-	-	-	-	-	-	565	4.4	0.20	563	4.4	0.20
C1 ^b	CO ₂	-	-	-	223	-50	0.68	-	-	-	223	-50	0.68
C2 ^a	CO ₂	-	-	-	223	-50	0.68	-	-	-	223	-50	0.68

^a Saturated liquid. ^b Saturated vapour. ^c Vapor quality 99.5%.

Figure 4.8 shows the exergy flow diagram of the CP plant and the polygeneration plant. Table 4.10 depicts the irreversibilities in each component for all the configurations studied. By far, the main source of irreversibilities in the CP plant is in the propane condenser. Because the temperature difference between propane and LNG streams is relatively high, irreversibilities are too. Thus, by exploiting the low-temperature exergy in cascade (firstly in the DB vaporizer for refrigeration production at -50°C, and later for power production and conventional refrigeration applications), irreversibilities are reduced considerably. Nevertheless, irreversibilities in the DB heat exchanger are still very high and account 63-65% of the total exergy destroyed in the CCP-(i) and the polygeneration units, respectively.

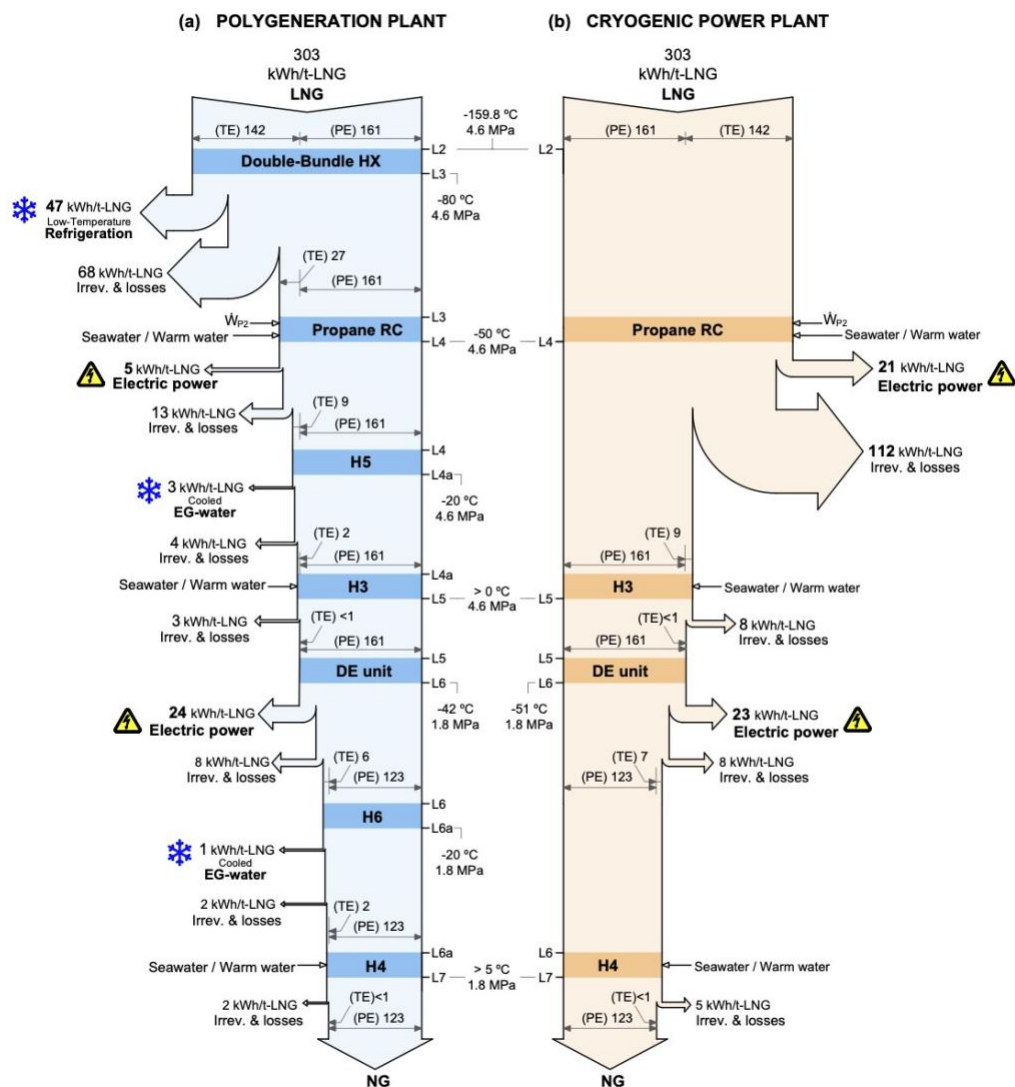


Figure 4.8. Exergy flow diagrams of (a) the CP plant and (b) the CCP system at design conditions. TE: Temperature component of LNG physical exergy, PE: Pressure component of LNG physical exergy.

Irreversibilities could be reduced even more if the DB heat exchanger were replaced by a more compact technology (e.g., fin-plate heat exchanger) and using a heat transfer fluid with a lower freezing-point than CO₂ to produce refrigeration at a lower temperature. In the case of the CCP-(ii) configuration, irreversibilities are reduced only by 2% with respect to the CP plant since the refrigeration for air-conditioning applications is poor in terms of “quality”.

Table 4.10. Irreversibilities (\dot{I}) of each system component of both the different configurations studied for the base-case operation.

Component	CP		CCP-(i)		CCP-(ii)		Polygeneration	
	\dot{I} , kW	\dot{I} , %	\dot{I} , kW	\dot{I} , %	\dot{I} , kW	\dot{I} , %	\dot{I} , kW	\dot{I} , %
LNG pump (P1)	387.5	1.9	387.5	2.4	387.5	1.9	387.5	2.5
LPG pump (P2)	23.1	0.1	5.1	0.0	23.8	0.1	5.5	0.0
Double-bundle HX	-	-	10,136.0	63.0	-	-	10,136.0	65.0
Propane condenser (H1)	12,924.0	62.7	1,163.0	7.2	12,924.0	64.3	1,163.0	7.5
Propane vaporizer (H2)	2,491.0	12.1	526.5	3.3	2,493.0	12.4	527.4	3.4
LNG heater No.1 (H3)	1,316.0	6.4	1,295.0	8.0	417.2	2.1	413.3	2.6
LNG heater No.2 (H4)	1,146.0	5.6	1,129.0	7.0	389.0	1.9	382.7	2.5
EG-water HE No.1 (H5)	-	-	-	-	534.0	2.7	534.2	3.4
EG-water HE No.2 (H6)	-	-	-	-	271.4	1.4	266.5	1.7
Chilled water HE (H7)	-	-	-	-	310.5	1.5	309.3	2.0
Propane turbine (T1)	1,115.0	5.4	246.5	1.5	1,132.0	5.6	255.1	1.6
DE unit (T2)	1,202.0	5.8	1,202.0	7.5	1,217.0	6.1	1,217.0	7.8
Total	20,605	100.0	16,091	100.0	20,099	100.0	15,597	100.0

4.4.1.2. Off-design performance

According to the results presented above for the base case operation, the polygeneration configuration stands as the most efficient system regarding the combined production of electricity and refrigeration. However, some of the operating parameters of an LNG physical exergy recovery system can vary considerably. Therefore, an off-design analysis may provide extra helpful information regarding the performance of the proposed systems [95]. The main considered input variables that could vary are:

- *Heat source water temperature.* The temperature of seawater is subjected to seasonal fluctuations, and the source of the heat source water could be diverse (e.g., cooling tower water, very low-temperature process heat, and so forth).
- The *LNG regasification flow rate* could vary depending on natural gas demands [144].
- The *LNG regasification pressure* may also affect the performance.

Figure 4.7 depicts the variation of some key performance indicators with the heat source temperature for all the configurations studied. On the other hand, Figure 4.9 shows the performance results obtained for both the CP cycle (as a reference configuration) and

the polygeneration plant for a heat source fluid temperatures range between 6°C to 40°C and LNG flow rates between 90 and 150 t-LNG/h. Additionally, [Figure 4.10](#) illustrates the effect of the regasification pressure on some of the performance indicators. According to the simulation results, the following observations can be made:

- The higher the heat source temperature, the best is the performance of both systems regardless of the regasification pressure and LNG flow rate. This fact is even more remarkable for the CP plant. The main reason is that the electric output of the Rankine cycle largely depends on the heat source temperature due to its influence on the saturation temperature and pressure of propane in the cycle. Besides, the Rankine cycle holds the major contribution to the total power capacity of the CP plant. As an example, if the heat source temperature drops from 30°C to 6°C, the net power produced decreases 37% and 24% for the CP plant and the polygeneration plant, respectively (see [Figure 4.9 \(a\)](#)), at the default LNG flow rate and pressure. On the other hand, the refrigeration production is unaffected by the heat source temperature. Thus, the cold recovery ratio (see [Figure 4.9 \(b\)](#)), the equivalent electricity production ([Figure 4.9 \(c\)](#)) and the exergetic efficiency (see [Figure 4.9 \(d\)](#)) of the polygeneration plant decreases with a heat source temperature drop but not as sharply as in the case of the reference CP unit.
- The higher is the LNG flow rate, the higher the total net power produced in all the systems and also the refrigeration produced in the polygeneration plant (see [Figure 4.9 \(a\)](#)). But the trend for the rest of indicators is the opposite. The reason is that the temperature difference between the input and output LNG streams increases in all heat exchangers as the LNG flow rate decreases below the design value used for the sizing of the heat transfer areas. This leads into a better temperature approach between the streams leaving the heat exchangers and into a higher enthalpy drop of LNG in the plant. As a result, irreversibilities decrease, and exergetic efficiency climbs. Moreover, the propane cycle operates at a higher temperature and pressure level at lower LNG flow rates. For instance, if the LNG flow rate decreases from 150 to 90 t/h for the default heat source temperature, the *EEP* increases by 12% and 9% in the only-power plant and the polygeneration system, respectively. For the same flow reduction, the exergetic efficiency increases from 23.7% to 26.7% in the CP plant and from 42.2% to 45.5% in the polygeneration plant. Besides, the *CRR* increases from 0.15 to 0.17 (reference CP plant) and from 0.82 to 0.84 (polygeneration plant).
- As shown in [Figure 4.7 \(b\)](#) the *CRR* reported by the polygeneration configuration is the only performance indicator which decreases (although very slightly) as the temperature of the heat source increases. The reason for this is the higher temperature of the NG stream leaving the DE unit which produces a lower refrigeration production at 4.4°C in the heat exchanger H6. Although the performance of the DE unit and the propane RC improves, the reduction in the refrigeration produced damages the global *CRR*. The refrigeration produced by the CCP-(ii) system also follows this trend. However, this decrease is offset by a higher power generation in

the RC which has much more weight on the total energy output of the system than that in the polygeneration plant.

- Figure 4.10 (b) shows that there is an LNG regasification pressure that maximizes the net power produced by the only-power plant for a given heat source temperature and LNG flow rate. This observation is consistent with the findings of other authors [282]. Higher pressures boost the shaft power of the turbine T2 (DE unit) because its pressure ratio is enlarged, although the energy consumed by pump P1 also increases.

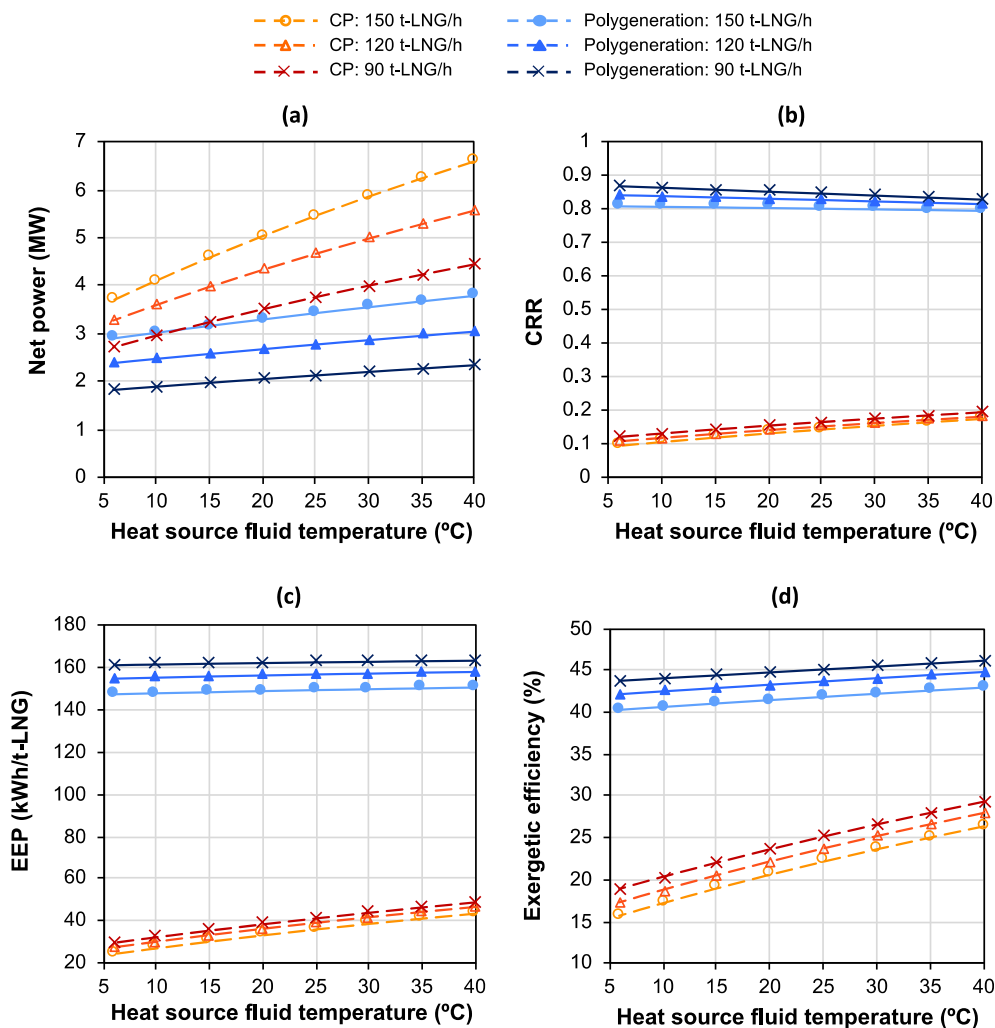


Figure 4.9. Performance indicators obtained for the polygeneration plant and the reference CP unit for different heat source fluid temperatures and LNG flow rates: (a) Net electric power, (b) Cold Recovery Ratio *CRR*, (c) Equivalent Electricity Production *EEP*, and (d) Exergetic efficiency.

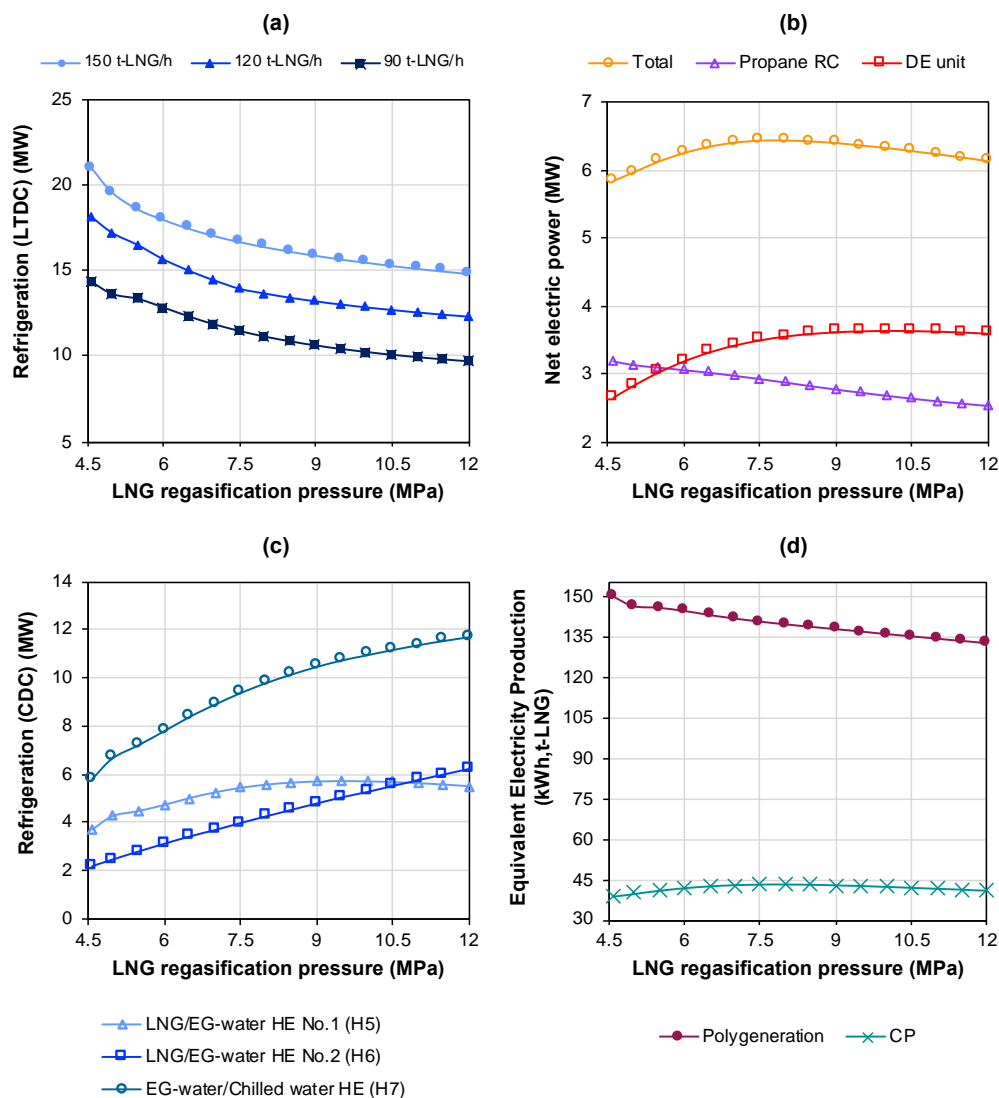


Figure 4.10. Effect of the variation of LNG regasification pressure on: (a) The low-temperature refrigeration produced by the CCP-(i) and the polygeneration systems, (b) the net power (total, propane RC and DE unit) of the CP plant, (c) the refrigeration for the conventional DC network, and (d) the EEP of the CP unit and the polygeneration plant.

Hence, the net power of the DE unit decreases beyond a certain LNG pressure. On the other hand, the low-temperature exergy of LNG stream L2 (see Figure 4.1) decreases as the pressure rises, so the temperature and pressure level of propane in the RC unit rise. However, the propane flow rate decreases ought to a lower condensation capacity in the heat exchanger H1. Since the flow rate dominates, the

net power delivered by the RC drops. In any case, to achieve a small enhancement of the total net power implies to operate at much higher pressures. As shown in [Figure 4.10 \(b\)](#), the power produced could be boosted from 5.8 to 6.4 MW (improvement of 9%), but this implies to increase the LNG pressure from the default (4.6 MPa) to 8 MPa.

- [Figure 4.10 \(a\)](#) shows that the low-temperature refrigeration production decreases significantly with the LNG regasification pressure, whilst the chilled water produced for air-conditioning applications increases. This phenomenon can be explained through the variation of the heat capacity of LNG with the temperature and pressure. As illustrated in [Figure 4.11](#), this variation is somewhat peculiar for regasification pressures close and above the critical point. The heat capacity of an LNG stream decreases with the pressure for temperatures between -160°C and temperatures close to the critical point (i.e., -82.6°C) which is the LNG temperature gap utilized to produce low-temperature refrigeration in the double-bundle heat exchanger. As a result, the capacity for producing low-temperature refrigeration decreases as the LNG pressure increases.
- In contrast, the specific heat increases for an LNG temperature of around -20°C as the regasification pressure does. Since the LNG stream L5 is exploited at this temperature for cooling the EG-water circuit, the capacity for producing low-temperature refrigeration increases as the LNG pressure does. Besides, for a given outlet pressure, the temperature of the gas stream leaving the DE unit is lower as the pressure at the inlet of the expander increases. This effect is illustrated in [Figure 4.12](#). As a result, the refrigeration effect in the heat exchanger H6 increases as the LNG regasification pressure does (see [Figure 4.10 \(c\)](#)). But all in all, as shown in [Figure 4.10 \(d\)](#), the effect of increasing the regasification pressure is clearly damaging for the equivalent production of electricity and power of the polygeneration plant. The production of the low-temperature refrigeration has a greater influence on the performance indicators.

4.4.2. Economic performance

As a baseline scenario, an electricity price (C_e) of 106.50 USD/MWh (~ 95.85 EUR/MWh) was considered which denotes an average value for industrial electricity consumers of the OECD countries in 2018 [\[283\]](#). Furthermore, its influence on the economic viability of the polygeneration plant, based on *DPBT*, was analysed using the lowest and highest electricity prices (i.e., 68.11 and 174.39 USD/MWh, respectively) of the same industries of OECD countries in 2018. Another key factor that has an effect on the economic performance of the polygeneration plant is the carbon tax imposed on emissions of greenhouse gases. Since the notion and status of putting carbon tax are not the same worldwide, three representative scenarios are considered:

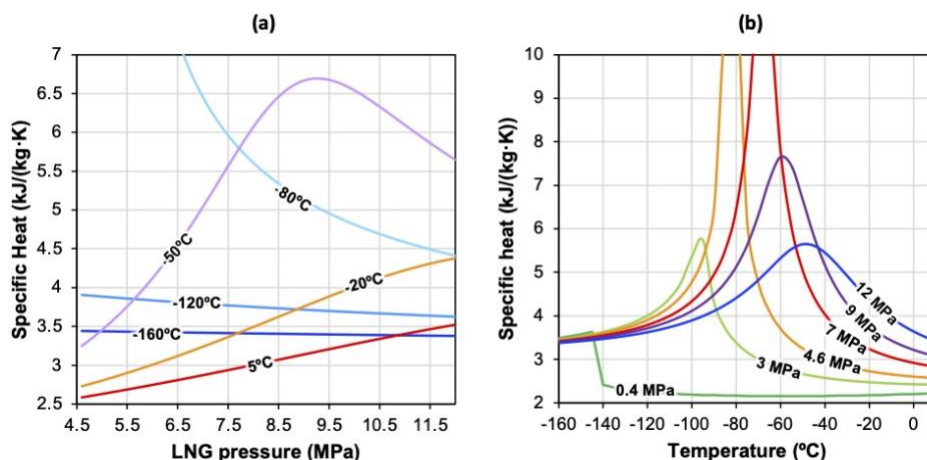


Figure 4.11. Variation of the specific heat of LNG (assumed as pure methane) (a) for. Properties calculated using REFPROP [235].

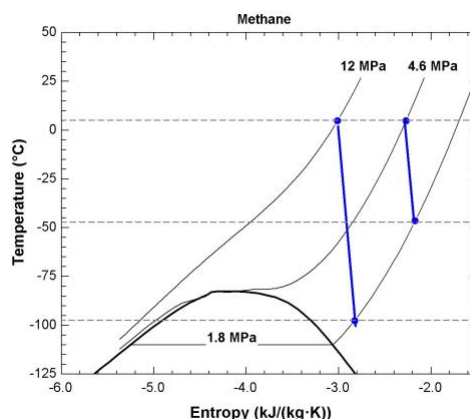


Figure 4.12. T-s diagram. Temperature of the gas stream leaving the DE unit in function of the inlet pressure (i.e., the regasification pressure).

- *Idle scenario.* No taxes yet applied to the GHGs emissions (i.e., countries without a carbon tax).
- *Baseline scenario.* It corresponds to countries with proactive environmental policies towards the temperature target set by the Paris Agreement. For example, carbon pricing between 40 – 80 USD/t-CO₂e needed by 2020 [284]. A mean carbon tax of 60 USD/t-CO₂e (~54 EUR/t-CO₂e) is chosen.
- *Ambitious scenario.* Countries with carbon tax greater-than 100 USD/t-CO₂e (~90 EUR/t-CO₂e), e.g., Sweden.

4.4.2.1. Base case

The results of the economic evaluation corresponding to the base-case scenario (106.50 USD/MWh electricity price and 60 USD/t-CO₂e carbon tax) are summarized in [Table 4.11](#). Additionally, a breakdown of the estimated purchase cost of each equipment is shown in [Table 4.12](#). *It should be noted that the economic results obtained are strictly subject to the particular assumptions, cost estimating correlations and economic parameters considered as a reference in this paper.* The following observations can be made:

- The LNG expander is the most expensive component of the polygeneration plant and represents 21% of the total cost of equipment, followed by the double-bundle heat

Table 4.11. Base-case scenario for the economic and environmental evaluation of the different types of configurations for an LNG regasification rate of 150 t/h. Values are given in million USD.

System component	Configuration			
	CP	CCP-(i)	CCP-(ii)	Polygeneration
Total capital investment, million USD (USD/kW_{eq,el})	72.6 (~12,400)	93.8 (~4,500)	80.6 (~10,700)	101.7 (~4,500)
- Total purchase cost of equipment	11.5	14.8	12.8	16.1
- Fixed Capital Investment (FCI)	49.4	63.8	54.8	69.2
- Other outlays	23.2	30.0	25.8	32.5
- Avoided capital costs (*)	6.5	46.1	13.0	53.6
- Net capital investment (Total – avoided)	66.1	47.7	67.6	48.1
Annual electricity savings (GWh/y)	47.0	128.6	54.2	135.7
- Net directly generated	42.4	24.4	43.9	25.7
- Equivalent electricity for LT refrigeration	0.0	98.7	0.0	98.7
- Equivalent electricity for conventional DC	0.0	0.0	5.8	5.7
- By net reduction of seawater pumping	4.6	5.6	4.6	5.6
Annual avoided emission of GHGs (t-CO₂e)	13,998	38,335	16,161	40,453
Net annual economic saving (million USD/y)	0.0	11.8	0.8	12.7
- Annual O&M	-0.5	-0.6	-0.5	-0.7
- Annual I&T	-3.0	-3.8	-3.3	-4.2
- Annual depreciation	-2.4	-3.1	-2.7	-3.4
- Annual overheads	-0.5	-0.6	-0.5	-0.7
- Total expenditures	-6.4	-8.2	-7.1	-8.9
- O&M, I&T, depreciation and overheads of avoided systems	0.6	4.0	1.1	4.7
- Avoided taxes due to GHGs emissions	0.8	2.3	1.0	2.4
- Benefit due to electricity savings	5.0	13.7	5.8	14.5
Economic indicators				
- Net present value	Unfeasible	61.0	Unfeasible	71.2
- Discounted Payback Time (DPBT)	Unfeasible	5.6	Unfeasible	5.0
- Internal Rate of Return (IRR)	Unfeasible	24.1%	Unfeasible	26.3%

(*) Avoided capital cost of: (1) ORV, (2) low-temperature chillers and (3) chiller plant for the conventional DC network.

Base-case scenario: electricity price: 160.50 USD/MWh; Carbon tax: 60 USD/t-CO₂e; CUF for electric generation: 90%; CUF for LT refrigeration: 70%; and CUF for conventional air-conditioning applications: 50%.

Table 4.12. Breakdown of Purchase Equipment Cost (reference year 2018) and share of each system component for the different configurations considered and using the cost functions listed in Table 4.5. Cost are given in thousand USD.

System component	Configuration							
	CP		CCP-(i)		CCP-(ii)		Polygeneration	
	Cost, 10 ³ USD	Share, %	Cost, 10 ³ USD	Share, %	Cost, 10 ³ USD	Share, %	Cost, 10 ³ USD	Share, %
LNG Pump (P1)	236	2.1%	236	1.6%	236	1.9%	236	1.5%
Propane Pump (P2)	45	0.4%	14	0.1%	45	0.4%	14	0.1%
ORC Turbine (T1)	3336	29.0%	1104	7.3%	3336	26.6%	1104	6.9%
DE Unit (T2)	3317	28.9%	3442	22.9%	3317	26.4%	3442	21.4%
Double bundle (DB-HE)	0	0.0%	2730	18.2%	0	0.0%	2730	17.0%
Propane Condenser (H1)	1020	8.9%	449	3.0%	1020	8.1%	449	2.8%
Propane Vaporizer (H2)	1135	9.9%	514	3.4%	1135	9.0%	514	3.2%
NG Heater (H3)	331	2.9%	357	2.4%	331	2.6%	357	2.2%
NG Heater (H4)	424	3.7%	449	3.0%	424	3.4%	449	2.8%
LNG/EG-Water HE No. 1 (H5)	-	-	-	-	493	3.9%	493	3.1%
LNG/EG-Water HE No.2 (H6)	-	-	-	-	533	4.2%	533	3.3%
EG-Water/Chilled Water (H7)	-	-	-	-	30	0.2%	44	0.3%
Piping low-temp. DC network (supply line)	-	-	868	5.8%	-	-	868	5.4%
Piping low-temp. DC network (return line)	-	-	3666	24.4%	-	-	3666	22.8%
Electric generator	1645	14.3%	1201	8.0%	1645	13.1%	1201	7.5%
Total PEC₂₀₁₈	11,490	100	15,029	100	12,545	100	16,099	100

exchanger (17% of total). The pipes of the low-temperature DC network also entail a high cost (around 216 USD/kW). However, this specific cost is much lower than the estimated cost for conventional low-temperature chillers (1,936 USD/kW for refrigeration load at -25°C) [280]), which forecast an important economic saving. A similar analysis can be drawn for the CCP-(i) system. Regarding the cryogenic power plant and the CCP-(ii) system, the cost of the LNG DE unit and the ORC turbine accounts together more than half of the total cost of equipment.

- The total capital investment estimated for the polygeneration plant is around 101.7 million USD. This figure is approximately 40% and 7% higher than the required by a cryogenic power plant or the CCP-(i) system, respectively. However, the specific cost of the plant estimated is one of the lowest among the configurations considered: around 4,500 USD per kW of equivalent electricity generated. Besides, the *net* capital investment of the polygeneration plant is estimated to decrease up to around 48 million USD due to the avoided capital cost of conventional units (ORV and chillers).
- The electricity savings and avoided GHGs emissions of the polygeneration plant (137.5 GWh/y and 40 t-CO₂e/y, respectively) results in an annual economic benefit of 14.5 million USD. Indirectly, up to around 4.7 million USD may be saved each year because of the avoided expenditures of conventional systems. By subtracting their inherent annual expenditures (~9 million USD), the polygeneration plant saves

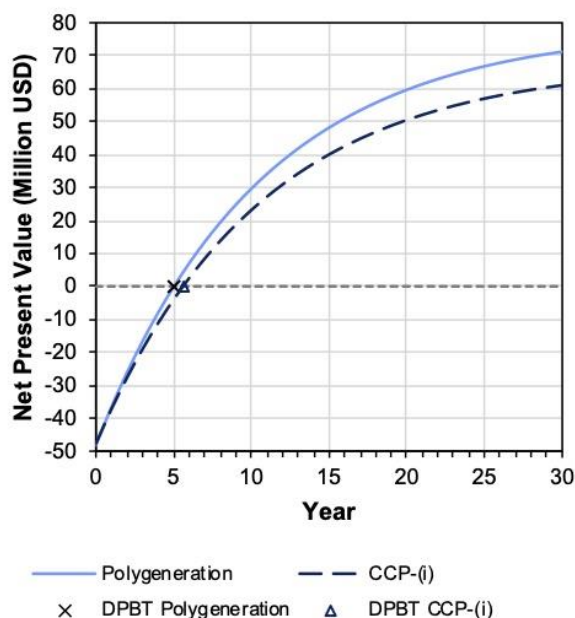


Figure 4.13. Evolution of the Net Present Value for the base-case scenario and the different configurations considered.

annually a net amount of 12.7 million USD, which is the highest saving among the configurations analysed.

- The discounted payback time of the polygeneration plant is estimated in approximately 5 years for the base-case scenario with an *IRR* of 26.3% at the end of the plant's lifetime. Although, slightly, the polygeneration plant improves the economic advantages over the CCP-(i) system, which has a payback time of 5.6 years and an *IRR* of 24.1%. Figure 4.13 shows the net present value of both configurations. At the end of plant's lifetime, the net present value of the polygeneration plant is 71.2 million USD which is 19% higher than the value obtained by the CCP-(i) system (61.0 million USD). Furthermore, the improvement of the polygeneration plant goes beyond an economic benefit, promoting a more sustainable refrigeration system and the phase-out of refrigerants with adverse environmental impact – *where their penalties have not been considered in the economic analysis of the plant.*

Regarding the cryogenic power plant and the CCP-(ii) system, their annual economic savings are not enough to recover the capital investment over the systems' lifetime (i.e. 30 years) and the annual expenditures at the considered base-case scenario (i.e. electricity tariff, carbon tax, and estimated capital investment). However, these systems could be economically feasible at different scenarios defined by high electricity tariff, more ambitious carbon tax, and/or lower capital investment (reduced plant equipment cost). This point is discussed in the next subsection.

4.4.2.2. Sensitivity analysis

As previously mentioned, the price of electricity and GHGs emission penalties are largely dependent on the specific location (or country) where the polygeneration plant deployed, to exploit the physical exergy of the LNG, the economic viability of the plant is mainly dependent on these circumstances. As stated previously, different values of these parameters are considered to investigate their influence on the *DPBT* of the project. Also, the economic evaluation of the plant is highly dependent on the accuracy of the estimated plant capital investment. Hence, the uncertainty in the estimation of the capital cost is also included in the sensitivity analysis. Thus, to assess the influence of these parameters on the economic performance (i.e., *DPBT*) the following specific typical values are considered:

- **Electricity prices** (USD/MWh): 68.11; 106.50 (base-case scenario); and 174.39.
- **Carbon tax** (USD/t-CO₂e): 0 (idle scenario); 60 (base-case scenario); and 120 (ambitious scenario).
- **Total capital cost:** Variation of $\pm 50\%$ relative to the estimated total capital cost at base-case scenario in steps of 25%. This variation is also applied to the avoided capital costs.

A sensitivity analysis is carried out to evaluate the variation of the discounted payback time under the different scenarios that arise from the combination of these parameters. Thereby, [Figure 4.14](#) illustrates the results obtained under different scenarios. In addition to the results of the polygeneration plant, the obtained cryogenic power plant results are also shown as a benchmark. The findings of the sensitivity analysis are summarized as follows:

- The capital investment of the cryogenic power plant is recovered when (1) high electricity prices are considered (such as 174.39 USD/MWh), (2) a carbon tax imposed, and (3) the capital investment is reduced by 25-50%. If carbon taxes are not obligatory, the system is viable only with the highest electricity price (174.39 USD/MWh) and reduced capital investment (reduced by 50%). If the electricity tariff is 106.5 USD/kWh, the capital investment of the cryogenic power plant is recovered only if the base-case capital cost estimated is reduced a half and if a carbon tax is compulsory. In all the cases, the cryogenic power plant is economically unfeasible for the lowest electricity price (68.11 USD/MWh). However, albeit the cryogenic power plant is economically feasible under some scenarios, long payback periods (> 6.2 years) were estimated. This may partly rationalize the low degree of implementation of such types of electric power generation systems in the LNG receiving terminals worldwide.

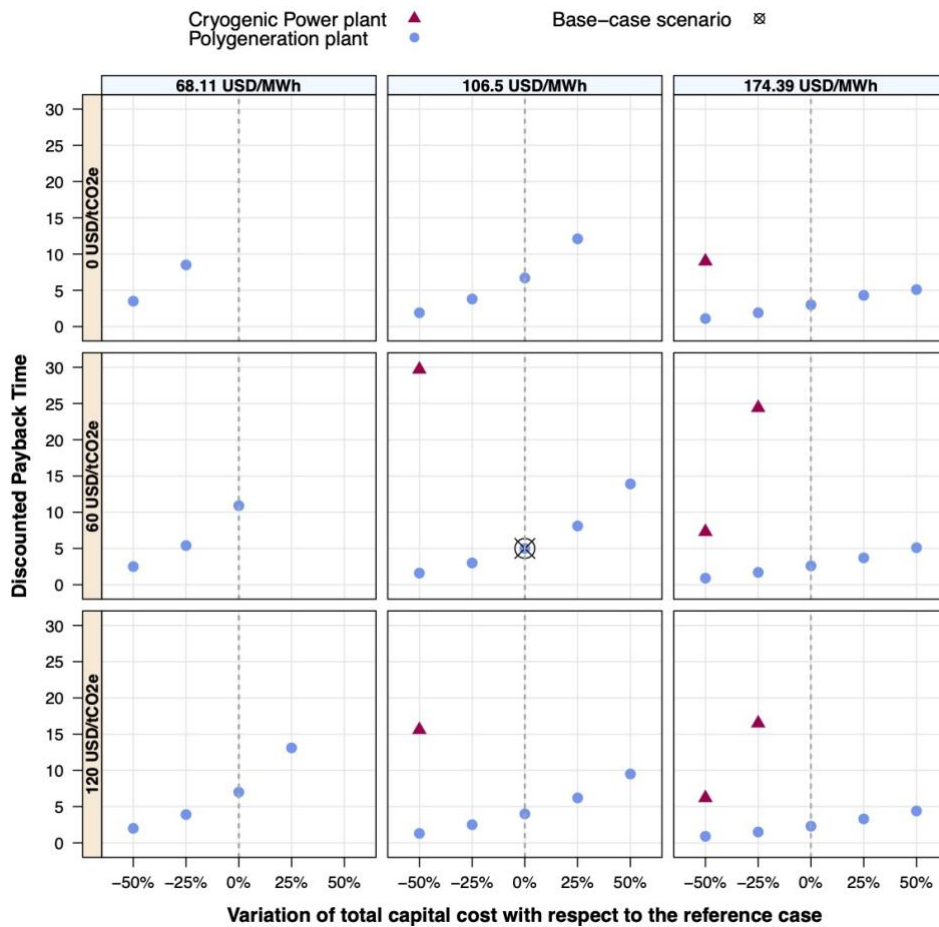


Figure 4.14. Variation of the discounted payback time of the polygeneration plant and the reference cryogenic power system with the electricity and carbon prices, and the variation in the capital cost. Figure published in [55].

- The most advantageous scenario is dominated by the combination of the highest electricity tariff (174.39 USD/MWh), the highest carbon tax (120 USD/MWh), and capital investment which is reduced in half with respect to the base-case. In that case, the plant could have a discounted payback time of 0.9 years. On the other hand, regardless of the electricity tariff, the payback time is always below 11 years if the capital investment is equal or lower than the estimated amount at the base-case scenario and when a carbon tax becomes obligatory. However, the project of the polygeneration plant could be economically unfeasible, for example, in a scenario where the electricity price is the lowest (68.11 USD/MWh) and no obligation on the

GHGs emissions (i.e., no carbon tax imposed) and the plant capital investment is maintained at its base-case estimated amount.

- The relative effect of each parameter on the payback time of the polygeneration plant is also analysed. Concerning the base-case scenario (marked in [Figure 4.14](#)), the estimated payback time of the polygeneration plant is extended up to 6.7 years ($\uparrow 34\%$) if no carbon tax is applicable, and decreases up to 4 years ($\downarrow 20\%$) if the carbon tax is increased to 120 USD/t-CO_{2e}. The sensitivity of the economic performance related to electricity prices is even more significant compared to the other parameters. For instance, the payback extends to ~11 years if the electricity price is 68.11 USD/MWh and it is reduced to 2.6 years ($\downarrow 48\%$) if the electricity price is 174.39 USD/MWh. But the major influence on the economic performance derives from variations on the capital cost of the plant. The base-case payback time is shortened up to 1.6 years ($\downarrow 68\%$) if the capital cost is reduced to half of the estimated amount, while it is extended up to ~14 years if the capital cost is twice the estimated amount.

4.5. Conclusions

The cascaded systems presented in [Chapter 3](#) and many other configurations proposed in the literature improves the efficiency of single-application systems, but their structures are complex and with much equipment. Thus, their economic feasibility could be an issue. This chapter aimed to enhance the competitiveness and promote the implementation of LNG physical exergy systems by developing relatively simple but efficient configurations for the combined production of electric power and refrigeration at different temperatures and built upon an existing cryogenic power unit. The configurations proposed have been modelled in sufficient detail, so that their techno-economic feasibility can be evaluated. The main conclusions drawn from the results reported in this chapter are:

- 1) The benchmark system consisted of a 6 MW power and LNG regasification unit integrated by a propane Rankine cycle and a direct expansion unit. The thermodynamic modelling developed for this reference configuration has been validated by using data available in the open literature. From that reference system, other three cascaded configurations have been developed and using only natural working fluids and heat transfer fluids: (1) the CCP-(i) plant that includes the production of low-temperature refrigeration at -50°C which is yield to agro-food industry warehouses through a CO₂ District Cooling network; (2) the CCP-(ii) plant that includes the production of refrigeration for air-conditioning applications in buildings located inside the regasification terminal; and (3) the polygeneration plant which is a combination of the two.

- 2) According to the simulation results obtained, the polygeneration configuration achieves the best trade-off between simplicity, efficiency, and environmental benefit. Although its electric power output decreases by 40% with respect to the reference cryogenic power plant for the same regasification capacity, the refrigeration produced boosts the performance of the plant. Its equivalent electricity production was nearly 150 kWh/t-LNG, the exergetic efficiency was 42%, and around 40 thousand t-CO₂e of annual emissions could be avoided if that system were implemented in an LNG receiving terminal. These indicators were the most promising among the considered configurations. In addition, installing cold thermal energy storages would be an attractive future option to increase the usage of the LNG low-temperature exergy available and improve the performance of both the low-temperature and the conventional DC networks. And although it was not considered in this chapter, the integration of renewable energies as heat source instead of using seawater/process water could enhance the indicators of the configurations analysed.
- 3) The off-design analysis showed that higher heat source temperatures are beneficial for the performance of the different configurations studied. Only the refrigeration production for air-conditioning applications becomes worse as the heat source temperature increases, but it has a minor impact on the overall performance. On the other hand, both the net power and the refrigeration produced increases with the LNG flow rate. In contrast, the specific indicators as well as the exergetic efficiency improves as the LNG flow rate decreases because of a better temperature approach between streams in the heat exchangers and the lower irreversibilities. Finally, there is a regasification pressure that optimizes the net power produced. However, the low-temperature refrigeration production decreases sharply as the regasification pressure increases. Because of its high impact on the overall performance of the polygeneration plant and the CCP-(i) system, the equivalent electricity production also decreases with the regasification pressure.
- 4) The economic performance of the polygeneration plant clearly improves that of a reference cryogenic power plant and the CCP-(ii) configuration. The polygeneration unit also slightly enhances the economic perspectives with respect to the CCP-(i) system. The base-case discounted payback time obtained for the polygeneration plant proposed in this chapter was 5 years with an internal rate of return of 26%. Although viability might be achieved for most of scenarios considered, ultimately, the economic feasibility depends largely on the capital investment, and factors that depend on the location such as the electricity tariff or carbon taxes applied. Very low electricity prices or too high capital investments could risk the viability of the system. But definitely, the introduction of carbon taxes boosts the competitiveness of this system and opens a new horizon of opportunity for LNG physical exergy utilization systems.

UNIVERSITAT ROVIRA I VIRGILI

EXERGY RECOVERY FROM LNG-REGASIFICATION FOR POLYGENERATION OF ENERGY

Antonio Atienza Márquez

Chapter 5. LNG low-temperature exergy utilization in satellite plants

5.1. Introduction

As concluded in [Chapter 2](#), most of the literature dealing with the utilization of the LNG physical exergy and the few existing plants exploiting that exergy are focused upon large-scale terminals. In contrast, the literature tackling this technical challenge on small-scale facilities (so-called “*satellite*”) is scarce. **In the case of operating satellite LNG plants, the exergy recovery has been hardly addressed.** But due to the huge number of these type of plants worldwide, there is an excellent potential to exploit a “*free*” physical exergy that should not be ignored.

[Figure 5.1](#) shows the LNG supply chain from large-scale harbour terminals to small-scale regasification facilities located in those places where conventional natural gas distribution pipelines do not exist. Usually, these regions are located far away from large-scale terminals, so LNG has to be transported through land transport (e.g., trucks, railway in iso-containers, and so forth) creating “*virtual pipelines*”. For the particular case of archipelagos, LNG can be transported from large-scale terminals to small-scale facilities in mini tankers.

So far only a few authors tackled the small-scale LNG low-temperature exergy utilization. Xu et al. [\[108\]](#) proposed a novel air separation process with LNG cold utilization and with potential application in satellite plants. Also, in [\[285\]](#) it was presented an optimized analysis of a pioneer demonstration project for storing the cold

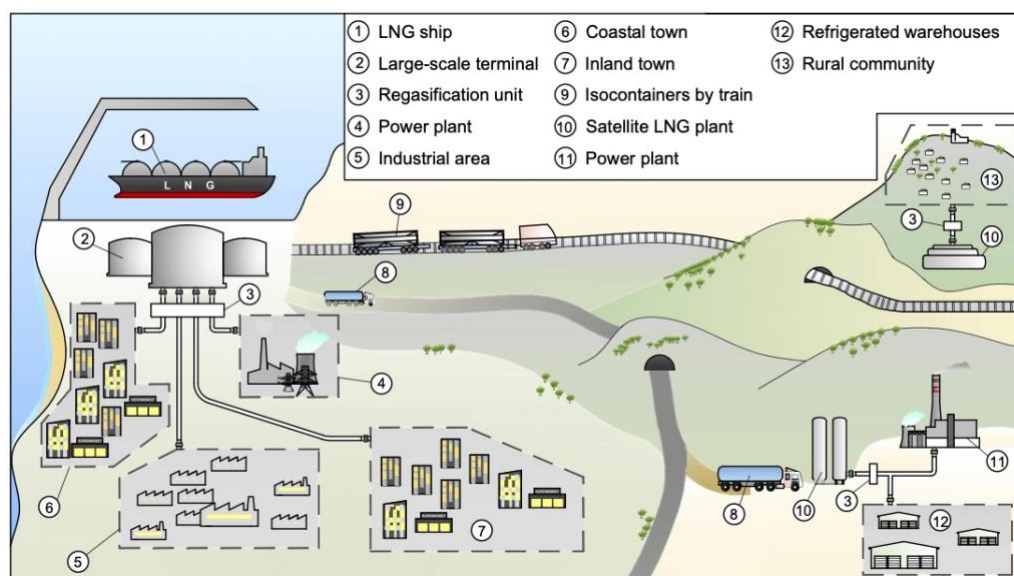


Figure 5.1. LNG supply chain from harbour large-scale terminals to satellite plants.

recovered from LNG-regasification in a satellite plant located in China. In that country, the importance of LNG and satellite plants was highlighted by Lin et al. [286]. On the other hand, Roszak and Chorowski [81] proposed the use of LNG low temperature for filling Adsorbed Natural Gas tanks. Kanbur et al. [287–289] studied different micro-cogeneration systems, and Ning et al. [216] analysed a small-scale system for the combined production of power and cold at different temperature levels. Also, other authors have proposed the utilization of LNG cold for CO₂ capture applications [290–292].

This chapter of the thesis addresses the techno-economic feasibility of the LNG low-temperature exergy recovery in satellite plants and its utilization for low-temperature refrigeration applications in the agro-food industry. Different configurations are proposed to exploit that exergy in different scenarios (i.e., types of satellite plant). The influence of the climate on the techno-economic feasibility is analysed. Furthermore, it is evaluated the feasibility of developing polygeneration systems by introducing PV technology in combination with the LNG physical exergy utilization. On the other hand, a simple methodology is proposed for estimating both the energy and natural gas demands in the absence of monitoring systems or real operating data, which may be a useful tool for researchers and engineers to perform preliminary techno-economic evaluations. It should be remarked that the results and conclusions obtained in this chapter of the thesis are valid for both the regasification of fossil LNG and bio-LNG.

5.2. Satellite plants: Description and operation

In this chapter, satellite LNG plants are classified in function of their size (i.e., the nameplate vaporization capacity) and their type, which depends on the final use of the regasified natural gas as fuel and on the number of users provisioned. Figure 5.2 shows some examples of operating satellite regasification facilities with some details about their sizes, vaporization capacities or natural gas end-use. For instance, these plants can supply natural gas to industry as shown in Figure 5.2 (a) and Figure 5.2 (b), to an electric power plant (Figure 5.2 (c)), for mining activities (Figure 5.2 (d)) or can feed natural gas into a local distribution network of a small town or village as shown in Figure 5.2 (e) and Figure 5.2 (d), among other uses. The above-mentioned types of satellite plants are some of the most typical, although are many more (e.g., vehicles refuelling stations).

The basic structure and the operating principle of a satellite plant are illustrated in Figure 5.3 These regasification facilities are integrated by the following main components:

- Unloading system.
- Cryogenic tanks.
- Pump (optionally, depending on the send-out pressure required).

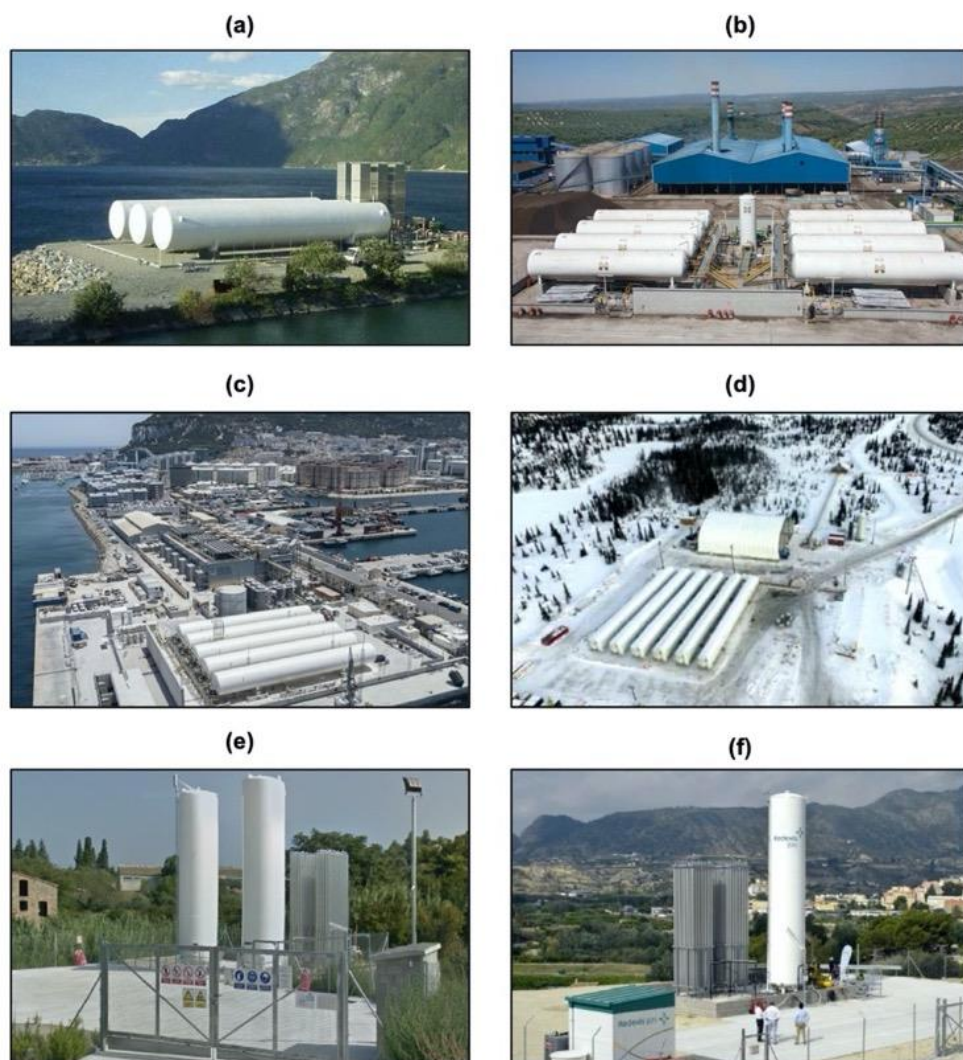


Figure 5.2. Examples of operating satellite LNG plants: (a) *Sunndalsora, Norway*. Gas supplied to an aluminium foundry with 1,500 m³ (3×500 m³) storage, 4,200 Nm³/h vaporization capacity [293]. (b) *Jaen, Spain*. Gas supplied to an olive-pomace sludge drying industry, 8×120 m³ storage and 7,200 Nm³/h vaporization capacity, send-out pressure 36-37 bar(g) [294]. (c) *Gibraltar United Kingdom*. Gas supplied to an electric power plant with an installed electric capacity of 86 MW. (d) *Far North Quebec, Canada*. 6×303 m³ storage, regasified natural gas is used for seven 2.1. power generation sets at a diamond mine [295]. (e) *Falset, Spain*. 60 m³ total storage, vaporization capacity 600 Nm³/h. Gas is supplied through a local pipeline network of 4 km to 400 houses and commercial buildings [296]. (f) *Abarán, Spain*. Plant with a storage of 30 m³ and vaporization capacity of 1,000 Nm³/h. Natural Gas fed into a pipeline network that supplies gas to 13,000 people, 2,000 dwellings, shops and also small industries, send-out pressure 0.4 bar(g) [297].

- Vaporization system.
- Security, regulation, odorization.
- Control system.

The working principle of a typical satellite LNG plant is as follows. Firstly, LNG is unloaded from trucks or iso-containers where LNG is stored at 80 - 160 kPa(g) to storage tanks by a cryogenic discharge pump or by pressure discharge (i.e., by creating a pressure difference between the tank truck and the LNG storage tank using an atmospheric unloading vaporizer). The second one is based on the pressure difference between the higher pressure of the gas phase in the truck and the lower pressure in the tank. The pressure is kept constant while filling the tank. The typical LNG storage pressure is between 200-450 kPa(g) with a maximum value of 500 kPa(g). An LNG pump could be used if higher send-out pressures are required. However, the regasification pressure in satellite facilities is generally lower than that in large-scale harbour terminals. Thus, the benefit of installing turboexpanders instead of pressure reducing valves to convert the pressure drop at regulation stations into electricity would be extremely limited. This is the reason why, in satellite plants, we refer only to the LNG *low-temperature exergy* utilization rather than the *physical exergy*, which also includes the mechanical – or pressure – exergy component.

The typical individual sizes of vacuum insulated cryogenic tanks installed ranges between 5-320 m³ (although can be even higher, e.g., >1,000 m³ depending on the type of satellite plant) with a maximum filling of 90% of their geometric capacity and can be

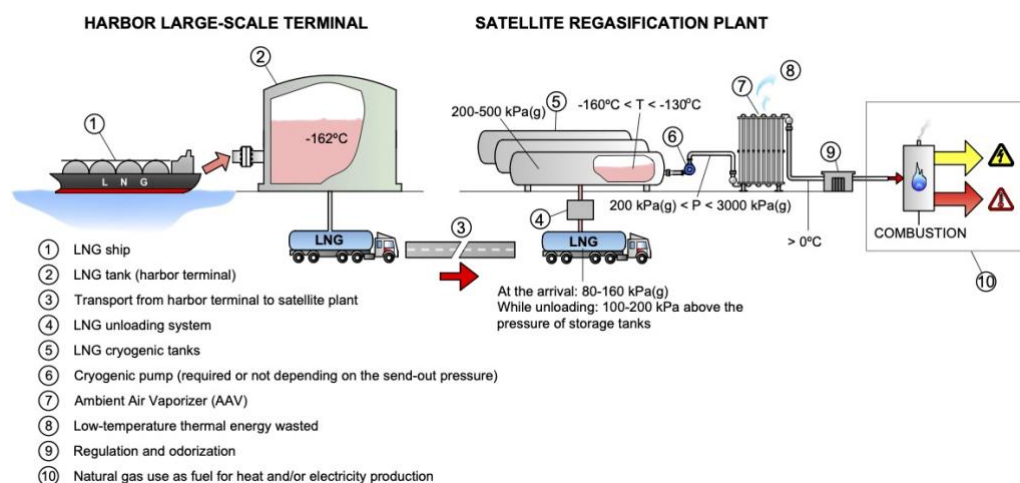


Figure 5.3. Schematic diagram of the conventional regasification process in an LNG satellite terminal without low-temperature exergy recovery.

installed vertically or horizontally depending on the space available or their capacities. Tanks are sized for autonomy of 4-5 days, and the total storage capacity of a satellite plant is typically between 1-1,500 m³. To avoid too high pressures, these tanks are equipped with security pressure relief valves.

On the other hand, the temperature of the stored LNG because it is a key parameter to determine the amount of cold available. At harbour large-scale terminals, LNG is unloaded from tankers and stored at around -162°C and at a pressure slightly higher than the ambient pressure. However, the temperature of LNG will increase in the process of loading trucks as well on the road to satellite facilities. The longer is the transport distance, the higher the temperature increase. Once at the cryogenic tanks, the temperature of the LNG will increase up to approximately -130°C. Consequently, because of the highest storage temperature, the low-temperature exergy content available in satellite terminals is lower than that in large-scale regasification plants.

As in large-scale terminals, LNG has to be regasified before being supplied to final customers. Usually, the technology of vaporizer utilized in these small terminals is Ambient Air Vaporizers (AAVs, described in [Chapter 1](#)) without low-temperature thermal energy recovery. The utilization of more than a single AAV operating in parallel is required for a reliable LNG-regasification, for example, when one of the AAV undergoes a defrosting cycle. Regasification capacities of typical AAVs are 200-5,000 Nm³/h. In moderate or cold climates, is usually required further heating by an electric or a water heater or any other kind of auxiliary heating system [293].

But, as illustrated in [Figure 5.4](#) the regasification entails an excellent opportunity to exploit the LNG low-temperature exergy content for multiple applications from its storage temperature up to a temperature that will depend on the specific application. In this chapter of the thesis, the low-temperature exergy is utilized for refrigeration production in freezing rooms. Notice that the utilization of an AAV is still required to heat the regasified natural gas above 0°C.

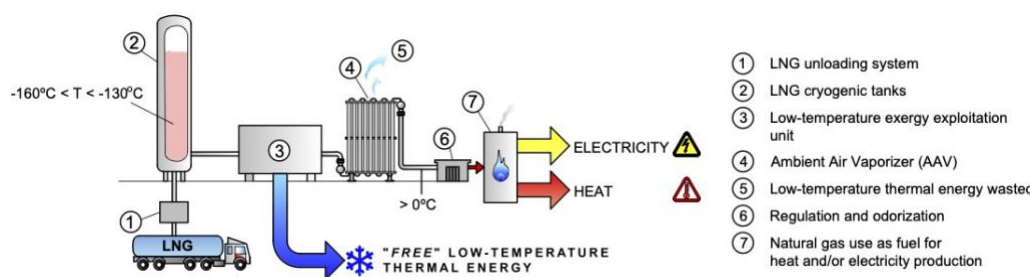


Figure 5.4. LNG unloading at harbour large-scale plants, road transport towards a satellite facility, and regasification with low-temperature exergy utilization.

Concerning commercial products for exploiting LNG low-temperature exergy, most of them are focused on refrigeration since it is one of the most direct applications. The company *Kälte-Klima-Sachsen GmbH* [298] built-in 2015 a pilot satellite facility that produced 3.3 kW from LNG of cold at -50°C . Figure 5.5 shows a picture of this installation with a detail of the heat exchanger utilized to recover the low-temperature thermal energy. A subsidiary of that company, *Eco Ice Kälte GmbH* [299] worked in cold recovery from liquefied cryogenic gases. In 2018 this business was transferred to *LNGCold Solutions GmbH* [300] which currently provides solutions for cold recovery from LNG-regasification in large-scale terminals and satellite plants.

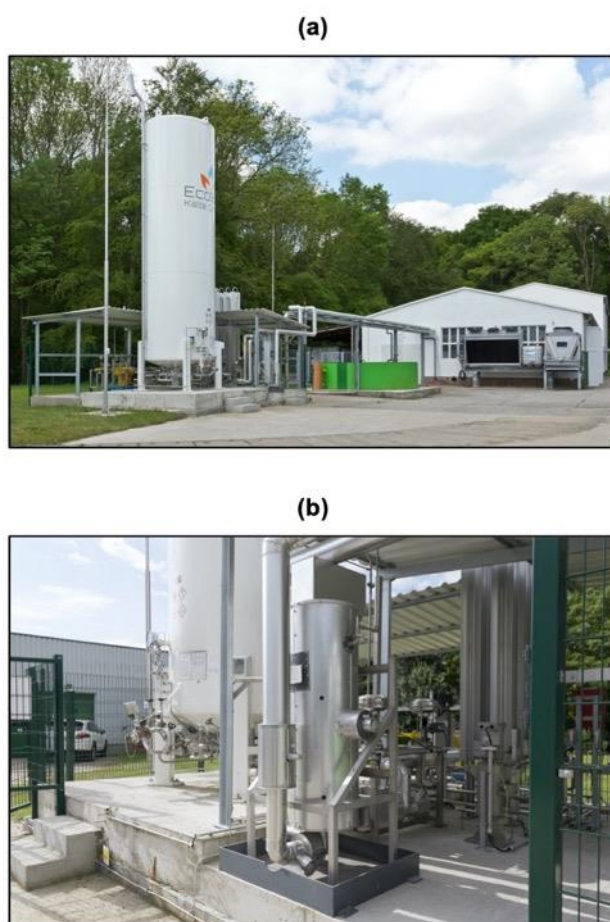


Figure 5.5. Pilot plant built in 2015 by *Eco Ice Kälte GmbH* in Borna, Germany. (a) Regasification site where LNG low-temperature exergy is exploited, and (b) heat exchanger utilized to recover the low-temperature thermal energy from LNG-regasification. Source: *Eco Ice Kälte GmbH* website [299].

5.3. Opportunities and challenges

The amount of low-temperature thermal energy available in a satellite plant is lower than that of a harbour large-scale terminal because of the much lower LNG regasification rates. Also, as mentioned before, the storage temperature is higher, which reduces the exergetic potential. Figure 5.6 depicts the low-temperature thermal energy that could be recovered for different LNG regasification pressures, assuming LNG as pure methane at saturated liquid state and for a heating process up to -70°C from storage temperatures between -160°C and -135°C .

Nonetheless, small- and medium-scale LNG is an expanding market [301]. Most of the growth is in China [302]. Spain accounts nearly 900 satellite LNG plants [303,304], and in Japan, the growing ratio is around ten new satellite terminals per annum [58,151]. Other countries, such as Norway, Netherlands, Turkey, Portugal or Switzerland, among others, are active in the small-scale LNG business. Also, it is a market in expansion in South America. As a result, there are thousands of satellite facilities where LNG cold energy could be utilized, thus contributing to the sustainability of refrigeration systems [71].

On the other hand, satellite plants allow the fuel shifting from diesel/fuel oil or coal to LNG [305] with a competitive price, a lower environmental impact and higher

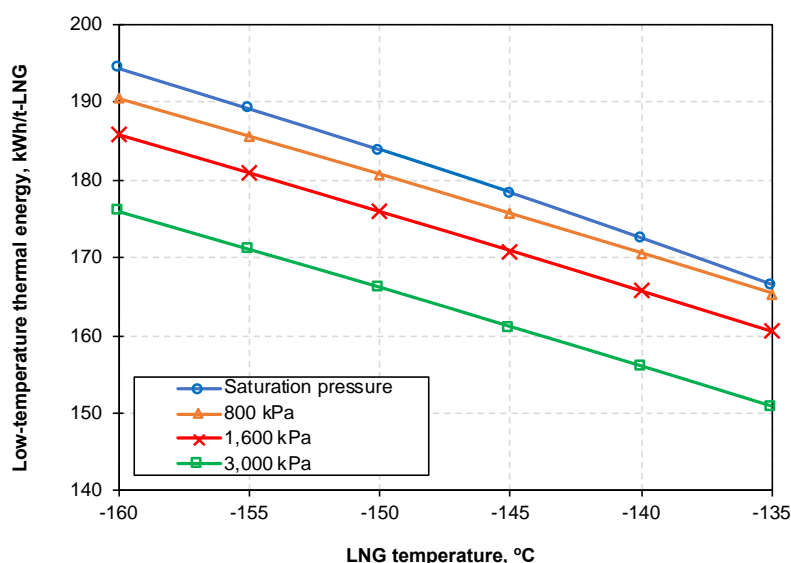


Figure 5.6. LNG (assumed as pure methane) cold energy recovery potential thorough its heating process from temperatures between -160°C to -135°C up to -70°C and considering different regasification pressures.

operational flexibility [301,306–308]. This fuel shifting is the motivation of new energy policies in Indonesia [309], and in other insular countries like Greece [310] or the Philippines [311]. The main power plant of Gibraltar is another example of successful fuel shifting from diesel to LNG [312]. The fuel shifting to bio-LNG or any other cryogenic biofuel is an even more environmentally friendly alternative.

The coal-to-LNG or diesel/heavy fuel oil-to-LNG switching may also add the extra value of producing “free” cold from the LNG-regasification process. Furthermore, the use of LNG is compatible with renewable energies in integrated local energy grids and may gain a foothold in the new model of cooling as a service (CaaS). Therefore, the use of LNG supports a sustainable development and has social benefits since it could promote new job opportunities in rural areas with problems of depopulation and contribute to developing local economies.

But there are some *bottlenecks*. Alike in large-scale terminals, there is no ideal heat transfer fluid to transport the cold energy recovered from the regasification sites to the facilities where it could be used [82]. In addition, there are some technical factors related specifically to the LNG-regasification in satellite plants that should be considered to evaluate the cold recovery potential, such as:

- **The amount of cold available.** It depends on the regasification capacity, the temperature at which cold is used and the regasification pressure. If the amount of cold recovered is always higher than the refrigeration load, then no back-up systems will be required. Otherwise, as illustrated in Figure 5.7, the conventional refrigeration systems should deal with a fraction of the total refrigeration load.
- **Fluctuating LNG vaporization rate.** In many types of satellite plants, the LNG send-out rate (and, thus, the cold available) varies over time in function of the natural gas demand as fuel. Figure 5.7 illustrates this fact. The fluctuation on the exploited LNG low-temperature exergy, introduces uncertainty in the refrigeration supplying system so that back-up refrigeration systems may be required. Notice that a refrigeration outage may break the cold chain of the foodstuff products, which entails health hazards for customers.
- **Mismatch between natural gas and refrigeration demands.** As shown in Figure 5.7, the periods of high refrigeration load and the periods with a high amount of cold available from LNG-regasification may take place at different moments. Thus, back-up systems are necessary, and cold energy storage systems are a solution to reduce the LNG cold wasted but increase the cost and the complexity of the installation.

5.4. Configurations

In this chapter, the low-temperature thermal energy (or “cold energy”) recovered from LNG-regasification is utilized for refrigeration applications at -18°C in deep-freezing

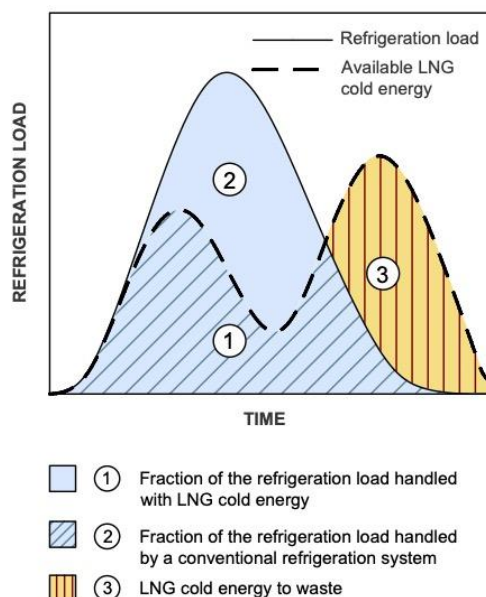


Figure 5.7. Conceptual example of the variation of a warehouse's refrigeration load and the cold available from LNG-regasification in a satellite plant.

rooms of either existing or new-built foodstuff warehouses. Two cold utilization configurations are proposed:

- **Direct** cold utilization (see [Figure 5.8 \(a\)](#)).
- **Indirect** cold utilization (see [Figure 5.8 \(b\)](#)).

Since the cold available in a satellite plant is very limited, it is considered that the cold is harnessed only by a single warehouse located a few meters far from the regasification site. Nevertheless, if the amount of cold available would be high enough, multiple users could take advantage of the cold through a District Cooling network, as illustrated in [Figure 5.8 \(c\)](#). Below is given a detailed description of both low-temperature exergy utilization configurations, and a discussion about the most suitable heat transfer fluids that could be utilized.

5.4.1. Direct configuration

[Figure 5.8 \(a\)](#) shows the schematic layout of configuration for the direct low-temperature exergy exploitation. This configuration stands-out because no vapour-compression refrigeration (VCR) systems are required, and its almost null electricity consumption. This is positive from an economic perspective.

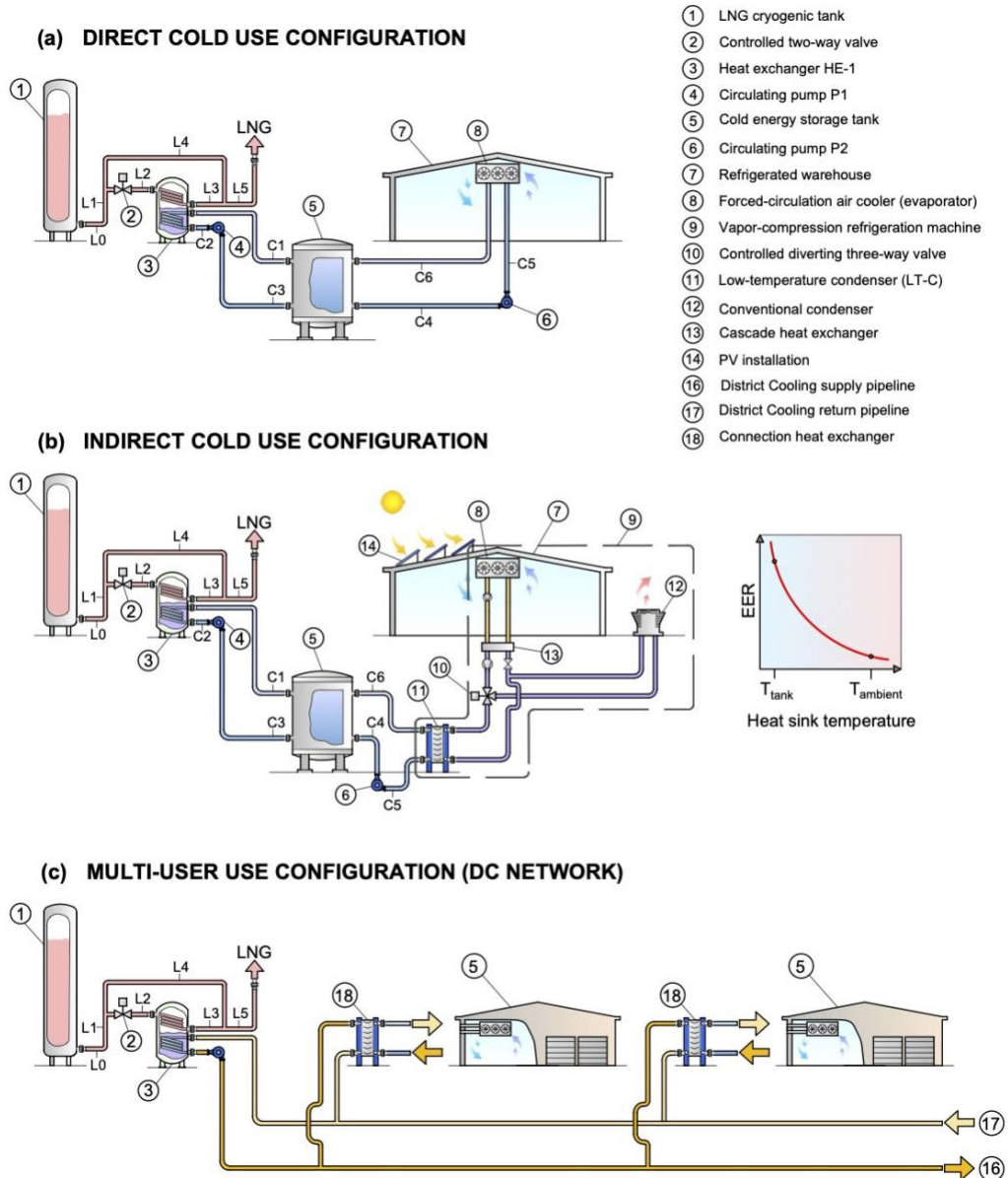


Figure 5.8. Schematic layout of the (a) Direct and (b) Indirect cold utilization configurations in satellite LNG plants; and (c) utilization of the cold by multiple users connected to a low-temperature District Cooling network.

The operation of this configuration is as follows. The LNG absorbs the heat from a heat transfer fluid in the heat exchanger HE-1. Then, the cooled heat transfer fluid yields the cold directly to freezing rooms through forced-circulation air coolers. An all-liquid cold

distribution circuit is assumed for the sake of operational reliability. At design conditions, the heat transfer fluid leaves the heat exchanger HE-1 at -32°C and returns at -25°C . A sensible cold thermal energy storage tank is utilized to mitigate the uncertainty in the supplying refrigeration system introduced by the fluctuations and mismatch of demands or caused by any eventual failure of the system.

However, this configuration could be implemented only in scenarios of satellite plants with very specific conditions. The amount of cold energy available (constrained by the instantaneous LNG vaporization rate) has to be always enough to handle the whole refrigeration load of freezing rooms. Also, constant or baseload regasification rates are preferable. Otherwise, fluctuations in the LNG regasification rate introduces uncertainty in the refrigeration supplied. But although having a baseload LNG send-out rate is quite common in large-scale harbour plants, this is rarely to exists in satellite regasification facilities since natural gas demand is highly fluctuating.

5.4.2. Indirect configuration

Figure 5.8 (b) shows the schematic layout of the configuration for the indirect exploitation of the LNG low-temperature exergy. It combines a VCR machine (which consists of an indirect NH_3/CO_2 refrigeration system) with the utilization of LNG cold energy as heat sink. This hybrid system increases the complexity, investment and annual expenditures (e.g., maintenance) with respect to the direct configuration described in the previous subsection. But instead, the indirect configuration provides further reliability and flexibility.

The indirect cold utilization configuration is based on the thermodynamic principle that the refrigeration efficiency of a VCR cycle (expressed by the Energy Efficiency Ratio, *EER*, which is defined as the ratio of the refrigeration capacity to the electricity consumed by compression) increases as the condensation temperature of the refrigerant decreases. Therefore, the cold energy of LNG could be utilized to condense the refrigerant below the ambient temperature and reduce electricity consumption. An indirect benefit of this configuration is the flattening of the electricity consumption peaks; thus, the electric power contracted can be adjusted and extra charges due to overpowering periods could be reduced. Furthermore, PV technology could be integrated into the system (e.g., through an inter grid-tie system) to offset part of the electricity consumption of the system to reduce the electricity bills.

As shown in Figure 5.8 (b), part of the LNG cold energy is transferred in the heat exchanger HE-1 to a secondary coolant circuit. A tank is used as cold thermal energy storage to stabilize the operation of the system avoiding continuous heat sink shifting, and also mitigates the impact of fluctuation and asynchrony of energy demands. For instance, the excess LNG cold energy in off-peak refrigeration demand periods can be stored to be used later if the refrigeration load increases and there is a lack of “free” cold

energy from LNG due to low gas demand. The set-point temperature of the coolant in the tank is -5°C . The low-temperature exergy contained in the tank is exploited through the heat exchanger LT-CD that plays the role of the condenser of the VCR cycle as an alternative to the conventional condenser (e.g., air-cooled or evaporative condensers).

To promote its commercialization, this configuration seeks to modify the least as possible the VCR machine and to increase the operational flexibility with reliability in the refrigeration supply. What is required to install a controlled diverting three-ways valve downstream the compressor to direct the refrigerant flow to the most convenient condenser (from the efficiency point of view). In [section 5.6.3](#) is given a detailed description of the control strategy utilized.

As a summary, [Table 5.1](#) shows the main features of both the direct and the indirect configuration.

Table 5.1. Summary of features of the direct and the indirect configurations for the utilization of the LNG low-temperature exergy.

Configuration for cold use	Simplicity	Reliability	Flexibility	VCR system	Cost and maintenance	Main advantages and weaknesses
- Direct (Figure 5.8 (a))	(+)	(-)	(-)	No	(+)	The energy management is simple but is required an instantaneous amount of LNG cold available enough to cover the refrigeration load. LNG vaporization fluctuations and mismatch between demands complicate the refrigeration supply.
- Indirect (Figure 5.8 (b))	(-)	(+)	(+)	Yes	(-)	LNG low-temperature exergy can be exploited even if it is lower than the refrigeration load. Problems related to gas fluctuation and mismatch between demands does not affect the refrigeration supply, but the complexity energy management increases.

5.4.3. The heat transfer fluids

As mentioned in [Chapter 3](#), the heat transfer fluids play a crucial role in any LNG physical exergy utilization system. [Table 5.2](#) provides a list of candidates with some of their relevant thermo-physical properties at the operating temperatures of the direct and the indirect configuration described above, their classification depending upon their safety issues and information about their environmental impact, which is much lower in comparison with fluorinated refrigerants (e.g., HFC-404A, HFC-32, PCF-14 or HFC-410A, among others).

Hydrocarbons have very low freezing temperatures, so they can be used as heat transfer fluids to recover the LNG cold through compact heat exchanger technologies without freezing concerns. By cons, they have flammability hazards. Alternatively, carbon

dioxide (CO₂) is safe, (i.e., not corrosive nor flammable or toxic), environmentally friendly and naturally abundant. Its low viscosity and specific volume at low temperatures and high conductivity are other of its strengths. However, CO₂ has a relatively high freezing point (-56°C), and its operating pressure is high. The use of CO₂ is quite attractive to transport the low-temperature thermal energy over long distances (order of kilometres) [119,140,211,223], although in satellite plants the distances are very short. Alternatives to CO₂ such as HFC-23 has been considered in the literature as an intermediate fluid to distribute the cold to cold rooms [117], but is out of choice in this thesis due to its huge environmental impact. On the other hand, ammonia (anhydrous) is a natural fluid widely used for industrial refrigeration applications, with very good heat transfer properties, and null environmental impact. But its freezing temperature (-77°C) is above the temperature of LNG, and it is flammable and highly toxic [228]. Thus, fluids without major security issues are preferable to mitigate damages if leakages occur, especially in enclosed areas such as freezing rooms.

In the indirect configuration (Figure 5.8 (b)), the operating temperature is higher than that for the direct scheme, so aqueous glycol solutions are an attractive option as heat transfer fluid. Despite the oral toxicity of Ethylene Glycol (EG), the secondary coolant circuit is installed outside and has no contact with the foodstuff. Besides, EG has better heat transfer properties than Propylene Glycol and can be pumped at a lower temperature [228]. For instance, the freezing point of 40% (by mass) EG – water solution (-24°C) is consistent with the operating temperatures of the indirect configuration (see Appendix D). Moreover, the operating pressure is much lower than that for CO₂. Higher EG concentrations further reduce the freezing point of the solution, but at the cost of a high viscosity and electricity consumption by pumping. The use of ice slurries could be an interesting choice [314,315], although in this study it is considered a single-phase heat transfer circuit as in traditional indirect circuits of refrigeration installations.

Table 5.2. Thermophysical properties, environmental and safety data of the candidate heat transfer fluids [88,236,237,313].

Fluid	T_{fr} , °C	$p_{vap}^{25^\circ C}$, kPa	Saturated liquid at -32°C				
			ρ , kg/m ³	μ , μPa·s	C_p , kJ/(kg·K)	k , W/(m·K)	p_{vap} , kPa
Propane	-187.6	952.1	569	176	2.30	0.123	155.0
Propylene	-185.2	1,154	590	166	2.26	0.142	195.8
Ethane	-182.8	4,190	463	86.7	2.86	0.117	1,002
Ethylene	-169.2	- ^a	444	73.8	3.07	0.115	1,832
Isobutane	-159.4	350.7	616	294	2.13	0.112	42.5
Butane	-138.3	243.3	634	289	2.18	0.130	25.5
Ammonia	-77.7	1,003	680	251	4.45	0.661	108.3
CO ₂	-56.6	6,434	1,084	170	2.06	0.149	1,334
PG – water ^b	-20.8	-	-	-	-	-	-
EG – water ^c	-23.9	2.57	-	-	-	-	-

Table 5.2 (cont.).

Fluid	Saturated liquid at -5°C					GWP	Safety group
	ρ , kg/m ³	μ , μPa·s	C_p , kJ/(kg·K)	k , W/(m·K)	p_{vap} , kPa		
Propane	535	132	2.46	0.109	406.0	~ 20	A3
Propylene	553	127	2.40	0.129	501.6	< 20	A3
Ethane	412	62.5	3.43	0.095	2,111	~ 20	A3
Ethylene	364	88.9	3.07	0.089	3,652	< 20	A3
Isobutane	586	210	2.26	0.101	131.0	~ 20	A3
Butane	606	213	2.29	0.117	85.1	~ 20	A3
Ammonia	645	180	4.59	0.576	354.8	< 1	B2L
CO ₂	956	108	2.41	0.117	3,046	1	A1
PG – water ^b	1,044	15,620	3.72	0.385	-	n/a	n/a ^d
EG – water ^c	1,063	7,188	3.41	0.406	0.333	n/a	n/a ^d

Nomenclature: T_{fr} – Freezing temperature; p_{vap} – vapor pressure; ρ – density; μ – dynamic viscosity; C_p – specific heat; k – Thermal conductivity; GWP – 100 years-Global Warming potential; PG – Propylene glycol; EG – Ethylene glycol; n/a – Not Available.

^a Critical temperature and pressure of ethylene 9.2°C and 5,042 kPa, respectively.

^b 40 mass-% PG.

^c 40 mass-% EG.

^d Hazard statement code: H302 - Harmful if swallowed [316].

Taking all the pros and cons of each candidate fluid into consideration for the utilization of the LNG low-temperature exergy, **CO₂ and a 40% (by mass) EG-water solution are selected as heat transfer fluids for the direct and the indirect configurations, respectively.** But the freezing point of these fluids is above the temperature of LNG, so special and custom-engineered heat exchanger technologies are required to prevent freezing issues. As discussed in previous chapters of the thesis, double-bundle heat exchangers are a promising technology solution. On the other hand, the company *Eco-ice Kälte* [299] has developed patents and technology in this line, including a vertical double-bundle heat exchanger [317,318] which has been installed in the demonstration facility shown above in Figure 5.5. As illustrated in configurations depicted in Figure 5.8, this technology can be a solution to recover LNG cold.

5.5. Scenarios analysed

As a whole, the scenarios with LNG low-temperature exergy utilization analysed in this study are integrated by: (1) A satellite LNG regasification plant, and (2) a foodstuff warehouse located in-situ or nearby the regasification site and where the low-temperature exergy of LNG is exploited (directly or indirectly) for refrigeration

production in cold rooms. As a whole, the scenarios analysed conform polygeneration systems that provide the following services:

- **LNG regasification.**
- **LNG low-temperature exergy utilization** to cover the whole or partially the refrigeration load of the cold rooms.
- **Heating** (e.g., hot water, process steam, space heating, and so on) and/or **electricity** production by using natural gas as fuel.
- Optionally, **PV panels** can be introduced to cover part of the electricity consumption of the refrigeration system installed in the warehouse.

However, there are multiple types of satellite plants. Likewise, there are almost infinite types of customers that could utilize the LNG cold energy, each one with their particular energy demands. A contribution of this chapter is to identify these most common scenarios, with the aim to draw strong conclusions about the potential of the LNG low-temperature exergy utilization in satellite facilities. Figure 5.9 depicts the scenarios analysed, which are determined by the following types of satellite plant:

- 1) **Satellite plant for a single consumer** (Figure 5.9 (a)). The regasified gas is consumed as fuel in the same warehouse where the freezing rooms are in.
- 2) **Satellite terminal for a baseload electric power plant** (Figure 5.9 (b)).
- 3) **Local satellite terminal** that supplies natural gas to a rural community (Figure 5.9 (c)).

Below is given a detailed description of these scenarios.

5.5.1. Scenario (1): Satellite plant for a single consumer (on-site LNG Terminal)

Figure 5.9 (a) shows the simplified schematic layout of a satellite plant owned by a single user (warehouse). The LNG system is installed just a few meters far from the warehouse with refrigeration demand. In this scenario, the low-temperature exergy of LNG is partially exploited in the heat exchanger HE-1. In the conventional case, once completely regasified in an Ambient Air Vaporizer, the gas is used on-site as fuel for heating production (i.e., hot water or process steam). In the case of an off-grid warehouse, the gas is also used as fuel for electricity production using, for example, internal combustion engines. Anyhow, the LNG vaporization rate and therefore, the availability of low-temperature thermal energy, is extremely irregular in this scenario since is determined by the energy demand (i.e., heat and/or electricity) in the warehouse which fluctuates strongly over time. That variation depends on factors like the activity schedule if it is a workday or weekend, the weather conditions, and so forth. Such

variability introduces uncertainty in the refrigeration supply, which is a serious handicap for using the low-temperature exergy of LNG directly.

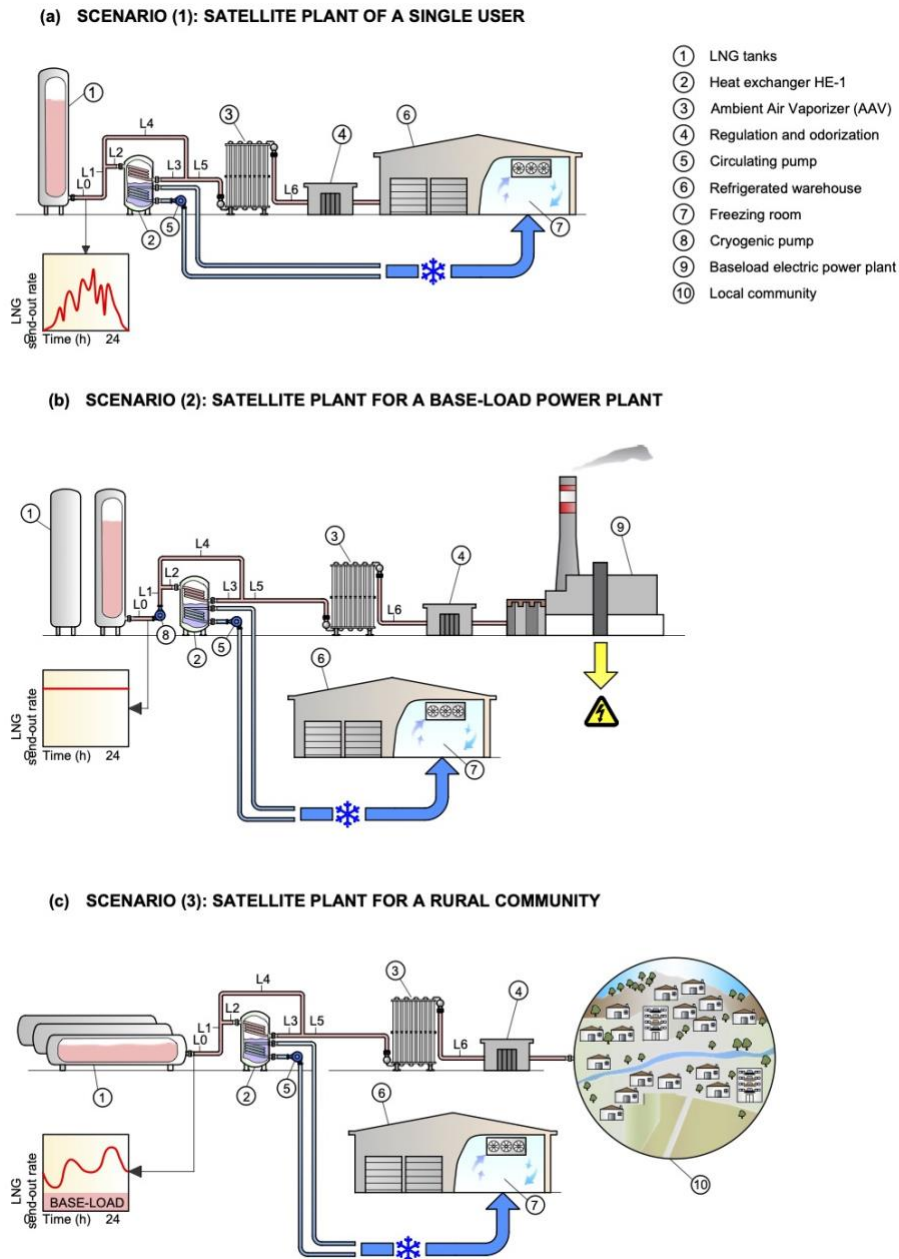


Figure 5.9. Schematic diagram of the different scenarios of satellite plants to recover the low-temperature exergy of LNG for foodstuff refrigeration applications.

5.5.2. Scenario (2): Satellite plant for electric power generation (on-site LNG Terminal)

The utilization of LNG as fuel for electric power generation is a promising option in some countries [319]. Figure 5.9 (b) shows the scenario of a satellite plant that supplies natural gas to a power plant for baseload electricity generation and with low-temperature exergy recovery from LNG-regasification. A key feature of this scenario is that the LNG send-out rate is constant throughout the year. Therefore, there is always rated cold energy available in a quantity that depends on the nameplate electric capacity of the power plant which determines the nameplate vaporization capacity of the satellite facility. This scenario is quite advantageous for the direct cold use configuration, except if the power plant is idle due to any failure or a scheduled maintenance stop and, therefore, there is no cold energy available. On the other hand, the send-out pressure depends on the requirements of the specific prime movers utilized in the power plant, so the use of a cryogenic pump may be necessary as illustrated in Figure 5.9 (b). This type of satellite plant is common in geographies with a distributed energy system or in off-grid locations. Although diesel or fuel-oil are typically used, the fuel shifting to LNG may encourage industry holders to install their foodstuff warehouses near to the regasification site to exploit the “free” LNG cold energy available.

5.5.3. Scenario (3): Satellite terminal of a local community (off-site LNG terminal)

Figure 5.9 (c) illustrates a local satellite terminal that lies on the outskirts of a village/town and supplies natural gas to dwellings as fuel for space heating, domestic hot water production and cooking. In this scenario, the LNG vaporization pattern fluctuates strongly in function of the hourly gas demand for household uses. This is an important constraint for using the low-temperature exergy of LNG directly without back-up refrigeration systems, which should be limited to exploiting only the cold energy corresponding to a theoretical LNG baseload fraction. But that amount is really difficult to determine since it depends on multiple factors, so the refrigeration supply to cold rooms could be not guaranteed every time. Therefore, the direct utilization of the LNG low-temperature exergy is considered as technically unsuitable in this scenario.

5.6. Modelling

5.6.1. Mathematical modelling and indicators

The different scenarios of satellite LNG plants with waste cold recover are modelled and simulated throughout a typical operating year using TRNSYS [320]. Properties of fluids

are obtained from REFPROP 9.1 [313]. Table 5.3 depicts the design parameters utilized in the different scenarios analysed. Also, the following modelling assumptions are made:

- Thermal and pressure losses are not considered both in equipment and pipes.
- Kinetic and gravitational energies are not considered.
- LNG is assumed as pure methane regarding thermodynamic properties calculations.
- Leakages of fluids to the environment are neglected.
- Parasitic electricity consumptions of circulating pumps are neglected.
- Electricity consumption of the fans of the conventional refrigeration machines is not considered.
- Temperature of air in the freezing chambers is assumed ideally maintained at the set-point (-18°C).
- Scheduled maintenance shutdowns are not considered in the calculations.
- Thermal efficiency for hot water or process steam production is set to 90%.

The heat transfer in heat exchangers is calculated from the energy balances and the heat transfer equations utilized in previous chapters of the thesis. The low-temperature thermal energy available in the double-bundle heat exchanger is calculated as follows:

$$\dot{Q}_{\text{LNG}} = \dot{m}_{L3}(h_{L3} - h_{L2}) \quad (5.1)$$

The energy balance in the cold energy storage tank (modelled with TRNSYS Type 4) shown in Figure 5.8 is calculated as follows:

$$\rho V C_p \frac{dT}{dt} = \dot{m}_{C1} C_p (T_{C1} - T_{C3}) - \dot{m}_{C4} C_p (T_{C6} - T_{C4}) - UA(T_o - T_{\text{tank}}) \quad (5.2)$$

The volume of the tank (V) is sized to handle the peak refrigeration load (or, in the indirect configuration, absorb the condensation heat released from the refrigerant of the VC machine) during 1.5 hours for a temperature range (ΔT) of 10°C. A well-insulated (i.e., $U \approx 0 \text{ W}/(\text{m}^2 \cdot \text{K})$) and a fully mixed tank is considered.

On the other hand, the coolant circulating pumps (modelled with TRNSYS Type 114) are sized accordingly with the following mathematical expression:

$$\dot{W}_P = \left(\frac{\dot{m}}{\rho} \times \Delta P \right) (\eta_P \times \eta_m)^{-1} \quad (5.3)$$

The pressure increase (Δp) required is calculated from the Darcy-Weisbach equation assuming a representative equivalent straight length of the circuit of 20 m and for 2 m/s

Table 5.3. Design parameters for each scenario of satellite LNG plant.

Parameter	Cold utilization configuration	
	Direct	Indirect
LNG tank temperature (T_{L1}), °C	-145	-145
LNG tank pressure (p_{L1}), kPa	328.2	328.2
Regasified NG supply temperature (T_{L5}), °C	5	5
LNG regasification pressure, kPa	328.2 ^a , 800.0 ^b 328.2 ^c	328.2 ^a , 800.0 ^b 328.2 ^c
LNG temperature at the outlet of HE-1 (T_{L3}), °C	-70	-70
Heat transfer fluid	CO ₂	40%-mass EG – water
Coolant inlet/outlet temperature in HE-1 (T_{C1} , T_{C2}), °C	-25 / -32	5 / -5
Circulating pumps discharge pressure, kPa	1,700	300
Set-point temperature of the cold energy storage tank, °C	-32	-5
EG-water inlet (T_{C5}) / outlet (T_{C6}) temperature in LT-CD, °C	-	-5 / 5

^a Scenario (1): Satellite plant owned by a single user.

^b Scenario (2): Satellite plant for a base-load power plant. Supply pressure suitable for commercial dual-fuel 4-stroke engines [321].

^c Scenario (3): Local satellite plant.

tube-side velocity. Smooth pipes are considered. The overall pump efficiency (η_P) and the motor efficiency (η_m) are assumed 70% and 95%, respectively.

Performance indicators

The following indicators are utilised to evaluate the overall performance of each configuration and scenario:

- The **Cold Recovery Ratio** (CRR) is a dimensionless quantity that indicates the amount of LNG cold thermal energy which is transferred in the heat exchanger HE-1 (see Figure 5.8 and Figure 5.9) with respect to the maximum amount available (i.e., which an ideal system could entirely convert into a useful energy output).

$$CRR = \frac{\dot{Q}_{HE1}}{\dot{m}_{LNG}(h_{L5} - h_{L1})} \quad (5.4)$$

- The **electricity saving** ($\nabla \dot{W}_{el,R}$, in kWh) achieved with respect to a reference case (ref) without LNG cold energy utilization. Parasitic consumptions of fans or defrosting devices are not considered. It is calculated as follows:

$$\nabla \dot{W}_{el,R} = \frac{\dot{Q}_R}{EER_{ref}} - \left(\frac{\dot{Q}_R}{EER} + \sum \dot{W}_P \right) \quad (5.5)$$

The Energy Efficiency Ratio (EER , in W/W) is determined from the modelling of the refrigeration machine described below.

- The **exergetic efficiency** determines how efficiently the initial physical exergy content of LNG translates into a reduction of the electricity consumed for refrigeration stuff. Its mathematical definition is as follows:

$$\eta_{ex} = \frac{\nabla \dot{W}_{el,R}}{(\dot{E}x_{ph,L0} - \dot{E}x_{ph,L6}) + \dot{W}_{el,R}} \times 100\% \quad (5.6)$$

The reference environment is set to the ambient temperature (time-dependent) and 101.325 kPa.

Finally, the avoided GHGs emissions (GHGA, in t-CO_{2,e}/year) are utilized to evaluate the positive effect of the configurations proposed to exploit the LNG cold thermal energy on the environment assuming an:

$$GHGA = EF \times \nabla \dot{W}_{el,R} \quad (5.7)$$

As in the previous chapters, an emission factor (*EF*) of 0.298 kg-CO_{2,e}/kWh is utilized.

Vapor-compression Refrigeration (VCR) machine modelling

The thermodynamic model of the indirect NH₃/CO₂ refrigeration system utilized in the indirect cold use configuration is based on the technology “*NewTon*” developed by Mayekawa Mfg. Co., Ltd. [322,323]. Figure 5.10 depicts a schematic layout of the system modelled. The ammonia VC cycle includes a double economizer system. CO₂ is the secondary coolant, and its latent heat is harnessed. The temperatures of the liquid CO₂ and the ammonia stream leaving the evaporator are -32°C (saturated liquid) and -35°C (saturated vapour), respectively. The temperature approach and subcooling in the ammonia condenser are set to 3°C and 1°C, respectively.

The *EER* (in W/W) of the machine is calculated through the following equation:

$$EER = \frac{\dot{Q}_R}{\dot{W}_{C,el}} = \frac{\dot{Q}_R}{\dot{W}_{C,is} \times \eta_C^{-1}} \quad (5.8)$$

For the sake of modelling simplicity, fans and defrost power consumption are not considered in the calculation of the *EER*. The electricity input to the motor of the compressor ($\dot{W}_{C,tot}$) is determined from the product of the work required for an isentropic compression ($\dot{W}_{C,is}$) and the total compressor efficiency (η_C), which is calculated as the product of the isentropic efficiency and the motor’s efficiency:

$$\eta_C = \eta_{C,is} \times \eta_m \quad (5.9)$$

The isentropic efficiency (η_{is}) determines the ratio of work required by an isentropic compression to the shaft work ($\dot{W}_{C,shf}$) [324]. It has been assumed equal to the volumetric efficiency in the modelling [325]. Based on the manufacturer data of an

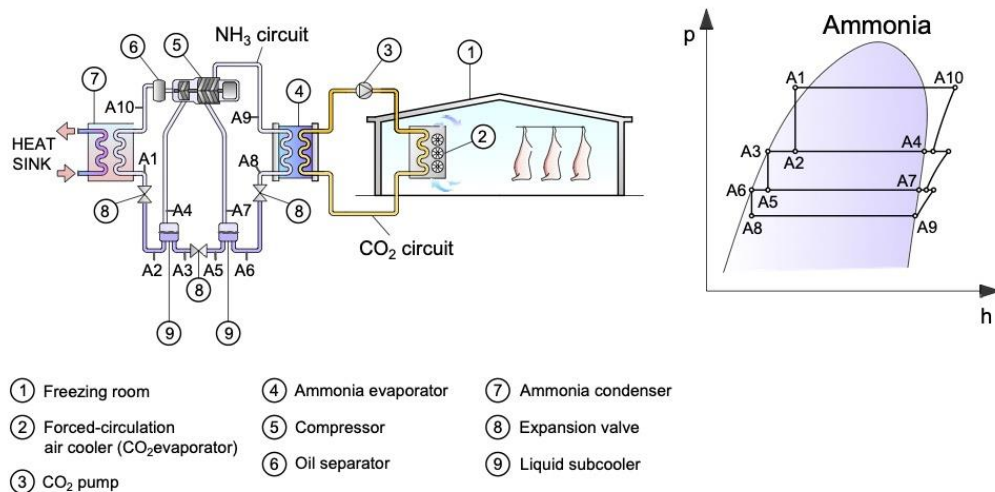
INDIRECT REFRIGERATION SYSTEM (NH₃/CO₂)

Figure 5.10. Schematic diagram of the NH₃/CO₂ refrigeration machine modelled.

ammonia (semi-hermetic type) screw compressor [326], we have developed the following correlation to calculate the isentropic efficiency as a function of the compression ratio:

$$\eta_{is} = \frac{\dot{W}_{C,is}}{\dot{W}_{C,shf}} = 0.79 - 0.0086 \times \left(\frac{p_{high}}{p_{low}} \right) \quad (5.10)$$

The data utilized to obtain that expression and the detailed procedure are provided in [Appendix D](#). Besides, the compressor shaft power (\dot{W}_{shf}) decreases in proportion to the cooling capacity at part-load operation due to the use of inverter technology. The model assumes this even at very low part-load fractions. The *EER* (in W/W) of the VCR machine is calculated from the following regression model:

$$EER = f(T_o, PLR) = A \times T_o^3 + B \times T_o^2 + C \times T_o + D \quad (5.11)$$

$$A = f(PLR) = -0.000054 \times PLR + 0.000007$$

$$B = f(PLR) = 0.0056 \times PLR - 0.0006$$

$$C = f(PLR) = -0.2277 \times PLR - 0.0002$$

$$D = f(PLR) = -7.0013 \times PLR^2 + 12.906 \times PLR - 0.3134$$

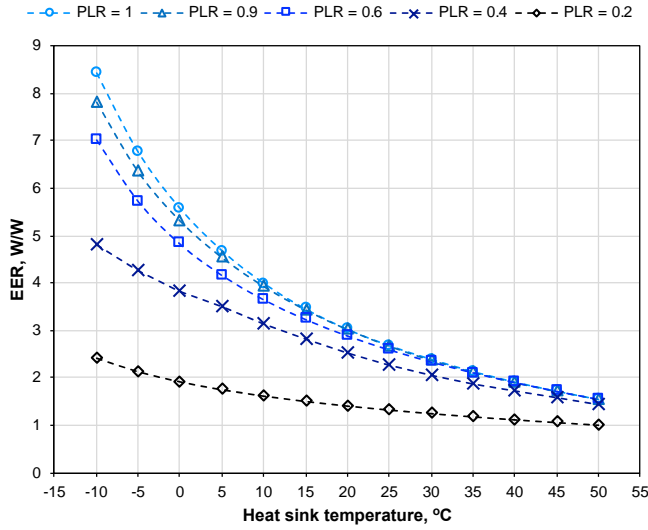


Figure 5.11. EER curves for different heat sink temperatures and part load ratios for a given temperature of the refrigerated rooms of -18°C .

where, T_o is the temperature of the heat sink and PLR denotes the part load ratio, defined as the ratio of the refrigeration load to the peak refrigeration load. Figure 5.11 depicts the EER of the VCR machine modelled for heat sink temperatures ranging between -10°C to 50°C at full load and part load operating conditions.

PV panels modelling

A PV grid-inter tied and a net-metering scenario is considered to evaluate the techno-economic feasibility of integrating PV technology with the indirect LNG low-temperature exergy utilization configuration (Figure 5.8 (b)). The PV generator is sized to cover the half of the average daily electricity consumption of the warehouse for refrigeration production, assuming a losses factor of 0.9 and for the tilt angle that maximizes the annual electricity production in each specific location ($3.7 + 0.69|\phi|$). The electricity output of the PV panels is calculated as a function of the irradiance on the panels' surface (I_T , calculated using the isotropic model [327]), the total surface of PV panels installed ($A_{tot,PV}$), the electric efficiency of the PV cells (η_{el}), the annual degradation rate of the cells (d) each year (n) since its operation starts and the efficiency of the inverter (η_{inv} , set as 95%):

$$\dot{W}_{el,PV} = I_T \times A_{tot,PV} \times \eta_{el,PV} \times (1 - d)^n \times \eta_{inv} \quad (5.12)$$

$$\eta_{el} = \eta_{el,ref} [1 - \beta(T_c - T_{ref})] \quad (5.13)$$

where the cells temperature (T_c) is calculated as follows:

$$T_c = T_o + (NOCT - 20^\circ\text{C}) \frac{I_T}{800} \quad (5.14)$$

The performance parameters utilized for the modelling are based on those of the commercial PV panels Panasonic Slim VBHN250SJ25 (250 W) [328]: reference electric efficiency $\eta_{el,ref}$: 19.8%, Normal Operating Cell Temperature (NOCT) = 40°C, Temperature coefficient β = 0.0000 1/K, annual degradation (d) 0.045% of PV cells each year from its start-up operation, n and reference temperature, T_{ref} , 25°C.

5.6.2. Energy demands

The assessment of the low-temperature exergy recovery potential in a satellite LNG plant needs information upon (1) *the natural gas demand as fuel*, and (2) *the refrigeration demand of the warehouse* that aims to exploit that “free” cold. However, these demands are different for each particular scenario, and the monitoring of the facilities is the only way to gather accurate data. Since this work is not focused on a case-study but seeks for establishing a methodology for assessing the feasibility in different conditions, both the energy and natural gas demands are estimated through the simple methods described below.

5.6.2.1. Energy demand of warehouses

The total energy demand (D_{tot}) of a refrigerated warehouse for groceries preservation splits into heat demand (\dot{Q}_H), for example, for hot water and/or steam process production, and electricity demand (\dot{W}_{el}) for refrigeration production ($\dot{W}_{el,R}$) and for other utilities ($\dot{W}_{el,O}$, e.g., lighting, machinery, electric defrost, and so on). The share of these energy demands to the total depends to a large degree in the activity sector (i.e., meat, horticulture, dairy, fisher, and so forth). The following two cases are considered:

- **Case A**, typical meat industry [329]: 50% electricity; 50% heat.
- **Case B**, typical horticultural industry [330]: 85% electricity; 15% heat.

For the sake of simplicity, it is assumed that both the heating and the electricity demand for uses beyond refrigeration depends only on the activity of workers in the warehouses and are estimated from the following equations:

$$\dot{Q}_H = \xi \times \dot{Q}_{h,max} \quad (5.15)$$

$$\dot{W}_{el,O} = \xi \times \dot{W}_{el,O,max} \quad (5.16)$$

where ξ represents the activity factor ($0 \leq \xi \leq 1$) that is based on the following schedule:

- *Midweek working day*: full activity ($\xi = 1$) from 6:00 to 22:00.
- *Saturday*: full activity from 6:00 to 14:00.
- *Any other case*: minimum activity ($\xi = 0.05$).

The electricity demand for refrigeration production is assumed 50% of the total electricity consumption [331]. The refrigeration load (\dot{Q}_R) is synchronised with the outdoor temperature [332], and also depends on the activity in the freezing rooms. It is estimated from the following correlation based on the peak refrigeration load ($\dot{Q}_{R,max}$):

$$\dot{Q}_R = (\beta_1 \times \xi + \beta_2 \times \phi) \dot{Q}_{R,max} \quad (5.17)$$

The temperature factor (ϕ) is defined as the variation of the temperature difference between the outdoor temperature (T_o) and the freezing room temperature (T_r , -18°C), with respect to that temperature difference at the design point. Its definition agrees with a linear variation with the outdoor temperature, and its mathematical expression is as follows:

$$\phi = \frac{\Delta T_{o-r}}{\Delta T_{o,max-r}} = \frac{T_o - T_r}{T_{o,max} - T_r} \quad (5.18)$$

To analyse the influence of the climate on the low-temperature exergy recovery potential, simulations are conducted for three locations representative of a Tropical, Mediterranean and Continental climate: Bangkok (13.92° N , 100.6° W), Thailand; Tarragona (40.82° N , 0.49° W), Spain; and Oslo (59.90° N , 10.62° W), Norway; respectively. The weather files from the EnergyPlus database are utilized in the modelling [333].

The parameters β_1 and β_2 in Eq. (5.17) are the weighing factors that take account of the relative influence of the activity and the outdoor temperature, respectively, on the refrigeration load. In a practical case, that influence depends on several factors such as the insulation of the freezing rooms, ventilation rates, particular working schedule, and so forth. In this study, the values assigned to β_1 and β_2 are 0.7 and 0.3, respectively, which are consistent with the variation of the energy demands in a typical agro-food industry warehouse [334].

On the other hand, the **Refrigeration Capacity Index** (RCI) is a dimensionless parameter which allows defining the peak refrigeration capacity of a warehouse ($\dot{Q}_{R,peak}$) in relation to the maximum cold energy that could be recovered from the

regasification of the nameplate LNG vaporization rate of a satellite plant ($\dot{m}_{LNG,np}$). Its mathematical expression is as follows:

$$RCI = \frac{\dot{Q}_{R,max}}{\dot{Q}_{LNG,max}} = \frac{\dot{Q}_{R,max}}{\dot{m}_{LNG,np}(h_{L3}-h_{L2})} \quad (5.19)$$

According to the definition given above, an $RCI > 1$ indicates that the peak refrigeration load of the cold rooms is higher than the maximum “free” low-temperature thermal energy that could be recovered throughout the LNG-regasification process; therefore, back-up refrigeration systems are required and the direct configuration for exploiting the LNG low-temperature exergy cannot be used.

5.6.2.2. Natural Gas demand

The LNG regasification rate varies for each of the scenarios described in [sections 5.5.1-5.5.3](#). The LNG send-out rate in a satellite plant for single consumer ([Figure 5.9 \(a\)](#), [section 5.5.1](#)) with or without connection to the electricity grid is determined from [Eq. \(5.20\)](#) and [Eq. \(5.21\)](#), respectively:

$$\dot{m}_{LNG} = \frac{\dot{Q}_H}{\eta_b \times LHV} \quad (5.20)$$

$$\dot{m}_{LNG} = \underbrace{\frac{\dot{Q}_H}{\eta_b \times LHV}}_{\text{Heating}} + \underbrace{\frac{\dot{Q}_R - \dot{m}_{LNG}(h_{L3} - h_{L2})}{EER \times \eta_{el} \times LHV}}_{\text{Electricity for refrigeration production}} + \underbrace{\frac{\dot{W}_{el,O}}{\eta_{el} \times LHV}}_{\text{Electricity for other uses}} \quad (5.21)$$

where η_b and η_{el} are the efficiencies of the boiler and the electric generator, respectively. The lower heating value (LHV) of natural gas is assumed 13.4 kWh/kg. Notice that, as shown in [Eq. \(5.21\)](#), the utilization of the LNG cold energy leads into a fuel-saving.

On the other hand, the LNG flow in the scenario of a satellite plant for a base-load power plant ([Figure 5.9 \(b\)](#), [section 5.5.2](#)) is calculated as a function of the electric output of the plant ($\dot{W}_{el,plant}$):

$$\dot{m}_{LNG} = \frac{\dot{W}_{el,plant}}{\eta_{el} \times LHV} \quad (5.22)$$

The regasification pattern in a local satellite plant that supplies gas to dwellings ([Figure 5.9 \(c\)](#), [section 5.5.3](#)) and that of large-scale harbour terminals look alike. The LNG send-out rate depends on the hour and the type of day (i.e., weekday or weekend) which affects the user’s behaviour and their energy consumptions, and also on the weather (mainly on the outdoor temperature [335]). It is assumed that the use of the regasified natural gas as fuel for space heating increases linearly as the outdoor temperature

decreases, and it is null when the outdoor temperature climbs above 18°C [336]. On the other hand, the use for other household stuff (i.e., cooking or domestic hot water production) is assumed to be independent of the weather throughout the year [337].

The following regression model is used to estimate the relationship between the LNG send-out rate at any simulation time-step and the nameplate regasification capacity ($\dot{m}_{LNG,np}$) in a local satellite plant:

$$\frac{\dot{m}_{LNG}}{\dot{m}_{LNG,np}} = \left[\beta_1 + \beta_2 \times \frac{\max(0, 18^\circ\text{C} - T_o)}{\max(0, 18^\circ\text{C} - T_{o,min,year})} \right] \times \tau \quad (5.23)$$

The parameter τ determines the shape of the regasification pattern, as illustrated in Figure 5.12. The gas demand decreases dramatically at night and exhibits peaks of demand when the daily activity begins and also at the end of the day. The peaks of demand are delayed on weekends.

The parameters β_1 and β_2 determine the share of the natural gas utilization for cooking and domestic hot water production, and the use for space heating, respectively, to the total natural gas consumption. These parameters should be consistent with the weather conditions of each location. For instance, whether the outdoor temperature of a location is very high throughout most the year the use of natural gas for space heating is almost negligible, so $\beta_1 \approx 1$ and $\beta_2 \approx 0$. The ratio β_1/β_2 set for each location is: 1/0 in Bangkok, 0.4/0.6 in Tarragona; and 0.2/0.8 in Oslo. Figure 5.13 shows the variation of the ambient temperature and the refrigeration load during a year in these locations. Also, the variation of the monthly average LNG demand in a local satellite plant is illustrated.

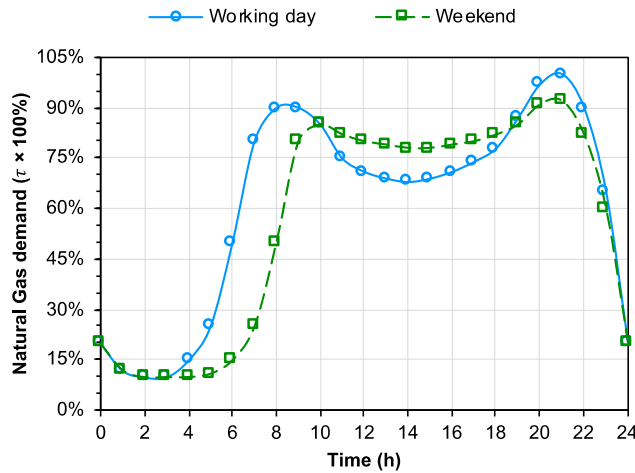


Figure 5.12. Natural demand pattern for household applications for typical weekdays and weekends.

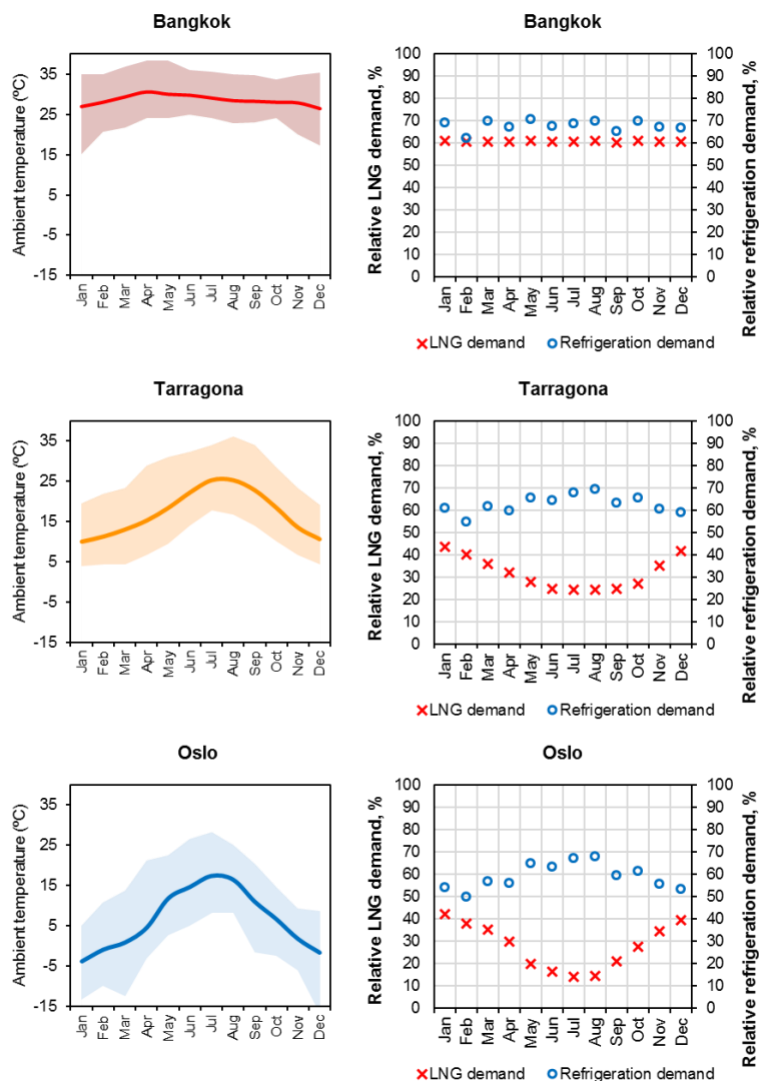


Figure 5.13. Monthly average relative LNG and refrigeration demands and evolution of the annual dry temperature in a typical year in (a) Bangkok, Thailand; (b) Tarragona, Spain; and (c) Oslo, Norway. Weather data obtained from EnergyPlus database [334].

5.6.3. Control system

The control system plays a key role for successful energy management in the cold utilization configurations and scenarios considered and its simplicity is an important practical restriction.

As shown in Figure 5.14 (a), a proportional controller prevents an excessive subcooling of the heat transfer medium in the double-bundle heat exchanger, thereby avoiding freezing problems. To do that, the position of the two-way valve installed upstream of the upper tube bundle is modulated to limit the LNG flow rate entering in function on the thermal load of the freezing room. The coolant flow rate is assumed constant, and the temperature of the warm return stream (stream C1) is monitored each simulation time-step (set to 5 minutes). In function of that temperature and the set-point temperature of the cooled coolant stream, leaving the bottoming tube bundle (stream C2), the control output signal (γ) is obtained from the following expression:

$$\gamma = \frac{\dot{m}_{L2}}{\dot{m}_{L2,design}} = \frac{1}{(T_{C2} - T_{C1})_{SP}} \times \max(0, T_{C1,SP} - T_{C1}) + 1 \quad (5.20)$$

The valve is fully open ($\gamma = 1$) when the refrigeration load of the freezing rooms corresponds to the peak value, whilst is fully close ($\gamma = 0$) when the refrigeration demand is null.

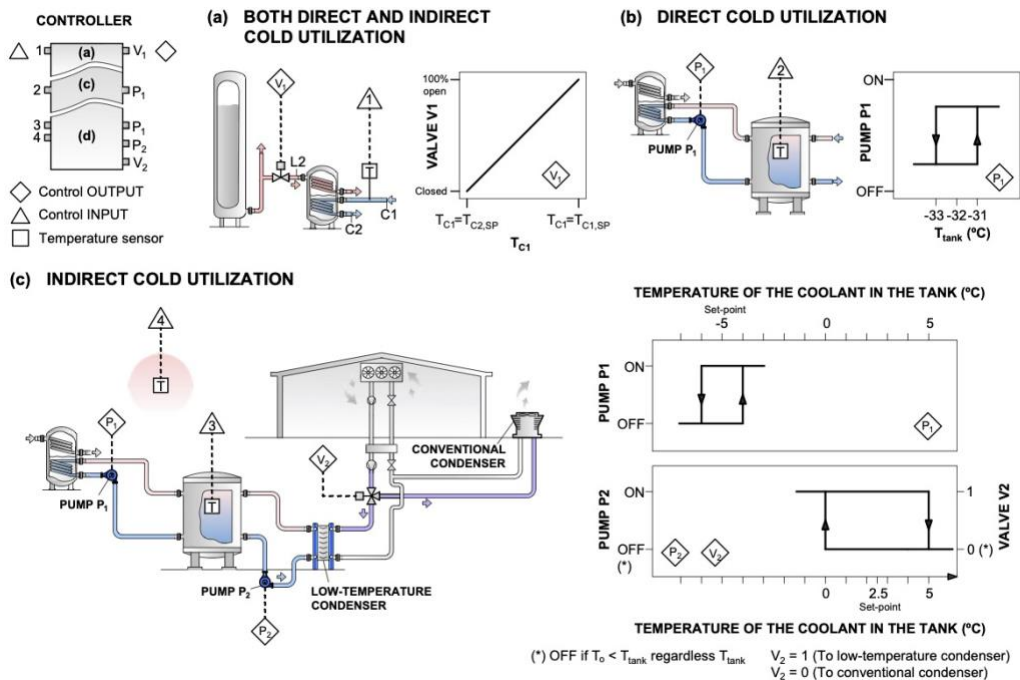


Figure 5.14. Control system. (a) Modulation of the LNG flow rate entering the double-bundle heat exchanger both in the direct and the indirect cold use configurations, (b) Control of the pump P1 in the direct configuration and (c) Energy management in the indirect cold use configuration.

As illustrated in [Figure 5.14 \(b\)](#) and [Figure 5.14 \(c\)](#), a two-position (on/off) controller starts/stops the motor of the pump P1 in function of the set-point temperature of the coolant in the tank (-5°C) with a differential of $\pm 1^{\circ}\text{C}$ to avoid very short on-and-off cycles. An on/off control mode is also utilized for managing the operation of the pump P2 and the diverting three-way valve installed in the VC circuit in the indirect cold utilization configuration. For controlling these components, it is used a set-point for the temperature of the cold energy storage tank of 2.5°C with a differential of $\pm 2.5^{\circ}\text{C}$ to avoiding very-short shifting of condenser. Whether the ambient temperature is below the temperature of the coolant in the cold storage tank, the pump P2 is turned off, and the refrigerant is condensed in the conventional unit.

5.6.4. Economic analysis

The economic analysis for the LNG cold energy recovery in satellite plants is based on the annual simulation results of the configurations and scenarios defined in the previous sections. The following assumptions are made for economic analysis:

- A new-built refrigerated warehouse is considered.
- The system's lifetime (n) is assumed for 30 years.
- The annual discount rate (r) is set to 10%.
- The electricity tariff (C_e) is 0.12 USD/kWh.
- No carbon taxes are applied in the base case.
- Neither renewable energies subsidies nor government incentives are considered.

The purchase equipment cost (PEC) of the main system components are estimated from the cost functions listed in [Table 5.4](#). To consider the inflation since these correlations were published and brought the PEC estimated up to the reference year (considered 2018), the *Chemical Engineering Plant Cost Index (CEPCI)* annual average composite values are used:

$$PEC = PEC_y \times \frac{CEPCI_{ref}}{CEPCI_y} \quad (5.24)$$

The Fixed Capital Investment (FCI) of the system splits into Cost of main equipment (PEC), the installation of equipment (10% of PEC), piping (10% of PEC), instrumentation and control (6% of PEC) and electric equipment and material (10% of PEC). The Total Capital Investment (TCI) also includes the working capital and the start-up cost, which are assumed 15% and 5% of the FCI , respectively. On the other hand, apart from the electricity bills, the annual expenditures of the system are due to fuel expenditures ($Fuel$), operation and maintenance ($O\&M$), insurance and taxes ($I\&T$) and annual overheads costs (OC) which are set as 6% (12 USD/kW in the case of a PV

system), 1% and 1% of the *FCI*, respectively. Notice that the fuel expenditures are only considered in the case of an off-grid warehouse.

Table 5.4. Purchase cost functions (in USD) for the main system components.

System component	Purchase cost function (USD)	Source
- Pumps	$1120 \times \dot{W}_{(kW)}^{0.8}$	[273]
- Double-bundle heat exchanger ^a	$3.28 \times 10^4 (A_{(m^2)}/80)^{0.68} \times f_m \times f_p$	[275]
- Low-temperature condenser ^a	$635.14 \times A_{(m^2)}^{0.778}$	[276]
- Cold storage tank ^b	$5700 + 700 \times V_{(m^3)}^{0.7}$	[277]
- Forced air-cooled coil ^b	$1.56 \times 10^5 (A_{(m^2)}/200)^{0.89} \times f_p$	[275]
- VCR machine	$4900 + 720 \times Q_{(kW)}^{0.9}$	[277]
- Photovoltaic installation	$2.10 \times \dot{W}_{el,PV(kW)}$	[338]

Note: The following reference overall heat transfer coefficient is utilized to estimate the heat transfer area of heat exchangers: 0.2 kW/(m²·K) for the double-bundle heat exchanger; 0.6 kW/(m²·K) for the heat exchanger HE-3 (assumed plate-and-frame type) and the 0.5 kW/(m²·K) for the forced air-cooled coil.

^a Material factor (f_m) = 2.4 (stainless-steel 304L); Pressure factor (f_p) = 1.5 for the direct cold use configuration and 1 for the indirect cold use configuration.

^b Pressure factor (f_p) = 1.5.

The economic feasibility of the systems proposed in this study is evaluated through the Levelized Cost of Refrigeration (*LCOR*), which is a parameter that indicates the present value of the total cost of producing a unit of refrigeration over the whole system's lifetime (in USD/kWh). Its mathematical definition is as follows:

$$LCOR = \frac{TCI + \sum_1^n (\dot{W}_{el,R} \times C_e + Fuel + O\&M + I\&T + OC) / (1+r)^n}{\sum_1^n \dot{Q}_R / (1+r)^n} \quad (5.25)$$

5.7. Results and discussion

5.7.1. Plant owned by a single user

Table 5.5 shows a breakdown of the energy demands and depicts the cold recovery potential in a satellite plant owned by a single-user (see Figure 5.9 (a)) with a total energy demand of 1 MW and with the typical demand mix set in section 5.6.2. The following observations can be made:

- The cold that could be recovered from LNG-regasification represents only 2-3% of the peak refrigeration demand of an off-grid warehouse, whilst is almost negligible if the natural gas is consumed only for heating production. Therefore, the direct LNG

cold utilization configuration is unfeasible to handle the whole refrigeration load of the warehouse in a satellite installation of a single warehouse, and a back-up refrigeration system is required. The cold would be directly utilized only in an individual freeze room of the warehouse whose refrigeration load is much than the total refrigeration demand.

- Regardless of the climate, when the gas is used only for heat production, the electricity-saving from the indirect utilization of the cold of the LNG regasified is extremely low ($\sim 1\%$). Since the cold available is extremely low, the cold storage tank has a too long cooling time, and the low-temperature condenser is rarely utilized (less than 4% of the year in the most advantageous case). In the case of an off-grid warehouse, figures obtained improve but are still poor. The electricity consumption of the VCR machine decreases between 1.2-3.9%, and the LNG saving as fuel is 0.6-1.8%; therefore, the reduction of GHGs emissions is also negligible.

Table 5.6 compares the annual energetic and economic results of both a conventional refrigeration system without LNG cold use and of a system that utilizes that cold indirectly (see Figure 5.8 (b)) in the case of a typical off-grid warehouse of the meat industry. The electricity saving achieved from the utilization of the LNG cold leads into a slight LNG saving as fuel ($< 1.3\%$). Nevertheless, the reduction of fuel expenditures is not well enough to outweigh the higher capital investment, and the *LCOR* obtained by both systems is alike.

5.7.2. Satellite plant for electric power production

Figure 5.15 shows the annual results obtained for the different LNG cold energy utilization configurations in a satellite plant for electric power production and for a range of refrigeration capacity indexes between 0.5 and 5.5. Since the results are analysed through dimensionless quantities, the conclusions obtained are valid for any size of the satellite LNG plant. The following observations can be made:

- As shown in Figure 5.15 (a), as the design refrigeration demand increases in relation to the LNG cold available, the cold recovery ratio increases, and the cold energy wastes decreases. When $RCI \leq 1$, the direct configuration utilizes a higher fraction of the total LNG cold available than the indirect configuration. For instance, if the peak refrigeration load matches the maximum LNG cold available (i.e., $RCI = 1$) the direct cold utilization exploits up to ~ 45 -51% of the LNG cold energy available throughout the year, whilst the indirect configuration utilizes only $\sim 30\%$. The indirect configuration achieves higher cold utilization ratios as the *RCI* increases. But from an $RCI \simeq 2.5$ hereunder, the LNG cold utilization ratio grows at a slower pace until is stabilized at around 70-80%. This is because, as the *RCI* increases, the LNG cold energy available becomes increasingly scarce to deal with the refrigeration load of the freezing rooms. Generally, the warmer is the climate, the higher both refrigeration

Table 5.5. Results of design energy demands and LNG cold recovery potential in a satellite plant owned by a single user of two type of agro-food industries. Values referenced to total energy demand of 1 MW (Electricity + Heat).

Case ^a	Public electrical grid connection	Electricity, kW			Heat, kW	Peak Refrigeration load ^b , kW	LNG consumption as fuel ^c , kg/h			Max. LNG cold energy available, kW
		Total	Refrigeration machines	Other utilities			Total	Heat production	Electricity production	
A	Yes	500	250	250	500	~ 570	41.5	41.5	0	7.4 (~ 1% ^d)
	No	500	250	250	500	~ 570	99.8	41.5	41.5	17.8 (~ 3% ^d)
B	Yes	850	425	425	150	~ 969	12.4	12.4	0	2.2 (< 1% ^d)
	No	850	425	425	150	~ 969	112.3	12.4	99.9	20.0 (~ 2% ^d)

^a Case A (typical meat industry): 50% electricity; 50% heat; Case B (typical horticultural industry): 85% electricity; 15% heat (see [section 5.6.2](#)).

^b Reference Energy Efficiency Ratio (*EER*): 2.28 W/W, assuming a heat sink at 32°C and full refrigeration load conditions.

^c Efficiencies of heating and electricity production assumed at 90% and 47%, respectively.

^d Share of the peak refrigeration load.

Table 5.6. Annual energetic and economic results for an off-grid refrigerated warehouse with and without LNG cold energy utilization in different locations and for different total energy demands.

Total energy demand ^a , MW	Location	Conventional case without LNG cold energy recovery				Indirect LNG cold energy utilization ^b			
		Electricity consumption, MWh/y	LNG consumption, t/y	<i>TCI</i> , thousand USD	<i>LCOR</i> ^c , USD/kW	Electricity consumption, MWh/y	LNG consumption, t/y	<i>TCI</i> , thousand USD	<i>LCOR</i> ^c , USD/kW
1	Bangkok	1,885	729	491	0.40	1,831 (↓ 2.9%)	719 (↓ 1.3%)	521	0.40
	Tarragona	1,347	643	491	0.40	1,320 (↓ 2.1%)	637 (↓ 1.0%)	521	0.40
	Oslo	989	586	491	0.39	978 (↓ 1.1%)	582 (↓ 0.8%)	521	0.40
5	Bangkok	9,427	2,804	2,056	0.31	9,202 (↓ 2.4%)	2,768 (↓ 1.3%)	2,118	0.31
	Tarragona	6,737	2,376	2,056	0.31	6,634 (↓ 1.5%)	2,352 (↓ 1.0%)	2,118	0.31
	Oslo	4,944	2,092	2,056	0.30	4,909 (↓ 0.7%)	2,075 (↓ 0.8%)	2,118	0.30
10	Bangkok	18,854	5,397	3,826	0.30	18,454 (↓ 2.1%)	5,329 (↓ 1.3%)	3,919	0.30
	Tarragona	13,475	4,543	3,826	0.29	13,283 (↓ 1.4%)	4,496 (↓ 1.0%)	3,919	0.29
	Oslo	9,888	3,973	3,826	0.28	9,814 (↓ 0.7%)	3,941 (↓ 0.8%)	3,919	0.28

^a The total is sum of the electricity and heat. Case A (typical meat industry): 50% electricity; 50% heat. An off-grid warehouse is considered (see [section 5.6.2](#)).

^b Quantities between parenthesis indicate the difference (in %) with respect to the case without LNG cold energy utilization.

^c Assuming an LNG price as fuel of 6 USD/MMBtu.

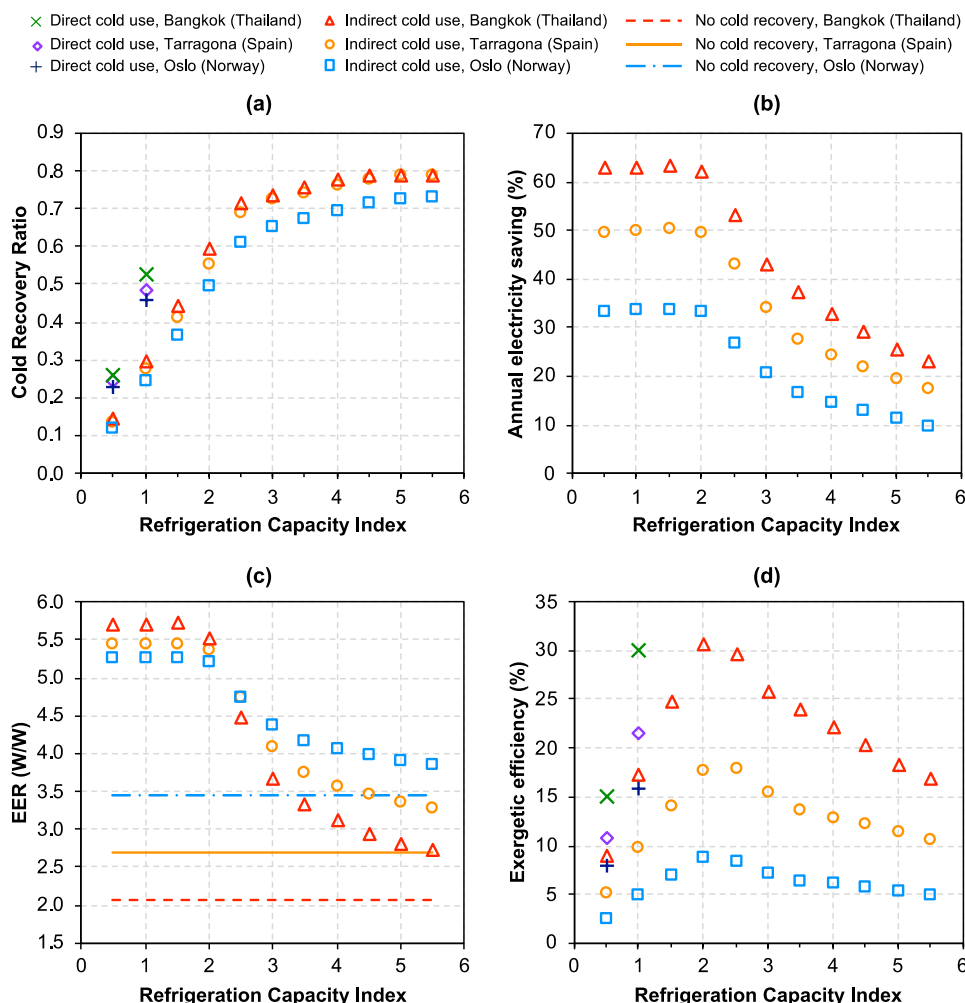


Figure 5.15. Annual results for a satellite LNG for power generation. (a) Cold Recovery Ratio, (b) Annual electricity-saving, (c) Energy Efficiency Ratio, EER , of the VCR machine, (d) Exergetic efficiency.

demand and cold recovery ratio, and vice versa. But as the RCI increases, the influence of the climate on the cold recovery ratio tends to wear off.

- Figure 5.15 (b) illustrates the annual electricity savings achieved by the indirect configuration with respect to the conventional refrigeration system without LNG cold energy recovery. For an $RCI < 2$, the electricity-saving is around 63%, 50%, 33% in Bangkok, Tarragona and Oslo, respectively. For example, the indirect utilization of the LNG cold in a satellite plant that supplies gas to a 50 MW electric power plant

and for an *RCI* of 1, reports an annual electricity saving of 2.5, 1.4 and 0.7 GWh/year in Bangkok, Tarragona and Oslo, respectively.

As shown in [Figure 5.15 \(a\)](#), the higher cold recovery ratios in warm climates imply a major improvement upon the *EER* of the VCR machine (see [Figure 5.15 \(c\)](#)) and, therefore, in a high electricity saving. But the electricity-saving decreases sharply when the design refrigeration load is more than twice the maximum LNG cold available. As the *RCI* increases (i.e., > 2), the conventional air condensing unit is utilized more often, and the *EER* of the VCR machine approaches that of the scenario without cold utilization.

- [Figure 5.15 \(d\)](#) depicts the exergetic efficiencies obtained. The direct configuration reports exergetic efficiencies of 30%, 22% and 16% in Bangkok, Tarragona and Oslo, respectively, when the design refrigeration load matches the maximum LNG cold available (i.e., $RCI = 1$). Notice that lower *RCIs* and coldest climates entail higher LNG cold wastes and, therefore, lower exergetic efficiencies. In any case, these efficiencies are higher than the obtained by the indirect configuration due to the lower sources of irreversibilities. A remarkable fact in the case of the indirect cold utilization configuration, is that there is an optimum exergetic efficiency for an *RCI* between 2.0-2.5: 30%, 17%, 9% in Bangkok, Tarragona and Oslo, respectively. The higher is the outdoor temperature of the location, the more valuable is LNG as low-temperature exergy source.

Regarding the environmental performance, the same observations made above for the influence of the climate and the *RCI* on the electricity-saving are valid for the avoided GHGs emissions. The direct configuration avoids nearly 100% of the annual GHGs emission with respect to a conventional refrigeration system without LNG cold energy utilization. For instance, in a satellite plant that supplies gas to a 50 MW electric power plant and for an *RCI* of 1, the estimated GHGs emissions avoided by exploiting the LNG cold energy directly are: 1,167, 834 and 611 t-CO₂/year in Bangkok, Tarragona and Oslo, respectively. Likewise, the GHGs emissions avoided by the indirect configuration estimated in the same scenario are 738, 418 and 206 t-CO₂/year in Bangkok, Tarragona and Oslo, respectively.

5.7.2.1. Economic performance

Regarding the economic feasibility, [Table 5.7](#) shows the total capital investment of each configuration considered for different electricity generation capacities of the power plant (1-200 MW) and, therefore, different sizes of satellite LNG plant (i.e., nameplate vaporization capacities between 245-48,342 Nm³/h). An *RCI* of 1 and also an *RCI* of 2 in the case of the indirect configuration are considered. On the other hand, [Figure 5.16](#) shows the *LCOR* estimated in each case. The *LCOR* estimated for the direct configuration is in the range 0.10-0.45 USD/kWh, which is, by far, the lowest among the different configurations considered.

Table 5.7. Total capital investment (in thousand USD) estimated for the different configurations considered and refrigeration capacity indexes, and for a satellite LNG plant for baseload power generation.

Configuration	Electric power capacity, MW	Refrigeration Capacity Index (Eq. 5.19) equal to 1					Refrigeration Capacity Index (Eq. 5.19) equal to 2				
		Peak refriger. load, kW	TCI, thousand USD (USD/kW ^f)	Electricity consumption, MWh/y			Peak refriger. load, kW	TCI, thousand USD (USD/kW ^f)	Electricity consumption, MWh/y		
				Bangkok	Tarragona	Oslo			Bangkok	Tarragona	Oslo
<i>Conventional</i> refrigeration system without LNG cold use	1 ^a	28	43 (1,500)	78	56	41	56	70 (1,250)	157	112	82
	10 ^b	278	263 (950)	785	561	412	557	481 (860)	1,570	1,122	823
	50 ^c	1,392	1,084 (780)	3,924	2,804	2,058	2,784	2,013 (720)	7,848	5,609	4,116
	100 ^d	2,784	2,013 (720)	7,848	5,609	4,116	5,567	3,746 (670)	15,695	11,217	8,231
	200 ^e	5,567	3,746 (670)	15,695	11,217	8,231	11,134	6,981 (630)	31,391	22,434	16,463
<i>Direct</i> LNG cold use configuration (Figure 5.8 (a))	1 ^a	28	66 (2,360)	1.0	1.0	0.9	-	-	-	-	-
	10 ^b	278	338 (1,210)	2.7	2.7	2.4	-	-	-	-	-
	50 ^c	1,392	1,205 (870)	5.3	5.2	4.7	-	-	-	-	-
	100 ^d	2,784	2,116 (760)	7.1	7.0	6.3	-	-	-	-	-
	200 ^e	5,567	3,738 (670)	9.6	9.4	8.5	-	-	-	-	-
<i>Indirect</i> LNG cold use configuration (Figure 5.8 (b))	1 ^a	28	76 (2,710)	31	30	29	56	107 (1,910)	63	60	58
	10 ^b	278	371 (1,330)	293	283	276	557	609 (1,090)	601	572	555
	50 ^c	1,392	1,384 (999)	1,447	1,400	1,366	2,784	2,373 (850)	2,976	2,835	2,752
	100 ^d	2,784	2,488 (890)	2,888	2,794	2,726	5,567	4,319 (780)	5,941	5,660	5,495
	200 ^e	5,567	4,503 (810)	5,767	5,579	5,444	11,134	7,898 (710)	11,867	11,305	10,977

- Nameplate vaporization rate of the satellite LNG plant (Eq. 5.22): ^a 245 Nm³/h (0.16 t/h); ^b 2,417 Nm³/h (1.6 t/h); ^c 12,082 Nm³/h (7.9 t/h); ^d 24,171 Nm³/h (15.9 t/h); ^e 48,342 Nm³/h (31.8 t/h).

- Maximum LNG cold energy available: ^a 28 kW; ^b 278 kW; ^c 1,392 kW; ^d 2,784 kW; ^e 5,567 kW.

^f Values between parenthesis indicates the specific cost of the refrigeration system in USD/kW, defined as the ratio between the total capital investment and the peak refrigeration load.

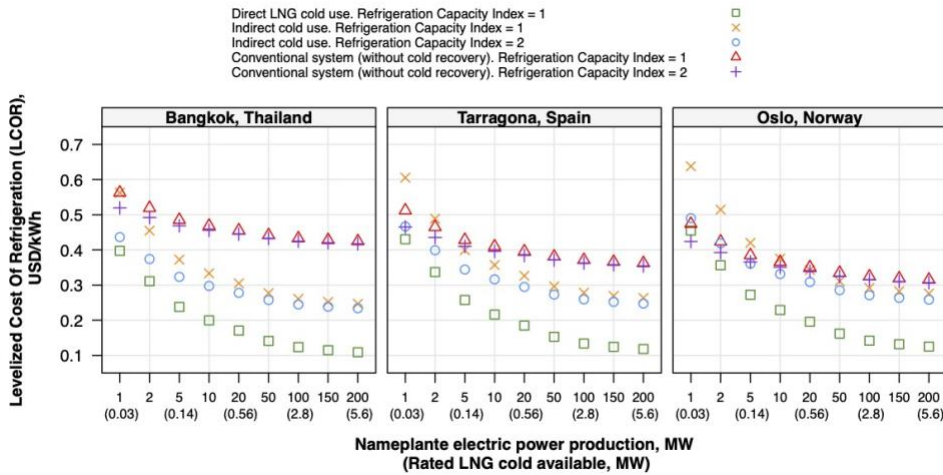


Figure 5.16. Levelized Cost of Refrigeration (*LCOR*) as a function of the size of satellite LNG plant (determined by the nameplate capacity electric power plant) for the direct, indirect and the conventional VCR system without LNG low-temperature exergy utilization in different locations.

Although the maximum refrigeration yields by the direct configuration to freezing rooms is constrained by the peak LNG cold energy available, the capital investment required is the lowest, and the electricity consumption is almost null. In contrast, the indirect configuration requires the highest specific capital investment per unit of LNG cold energy utilized (i.e., in USD/kW) with an *LCOR* estimated in the range 0.25-0.64 USD/kWh for an *RCI* of 1, and 0.23-0.49 USD/kWh for an *RCI* of 2; and a very limited economic competitiveness in cold climates. On the other hand, the impact of the *RCI* on the economic performance of the indirect configuration is only important in the case of very small plant sizes.

As shown in Table 5.7, although the total cost increases with the size of the systems, the specific investment per unit of refrigeration produced decreases and the absolute annual electricity saving increases. Thus, the economic competitiveness of the LNG cold utilization systems increases as the size of the satellite plants does. But in the case of small power plants (i.e., < 5 MW), the *LCOR* estimated for the conventional system without LNG cold energy utilization is similar or even lower than that of the indirect cold use configuration.

5.7.3. Local satellite plant

Figure 5.17 shows the annual dimensionless results obtained for the indirect LNG cold energy utilization in a local satellite facility for refrigeration capacity indexes ranging between 0.2 and 2. On the other hand, Table 5.8 shows the capital investment estimated

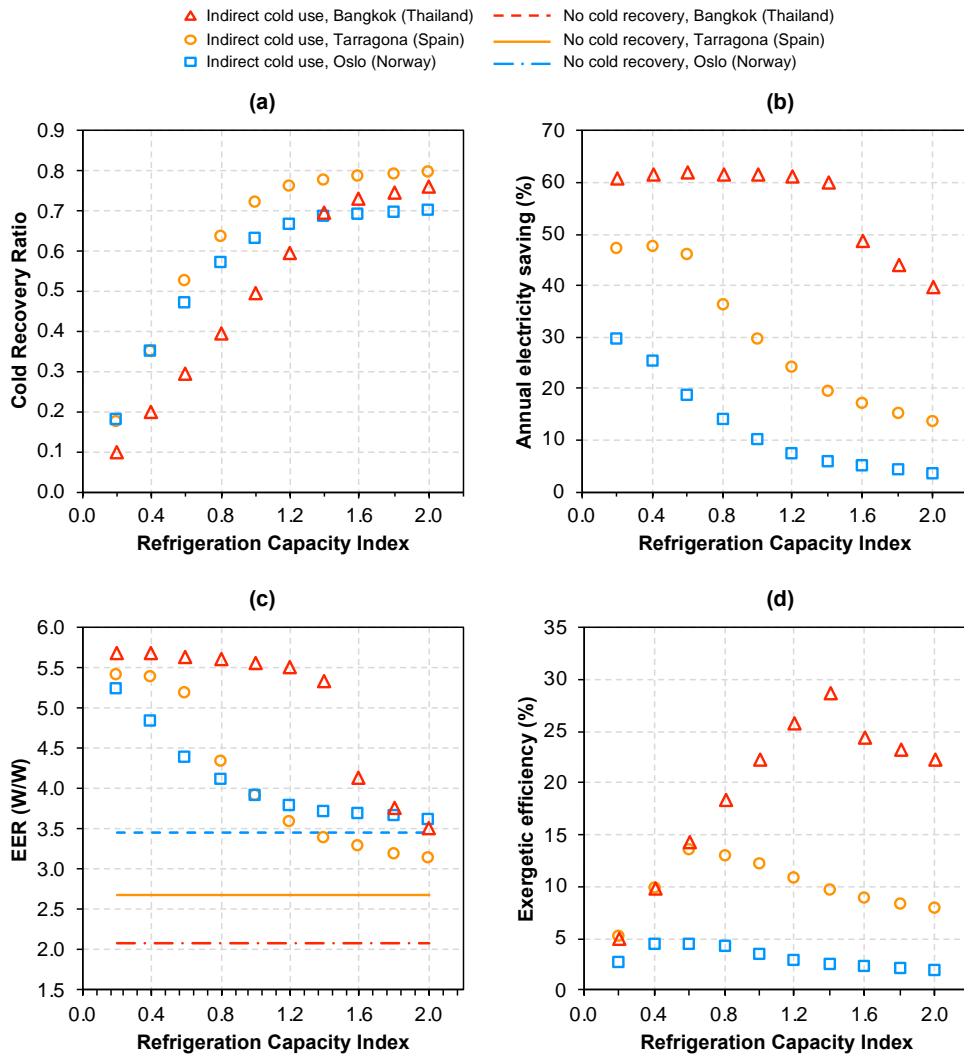


Figure 5.17. Monthly results obtained for a *satellite LNG plant for base-load power production* in three different climate conditions analysed (Tarragona – TGN, Bangkok – BKK and Oslo – OSL). (a) Cold Recovery Ratio, (b) Electricity saving, (c) Energy Efficiency Ratio, *EER*, of the VCR machine and (d) Exergetic efficiency.

and the electricity consumption calculated for both the indirect cold utilization configuration and for the refrigeration system without LNG cold energy utilization. The following observations are withdrawn:

- As shown in [Figure 5.17 \(a\)](#), the cold utilization ratio increases with the *RCI*. But the climate determines the performance of the LNG cold energy utilization systems strongly. The reason is the different seasonal variation of the LNG consumption and,

therefore, the unequal availability of “free” cold energy. For a given size of satellite plant, the LNG consumption is estimated nearly constant throughout the year in climates with high and constant temperature like in Bangkok (see [Figure 5.13](#)). In contrast, in cold climates like in Oslo, there is a wide variation since the gas demand for space heating decreases dramatically in summer. Consequently, the season of highest refrigeration load (i.e., summer) matches the season of lowest LNG consumption and the cold energy available falls short for lower *RCIs* than in warmer climates.

- [Figure 5.17 \(b\)](#) shows that, in Bangkok, the maximum electricity-saving achieved with respect to the conventional refrigeration system without LNG cold use is ~ 61%, ~ 47% in Tarragona, and ~ 30% in Oslo. For instance, as shown in [Table 5.8](#), in a typical local satellite plant with a nameplate vaporization capacity of 1,500 Nm³/h and considering that the design refrigeration load of the freezing rooms matches the maximum LNG cold energy available (i.e., *RCI* = 1), the electricity-saving by exploiting indirectly the LNG low-temperature exergy estimated is 310, 107 and 26 MWh/year in Bangkok, Tarragona and Oslo, respectively. As illustrated in [Figure 5.17 \(c\)](#), the improvement on the *ERR* of the VCR machine with respect the case without LNG cold use has a greater impact in warm locations, which leads into higher electricity savings.
- The electricity savings achieved are kept closer to the maximum for higher *RCIs* in warm climates than in cold climates, mainly because of a better match between the refrigeration load and the LNG cold energy available throughout a year. Again, as the *RCI* increases, there is an increasing shortage of LNG cold energy in relation to the refrigeration load, so the air-condensing unit is activated more often and the *EER* trends to approach that of the scenario without cold utilization. On the other hand, an optimum exergetic efficiency for each location is observed in [Figure 5.17 \(d\)](#): 29% (*RCI* = ~ 1.4), 14% (*RCI* = ~ 0.6) and 4% (*RCI* = ~ 0.4) in Bangkok, Tarragona and Oslo, respectively. In such optimum point, the environmental performance in a local satellite plant with a nameplate vaporization capacity of 1,500 Nm³/h and for in a local satellite plant, the annual avoided GHGs emissions are 92, 32 and 8 t-CO_{2,eq} in Bangkok, Tarragona and Oslo, respectively.

5.7.3.1. Economic performance

The economic performance of the indirect LNG cold utilization configuration in local satellite plants is evaluated for the following three different plant sizes (i.e., nameplate vaporization capacities):

- *Small-size* plant: 300 Nm³/h (0.2 t-LNG/h).
- *Medium-size* plant: 1,500 Nm³/h (1.0 t-LNG/h).
- *Large-size* plant: 5,000 Nm³/h (3.3 t-LNG/h).

Table 5.8. Capital investment estimated and annual electricity consumption calculated for the conventional refrigeration system without LNG cold energy utilization and the indirect LNG cold utilization configuration **in local satellite plants** with different sizes.

Plant size	Refrig. Capacity Index (Eq. 5.19)	Peak refriger. load, kW	Configuration								
			Conventional refrigeration system without LNG cold use						Indirect LNG cold use configuration (Figure 5.8 (b))		
			TCI, thousand USD (USD/kW ^d)	Electricity consumption, MWh/y			TCI, thousand USD (USD/kW ^d)	Electricity consumption, MWh/y			
Bangkok	Tarragona	Oslo		Bangkok	Tarragona	Oslo					
Small ^a	0.2	7.03	20.0 (2,840)	20	14	11	40.9 (5,820)	9	9	8	
	0.6	21.1	35.5 (1,680)	60	43	32	65.1 (3,090)	24	25	27	
	1	35.2	50.0 (1,420)	101	72	53	86.3 (2,450)	41	53	49	
	1.4	49.2	63.8 (1,290)	141	101	74	102.1 (2,080)	59	83	72	
	2	70.3	83.9 (1,190)	202	144	106	124.8 (1,770)	104	127	104	
Medium ^b	0.2	35.2	50.0 (1,420)	101	72	53	86.3 (2,450)	39	38	37	
	0.6	105.4	116.0 (1,100)	302	216	159	178.3 (1,690)	115	117	129	
	1	175.7	177.4 (1,010)	504	360	264	260.2 (1,480)	194	253	238	
	1.4	246.0	236.3 (1,070)	705	504	370	325.0 (1,320)	281	406	349	
	2	351.5	321.7 (920)	1,008	720	529	418.5 (1,190)	606	624	510	
Large ^c	0.2	117.2	126.5 (1,080)	336	240	176	192.5 (1,642)	127	123	120	
	0.6	351.5	321.7 (920)	1,008	720	529	446.7 (1,270)	378	381	423	
	1	585.8	503.1 (860)	1,680	1,200	881	674.9 (1,152)	637	834	785	
	1.4	820.2	677.3 (830)	2,351	1,681	1,233	862.9 (1,050)	927	1,342	1,154	
	2	1,172	929.8 (790)	3,359	2,401	1,762	1,134.0 (970)	2,010	2,067	1,690	

- Nameplate vaporization rate: ^a 300 Nm³/h (0.2 t/h); ^b 1,500 Nm³/h (1.0 t/h); ^c 5,000 Nm³/h (3.3 t/h).

- Maximum LNG cold energy available: ^a 32.5 kW; ^b 175.7 kW; ^c 585.8 kW.

^d Values between parenthesis indicates the specific cost of the refrigeration system in USD/kW, defined as the ratio between the total capital investment and the peak refrigeration load.

On the other hand, [Figure 5.18](#) shows the variation of the *LCOR* estimated. According to the results, the indirect LNG cold recovery system is economically unfeasible in cold climates since the electricity savings achieved are not enough to offset the high capital investment (see [Table 5.8](#)). Although the economic performance improves for warmer climates and larger plant sizes, the LNG cold utilization system is only clearly competitive in locations with high and constant temperatures throughout the year and for large-size plants.

As shown in [Figure 5.18](#), in those cases where the LNG cold recovery system is economically more competitive than the conventional refrigeration system, the lowest values of *LCOR* estimated correspond to the *RCI* that optimizes the exergetic efficiency.

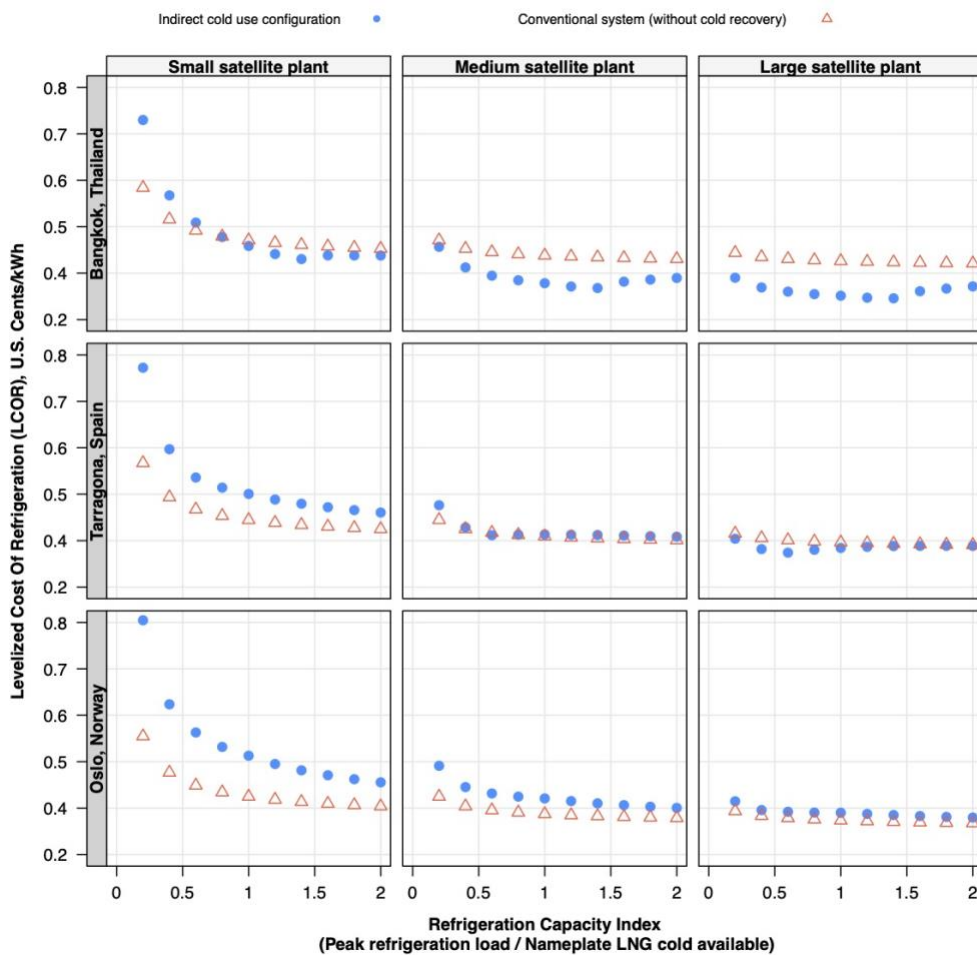


Figure 5.18. Levelized Cost of Refrigeration (*LCOR*) obtained for a **local satellite LNG plant** that supplies natural gas to a rural community in different locations, plant sizes (Small – 300 Nm³/h; Medium – 1,500 Nm³/h; and Large 5,000 Nm³/h) and refrigeration capacity indexes.

For instance, in Bangkok, the *LCOR* estimated for an *RCI* of 1.4 and a medium-size and large-size plants are 0.34 and 0.29 USD/kWh, respectively. In Tarragona, the lowest *LCOR* estimated is 0.35 USD/kWh which corresponds to a large-size plant and an *RCI* of 0.6

5.7.4. The integration of PV technology

Figure 5.19 depicts the economic performance through the levelized cost of refrigeration (Eq. 5.24) of the indirect LNG cold utilization system (see Figure 5.8 (b)) and of the conventional VCR system without LNG low-temperature exergy utilization, both with PV integration to cover the half of the electricity consumption for refrigeration production. As one of the most typical type of plant, a medium-size local satellite plant with a nameplate vaporization capacity of 1,500 Nm³/h is used as a reference case to evaluate the feasibility of introducing PV panels.

Results are analysed for different climates and electricity prices ranging between 2-30 USD-cent/kWh. Regarding the imposition of a carbon tax, two cases are considered: (1) no carbon tax imposed, and (2) a carbon tax imposed of 120 USD/t-CO_{2,eq}, which would correspond an ambitious environmental policy. A refrigeration capacity index (see Eq. 5.19) equal to 1 is assumed. On the other hand, Table 5.9 shows the capital investment, details about the PV generator and also the GHGs emissions for each location. *It should be noted that the results shown are strictly subject to the particular assumptions and cost estimating correlations considered in section 5.6.4.*

According to the results, the conventional system, combined with a PV installation, does not provide neither economic nor environmental improvement with respect to the LNG cold utilization system. Moreover, it requires to install a much larger PV generator with the corresponding higher capital investment. However, despite a remarkable environmental benefit, the introduction of PV technology in the LNG low-temperature exergy utilization system has a very limited economic competitiveness. Indeed, in cold locations and with low radiation levels (e.g., Oslo), the economic performance of the LNG cold utilization system gets worst when PV technology is introduced (even for high electricity tariffs). In such locations, the electricity savings achieved are insufficient to offset the expenditures of the PV installation.

The economic perspectives, when introducing PV technology improve when a carbon tax is imposed and in warmer climates and with higher radiation levels due to the higher electricity savings achieved. But, ultimately, the economic feasibility depends on the electricity tariff. For example, if no carbon taxes are imposed, the hybrid system (PV + LNG cold utilization) is economically advantageous from electricity prices beyond approximately 18 and 20 USD-cent/kWh, in Bangkok and Tarragona, respectively. If a carbon tax of 120 USD/t-CO_{2,eq} is imposed, the hybrid system is economically feasible

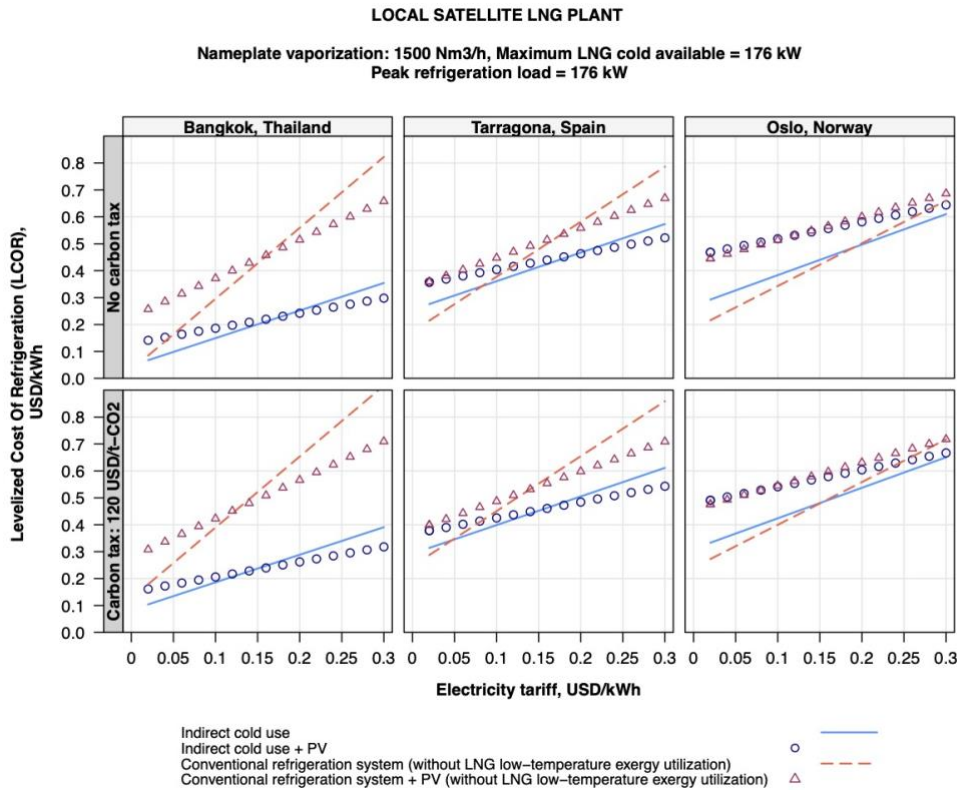


Figure 5.19. Levelized Cost of Refrigeration (*LCOR*) as a function of the electricity tariff in a medium-size satellite LNG plant for the indirect cold utilization and for the conventional vapour-compression refrigeration system both with and without PV integration (coverage of 50% of the electricity consumption) and in different locations. A refrigeration capacity index (Eq. 5.19) equal to 1 is assumed.

from electricity prices beyond approximately 14 and 16 USD-cent/kWh in Bangkok and Tarragona, respectively.

5.8. Conclusions

This chapter of the thesis tackled the utilization of the LNG low-temperature exergy throughout its regasification process in satellite facilities for sustainable refrigeration applications in the agro-food industry. Two configurations were proposed for exploiting that exergy content directly without back-up refrigeration systems or indirectly by adapting the conventional refrigeration installation. On the other hand, three types of satellite plant have been considered as representative scenarios to evaluate the techno-economic feasibility of these configurations taking into account the influence of the

Table 5.9. Integration of PV technology in both a configuration for utilizing the LNG cold energy indirectly in a local medium-size satellite plant (Nameplate vaporization: 1,500 Nm³/h and peak refrigeration load assuming an $RCI = 1$ (Eq. 5.19): 175.7 kW) and in a conventional refrigeration system: Size of the PV generator, capital investment and GHGs emissions of during the whole systems' lifetime.

Configuration	Location	Annual-average total radiation on PV panels' surface, kWh/(m ² ·day)	PV capacity installed, kW	No. of PV panels ^a	TCL, thousand USD (USD/kW ^b)	GHGe ^c , t-CO _{2,eq} /30-year
- VCR system without LNG cold use + PV	Bangkok	4.96	742.5	2,970	1,736 (9,880)	12,537
	Tarragona	4.49	114.3	457	417 (2,370)	1,789
	Oslo	2.27	160.5	642	514 (2,930)	1,314
- Indirect LNG cold energy use + PV	Bangkok	4.96	287.3	1,149	863 (4,910)	4,892
	Tarragona	4.49	58.0	232	382 (2,170)	950
	Oslo	2.27	111.8	447	495 (2,820)	957

^a The PV generator is sized to cover 50% of the average electricity consumed for refrigeration production in the warehouse. Model of PV panel: Panasonic Slim VBHN250SJ25 (250 W) [328].

^b Values between parenthesis indicates the specific cost of the refrigeration system in USD/kW, defined as the ratio between the total capital investment and the peak refrigeration load.

^c Emissions during the whole system's lifetime and considering an emission factor of 0.298 kgCO₂-eq/kWh.

climate. It was also discussed the convenience of introducing PV panels to enhance the competitiveness of the configurations developed. The main conclusions are:

- 1) The technical feasibility of the direct utilization of the LNG low-temperature exergy is limited to very specific scenarios. Since no back-up refrigeration systems are utilized in this configuration, a constant or baseload LNG vaporization rate throughout the year is required to ensure that a minimum amount of “free” low-temperature thermal energy is available to avoid refrigeration outages. The direct configuration is unsuitable in a satellite plant owned by a single user since in these types of facilities the “free” low-temperature thermal energy available from LNG-regasification is much lower than the refrigeration demand of the freezing rooms. The direct configuration is also unfeasible in a local satellite plant due to the fluctuating LNG vaporization pattern in these types of terminals and the difficulty to determine a baseload fraction. A promising scenario of a satellite plant where the LNG low-temperature could be exploited directly, and with excellent economic competitiveness regardless the climate is a satellite plant that supplies natural gas to a baseload power plant because of the constant LNG vaporization rate and, therefore, the constant amount of low-temperature thermal energy available. However, even in that scenario, any failure or maintenance shutdown at the natural gas regasification side could put at risk the refrigeration supply.
- 2) The indirect configuration proposed in this chapter of the thesis (whose working principle is based on lowering the condensation temperature of the vapour-compression machines to boost the refrigeration efficiency and to reduce the electricity consumption) overcomes the unreliability of the direct configuration. This

configuration could reduce the electricity consumption of the refrigeration machines up to 60% in satellite plants located in warm climates that supply gas for a power plant or in a local satellite plant but at the expenses of a high capital investment which constraint the economic feasibility. Generally, the economic competitiveness of the indirect configuration improves as the amount of “*free*” low-temperature thermal energy exploited increases due to the lower specific cost of the equipment. On the other hand, the economic competitiveness enhances considerably in warmer climates because of a greater improvement of the refrigeration efficiency of the vapour-compression refrigeration machine with respect to the conventional case without LNG exergy utilization. In cold climates, the electricity-saving achieved throughout the year is not enough to outweigh the high capital investment required, and the indirect configuration would not be economically feasible. From a technical perspective, the indirect configuration could be introduced in the scenario of a satellite plant owned by a single user to reduce the energy consumption, but the LNG cold energy available in relation to the refrigeration load and the electricity (or fuel) savings are so small that the economic benefit would be null.

- 3) The ratio between the refrigeration load of freezing rooms with respect to the maximum LNG low-temperature thermal energy available should be carefully determined for any engineering project aiming to utilize the LNG low-temperature exergy in satellite facilities for refrigeration in freezing rooms. This ratio, apart from the climate and the overall size of the installation, has a noteworthy influence on the exergetic efficiency and on the economic feasibility. On the other hand, the combination of a grid-tie PV installation with the indirect LNG low-temperature exergy utilization system may enhance the economic competitiveness but only in locations where electricity prices are high (approximately beyond 18-20 USD/kWh), in warm climates and with high radiation levels. With the aim to perform a conservative base-case economic analysis, nor the imposition of carbon taxes, neither subsidies/government incentives have been considered in the base-case scenario. But definitely, all these factors could boost the economic competitiveness of the LNG exergy utilization systems (and the integration of PV technology as well) and promote their widespread use in satellite regasification facilities.

UNIVERSITAT ROVIRA I VIRGILI

EXERGY RECOVERY FROM LNG-REGASIFICATION FOR POLYGENERATION OF ENERGY

Antonio Atienza Márquez

Chapter 6. General conclusions and future outlook

6.1. Conclusions

Because of its cryogenic temperature and usually high regasification pressure, LNG is a *premium quality* source of physical exergy which can be exploited for multiple applications. However, that potential is wasted in most of the regasification terminals worldwide. The main bottleneck lies in the low efficiencies and weak economic competitiveness. To enhance the efficiency with respect to single-application configurations, several research works tackled the utilization of LNG physical exergy through polygeneration configurations. However, complexity and capital investments of proposed configurations are much higher. And more often than not, the proposed polygeneration plants are purely theoretical without a practical approach so that their implementation into the market will be challenging. Additionally, the vast majority of studies are focused on large-scale terminals, whilst the literature dealing with satellite facilities is scarce.

In this thesis, different *non-combustion* polygeneration systems were proposed to regasify LNG and exploit its physical exergy as a by-product through cascaded configurations. The models developed aims to determine the potential of that technical solution and to address critical issues such as the selection of the operating fluids. Also, the objective was to achieve the techno-economic feasibility by boosting the efficiency but with a moderate increase of the structural complexity. The production of electricity and refrigeration at different temperatures were the applications studied. Furthermore, both large-scale harbour terminals and satellite facilities were considered.

6.1.1. Large-scale regasification facilities

The first large-scale polygeneration plant presented was integrated by different power units (RCs and a DE unit) arranged in cascade and by a DC network that distributes low-temperature thermal energy to users with refrigeration demand at different temperature levels. The design was consistent with the availability of resources and type of industries located near the Barcelona LNG Terminal (Spain). The plant was utilized as a case-study to discuss the selection of the most suitable working fluids and heat transfer fluids depending on the application and the thermal boundary conditions. The performance simulation showed the following facts:

- 1) None of the fluids selected matched all the features of an ideal candidate but was the one that achieved the best trade-off between all the indicators. Methane, was selected as working fluid for the RC cycle that uses seawater as heat source and operates between 10°C and -130°C; Carbon Dioxide was selected both as working fluid of the RC that operates between 30°C and -30°C and as heat transfer fluid of the low-temperature DC network: and propane was selected as working fluid for the RC cycle that uses biomass as heat source and operates between 300°C and -10°C.

- 2) At the baseline case considered (i.e., 180 t-LNG/h, regasification and send-out pressure: 7.2 and 3.0 MPa, respectively) and operating with the selected fluids the plant produced equivalent electricity of 125.3 kWh/t-LNG (i.e., 13.2 MW of net electric power, 16.4 MW of refrigeration: 8.2 MW at -25°C; 6.6 MW at -10°C; and 1.6 MW at 5°C). The exergetic efficiency reported was 40%, the double than the reported by existing cryogenic power generation units based on RC cycle. Moreover, the plant could ideally avoid the annual emission of 59 thousand tonnes of GHGs and achieve an annual primary energy and seawater savings of 380 GWh and 60%, respectively, with respect to the conventional regasification process without LNG physical exergy utilization.
- 3) The fluids selected for that specific case-study plant will not necessarily be the most suitable for other configurations. The selection of fluids is an issue that has to be addressed carefully for each specific case study and considering the particular operating conditions. However, the fluids preselection tips and recommendations provided in this chapter as well as the decision-making process presented can be utilized as a sort of guideline in future studies and projects on this subject. The major conclusion is that natural fluids are suitable to operate in LNG physical exergy recovery systems and even could report a better system performance than, for example, HFCs (among other human-made fluids).

Afterwards, the large-scale polygeneration configurations subsequently presented in the thesis were built upon an existing 6 MW power generation unit which consists of a propane cryogenic RC (driven by seawater or process water) and a DE unit. The objective was to address the techno-economic issue in depth. Operating data were collected from the literature, and the model of the benchmark cryogenic power plant was calibrated. Also, the information available regarding constructive details of the main components enabled to evaluate the economic performance. Apart from the regasification of LNG and the production of electricity, the configurations developed from the reference power unit and their services provides the following. A CCP system (type i) that produced low-temperature (-50°C) refrigeration in a double-bundle heat exchanger and distributed through a CO₂ DC network; a CCP system (type ii) that produced refrigeration (4.4°C) for air-conditioning applications; and a polygeneration unit that combined the two CCP units. All the configurations operated only with natural fluids. The simulation results drawn the following conclusions:

- 1) At the baseline operating conditions (i.e., 150 t-LNG/h regasification and send-out pressure: 4.6 MPa and 1.8 MPa, respectively), the polygeneration configuration reported the both highest equivalent electricity production and exergetic efficiency: 150 kWh/t-LNG and 42%, respectively. Indeed, up to 80% of the low-temperature thermal energy that could be ideally recovered was transformed into useful energy. Although the net electric output (3.5 MW) decreases 40% with respect to the benchmark plant, the production of low-temperature refrigeration (21 MW) and refrigeration at 4.4°C (5.8 MW) boosts the performance of the system. The avoided

GHGs emissions by the system were estimated at 44.6 kg-CO₂e per metric tonne of LNG regasified.

- 2) The off-design performance analysis showed that the overall production improves as the heat source temperatures and LNG flow rates increase, and low regasification pressures are preferable for the systems that produce low-temperature refrigeration.
- 3) Polygeneration could make the physical exergy recovery from LNG-regasification economically viable. For the base-case scenario (electricity tariff of 106.5 USD/MWh and carbon tax of 60 USD/t-CO₂e) the polygeneration unit reports a payback time of 5 years. The economic performance of the CCP-(i) unit was also very promising reporting a payback slightly lower than the polygeneration unit. However, the economic analysis also showed the weak competitiveness of single application systems as in the case of the reference power unit. Also, it was observed the poor economic performance of systems that produce only energy services with low quality (from the exergy point of view) such as the refrigeration for air-conditioning applications. The electricity tariff and the level of the imposition of carbon prices are major factors that ultimately determine the economic viability.

6.1.2. Satellite regasification facilities

The last part of the thesis tackled the LNG low-temperature exergy utilization in satellite plants for refrigeration applications in foodstuff industries located in-situ or nearby the regasification site. Two different strategies for exploiting the LNG low-temperature exergy were proposed: (1) *Direct*: without back-up refrigeration systems, and (2) *Indirect*: the aim is to improve the efficiency by reducing the condensing temperature of vapour-compression refrigeration machines. The main findings obtained from the techno-economic analysis in different climates and for different plant sizes were the following:

- The types of satellite plant with a constant LNG vaporization rate throughout the year (e.g., those that supplies gas to a base-load power plant) are the most attractive for exploiting the low-temperature exergy in the regasification process. By contrast, in the case of satellite plants of single users, the LNG cold that could be recovered is usually negligible with respect to the total refrigeration demand of a typical foodstuff warehouse. The economic competitiveness improves with the size of the plant and in warmer climates. Furthermore, for each specific case-study, there is a ratio of the peak refrigeration load of the cold rooms to the maximum cold available from the LNG-regasification that optimizes the economic performance. This ratio has to be carefully evaluated for each specific case-study.
- From an economic perspective, the direct utilization of the low-temperature thermal energy of LNG is the most attractive option. However, that strategy reported weak operational flexibility and reliability. It would be technically feasible only in those scenarios with a constant LNG flow rate (e.g., a satellite plant that supplies gas to

a baseload power plant), because there are not back-up refrigeration systems to face cold shortages derived from a fluctuating gas demand as occurs, for example, in a local satellite terminal.

- The indirect configuration provides security in the refrigeration supply and a versatile operation, so can be adapted to multiple scenarios and types of satellite plant. But both the structural complexity and the capital investment increase with respect to the direct configuration, and the energy management requires a more sophisticated control system. As a result, the economic viability of the indirect configuration is limited to medium-large size satellite plants located in areas with temperate/warm climates. In those most advantageous scenarios, electricity savings up to 60% could be obtained. On the other hand, with the current market prices, the integration of PV panels could improve the competitiveness of the indirect configuration for electricity tariffs above 180-200 USD/MWh. The imposition of carbon taxes would further improve economic perspectives.

6.2. Final remark and future outlook

As a final remark, the results of this doctoral thesis showcased that polygeneration is an economically feasible technical solution to squeeze the LNG physical exergy in cascade. The combined and simultaneous production of cryogenic power and refrigeration at different temperatures provides added value to the LNG regasification infrastructure in large-scale terminals. Likewise, in some scenarios of satellite regasification facilities, the use of the cryogenic temperature of LNG to produce low-temperature refrigeration will contribute to enhancing the competitiveness and sustainability of local industries.

In the near future, the decarbonization policies (e.g., regarding fuel shifting strategies, application of carbon taxes, refrigerants phase-out roadmaps, among other points) will largely determine the short-medium term expansion of the infrastructure and the further development of new technologies for exploiting the physical exergy of LNG in regasification terminals. Particularly, the bio-LNG market requires also regasification facilities. It can use and share the already existing infrastructure of conventional gas, and its potential expansion opens a promising horizon of opportunity for the systems developed in this thesis, especially for those focused on satellite facilities.

On the other hand, although several detailed energetic, environmental and economic analysis were presented in this thesis, there are still some pending aspects to be addressed. Further studies in both theoretical and experimental aspects are required. Some future works and lines of research are indicated in the following points:

- **Detailed study of the double-bundle heat exchanger** presented in the thesis for the production of low-temperature refrigeration using CO₂ as heating media. The construction of this type of unit requires of an exhaustive design. Therefore, a highly

accurate sizing the heat transfer areas are crucial to avoid, for example, an excessive subcooling of the CO₂ streams that could entail freezing risk. For this purpose, a more detailed thermodynamic modelling (e.g., applying finite difference methods) is required. But also, to estimate the film coefficient accurately for the different fluids involved is crucial to develop new “*customized*” empirical or semi-empirical correlations for the different fluids involved in the heat transfer and valid for the operating boundaries (i.e., mass fluxes, temperatures and pressures) expected for the unit. Thus, to build experimental set-ups would be required. Also, the construction of prototypes will be essential to study the operation and the practical limitations in depth.

- **Design and construction of a pilot plant to study the utilization of the LNG low temperature in satellite plants for refrigeration applications.** How some technical aspects affect the system performance could be studied, for example, the effect of the thermal load variations or the intermittency of the gas demand, which determines the availability of cold. Also, different **energy management control algorithms** could develop and tested to optimize system performance.
- **Techno-economic assessment of cold thermal energy storages integrated with LNG physical exergy recovery systems.** These systems could provide a technical solution to issues derived from the part-load operation. For example, the excess/lack of low-temperature thermal energy depending on the mismatch between the gas and refrigeration demands, which are subjected to hourly and seasonal variations. Besides, this line of research will involve the development of demonstration projects and several experimental works related to, for example, the technologies and materials utilized for the cold storage.

References

- [1] National Aeronautics and Space Administration (NASA), The Effects of Climate Change, (2020). <https://climate.nasa.gov/effects/> (accessed 28 March 2020).
- [2] International Institute of Refrigeration (IIR), Kyoto Protocol, 2017.
- [3] T. Vandyck, K. Keramidas, B. Saveyn, A. Kitous, Z. Vrontisi, A global stocktake of the Paris pledges: Implications for energy systems and economy, *Glob. Environ. Chang.* 41 (2016) 46–63. DOI: 10.1016/J.Gloenvcha.2016.08.006.
- [4] European Commission, The European Green Deal, *Eur. Comm.* (2019).
- [5] International Energy Agency (IEA), Data and statistics, (2020). [https://www.iea.org/data-and-statistics?country=WORLD&fuel=Energy supply&indicator=Total primary energy supply \(TPES\) by source](https://www.iea.org/data-and-statistics?country=WORLD&fuel=Energy supply&indicator=Total primary energy supply (TPES) by source) (accessed 26 March 2020).
- [6] BP p.l.c., BP Energy Outlook 2019 edition, (2019).
- [7] C. Kuzemko, M. Bradshaw, G. Bridge, A. Goldthau, J. Jewell, I. Overland, D. Scholten, T. Van de Graaf, K. Westphal, Covid-19 and the politics of sustainable energy transitions, *Energy Res. Soc. Sci.* 68 (2020) 101685. DOI: 10.1016/J.Erss.2020.101685.
- [8] B. Steffen, F. Egli, M. Pahle, T.S. Schmidt, Navigating the Clean Energy Transition in the COVID-19 Crisis, *Joule*. 4 (2020) 1137–1141. DOI: 10.1016/J.Joule.2020.04.011.
- [9] International Energy Agency (IEA), Outlook for biogas and biomethane. Prospects for organic growth, 2020.
- [10] I. Energy Agency, World Energy Outlook Special Report on Unconventional Gas, n.d.
- [11] International Energy Agency (IEA), The Role of Gas in Today’s Energy Transitions, 2019.
- [12] International Energy Agency (IEA), Statistics report. Natural Gas Information - Overview, Paris, 2020.
- [13] International Energy Agency (IEA), Gas 2020, Paris, 2020.
- [14] S. Mokhtab, J.Y. Mak, J. V Valappil, D.A. Wood, Handbook of Liquefied Natural Gas, Elsevier Science, 2013.
- [15] B. Kavalov, H. Petric, A. Georgakaki, Liquefied Natural Gas for Europe - Some Important Issues for Consideration, 2009. DOI: 10.2790/1045.
- [16] S.H. Ali, Greening Natural Gas Delivery – LNG versus Pipelines, 2014.
- [17] R. Bruno, P. Bevilacqua, N. Arcuri, Energy Recovery from the LNG Regasification Process, in: *Adv. Nat. Gas Emerg. Technol., InTech*, 2017. DOI: 10.5772/67771.
- [18] Y. Du, S. Paltsev, International Trade in Natural Gas : Golden Age of LNG ?, 2014.
- [19] C. Le Fevre, A review of demand prospects for LNG as a marine transport fuel, (2018) 35. DOI: 10.26889/9781784671143.
- [20] International Maritime Organisation (IMO), Studies on the feasibility and use of LNG as a fuel for shipping, 2016.
- [21] Gasnam, Motores marinos a gas natural (In Spanish), 2020. (n.d.). <https://gasnam.es/maritimo/motores-marinos-a-gas-natural/> (accessed 11 September 2020).
- [22] I. Smajla, D. Karasalihović Sedlar, B. Drljača, L. Jukić, Fuel Switch to LNG in Heavy Truck Traffic, *Energies*. 12 (2019) 515. DOI: 10.3390/En12030515.
- [23] A. Arteconi, C. Brandoni, D. Evangelista, F. Polonara, Life-cycle greenhouse gas analysis of LNG as a heavy vehicle fuel in Europe, *Appl. Energy*. 87 (2010) 2005–2013. DOI: 10.1016/J.Apenergy.2009.11.012.
- [24] National Renewable Energy Laboratory, Using LNG as a Fuel in Heavy-Duty Tractors, (1999) 28.

- [25] International Gas Union (IGU), 2020 World LNG Report, (2020).
- [26] International Gas Union (IGU), The natural gas industry: Methane emissions challenge, (2017) 23.
- [27] Cedigaz, Natural Gas and Liquefied Natural Gas Databases, (2020). <https://www.cedigaz.org/> (accessed 6 August 2020).
- [28] bp p.l.c., Statistical Review of World Energy, (2020). <https://www.bp.com/en/global/corporate/energy-economics/statistical-review-of-world-energy.html> (accessed 6 August 2020).
- [29] International Gas Union (IGU), Resources - IGU Reports, (2020). <https://igu.org/resources/> (accessed 6 August 2020).
- [30] International Group of Liquefied Natural Gas Importers (GIIGNL), GIIGNL Publications, (2020). <https://giignl.org/publications> (accessed 6 August 2020).
- [31] T. Okamura, M. Furukawa, H. Ishitani, Future forecast for life-cycle greenhouse gas emissions of LNG and city gas 13A, *Appl. Energy*. 84 (2007) 1136–1149. DOI: 10.1016/J.Apenenergy.2007.05.005.
- [32] T. Iannaccone, G. Landucci, A. Tugnoli, E. Salzano, V. Cozzani, Sustainability of cruise ship fuel systems: Comparison among LNG and diesel technologies, *J. Clean. Prod.* 260 (2020) 121069. DOI: 10.1016/J.Jclepro.2020.121069.
- [33] Y. Zhiyi, O. Xunmin, Life cycle analysis on liquefied natural gas and compressed natural gas in heavy-duty trucks with methane leakage emphasized, *Energy Procedia*. 158 (2019) 3652–3657. DOI: 10.1016/J.Egypro.2019.01.896.
- [34] M. Al-Breiki, Y. Bicer, Comparative life cycle assessment of sustainable energy carriers including production, storage, overseas transport and utilization, *J. Clean. Prod.* 279 (2021) 123481. DOI: 10.1016/J.Jclepro.2020.123481.
- [35] S. Sun, M. Ertz, Life cycle assessment and Monte Carlo simulation to evaluate the environmental impact of promoting LNG vehicles, *MethodsX*. 7 (2020) 101046. DOI: 10.1016/J.Mex.2020.101046.
- [36] N. Pavlenko, B. Comer, Y. Zhou, N. Clark, D. Rutherford, The climate implications of using LNG as a marine fuel, *ICCT Work. Pap.* 2020-02. (2020).
- [37] L. Langshaw, D. Ainalis, S. Acha, N. Shah, M.E.J. Stettler, Environmental and economic analysis of liquefied natural gas (LNG) for heavy goods vehicles in the UK: A Well-to-Wheel and total cost of ownership evaluation, *Energy Policy*. 137 (2020) 111161. DOI: 10.1016/J.Enpol.2019.111161.
- [38] R.A. Alvarez, D. Zavala-Araiza, D.R. Lyon, D.T. Allen, Z.R. Barkley, A.R. Brandt, K.J. Davis, S.C. Herndon, D.J. Jacob, A. Karion, E.A. Kort, B.K. Lamb, T. Lauvaux, J.D. Maasackers, A.J. Marchese, M. Omara, S.W. Pacala, J. Peischl, A.L. Robinson, P.B. Shepson, C. Sweeney, A. Townsend-Small, S.C. Wofsy, S.P. Hamburg, Assessment of methane emissions from the U.S. oil and gas supply chain, *Science* (80-.). 361 (2018) 186–188. DOI: 10.1126/Science.Aar7204.
- [39] J.C. Peters, Natural gas and spillover from the US Clean Power Plan into the Paris Agreement, *Energy Policy*. 106 (2017) 41–47. DOI: 10.1016/J.Enpol.2017.03.039.
- [40] GIE, Marcogaz, Potential ways the gas industry can contribute to the reduction of methane emissions, 2019.
- [41] T.J. Skone, G. Cooney, M. Jamieson, J. Littlefield, J. Marriott, Life cycle greenhouse gas perspective on exporting liquefied natural gas from the United States, 2014.
- [42] A. Sharafian, H. Talebian, P. Blomerus, O. Herrera, W. Mérida, A review of liquefied natural gas refueling station designs, *Renew. Sustain. Energy Rev.* 69 (2017) 503–513. DOI: 10.1016/J.Rser.2016.11.186.
- [43] International Energy Agency (IEA), Korea Energy Economics Institute, LNG Market Trends and Their Implications, 2019. DOI: 10.1787/90c2a82d-En.
- [44] A. Atienza-Márquez, J.C. Bruno, A. Coronas, Cold recovery from LNG-regasification for polygeneration applications, *Appl. Therm. Eng.* 132 (2018) 463–478. DOI:

- 10.1016/J.Applthermaleng.2017.12.073.
- [45] W. Mazyan, A. Ahmadi, H. Ahmed, M. Hoorfar, Market and technology assessment of natural gas processing: A review, *J. Nat. Gas Sci. Eng.* 30 (2016) 487–514. DOI: 10.1016/J.Jngse.2016.02.010.
- [46] O. Koku, S. Perry, J.K. Kim, Techno-economic evaluation for the heat integration of vaporisation cold energy in natural gas processing, *Appl. Energy.* 114 (2014) 250–261. DOI: 10.1016/J.Apenergy.2013.09.066.
- [47] M. Mehrpooya, M. Omid, A. Vatani, Novel mixed fluid cascade natural gas liquefaction process configuration using absorption refrigeration system, *Appl. Therm. Eng.* 98 (2016) 591–604. DOI: 10.1016/J.Applthermaleng.2015.12.032.
- [48] J. Pospíšil, P. Charvát, O. Arsenyeva, L. Klimeš, M. Špiláček, J.J. Klemeš, Energy demand of liquefaction and regasification of natural gas and the potential of LNG for operative thermal energy storage, *Renew. Sustain. Energy Rev.* 99 (2019) 1–15. DOI: 10.1016/J.Rser.2018.09.027.
- [49] M.S. Khan, I.A. Karimi, D.A. Wood, Retrospective and future perspective of natural gas liquefaction and optimization technologies contributing to efficient LNG supply: A review, *J. Nat. Gas Sci. Eng.* 45 (2017) 165–188. DOI: 10.1016/J.Jngse.2017.04.035.
- [50] I.S. Al-Mutaz, X. Liu, G. Mazza, Natural gas liquefaction technologies - An overview, *Oil Gas Eur. Mag.* 42 (2016) 213–218.
- [51] S. Kumar, H.T. Kwon, K.H. Choi, W. Lim, J.H. Cho, K. Tak, I. Moon, LNG: An eco-friendly cryogenic fuel for sustainable development, *Appl. Energy.* 88 (2011) 4264–4273. DOI: 10.1016/J.Apenergy.2011.06.035.
- [52] Qatargas - Future Fleet, (2014). <http://www.qatargas.com/English/AboutUs/Pages/FutureFleet.aspx> (accessed 7 September 2017).
- [53] Enagas, Barcelona Regasification Plant, (n.d.).
- [54] E. Querol, B. Gonzalez-Reguerol, J. García-Torrent, M.J. García-Martínez, Boil off gas (BOG) management in Spanish liquid natural gas (LNG) terminals, *Appl. Energy.* 87 (2010) 3384–3392. DOI: 10.1016/J.Apenergy.2010.04.021.
- [55] A. Atienza-Márquez, D.S. Ayoub, J. Carles Bruno, A. Coronas, Energy polygeneration systems based on LNG-regasification: Comprehensive overview and techno-economic feasibility, *Therm. Sci. Eng. Prog.* 20 (2020) 100677. DOI: 10.1016/J.Tsep.2020.100677.
- [56] R. Agarwal, T. Rainey, S. Rahman, T. Steinberg, R. Perrons, R. Brown, LNG Regasification Terminals: The Role of Geography and Meteorology on Technology Choices, *Energies.* 10 (2017) 2152. DOI: 10.3390/En10122152.
- [57] D. Patel, J. Mak, D. Rivera, J. Angtuaco, LNG vaporizer selection based on site ambient conditions, in: *Gas Process. Assoc. 30th Annu. Conf.*, Edinburgh, 2013.
- [58] K. Mori, The expansion of LNG use in Japan, *15th Int. Conf. Exhib. Liq. Nat. Gas.* (2007) 14.
- [59] G. Tsatsaronis, T. Morosuk, Advanced exergetic analysis of a novel system for generating electricity and vaporizing liquefied natural gas, *Energy.* 35 (2010) 820–829. DOI: 10.1016/J.Energy.2009.08.019.
- [60] Osaka Gas Co. Ltd., High-performance open rack LNG vaporizer SUPERORV, (n.d.). https://www.osakagas.co.jp/en/rd/technical/1198901_6995.html (accessed 6 August 2020).
- [61] C. Qi, W. Wang, B. Wang, Y. Kuang, J. Xu, Performance analysis of submerged combustion vaporizer, *J. Nat. Gas Sci. Eng.* 31 (2016) 313–319. DOI: 10.1016/J.Jngse.2016.03.003.
- [62] Sumitomo Precision Products Co. Ltd. - Heat Exchanger Division, Products. Various heat exchangers in energy market, (2020). <https://www.spp.co.jp/netsu/en/products/lng/> (accessed 9 November 2020).
- [63] Kobe Steel Ltd., Intermediate Fluid Vaporizer, (2019). <http://www.kobelco.co.jp/english/products/ecmachinery/lng/ifv.html> (accessed 22 March 2019).
- [64] S. Liu, W. Jiao, L. Ren, H. Wang, P. Zhang, Dynamic heat transfer analysis of liquefied natural

- gas ambient air vaporizer under frost conditions, *Appl. Therm. Eng.* 110 (2017) 999–1006. DOI: 10.1016/J.Applthermaleng.2016.09.016.
- [65] S. Xu, X. Chen, Z. Fan, Thermal design of intermediate fluid vaporizer for subcritical liquefied natural gas, (2016). DOI: 10.1016/J.Jngse.2016.04.031.
- [66] L. Pu, Z. Qu, Y. Bai, D. Qi, K. Song, P. Yi, Thermal performance analysis of intermediate fluid vaporizer for liquefied natural gas, *Appl. Therm. Eng.* 65 (2014) 564–574. DOI: 10.1016/J.Applthermaleng.2014.01.031.
- [67] European Commission, European Strategic Energy Technology Plan (SET-Plan), (2017) 13. https://setis.ec.europa.eu/system/files/integrated_setplan/%0Aissues_paper_action6_ee_industry_0.pdf (accessed 10 June 2018).
- [68] D. Coulomb, J.-L. Dupont, A. Pichard, The role of refrigeration in the economy, *IIR Inf. Notes Refrig. Technol.* 29 (2015).
- [69] International Energy Agency (IEA), The Future of Cooling. Opportunities for energy-efficient air conditioning, 2018.
- [70] U.S. Energy Information Administration (EIA), Annual Energy Outlook 2020 with projections to 2050, 2020.
- [71] The Carbon Trust, The Emerging Cold Economy. Sustainable solutions for rapidly increasing cooling needs, 2015.
- [72] J.L. Dupont, P. Domanski, P. Lebrun, F. Ziegler, The Role of Refrigeration in the Global Economy, 38th IIR Nformatory Note Refrig. Technol. (2019).
- [73] International Institute of Refrigeration (IIR), The impact of the refrigeration sector on climate change - 35th IIR Informatory Note on Refrigeration Technologies, 2017.
- [74] European Parliament, Council of the European Union, Regulation (EU) No 517/2014 of the European Parliament and of the Council of 16 April 2014 on fluorinated greenhouse gases and repealing Regulation (EC) No 842/2006, 2014.
- [75] The Economist Intelligence Unit, The Cooling Imperative. Forecasting the size and source of future cooling demand, 2019.
- [76] P. Van der Gaag, Bio-LNG: Improving eco-performance and quality of fossil LNG (in shipping). Options for Amsterdam, (2013).
- [77] M.A. Qyyum, J. Haider, K. Qadeer, V. Valentina, A. Khan, M. Yasin, M. Aslam, G. De Guido, L.A. Pellegrini, M. Lee, Biogas to liquefied biomethane: Assessment of 3P's—Production, processing, and prospects, *Renew. Sustain. Energy Rev.* 119 (2020) 109561. DOI: 10.1016/J.Rser.2019.109561.
- [78] F. Capra, F. Magli, M. Gatti, Biomethane liquefaction: A systematic comparative analysis of refrigeration technologies, *Appl. Therm. Eng.* 158 (2019) 113815. DOI: 10.1016/J.Applthermaleng.2019.113815.
- [79] A. Baccioli, M. Antonelli, S. Frigo, U. Desideri, G. Pasini, Small scale bio-LNG plant: Comparison of different biogas upgrading techniques, *Appl. Energy.* 217 (2018) 328–335. DOI: 10.1016/J.Apenenergy.2018.02.149.
- [80] A. Rehman, M.A. Qyyum, K. Qadeer, F. Zakir, Y. Ding, M. Lee, L. Wang, Integrated biomethane liquefaction using exergy from the discharging end of a liquid air energy storage system, *Appl. Energy.* 260 (2020) 114260. DOI: 10.1016/J.Apenenergy.2019.114260.
- [81] E.A. Roszak, M. Chorowski, Exergy analysis of combined simultaneous Liquid Natural Gas vaporization and Adsorbed Natural Gas cooling, *Fuel.* 111 (2013) 755–762. DOI: 10.1016/J.Fuel.2013.03.074.
- [82] A. Atienza-Márquez, J.C. Bruno, A. Akisawa, M. Nakayama, A. Coronas, Fluids selection and performance analysis of a polygeneration plant with exergy recovery from LNG-regasification, *Energy.* 176 (2019) 1020–1036. DOI: 10.1016/J.Energy.2019.04.060.
- [83] T. Morosuk, G. Tsatsaronis, Comparative evaluation of LNG – based cogeneration systems using

- advanced exergetic analysis, *Energy*. 36 (2011) 3771–3778. DOI: 10.1016/J.Energy.2010.07.035.
- [84] L. Zhao, J. Zhang, X. Wang, J. Feng, H. Dong, X. Kong, Dynamic exergy analysis of a novel LNG cold energy utilization system combined with cold, heat and power, *Energy*. 212 (2020) 118649. DOI: 10.1016/J.Energy.2020.118649.
- [85] T.K. Ibrahim, F. Basrawi, O.I. Awad, A.N. Abdullah, G. Najafi, R. Mamat, F.Y. Hagos, Thermal performance of gas turbine power plant based on exergy analysis, *Appl. Therm. Eng.* 115 (2017) 977–985. DOI: 10.1016/J.Applthermaleng.2017.01.032.
- [86] I. Dincer, M.A. Rosen, Chemical Exergy, in: I. Dincer, M.A. Rosen (Eds.), *Exergy*, Second Edi, Elsevier, 2013: pp. 31–49. DOI: 10.1016/B978-0-08-097089-9.00003-6.
- [87] T. Morosuk, G. Tsatsaronis, Splitting physical exergy: Theory and application, *Energy*. 167 (2019) 698–707. DOI: 10.1016/J.Energy.2018.10.090.
- [88] F-Chart Software, Engineering Equation Solver (EES), (2019).
- [89] Elsevier, Scopus, (2020). <https://www.scopus.com> (accessed 3 March 2020).
- [90] T. He, Z.R. Chong, J. Zheng, Y. Ju, P. Linga, LNG cold energy utilization: Prospects and challenges, *Energy*. 170 (2019) 557–568. DOI: 10.1016/J.Energy.2018.12.170.
- [91] B.B. Kanbur, L. Xiang, S. Dubey, F.H. Choo, F. Duan, Cold utilization systems of LNG: A review, *Renew. Sustain. Energy Rev.* 79 (2017) 1171–1188. DOI: 10.1016/J.Rser.2017.05.161.
- [92] G. Kashiyama, M. Nakagawa, Introduction of LNG Cryogenic Power Generation System, in: 13th Asian Int. Conf. Fluid Mach., Tokyo (Japan), 2015: pp. 1–10.
- [93] A. Atienza-márquez, J.C. Bruno, A. Coronas, An LNG-based system for the combined production of power and cooling, in: 2020. DOI: 10.18462/Iir.Rankine.2020.1202.
- [94] K. Jiang, Economic Analysis of LNG Cold Energy Utilization, in: X. Zhang, I. Dincer (Eds.), *Energy Solut. to Combat Glob. Warm.*, Springer International Publishing, Cham, 2017: pp. 119–132. DOI: 10.1007/978-3-319-26950-4_5.
- [95] W. Xia, Y. Huo, Y. Song, J. Han, Y. Dai, Off-design analysis of a CO₂ Rankine cycle for the recovery of LNG cold energy with ambient air as heat source, *Energy Convers. Manag.* 183 (2019) 116–125. DOI: 10.1016/J.Enconman.2018.12.098.
- [96] M.H. Ahmadi, M. Mehrpooya, S. Abbasi, F. Pourfayaz, J.C. Bruno, Thermo-economic analysis and multi-objective optimization of a transcritical CO₂ power cycle driven by solar energy and LNG cold recovery, *Therm. Sci. Eng. Prog.* 4 (2017) 185–196. DOI: 10.1016/J.Tsep.2017.10.004.
- [97] W. Stanek, T. Simla, B. Rutczyk, A. Kabaj, Z. Buliński, I. Szczygieł, L. Czarnowska, T. Krysiński, P. Gładysz, Thermo-ecological assessment of Stirling engine with regenerator fed with cryogenic exergy of liquid natural gas (LNG), *Energy*. 185 (2019) 1045–1053. DOI: 10.1016/J.Energy.2019.07.116.
- [98] M. Hou, Z. Wu, G. Yu, J. Hu, E. Luo, A thermoacoustic Stirling electrical generator for cold exergy recovery of liquefied nature gas, *Appl. Energy*. 226 (2018) 389–396. DOI: 10.1016/J.Apenergy.2018.05.120.
- [99] K. Wang, S. Dubey, F.H. Choo, F. Duan, Thermoacoustic Stirling power generation from LNG cold energy and low-temperature waste heat, *Energy*. 127 (2017) 280–290. DOI: 10.1016/J.Energy.2017.03.124.
- [100] M. Ge, X. Wang, Y. Zhao, S. Wang, L. Liu, Performance analysis of vaporizer tube with thermoelectric generator applied to cold energy recovery of liquefied natural gas, *Energy Convers. Manag.* 200 (2019) 112112. DOI: 10.1016/J.Enconman.2019.112112.
- [101] A. Franco, C. Casarosa, Thermodynamic analysis of direct expansion configurations for electricity production by LNG cold energy recovery, *Appl. Therm. Eng.* 78 (2015) 649–657. DOI: 10.1016/J.Applthermaleng.2014.11.062.
- [102] R. Ferreira García, J. Carbia Carril, J. Romero Gomez, M. Romero Gomez, Power plant based on three series Rankine cycles combined with a direct expander using LNG cold as heat sink, *Energy Convers. Manag.* 101 (2015) 285–294. DOI: 10.1016/J.Enconman.2015.05.051.

- [103] R. Ferreiro García, J. Jose, Carbia Carril, J. Romero Gómez, M. Romero Gómez, Combined cascaded Rankine and direct expander based power units using LNG (liquefied natural gas) cold as heat sink in LNG regasification, *Energy*. 105 (2016) 16–24. DOI: 10.1016/J.Energy.2015.09.051.
- [104] M.R. Gómez, R.F. Garcia, J.R. Gómez, J.C. Carril, Thermodynamic analysis of a Brayton cycle and Rankine cycle arranged in series exploiting the cold exergy of LNG (liquefied natural gas), *Energy*. 66 (2014) 927–937. DOI: 10.1016/J.Energy.2013.12.036.
- [105] M. S. Sadaghiani, M.H. Ahmadi, M. Mehrpooya, F. Pourfayaz, M. Feidt, Process development and thermodynamic analysis of a novel power generation plant driven by geothermal energy with liquefied natural gas as its heat sink, *Appl. Therm. Eng.* 133 (2018) 645–658. DOI: 10.1016/J.Applthermaleng.2018.01.077.
- [106] Z. Yan, P. Zhao, J. Wang, Y. Dai, Thermodynamic analysis of an SOFC–GT–ORC integrated power system with liquefied natural gas as heat sink, *Int. J. Hydrogen Energy*. 38 (2013) 3352–3363. DOI: 10.1016/J.Ijhydene.2012.12.101.
- [107] X. Yang, H. Zhao, Thermodynamic performance study of the SOFC-STIG distributed energy system fueled by LNG with CO₂ recovery, *Energy*. 186 (2019) 115860. DOI: 10.1016/J.Energy.2019.115860.
- [108] W. Xu, J. Duan, W. Mao, Process study and exergy analysis of a novel air separation process cooled by LNG cold energy, *J. Therm. Sci.* 23 (2014) 77–84. DOI: 10.1007/S11630-014-0679-5.
- [109] M. Mehrpooya, M. Kalhorzadeh, M. Chahartaghi, Investigation of novel integrated air separation processes, cold energy recovery of liquefied natural gas and carbon dioxide power cycle, *J. Clean. Prod.* 113 (2016) 411–425. DOI: 10.1016/J.Jclepro.2015.12.058.
- [110] A. Ebrahimi, M. Ziabasharhagh, Optimal design and integration of a cryogenic Air Separation Unit (ASU) with Liquefied Natural Gas (LNG) as heat sink, thermodynamic and economic analyses, *Energy*. 126 (2017) 868–885. DOI: 10.1016/J.Energy.2017.02.145.
- [111] T. Yuan, C. Song, J. Bao, N. Zhang, X. Zhang, G. He, Minimizing power consumption of boil off gas (BOG) recondensation process by power generation using cold energy in liquefied natural gas (LNG) regasification process, *J. Clean. Prod.* 238 (2019) 117949. DOI: 10.1016/J.Jclepro.2019.117949.
- [112] J. Park, F. You, H. Cho, I. Lee, I. Moon, Novel massive thermal energy storage system for liquefied natural gas cold energy recovery, *Energy*. 195 (2020) 117022. DOI: 10.1016/J.Energy.2020.117022.
- [113] I. Lee, F. You, Systems design and analysis of liquid air energy storage from liquefied natural gas cold energy, *Appl. Energy*. 242 (2019) 168–180. DOI: 10.1016/J.Apenergy.2019.03.087.
- [114] C.W. Ong, C.L. Chen, Technical and economic evaluation of seawater freezing desalination using liquefied natural gas, *Energy*. 181 (2019) 429–439. DOI: 10.1016/J.Energy.2019.05.193.
- [115] J. Chang, J. Zuo, K.J. Lu, T.S. Chung, Membrane development and energy analysis of freeze desalination-vacuum membrane distillation hybrid systems powered by LNG regasification and solar energy, *Desalination*. 449 (2019) 16–25. DOI: 10.1016/J.Desal.2018.10.008.
- [116] J. Xu, W. Lin, A CO₂ cryogenic capture system for flue gas of an LNG-fired power plant, *Int. J. Hydrogen Energy*. 42 (2017) 18674–18680. DOI: 10.1016/J.Ijhydene.2017.04.135.
- [117] S. Li, B. Wang, J. Dong, Y. Jiang, Thermodynamic analysis on the process of regasification of LNG and its application in the cold warehouse, *Therm. Sci. Eng. Prog.* 4 (2017) 1–10. DOI: 10.1016/J.Tsep.2017.08.001.
- [118] A. Messineo, G. Panno, LNG cold energy use in agro-food industry: A case study in Sicily, *J. Nat. Gas Sci. Eng.* 3 (2011) 356–363. DOI: 10.1016/J.Jngse.2011.02.002.
- [119] V. La Rocca, Cold recovery during regasification of LNG part one: Cold utilization far from the regasification facility, *Energy*. 35 (2010) 2049–2058. DOI: 10.1016/J.Energy.2010.01.022.
- [120] V. La Rocca, Cold recovery during regasification of LNG part two: Applications in an Agro Food

- Industry and a Hypermarket, *Energy*. 36 (2011) 4897–4908. DOI: 10.1016/J.Energy.2011.05.034.
- [121] A. Mugnini, G. Coccia, F. Polonara, A. Arteconi, Potential of District Cooling Systems: A Case Study on Recovering Cold Energy from Liquefied Natural Gas Vaporization, *Energies*. 12 (2019) 3027. DOI: 10.3390/En12153027.
- [122] M.A. Emadi, H. Pourrahmani, M. Moghimi, Performance evaluation of an integrated hydrogen production system with LNG cold energy utilization, *Int. J. Hydrogen Energy*. 43 (2018) 22075–22087. DOI: 10.1016/J.Ijhydene.2018.10.048.
- [123] J. Bao, T. Yuan, C. Song, X. Zhang, N. Zhang, G. He, Thermodynamic analysis of a new double-pressure condensation power generation system recovering LNG cold energy for hydrogen production, *Int. J. Hydrogen Energy*. 44 (2019) 17649–17661. DOI: 10.1016/J.Ijhydene.2019.05.107.
- [124] J. Lian, B. Xia, Y. Yin, G. Yang, Y. Yang, X. Gou, E. Wang, L. Liu, J. Wu, Research on High Efficient Utilization of LNG Cold Energy, in: 4th Int. Conf. Comput. Mechatronics, Control Electron. Eng. (ICCMCEE 2015), Atlantis Press, Hangzhou, Zhejiang, 2015: pp. 282–287. DOI: 10.2991/Iccmcee-15.2015.52.
- [125] Q. Wang, Z. Huang, Z. Liu, Overview of High-Value Reuse and Grinding at Sub-Zero Temperature of Scrap Rubber Tires, *IOP Conf. Ser. Mater. Sci. Eng.* 472 (2019) 012071. DOI: 10.1088/1757-899X/472/1/012071.
- [126] T. Gao, W. Lin, A. Gu, Improved processes of light hydrocarbon separation from LNG with its cryogenic energy utilized, *Energy Convers. Manag.* 52 (2011) 2401–2404. DOI: 10.1016/J.Enconman.2010.12.040.
- [127] H. Uwitonze, S. Han, C. Jangryeok, K.S. Hwang, Design process of LNG heavy hydrocarbons fractionation: Low LNG temperature recovery, *Chem. Eng. Process. Process Intensif.* 85 (2014) 187–195. DOI: 10.1016/J.Cep.2014.09.002.
- [128] L.N. Guo, B.L. An, L.B. Chen, J.X. Chen, J.J. Wang, Y. Zhou, Progress of liquefied natural gas cold energy utilization, *IOP Conf. Ser. Mater. Sci. Eng.* 502 (2019) 012148. DOI: 10.1088/1757-899X/502/1/012148.
- [129] S. Hirakawa, K. Kosugi, Utilization of LNG cold, *Int. J. Refrig.* 4 (1981) 17–21. DOI: 10.1016/0140-7007(81)90076-1.
- [130] M. Romero Gómez, R. Ferreiro Garcia, J. Romero Gómez, J. Carbia Carril, Review of thermal cycles exploiting the exergy of liquefied natural gas in the regasification process, *Renew. Sustain. Energy Rev.* 38 (2014) 781–795. DOI: 10.1016/J.Rser.2014.07.029.
- [131] Y. Fujiwara, T. Asakura, T. Yamamoto, M. Yamamoto, LNG cold energy supply for CO2 reduction and energy conservation in Mitsui chemicals ethylene plant, *Int. Gas Res. Conf. Proc.* (2011) P1-25.
- [132] P.A. Ferreira, I. Catarino, D. Vaz, Thermodynamic analysis for working fluids comparison in Rankine-type cycles exploiting the cryogenic exergy in Liquefied Natural Gas (LNG) regasification, *Appl. Therm. Eng.* 121 (2017) 887–896. DOI: 10.1016/J.Applthermaleng.2017.04.082.
- [133] M.H. Ahmadi, M. Mehrpooya, F. Pourfayaz, Thermodynamic and exergy analysis and optimization of a transcritical CO2 power cycle driven by geothermal energy with liquefied natural gas as its heat sink, *Appl. Therm. Eng.* 109 (2016) 640–652. DOI: 10.1016/J.Applthermaleng.2016.08.141.
- [134] K.H.K.C. Kim, K.H.K.C. Kim, Thermodynamic performance analysis of a combined power cycle using low grade heat source and LNG cold energy, *Appl. Therm. Eng.* 70 (2014) 50–60. DOI: 10.1016/J.Applthermaleng.2014.04.064.
- [135] Calnetix Technologies, Calnetix FreeSpin In-line Turboexpander. The Pressure-to-Power Solution, (2019). Gas Processor Association, 30th annual conference (accessed 9 November 2020).
- [136] Atlas Copco, Driving Expander Technology, (2019). <https://www.atlascopco.com/en-uk/compressors/products/ProcessAirGasEquipment/turboexpanders> (accessed 9 November 2020).

- [137] G. Oliveti, N. Arcuri, R. Bruno, M. De Simone, A rational thermodynamic use of liquefied natural gas in a waste incinerator plant, *Appl. Therm. Eng.* 35 (2012) 134–144. DOI: 10.1016/J.Applthermaleng.2011.10.015.
- [138] X. Shi, B. Agnew, D. Che, J. Gao, Performance enhancement of conventional combined cycle power plant by inlet air cooling, inter-cooling and LNG cold energy utilization, *Appl. Therm. Eng.* 30 (2010) 2003–2010. DOI: 10.1016/J.Applthermaleng.2010.05.005.
- [139] K. Kaneko, K. Ohtani, Y. Tsujikawa, S. Fujii, Utilization of the cryogenic exergy of LNG by a mirror gas-turbine, *Appl. Energy*. 79 (2004) 355–369. DOI: 10.1016/J.Apenenergy.2004.02.007.
- [140] C. Dispenza, G. Dispenza, V. La Rocca, G. Panno, V. La Rocca, G. Panno, V. La Rocca, G. Panno, Exergy recovery during LNG regasification: Electric energy production - Part one, *Appl. Therm. Eng.* 29 (2009) 380–387. DOI: 10.1016/J.Applthermaleng.2008.03.036.
- [141] C. Dispenza, G. Dispenza, V. La Rocca, G. Panno, Exergy recovery during LNG regasification: Electric energy production – Part two, *Appl. Therm. Eng.* 29 (2009) 388–399. DOI: 10.1016/J.Applthermaleng.2008.03.035.
- [142] M. Romero Gómez, R.F. Garcia, J.C. Carril, J. Romero Gómez, High efficiency power plant with liquefied natural gas cold energy utilization, *J. Energy Inst.* 87 (2014) 59–68. DOI: 10.1016/J.Joei.2014.02.007.
- [143] T. Lu, K.S. Wang, Analysis and optimization of a cascading power cycle with liquefied natural gas (LNG) cold energy recovery, *Appl. Therm. Eng.* 29 (2009) 1478–1484. DOI: 10.1016/J.Applthermaleng.2008.06.028.
- [144] T. Sung, K.C. Kim, LNG Cold Energy Utilization Technology, in: X. Zhang, I. Dincer (Eds.), *Energy Solut. to Combat Glob. Warm. Notes Energy*, vol. 33, Springer, 2017: pp. 47–66. DOI: 10.1007/978-3-319-26950-4_3.
- [145] T. Miyazaki, Y.. Kang, A. Akisawa, T. Kashiwagi, A combined power cycle using refuse incineration and LNG cold energy, *Energy*. 25 (2000) 639–655. DOI: 10.1016/S0360-5442(00)00002-5.
- [146] Y. Ueda, C. Kato, Stability analysis of thermally induced spontaneous gas oscillations in straight and looped tubes, *J. Acoust. Soc. Am.* 124 (2008) 851–858. DOI: 10.1121/1.2939134.
- [147] A. Akisawa, N. Tanaka, Y. Ueda, Optimal design of thermoacoustic engines driven by LNG using particle swarm optimization, *Trans. JSME (in Japanese)*. 82 (2016) 16–00248. DOI: 10.1299/Transjsme.16-00248.
- [148] Y. Ueda, B.M. Mehdi, K. Tsuji, A. Akisawa, Optimization of the regenerator of a traveling-wave thermoacoustic refrigerator, *J. Appl. Phys.* 107 (2010) 1–5. DOI: 10.1063/1.3294616.
- [149] R.E.H. Giametta, *Integration of LNG Regasification and Air Separation Units*, Norwegian University of Science and Technology, 2017.
- [150] D. Kim, R.E.H. Giametta, T. Gundersen, Optimal Use of Liquefied Natural Gas (LNG) Cold Energy in Air Separation Units, *Ind. Eng. Chem. Res.* 57 (2018) 5914–5923. DOI: 10.1021/Acs.iecr.7b04282.
- [151] T. Kanagawa, *Japan’s LNG Utilization and Environmental Efforts*, Tokyo (Japan), 2008.
- [152] A. Ebrahimi, M. Ziabasharhagh, Optimal design and integration of a cryogenic Air Separation Unit (ASU) with Liquefied Natural Gas (LNG) as heat sink, thermodynamic and economic analyses, *Energy*. 126 (2017) 868–885. DOI: 10.1016/J.Energy.2017.02.145.
- [153] M. Mehrpooya, M.M. Moftakhari Sharifzadeh, M.A. Rosen, Optimum design and exergy analysis of a novel cryogenic air separation process with LNG (liquefied natural gas) cold energy utilization, *Energy*. 90 (2015) 2047–2069. DOI: 10.1016/J.Energy.2015.07.101.
- [154] Z. Jieyu, L. Yanzhong, L. Guangpeng, S. Biao, Simulation of a Novel Single-column Cryogenic Air Separation Process Using LNG Cold Energy, *Phys. Procedia*. 67 (2015) 116–122. DOI: 10.1016/J.Phpro.2015.06.021.
- [155] Chiyoda Corporation, BOG Re-liquefaction System, (2017).

- <https://www.chiyodacorp.com/en/service/receive/bog/> (accessed 4 September 2020).
- [156] I.A. Fernández, M.R. Gómez, J.R. Gómez, L.M. López-González, H₂ production by the steam reforming of excess boil off gas on LNG vessels, *Energy Convers. Manag.* 134 (2017) 301–313. DOI: 10.1016/J.Enconman.2016.12.047.
- [157] L. Yin, Y. Ju, Design and analysis of a process for directly Re-liquefying BOG using subcooled LNG for LNG carrier, *Energy*. 199 (2020) 117445. DOI: 10.1016/J.Energy.2020.117445.
- [158] C. Song, Q. Liu, S. Deng, H. Li, Y. Kitamura, Cryogenic-based CO₂ capture technologies: State-of-the-art developments and current challenges, *Renew. Sustain. Energy Rev.* 101 (2019) 265–278. DOI: 10.1016/J.Rser.2018.11.018.
- [159] Osaka Gas Liquid Co. Ltd., Carbon dioxide business, (2020). https://www.liquidgas.co.jp/english/product/carbonic_acid.html (accessed 8 September 2020).
- [160] T. Yamamoto, Y. Fujiwara, The accomplishment of 100 % utilisation of LNG cold energy, 25th World Gas Conf. (2012) 1–19.
- [161] C. Dispenza, G. Dispenza, V. La Rocca, G. Panno, Exergy recovery in regasification facilities - Cold utilization: A modular unit, *Appl. Therm. Eng.* 29 (2009) 3595–3608. DOI: 10.1016/J.Applthermaleng.2009.06.016.
- [162] D.S. Ayoub, V. Eveloy, Integration of Municipal Air-Conditioning, Power, and Gas Supplies Using an LNG Cold Exergy-Assisted Kalina Cycle System, *Energies*. 13 (2020) 4599. DOI: 10.3390/En13184599.
- [163] F. Ayachi, Y. Lizhong, F.D. Magro, A. Meneghetti, A. Romagnoli, Assessment of LNG Cold Energy utilization for Road Vehicles and Data-Centres cooling using Liquid Air, *Energy Procedia*. 158 (2019) 5047–5052. DOI: 10.1016/J.Egypro.2019.01.656.
- [164] F. Ayachi, L. Yang, J.Y. Sze, A. Romagnoli, Cryogenic polygeneration for green data centre, *Energy Procedia*. 152 (2018) 15–20. DOI: 10.1016/J.Egypro.2018.09.052.
- [165] TeraCool LLC, Data Cent. Cool. from Waste LNG Refrig. Signif. Energy Sav. Environ. Benefits. (2013). <http://www.teracool-llc.com/> (accessed 9 September 2020).
- [166] T. Banaszkiwicz, M. Chorowski, W. Gizicki, A. Jedrusyna, J. Kielar, Z. Malecha, A. Piotrowska, J. Polinski, Z. Rogala, K. Sierpowski, J. Skrzypacz, M. Stanlik, K. Tomczuk, P. Dowżenko, Liquefied Natural Gas in Mobile Applications—Opportunities and Challenges, *Energies*. 13 (2020) 5673. DOI: 10.3390/En13215673.
- [167] H. Tan, Y. Li, H. Tuo, Theoretical and experimental study on a self-refrigerating system for LNG-fueled refrigerated vehicles, *J. Nat. Gas Sci. Eng.* 20 (2014) 192–199. DOI: 10.1016/J.Jngse.2014.06.022.
- [168] F. Yan, W. Yi, B. Xu, Y. Luo, Study on the Characteristics of Heat Exchanger for Cold Energy Recovery in LNG Vehicles, *Energy Procedia*. 104 (2016) 487–491. DOI: 10.1016/J.Egypro.2016.12.082.
- [169] P. Babu, A. Nambiar, T. He, I.A. Karimi, J.D. Lee, P. Englezos, P. Linga, A Review of Clathrate Hydrate Based Desalination To Strengthen Energy–Water Nexus, *ACS Sustain. Chem. Eng.* 6 (2018) 8093–8107. DOI: 10.1021/Acscschemeng.8b01616.
- [170] W. Cao, C. Beggs, I.M. Mujtaba, Theoretical approach of freeze seawater desalination on flake ice maker utilizing LNG cold energy, *Desalination*. 355 (2014) 22–32. DOI: 10.1016/J.Desal.2014.09.034.
- [171] W. Lin, M. Huang, A. Gu, A seawater freeze desalination prototype system utilizing LNG cold energy, *Int. J. Hydrogen Energy*. 42 (2017) 18691–18698. DOI: 10.1016/J.Ijhydene.2017.04.176.
- [172] C. Xie, L. Zhang, Y. Liu, Q. Lv, G. Ruan, S.S. Hosseini, A direct contact type ice generator for seawater freezing desalination using LNG cold energy, *Desalination*. 435 (2018) 293–300. DOI: 10.1016/J.Desal.2017.04.002.
- [173] T. He, S.K. Nair, P. Babu, P. Linga, I.A. Karimi, A novel conceptual design of hydrate based desalination (HyDesal) process by utilizing LNG cold energy, *Appl. Energy*. 222 (2018) 13–24.

- DOI: 10.1016/J.Apenergy.2018.04.006.
- [174] Z.R. Chong, T. He, P. Babu, J. Zheng, P. Linga, Economic evaluation of energy efficient hydrate based desalination utilizing cold energy from liquefied natural gas (LNG), *Desalination*. 463 (2019) 69–80. DOI: 10.1016/J.Desal.2019.04.015.
 - [175] T. He, Z.R. Chong, P. Babu, P. Linga, Techno-Economic Evaluation of Cyclopentane Hydrate-Based Desalination with Liquefied Natural Gas Cold Energy Utilization, *Energy Technol.* 8 (2020) 1900212. DOI: 10.1002/Ente.201900212.
 - [176] International Energy Agency (IEA), *The Future of Hydrogen for G20. Seizing today's opportunities*, 2019.
 - [177] Alternative Fuels Data Center (AFDC). U.S. Department of Energy, Hydrogen Production and Distribution, (2020). https://afdc.energy.gov/fuels/hydrogen_production.html (accessed 14 September 2020).
 - [178] United States Department of Energy, Hydrogen Production: Natural Gas Reforming, (2020). <https://www.energy.gov/eere/fuelcells/hydrogen-production-natural-gas-reforming> (accessed 10 September 2020).
 - [179] M. Ogawa, T. Seki, H. Honda, M. Nakamura, Y. Takatani, A hydrogen production method using latent heat of liquefied natural gas, *Electr. Eng. Japan (English Transl. Denki Gakkai Ronbunshi)*. 147 (2004) 32–42. DOI: 10.1002/Eej.10299.
 - [180] A. Mayyas, M. Ruth, B. Pivovar, G. Bender, K. Wipke, A. Mayyas, M. Ruth, B. Pivovar, G. Bender, K. Wipke, Manufacturing Cost Analysis for Proton Exchange Membrane Water Electrolyzers Manufacturin, *Natl. Renew. Energy Lab.* (2019) 65.
 - [181] S. Shiva Kumar, V. Himabindu, Hydrogen production by PEM water electrolysis – A review, *Mater. Sci. Energy Technol.* 2 (2019) 442–454. DOI: 10.1016/J.Mset.2019.03.002.
 - [182] M. Carmo, D.L. Fritz, J. Mergel, D. Stolten, A comprehensive review on PEM water electrolysis, *Int. J. Hydrogen Energy*. 38 (2013) 4901–4934. DOI: 10.1016/J.Ijhydene.2013.01.151.
 - [183] M.H. Taheri, A.H. Mosaffa, L.G. Farshi, Energy, exergy and economic assessments of a novel integrated biomass based multigeneration energy system with hydrogen production and LNG regasification cycle, *Energy*. 125 (2017) 162–177. DOI: 10.1016/J.Energy.2017.02.124.
 - [184] E. Akrami, I. Khazaei, A. Gholami, Comprehensive analysis of a multi-generation energy system by using an energy-exergy methodology for hot water, cooling, power and hydrogen production, *Appl. Therm. Eng.* 129 (2018) 995–1001. DOI: 10.1016/J.Applthermaleng.2017.10.095.
 - [185] International Gas Union (IGU), *2019 World LNG Report*, 2019.
 - [186] Y.A. Çengel, Power generation potential of liquified natural gas regasification terminals, *Int. J. Energy Res.* (2020) er.5116. DOI: 10.1002/Er.5116.
 - [187] R. Agarwal, Y. Hisazumi, A. Kegasa, T. Hori, Hampson type heat-exchanger technology and economic evaluation for LNG re- gasification and power generation At LNG receiving terminals, in: *Proc. Int. Conf. Power Eng., The Japan Society of Mechanical Engineers, Yokohama (Japan)*, 2015.
 - [188] Y. Hosoya, Power generation from cryogenic energy (in Japanese), *J. Cryog. Supercond. Soc. Japan*. 19 (1984) 3–11. DOI: 10.2221/Jcsj.19.3.
 - [189] T. Otsuka, Evolution of an LNG terminal: Senboku terminal of Osaka GAS, in: *23rd World Gas Conf., International Gas Union (IGU), Amsterdam (Netherlands)*, 2006: pp. 2617–2631.
 - [190] Osaka Gas Co. Ltd., *Senboku LNG Terminals*, (n.d.).
 - [191] Engineering Department of Osaka Gas Co.Ltd., *LNG Cold Energy Utilization at LNG Receiving Terminals*, (n.d.).
 - [192] M. Ikeda, CO₂ REDUCTION USING LNG COLD ENERGY, in: *LNG 15. Proc. 15th Int. Conf. Exhib. Liq. Nat. Gas, Barcelona (Spain)*, 2007: p. PO-52.
 - [193] Y. Akasaka, Power generation plant using LNG cold in Osaka Gas, *TEION KOGAKU (Journal*

- Cryog. Supercond. Soc. Japan). 19 (1984) 12–18. DOI: 10.2221/Jcsj.19.12.
- [194] Osaka Gas Co. Ltd., Cryogenic power generation system recovering LNG's cryogenic energy and generating power for energy and CO₂ emission savings, (2017). https://www.osakagas.co.jp/en/rd/technical/1198907_6995.html (accessed 6 June 2018).
- [195] M. Tada, A supercritical pressure cold energy utilization system of the cryogenic fluid (Liquefied gas supercritical pressure cold energy power generation system : LSG), Trans. JSME (in Japanese). 82 (2016) 15-00581-15-00581. DOI: 10.1299/Transjsme.15-00581.
- [196] M. Kusagawa, E. Hamatani, Y. Sakamoto, M. Takubo, E. Ogawa, K. Ikeda, H. Emi, A fully optimized cascaded LNG cold energy utilization system, in: 14th Int. Conf. Exhib. Liq. Nat. Gas, Doha, 2004: p. Poster PO-30.
- [197] D. Group, Introduction to power generation and supply bussiness in English. Cold energy utilizations, (2020). https://gps.osakagas.co.jp/daigas_gps/en/businessdomain/terminal/cold/ (accessed 16 September 2020).
- [198] H. Kim, Review on Economical Efficiency of Lng Cold Energy Use in South Korea, in: 23rd World Gas Conf., International Gas Union (IGU), Amsterdam (Netherlands), 2006: pp. 2870–2885.
- [199] The Cryostar Magazine, Issue #30 - Autumn 2017. (2017) 6–7.
- [200] J.C. Sánchez-Izquierdo, L.C.G. Pérez, Electricity generation in ENAGÁS' regasifying plant in Palos de la Frontera (Huelva), FuturEnergy. November (2013) 31–35.
- [201] Cogen España - Asociación Española para la Promoción de la Cogeneración, Quién es quién en cogen España 2015 (In Spanish), 2015.
- [202] Enagás Transporte S.A.U., Planta de Almacenamiento y Regasificación de Barcelona. Declaración/Memoria Ambiental 2018, 2019.
- [203] O. Nuñez, Regasification Plant Energy Efficiency. Innovative Solutions, in: 18th Int. Conf. Exhib. Liq. Nat. Gas, Perth (Australia), 2016.
- [204] Enagas, The sustainable cold logistics hub at the Enagás regasification plant in Huelva receives financing from ERDF funds and public aid from the CDTI, (2019). https://www.enagas.es/enagas/en/Comunicacion/NotasPrensa/2019_10_10_NP_Shaky_ES (accessed 10 July 2020).
- [205] D. Solera Rico, Proyecto ShakyUso del frío residual del GNL para el desarrollo de un almacén de congelación y la gestión de la cadena de suministro mediante el uso de pila de hidrógeno, Interempresas - Energías. (2019).
- [206] A. Coronas, Panel Discussion 1. Polygeneration Technologies: Present Status and Future Perspectives, in: Int. Conf. Polygeneration (ICP 2019), Fukuoka (Japan), 2019: pp. 1–6.
- [207] M. Mehrpooya, M.M.M. Sharifzadeh, A novel integration of oxy-fuel cycle, high temperature solar cycle and LNG cold recovery – energy and exergy analysis, Appl. Therm. Eng. 114 (2017) 1090–1104. DOI: 10.1016/J.Applthermaleng.2016.11.163.
- [208] M. Mehrpooya, R. Esfilar, S.M.A. Moosavian, Introducing a novel air separation process based on cold energy recovery of LNG integrated with coal gasification, transcritical carbon dioxide power cycle and cryogenic CO₂ capture, J. Clean. Prod. 142 (2017) 1749–1764. DOI: 10.1016/J.Jclepro.2016.11.112.
- [209] H. Ghaebi, T. Parikhani, H. Rostamzadeh, Energy, exergy and thermoeconomic analysis of a novel combined cooling and power system using low-temperature heat source and LNG cold energy recovery, Energy Convers. Manag. 150 (2017) 678–692. DOI: 10.1016/J.Enconman.2017.08.052.
- [210] R. Esfilar, M. Mehrpooya, S.M.A. Moosavian, Thermodynamic assessment of an integrated biomass and coal co-gasification, cryogenic air separation unit with power generation cycles based on LNG vaporization, Energy Convers. Manag. 157 (2018) 438–451. DOI: 10.1016/J.Enconman.2017.12.026.
- [211] A. Atienza-Márquez, J.C. Bruno, A. Akisawa, A. Coronas, Performance analysis of a combined cold and power (CCP) system with exergy recovery from LNG-regasification, Energy. 183 (2019)

- 448–461. DOI: 10.1016/J.Energy.2019.06.153.
- [212] M.A. Emadi, J. Mahmoudimehr, Modeling and thermo-economic optimization of a new multi-generation system with geothermal heat source and LNG heat sink, *Energy Convers. Manag.* 189 (2019) 153–166. DOI: 10.1016/J.Enconman.2019.03.086.
- [213] Z. Liu, I.A. Karimi, T. He, A novel inlet air cooling system based on liquefied natural gas cold energy utilization for improving power plant performance, *Energy Convers. Manag.* 187 (2019) 41–52. DOI: 10.1016/J.Enconman.2019.03.015.
- [214] M. Ebadollahi, H. Rostamzadeh, M.Z. Pedram, H. Ghaebi, M. Amidpour, Proposal and assessment of a new geothermal-based multigeneration system for cooling, heating, power, and hydrogen production, using LNG cold energy recovery, *Renew. Energy*. 135 (2019) 66–87. DOI: 10.1016/J.Renene.2018.11.108.
- [215] T. Parikhani, T. Gholizadeh, H. Ghaebi, S.M. Sattari Sadat, M. Sarabi, Exergoeconomic optimization of a novel multigeneration system driven by geothermal heat source and liquefied natural gas cold energy recovery, *J. Clean. Prod.* 209 (2019) 550–571. DOI: 10.1016/J.Jclepro.2018.09.181.
- [216] J. Ning, Z. Sun, Q. Dong, X. Liu, Performance study of supplying cooling load and output power combined cycle using the cold energy of the small scale LNG, *Energy*. 172 (2019) 36–44. DOI: 10.1016/J.Energy.2019.01.094.
- [217] X. She, T. Zhang, L. Cong, X. Peng, C. Li, Y. Luo, Y. Ding, Flexible integration of liquid air energy storage with liquefied natural gas regasification for power generation enhancement, *Appl. Energy*. 251 (2019) 113355. DOI: 10.1016/J.Apenergy.2019.113355.
- [218] Y. Liu, J. Han, H. You, Performance analysis of a CCHP system based on SOFC/GT/CO₂ cycle and ORC with LNG cold energy utilization, *Int. J. Hydrogen Energy*. 44 (2019) 29700–29710. DOI: 10.1016/J.Ijhydene.2019.02.201.
- [219] Y. Liu, J. Han, H. You, Exergoeconomic analysis and multi-objective optimization of a CCHP system based on LNG cold energy utilization and flue gas waste heat recovery with CO₂ capture, *Energy*. 190 (2020) 116201. DOI: 10.1016/J.Energy.2019.116201.
- [220] B. Ghorbani, K.B. Mahyari, M. Mehrpooya, M.-H.H. Hamed, Introducing a hybrid renewable energy system for production of power and fresh water using parabolic trough solar collectors and LNG cold energy recovery, *Renew. Energy*. 148 (2020) 1227–1243. DOI: 10.1016/J.Renene.2019.10.063.
- [221] N. Chitgar, M. Moghimi, Design and evaluation of a novel multi-generation system based on SOFC-GT for electricity, fresh water and hydrogen production, *Energy*. 197 (2020) 117162. DOI: 10.1016/J.Energy.2020.117162.
- [222] Y.A. Çengel, J.M. Cimbala, *Mecánica de fluidos : fundamentos y aplicaciones*, McGraw Hill, México DF, 2006.
- [223] D. Pineda Quijano, C. Infante Ferreira, W. Duivenvoorden, J. Mieog, T. Van Der Noortgaete, B. Van Der Velpen, Techno-economic feasibility study of a system for the transfer of refrigeration capacity from LNG regasification plants to industrial assets, in: 12th IEA Heat Pump Conf., Rotterdam, 2017.
- [224] ASHRAE, District heating and cooling, in: ASHRAE Handb. Heating, Vent. Air-Conditioning Syst., 2008.
- [225] A.A. Lakew, O. Bolland, Working fluids for low-temperature heat source, *Appl. Therm. Eng.* 30 (2010) 1262–1268. DOI: 10.1016/J.Applthermaleng.2010.02.009.
- [226] J. Bao, L. Zhao, A review of working fluid and expander selections for organic Rankine cycle, *Renew. Sustain. Energy Rev.* 24 (2013) 325–342. DOI: 10.1016/J.Rser.2013.03.040.
- [227] M. Badami, J.C. Bruno, A. Coronas, G. Fambri, Analysis of different combined cycles and working fluids for LNG exergy recovery during regasification, *Energy*. 159 (2018) 373–384. DOI: 10.1016/J.Energy.2018.06.100.

- [228] ASHRAE, ASHRAE Handbook-Refrigeration - SI Edition, 2014.
- [229] B. Koffi, A. Cerutti, M. Duerr, A. Iancu, A. Kona, G. Janssens-Maenhout, A. Ianku, A. Kona, G. Janssens-Maenhout, CoM Default Emission Factors for the Member States of the European Union - Version 2017, European Commission, Joint Research Centre (JRC), 2017.
- [230] G. Li, Organic Rankine cycle performance evaluation and thermoeconomic assessment with various applications part I: Energy and exergy performance evaluation, *Renew. Sustain. Energy Rev.* 53 (2016) 477–499. DOI: 10.1016/J.Rser.2015.08.066.
- [231] G. Li, M. Eisele, H. Lee, Y. Hwang, R. Radermacher, Experimental investigation of energy and exergy performance of secondary loop automotive air-conditioning systems using low-GWP (global warming potential) refrigerants, *Energy*. 68 (2014) 819–831. DOI: 10.1016/J.Energy.2014.01.018.
- [232] S. Quoilin, M. Van Den Broek, S. Declaye, P. Dewallef, V. Lemort, Techno-economic survey of Organic Rankine Cycle (ORC) systems, *Renew. Sustain. Energy Rev.* 22 (2013) 168–186. DOI: 10.1016/J.Rser.2013.01.028.
- [233] A.I. Papadopoulos, M. Stijepovic, P. Linke, On the systematic design and selection of optimal working fluids for Organic Rankine Cycles, *Appl. Therm. Eng.* 30 (2009) 760–769. DOI: 10.1016/J.Applthermaleng.2009.12.006.
- [234] W. Gang, S. Wang, F. Xiao, D. Gao, District cooling systems: Technology integration, system optimization, challenges and opportunities for applications, *Renew. Sustain. Energy Rev.* 53 (2016) 253–264. DOI: 10.1016/J.Rser.2015.08.051.
- [235] NIST, REFPROP 9.1, (2018). <https://www.nist.gov/srd/refprop> (accessed 19 March 2020).
- [236] J.M. Calm, G.C. Hourahan, Property, safety, and environmental data for alternative refrigerants, *Refrig. Sustain. Dev. Proc. 23rd Int. Congr. Refrig.* (2011) Paper 915.
- [237] ANSI/ASHRAE Standard 34, Designation and Safety Classification of Refrigerants, (2016).
- [238] A. Groniewsky, G. Györke, A.R. Imre, Description of wet-to-dry transition in model ORC working fluids, *Appl. Therm. Eng.* 125 (2017) 963–971. DOI: 10.1016/J.Applthermaleng.2017.07.074.
- [239] X. Xu, Y. Hwang, R. Radermacher, Performance comparison of R410A and R32 in vapor injection cycles, *Int. J. Refrig.* 36 (2013) 892–903. DOI: 10.1016/J.Ijrefrig.2012.12.010.
- [240] U. Drescher, D. Brüggemann, D. Brü, Fluid selection for the Organic Rankine Cycle (ORC) in biomass power and heat plants, *Appl. Therm. Eng.* 27 (2007) 223–228. DOI: 10.1016/J.Applthermaleng.2006.04.024.
- [241] H. Habibi, A. Chitsaz, K. Javaherdeh, M. Zoghi, M. Ayazpour, Thermo-economic analysis and optimization of a solar-driven ammonia-water regenerative Rankine cycle and LNG cold energy, *Energy*. 149 (2018) 147–160. DOI: 10.1016/J.Energy.2018.01.157.
- [242] B. Fankam Tchanche, G. Papadakis, G. Lambrinos, A. Frangoudakis, Fluid selection for a low-temperature solar organic Rankine cycle, *Appl. Therm. Eng.* 29 (2008) 2468–2476. DOI: 10.1016/J.Applthermaleng.2008.12.025.
- [243] S. Le, J.-Y. Lee, C.-L. Chen, Waste cold energy recovery from liquefied natural gas (LNG) regasification including pressure and thermal energy, *Energy*. 152 (2018) 770–787. DOI: 10.1016/J.Energy.2018.03.076.
- [244] S. Seidel, J. Ye, S.O. Andersen, A. Hillbrand, Not-in-Kind Alternatives To High Global Warming HFCs, *Cent. Clim. Energy Solut.* (2016) 27.
- [245] Total, Grow in LNG, an Energy for the Future, (2018). <https://www.ep.total.com/en/areas/liquefied-natural-gas/grow-lng-energy-future> (accessed 17 July 2018).
- [246] Osaka Gas Co., Ltd., (2019). <https://www.osakagas.co.jp/en/> (accessed 22 March 2019).
- [247] V. Eveloy, D. Ayou, Sustainable District Cooling Systems: Status, Challenges, and Future Opportunities, with Emphasis on Cooling-Dominated Regions, *Energies*. 12 (2019) 235. DOI: 10.3390/En12020235.

- [248] H. Han, Y. Yan, S. Wang, Y.-X. Li, Thermal design optimization analysis of an intermediate fluid vaporizer for liquefied natural gas, *Appl. Therm. Eng.* 129 (2018) 329–337. DOI: 10.1016/J.Applthermaleng.2017.10.043.
- [249] S. Xu, X. Chen, Z. Fan, Design of an Intermediate Fluid Vaporizer for Liquefied Natural Gas, *Chem. Eng. Technol.* 40 (2017) 428–438. DOI: 10.1002/Ceat.201500740.
- [250] G.F. Hewitt, *Heat Exchanger Design Handbook*, Begal House, Inc. New York, 2002.
- [251] A. Atienza-Márquez, J.C. Bruno, A. Akisawa, A. Coronas, Thermal design of a vaporizer for cold recovery from LNG-regasification using CO₂ as heat transfer media, *Refrig. Sci. Technol.* 2019-Augus (2019) 2448–2455. DOI: 10.18462/Iir.Icr.2019.1018.
- [252] International Institute of Refrigeration (IIR), *Cogeneration/Trigeneration - 33rd Informatory Note on Refrigeration Technologies*, 2017.
- [253] ASHRAE, *District Cooling Guide*, Atlanta, 2013.
- [254] Y. Hisazumi, T. Hori, C. Park, A. Kegasa, Study of LNG vaporization and power system for the next generation, *J. Japan Soc. Energy Resour.* 35 (2014) 10–17.
- [255] Y. Liu, K. Guo, A novel cryogenic power cycle for LNG cold energy recovery, *Energy.* 36 (2011) 2828–2833. DOI: 10.1016/J.Energy.2011.02.024.
- [256] J.K. Jensen, T. Ommen, W.B. Markussen, L. Reinholdt, B. Elmegaard, Technical and economic working domains of industrial heat pumps: Part 2 – Ammonia-water hybrid absorption-compression heat pumps, *Int. J. Refrig.* 55 (2015) 183–200. DOI: 10.1016/J.Ijrefrig.2015.02.011.
- [257] S. Kakaç, H. Liu, A. Pramuanjaroenkij, *Heat exchangers: Selection, rating, and thermal design*, Third Edit, CRC Press, 2012.
- [258] R.K. Sinnott, *Chemical Engineering Design*, Fourth Ed., Elsevier Science, 2005.
- [259] M. Nitsche, R.O. Gbadamosi, *Heat Exchanger Design Guide: A Practical Guide for Planning, Selecting and Designing of Shell and Tube Exchangers*, Elsevier Science, 2016.
- [260] J.J. McKetta, *Heat transfer design methods*, Marcel Dekker, Inc., 1988.
- [261] Z.G. Qu, Y.H. Bai, L. Pu, One-dimensional numerical study of thermal performance of an organic Rankine cycle system using liquefied natural gas as a cold source for cold energy recovery, *J. Nat. Gas Sci. Eng.* 26 (2015) 1399–1413. DOI: 10.1016/J.Jngse.2015.07.027.
- [262] M.M. Shah, Comprehensive correlations for heat transfer during condensation in conventional and mini/micro channels in all orientations, *Int. J. Refrig.* 67 (2016) 22–41. DOI: 10.1016/J.Ijrefrig.2016.03.014.
- [263] D. Jung, H. Lee, D. Bae, S. Oho, Nucleate boiling heat transfer coefficients of flammable refrigerants, *Int. J. Refrig.* 27 (2004) 409–414. DOI: 10.1016/J.Ijrefrig.2003.11.007.
- [264] D. Jung, S. Chae, D. Bae, S. Oho, Condensation heat transfer coefficients of flammable refrigerants, *Int. J. Refrig.* 27 (2004) 314–317. DOI: 10.1016/J.Ijrefrig.2003.09.006.
- [265] Y.-Y. Bae, H.-Y. Kim, Convective heat transfer to CO₂ at a supercritical pressure flowing vertically upward in tubes and an annular channel, *Exp. Therm. Fluid Sci.* 33 (2009) 329–339. DOI: 10.1016/J.Expthermflusci.2008.10.002.
- [266] K. Liang, B. Yang, Z. Zhang, Investigation of Heat Transfer and Coking Characteristics of Hydrocarbon Fuels, *J. Propuls. Power.* 14 (1998) 789–796. DOI: 10.2514/2.5342.
- [267] A. Zukauskas, Heat Transfer from Tubes in Cross Flow, in: S. Kakaç, R.K. Shah, W. Aung (Eds.), *Handb. Single-Phase Convect. Heat Transf.*, Wiley, New York, 1987.
- [268] Z.H. Ayub, Plate Heat Exchanger Literature Survey and New Heat Transfer and Pressure Drop Correlations for Refrigerant Evaporators, *Heat Transf. Eng.* 24 (2003) 3–16. DOI: 10.1080/01457630390218074.
- [269] D. Butterworth, Steam Power Plant and Process condensers, in: S. Kakaç (Ed.), *Boil. Evaporators Condens.*, Jonh Wiley & Sons, Inc., 1991.
- [270] J.W. Palen, Heat exchangers, vaporizers and condensers, in: M. Kutz (Ed.), *Mech. Eng. Handb.*,

- 2nd ed., John Wiley & Sons, Inc, 1998.
- [271] E. Cao, *Heat Transfer in Process Engineering*, McGraw-Hill, 2010.
- [272] P. Dorj, *Thermoeconomic Analysis of a New Geothermal Utilization CHP Plant in Tsetserleg, Mongolia*, University of Iceland, 2005.
- [273] A.H.H. Mosaffa, N.H. Mokarram, L.G. Farshi, Thermo-economic analysis of combined different ORCs geothermal power plants and LNG cold energy, *Geothermics*. 65 (2017) 113–125. DOI: 10.1016/J.Geothermics.2016.09.004.
- [274] Anish Modi, *Numerical evaluation of the Kalina cycle for concentrating solar power plants*, DTU Mechanical Engineering, 2015.
- [275] R. Smith, *Chemical Process Design and Integration*, John Wiley & Sons, Ltd, 2005. DOI: 10.1529/Biophysj.107.124164.
- [276] J.D. Kumana, Cost update on specialty heat exchangers, *Chem. Eng.* (1984).
- [277] G. Towler, R. Sinnott, *Chemical Engineering Design. Principles, practice and economics of plant and process design*, Elsevier, 2008.
- [278] A. Bejan, G. Tsatsaronis, M. Moran, *Thermal Design and Optimization*, Jonh Wiley & Sons, Inc., 1996.
- [279] U.S. Coast Guard and Maritime Administration, *Beacon Port Deepwater Port License Application: Environmental Impact Statement*, Washinton DC, 2006.
- [280] W.L. Luyben, Estimating refrigeration costs at cryogenic temperatures, *Comput. Chem. Eng.* 103 (2017) 144–150. DOI: 10.1016/J.Compchemeng.2017.03.013.
- [281] Y. Hisazumi, Y. Yamasaki, S. Sugiyama, Proposal for a high efficiency LNG power-generation system utilizing waste heat from the combined cycle, *Appl. Energy*. 60 (1998) 169–182. DOI: 10.1016/S0306-2619(98)00034-8.
- [282] H.K. Ersoy, S.O. Demirpolat, Using liquefied natural gas cold energy for power generation: case study for Marmara Ereglisi receiving terminal, *J. Energy Inst.* 82 (2009) 11–18. DOI: 10.1179/014426009X393991.
- [283] International Energy Agency (IEA), *Electricity Information: Overview*, Stat. Iea. (2019) 1–10.
- [284] World Banck Group, *State and Trends of Carbon Pricing 2019*, Washinton DC, 2019. DOI: 10.1596/978-1-4648-1435-8.
- [285] W. Xu, Z. Huang, S. Fan, Optimized Analysis of Cold Energy Utilization for Cold Storage Project of Xingtan LNG Satellite Station, in: I. Dincer, A. Midilli, H. Kucuk (Eds.), *Prog. Exergy, Energy, Environ., Springer International Publishing, Cham*, 2014: pp. 569–576. DOI: 10.1007/978-3-319-04681-5_53.
- [286] W. Lin, N. Zhang, A. Gu, LNG (liquefied natural gas): A necessary part in China’s future energy infrastructure, *Energy*. 35 (2010) 4383–4391. DOI: 10.1016/J.Energy.2009.04.036.
- [287] B.B. Kanbur, L. Xiang, S. Dubey, F.H. Choo, F. Duan, Thermoeconomic assessment of a micro cogeneration system with LNG cold utilization, *Energy*. 129 (2017) 171–184. DOI: 10.1016/J.Energy.2017.04.071.
- [288] B.B. Kanbur, L. Xiang, S. Dubey, F.H. Choo, F. Duan, Thermoeconomic and environmental assessments of a combined cycle for the small scale LNG cold utilization, *Appl. Energy*. 204 (2017) 1148–1162. DOI: 10.1016/J.Apenergy.2017.01.061.
- [289] B.B. Kanbur, L. Xiang, S. Dubey, F.H. Choo, F. Duan, B. Burak Kanbur, L. Xiang, S. Dubey, F. Hoong Choo, F. Duan, Finite sum based thermoeconomic and sustainable analyses of the small scale LNG cold utilized power generation systems, *Appl. Energy*. 220 (2018) 944–961. DOI: 10.1016/J.Apenergy.2017.12.088.
- [290] L. Zhao, H. Dong, J. Tang, J. Cai, Cold energy utilization of liquefied natural gas for capturing carbon dioxide in the flue gas from the magnesite processing industry, *Energy*. 105 (2016) 45–56. DOI: 10.1016/J.Energy.2015.08.110.

- [291] B.B. Kanbur, L. Xiang, S. Dubey, F.H. Choo, F. Duan, Thermoeconomic analysis and optimization of the small scale power generation and carbon dioxide capture system from liquefied natural gas, *Energy Convers. Manag.* 181 (2019) 507–518. DOI: 10.1016/J.Enconman.2018.11.077.
- [292] B.B. Kanbur, L. Xiang, S. Dubey, F.H. Choo, F. Duan, Life-cycle-integrated thermoeconomic and enviroeconomic assessments of the small-scale-liquefied natural gas cold utilization systems, *Int. J. Energy Res.* 43 (2019) 4104–4126. DOI: 10.1002/Er.4510.
- [293] V. Chrz, C. Emmer, LNG directly to customers stations, in: Gas Technology Institute (GTI), International Gas Union (IGU), I.I. of R. (IIR) (Eds.), 15th Int. Conf. Exhib. Liq. Nat. Gas (LNG 15), Barcelona (Spain), 2007: p. PO-12.
- [294] Compañía Energética Las Villas olive-pomace sludge reduction and treatment plant and treatment through cogeneration with a 25 MW gas turbine, *InfoPower*. (n.d.) 1–8.
- [295] Chart Inc., Case Study LNG #4 - Power Generation at Secluded Diamond Mine, 2017.
- [296] M. Bahillo, Priorat, viticultura heroica, *Gasactual*. 138 (2016).
- [297] Redexis Gas comienza el suministro de gas natural en Abarán, Murcia.Com. (2018).
- [298] Kälte-Klima-Sachsen GmbH, (n.d.). <http://kaelte-klima-sachsen.de/> (accessed 11 December 2019).
- [299] Eco ice Kälte GmbH, (n.d.). <http://www.eco-ice.net/es/> (accessed 14 October 2019).
- [300] LNGcold solutions GmbH, (2019). <http://lngcold.energy/> (accessed 5 December 2019).
- [301] G. Biscardini, R. Schmill, A. Del Maestro, Small going big. Why small-scale LNG may be the next big wave, *Strategy&* (Part of the PwC network), 2017.
- [302] International Gas Union (IGU) Program Committee (PGC) D3, Small Scale LNG, 2015.
- [303] T. Meixus Fernández, Best Practice Policy Guidance for Liquefied Natural Gas (LNG) Case Study: Small Scale LNG-Truck Loading, United Nations - Economic Commission for Europe, 2017.
- [304] International Gas Union (IGU), Flexible LNG Facilities Enhancing Functionality Across the LNG Value Chain, in: 27th World Gas Conf., Washington DC (USA), 2018.
- [305] K. Punnonen, Small and Medium size LNG for Power Production, Power Plant, Wärtsilä Finl. Oy, Finl. (2013) 1–18.
- [306] Asia Pacific Energy Research Centre (APEREC), Small-scale LNG in Asia-Pacific, Asia-Pacific Economic Cooperation (APEC), 2019.
- [307] Wärtsilä, Small-and medium-scale LNG terminals, (2018).
- [308] E. Strantzali, K. Aravossis, G. Livanos, N. Chrysanthopoulos, A Novel Multicriteria Evaluation of Small-Scale LNG Supply Alternatives: The Case of Greece, *Energies*. 11 (2018) 903. DOI: 10.3390/En11040903.
- [309] Nomura Research Institute, Study on Opportunities and Issues in introducing mini LNG facilities and equipments in Indonesia, (n.d.).
- [310] E. Strantzali, K. Aravossis, G.A. Livanos, Evaluation of future sustainable electricity generation alternatives: The case of a Greek island, *Renew. Sustain. Energy Rev.* 76 (2017) 775–787. DOI: 10.1016/J.Rser.2017.03.085.
- [311] F. Carron, Small Scale LNG Based Power Generation in the Philippines, in: *Power Genp Asia* 2014, 2014.
- [312] New LNG power plant at Gibraltar powered by MAN Energy Solutions, (2019). <https://www.man-es.com/discover/gibraltar-builds-a-modern-lng-power-plant> (accessed 30 November 2019).
- [313] E.W. Lemmon, M.L. Huber, M.O. McLinden, NIST Reference Fluid Thermodynamic and Transport Properties—REFPROP, (2013).
- [314] D.S. Ayoub, J.C. Bruno, A. Coronas, Integration of a mechanical and thermal compressor booster in combined absorption power and refrigeration cycles, (2017). DOI: 10.1016/J.Energy.2017.06.148.
- [315] J. Guilpart, E. Stamatou, A. Delahaye, L. Fournaison, Comparison of the performance of different

- ice slurry types depending on the application temperature, *Int. J. Refrig.* 29 (2006) 781–788. DOI: 10.1016/J.Ijrefrig.2005.11.009.
- [316] European Parliament and the Council of the European Union, Regulation (EC) 1272/2008, Off. J. Eur. Union. I. 333/1 (2008).
- [317] R. Braun, P. Otto, Method and heat exchanger for recovering cold during re-gasification of cryogenic liquids, WO 2017/114518, 2017.
- [318] R. Braun, O. Peter, L. Bihl, Refrigeration supply plant coupled to regasification apparatus of a Liquefied Natural Gas terminal, WO 2019/020135, 2019.
- [319] METI Japan, Study for LNG fired Combined Cycle Power Plant in Bangladesh - Final Report, (2018).
- [320] TRNSYS, (2017). <http://www.trnsys.com/> (accessed 19 March 2020).
- [321] Wärtsilä, Wärtsilä 50DF multi-fuel engine, (2019).
- [322] L. Mayekawa MFG. Co., NewTon, (2009). <https://mayekawa.com/lp/newton/> (accessed 13 April 2020).
- [323] H. Asano, N. Mugabi, Actual Energy Conservations By Using NH₃ / CO₂, in: *Int. Conf. Sav. Energy Refrig. Air-Conditioning*, Jeollanam-Do (South Korea), 2013: pp. ICSERA2013-3-C-2.
- [324] ASHRAE, Handbook - Heating, Ventilating, and Air-Conditioning Systems and Equipment (SI Edition), 2012.
- [325] J. Alberto Dopazo, J. Fernández-Seara, J. Sieres, F.J. Uhía, Theoretical analysis of a CO₂–NH₃ cascade refrigeration system for cooling applications at low temperatures, *Appl. Therm. Eng.* 29 (2009) 1577–1583. DOI: 10.1016/J.Applthermaleng.2008.07.006.
- [326] Kobe Steel Ltd., iZN Series Specifications - Semi-hermetic type (24 to 125kW motor rating compressor and racks) - Model iZN70W/TUW, (2020). https://www.kobelco.co.jp/english/products/standard_compressors/refrigerationunit/izn/spec.html (accessed 19 April 2020).
- [327] J.A. Duffie, W.A. Beckman, *Solar Engineering of Thermal Process*, Fourth, John Wiley & Sons, Inc, 2013.
- [328] Panasonic, Panasonic Solar HIT Photovoltaic Module, (2019).
- [329] M. Feliciano, F. Rodrigues, J.M.R.C.A. Santos, Assessment of Energy Use and Energy Efficiency in Two Portuguese Slaughterhouses, *Int. J. Environ. Earth Sci. Eng.* 8 (2014). DOI: 10.13140/2.1.4870.8640.
- [330] A. Latini, C. Viola, M. Scoccianti, C.A. Campiotti, *Manual de eficiencia energética en centrales hortofrutícolas*, 2014.
- [331] S. Goli, A. McKane, D. Olsen, Demand response opportunities in industrial refrigerated warehouses in California, in: *ACEEE Summer Study Energy Effic. Ind.*, Niagara Falls, NY, 2011.
- [332] D. Scott, R. Castillo, K. Larson, B. Dobbs, D. Olsen, *Refrigerated Warehouse Demand Response Strategy Guide*, 2015.
- [333] EnergyPlus - Weather Data, (2019). <https://energyplus.net/weather> (accessed 10 December 2019).
- [334] F.J. Cárcel Carrasco, J. Grau Carrión, Energy Monitoring for Control of Energy Consumption. A Case Study, *3C Tecnol.* 4 (2015) 19–31.
- [335] R. Hribar, P. Potočnik, J. Šilc, G. Papa, A comparison of models for forecasting the residential natural gas demand of an urban area, *Energy.* 167 (2019) 511–522. DOI: 10.1016/J.Energy.2018.10.175.
- [336] S.D. Watson, K.J. Lomas, R.A. Buswell, Decarbonising domestic heating: What is the peak GB demand?, *Energy Policy.* 126 (2019) 533–544. DOI: 10.1016/J.Enpol.2018.11.001.
- [337] I.H. Magnussen, *Energy consumption 2012 - Household energy consumption*, 2013.
- [338] R. Fu, D. Feldman, R. Margolis, U.S. Solar Photovoltaic System Cost Benchmark: Q1 2018, 2018.

- [339] F.P. Incropera, Fundamentals of heat and mass transfer, John Wiley, 2007.
- [340] A. Melinder, Thermophysical properties of liquid secondary refrigerants, International Institute of Refrigeration (IIR), Paris, 1997.
- [341] K.M. Tsamos, Y.T. Ge, Id. Santosa, S.A. Tassou, G. Bianchi, Z. Mylona, Energy analysis of alternative CO₂ refrigeration system configurations for retail food applications in moderate and warm climates, Energy Convers. Manag. 150 (2017) 822–829. DOI: 10.1016/J.Enconman.2017.03.020.
- [342] T.S. Lee, C.H. Liu, T.W. Chen, Thermodynamic analysis of optimal condensing temperature of cascade-condenser in CO₂/NH₃ cascade refrigeration systems, Int. J. Refrig. 29 (2006) 1100–1108. DOI: 10.1016/J.Ijrefrig.2006.03.003.
- [343] J. Steven Brown, S.F. Yana-Motta, P.A. Domanski, Comparative analysis of an automotive air conditioning systems operating with CO₂ and R134a, Int. J. Refrig. 25 (2002) 19–32. DOI: 10.1016/S0140-7007(01)00011-1.
- [344] S.M. Tarique, M.A. Siddiqui, Performance and economic study of the combined absorption/compression heat pump, Energy Convers. Manag. 40 (1999) 575–591. DOI: 10.1016/S0196-8904(98)00045-4.

Appendices

UNIVERSITAT ROVIRA I VIRGILI

EXERGY RECOVERY FROM LNG-REGASIFICATION FOR POLYGENERATION OF ENERGY

Antonio Atienza Márquez

Appendix A. Natural gas and LNG composition, properties and conversion factors

Table A.1 depicts the composition, the molar mass and the critical temperature and pressure of some of the most conventional types of LNG. Figure A.1 shows some of the thermophysical properties (i.e., density, viscosity, thermal conductivity and specific heat of the different types of natural gas depicted in Table A.1 as a function of the temperature. Table A.2 shows some approximate unit conversion factors widely used in the energy sector.

Table A.1. Different LNG compositions considered in the calculations. Source: REFPROP.

Component	Natural Gas composition (molar fractions)					
	Methane	Gulf Coast	Amarillo	Ekofisk	High CO ₂ /N ₂	High N ₂
Methane	100.0	96.5222	90.6724	85.9063	81.212	81.441
Ethane	0	1.8186	4.5279	8.4919	4.303	3.3
Propane	0	0.4596	0.828	2.3015	0.895	0.605
Hydrogen	0	0	0	0	0	0
Nitrogen	0	0.2595	3.1284	1.0068	5.702	13.465
Carbon Dioxide	0	0.5956	0.4676	1.4954	7.585	0.985
Isobutane	0	0.0977	0.1037	0.3486	0.151	0.1
Butane	0	0.1007	0.1563	0.3506	0.152	0.104
isopentane	0	0.0473	0.0321	0.0509	0	0
Pentane	0	0.0324	0.0443	0.048	0	0
Helium	0	0	0	0	0	0
Hexane	0	0.0664	0.0393	0	0	0
Molar mass (g/mol)	16.043	16.799	17.595	18.768	19.829	18.649
Critical temperature (°C)	-82.586	-72.745	-68.144	-52.403	-64.066	-77.669
Critical pressure (MPa)	4.5992	5.5135	6.0429	7.0068	6.2895	5.982

Table A.2. Approximate unit conversion factors for LNG. Values are approximated since depends on the composition of the natural gas.

From	To convert (multiply by)							
	LNG		Gas			Energy (referred to gross heating value)		
	t	m ³ LNG	bcm	Nm ³ (NG)	Scf	MWh	Mbtu	tep
t	1	2.32	1.35×10 ⁻⁶	1,346	50.2×10 ³	15.7	53.7	1.35
m ³ LNG	0.430	1	0.580×10 ⁻⁶	580	21.7×10 ³	6.8	23.2	0.584
bcm	743×10 ³	1.72×10 ⁶	1	1×10 ⁹	37.3×10 ⁹	11.7×10 ⁶	39.9×10 ⁶	1.01×10 ⁶
Nm ³ (NG)	0.743×10 ⁻³	1.72×10 ⁶	1×10 ⁻⁹	1	37.3	0.012	0.040	1.01×10 ⁻³
Scf (60°F)	0.020×10 ⁻³	0.046×10 ⁻³	0.027×10 ⁻⁹	0.027	1	0.313×10 ⁻³	1.070×10 ⁻³	27.0×10 ⁻⁶
MWh	0.064	0.147	85.5×10 ⁻⁹	85.5	3,190	1	3.41	0.086
Mbtu	0.019	0.043	25.0×10 ⁻⁹	25.0	935	0.293	1	0.025
tep	0.739	1.71	0.994×10 ⁻⁶	994	37.1×10 ³	11.6	39.7	1

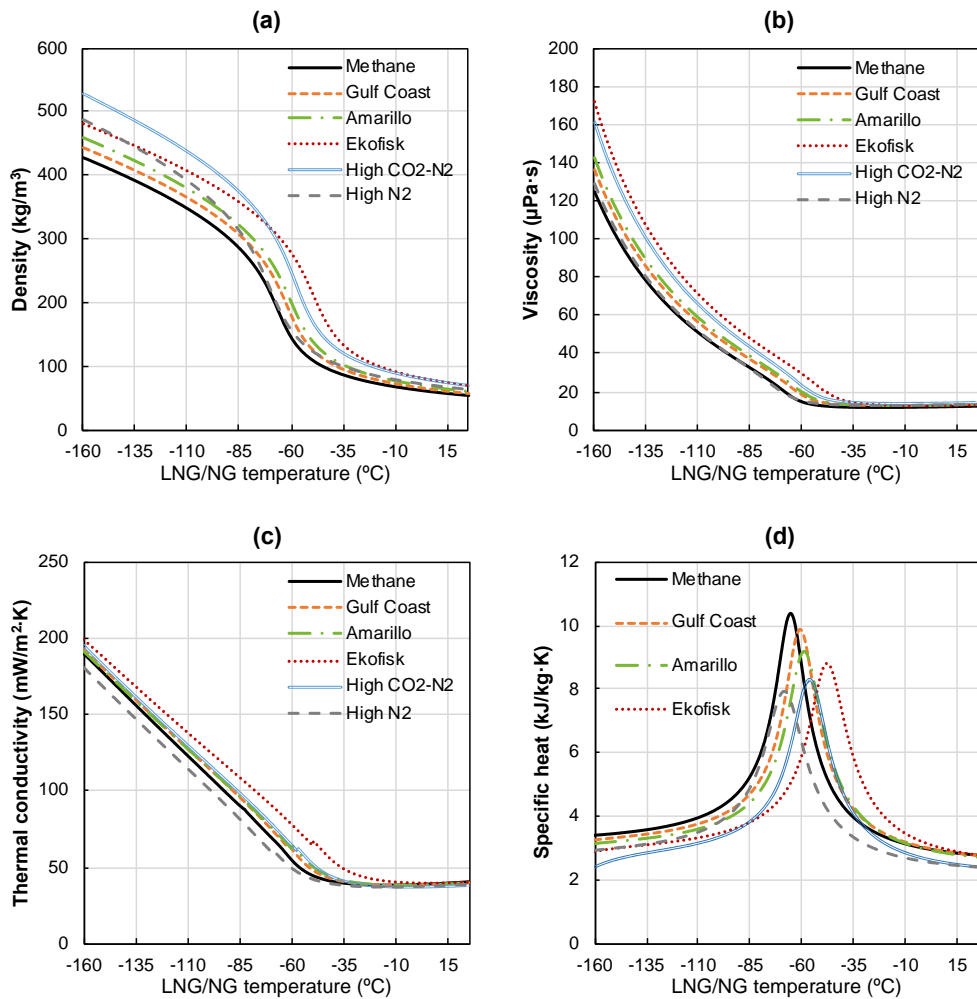


Figure A.1. Thermodynamic properties of different types of natural gas for an LNG/NG pressure of 7.5 MPa. (a) Density, (b) Viscosity, (c) Thermal conductivity, (d) Specific Heat.

Appendix B. Thermodynamic data of the polygeneration plant analysed in Chapter 3

Table B.1 depicts the energy and exergy balances of all the components that integrate the polygeneration plant presented in Figure 3.3. Table B.2 shows the thermodynamic data of each state point of the plant when it operates with the previously selected working fluids and heat transfer fluids.

Table B.1. Energy and exergy balance equations of all the components of the polygeneration plant.

Component	Energy balance	Exergy balance
Condenser C-1	$\dot{Q}_{C1} = \dot{m}_{LNG}(h_3 - h_2) = \dot{m}_{RC1}(h_{13} - h_{14})$	$\dot{I}_{C1} = \dot{E}x_2 + \dot{E}x_{13} - \dot{E}x_3 - \dot{E}x_{14}$
Condenser C-2	$\dot{Q}_{C2} = \dot{m}_{LNG}(h_4 - h_3) = \dot{m}_{DC\&RC2}(h_{20} - h_{21})$	$\dot{I}_{C2} = \dot{E}x_3 + \dot{E}x_{20} - \dot{E}x_4 - \dot{E}x_{21}$
Condenser C-3	$\dot{Q}_{C3} = \dot{m}_{LNG}(h_5 - h_4) = \dot{m}_{RC3}(h_{44} - h_{45})$	$\dot{I}_{C3} = \dot{E}x_4 + \dot{E}x_{44} - \dot{E}x_5 - \dot{E}x_{45}$
Heater H-1	$\dot{Q}_{H1} = \dot{m}_{RC1}(h_9 - h_{16}) + \dot{m}_{RC1}(h_{11} - h_{10}) = \dot{m}_{SW,H1}(h_{17} - h_{18})$	$\dot{I}_{H1} = \dot{E}x_{10} + \dot{E}x_{16} + \dot{E}x_{17} - \dot{E}x_9 - \dot{E}x_{11} - \dot{E}x_{18}$
Heater H-2	$\dot{Q}_{H2} = \dot{m}_{DC\&RC2}(h_{31} - h_{30}) = \dot{m}_{WH}(h_{38} - h_{39})$	$\dot{I}_{H2} = \dot{E}x_{30} + \dot{E}x_{38} - \dot{E}x_{31} - \dot{E}x_{39}$
Heater H-3	$\dot{Q}_{H3} = \dot{m}_{RC3}(h_{40} - h_{47}) + \dot{m}_{RC3}(h_{42} - h_{41})$	$\dot{I}_{H3} = \dot{E}x_{41} + \dot{E}x_{47} + \dot{Q}_{H3} \left(1 - \frac{T_0}{T_{bb}}\right) - \dot{E}x_{40} - \dot{E}x_{42}$
Heater H-4	$\dot{Q}_{H4} = \dot{m}_{LNG}(h_6 - h_5) = \dot{m}_{SW,H4}(h_{48} - h_{49})$	$\dot{I}_{H4} = \dot{E}x_5 + \dot{E}x_{48} - \dot{E}x_6 - \dot{E}x_{49}$
Heater H-5	$\dot{Q}_{H5} = \dot{m}_{LNG}(h_8 - h_7) = \dot{m}_{SW,H5}(h_{50} - h_{51})$	$\dot{I}_{H5} = \dot{E}x_7 + \dot{E}x_{50} - \dot{E}x_8 - \dot{E}x_{51}$
Pump P1	$\dot{W}_{P1} = \dot{m}_{LNG}(h_2 - h_1)$	$\dot{I}_{P1} = \dot{E}x_1 + \dot{W}_{P1} - \dot{E}x_2$
Pump P2	$\dot{W}_{P2} = \dot{m}_{RC1}(h_{15} - h_{14})$	$\dot{I}_{P2} = \dot{E}x_{14} + \dot{W}_{P2} - \dot{E}x_{15}$
Pump P3	$\dot{W}_{P3} = \dot{m}_{DC\&RC2}(h_{22} - h_{21})$	$\dot{I}_{P3} = \dot{E}x_{21} + \dot{W}_{P3} - \dot{E}x_{22}$
Pump P4	$\dot{W}_{P4} = \dot{m}_{RC3}(h_{46} - h_{45})$	$\dot{I}_{P4} = \dot{E}x_{45} + \dot{W}_{P4} - \dot{E}x_{46}$
Recuperator R-1	$\dot{Q}_{R1} = \dot{m}_{RC1}(h_{12} - h_{13}) = \dot{m}_{RC1}(h_{16} - h_{15})$	$\dot{I}_{R1} = \dot{E}x_{12} + \dot{E}x_{15} - \dot{E}x_{13} - \dot{E}x_{16}$
Recuperator R-2	$\dot{Q}_{R2} = \dot{m}_{RC3}(h_{43} - h_{44}) = \dot{m}_{RC3}(h_{47} - h_{46})$	$\dot{I}_{R2} = \dot{E}x_{43} + \dot{E}x_{46} - \dot{E}x_{44} - \dot{E}x_{47}$
Turbine T1 (HP)	$\dot{W}_{T1-HP} = \dot{m}_{RC1}(h_9 - h_{10})$	$\dot{I}_{T1-HP} = \dot{E}x_9 - \dot{E}x_{10} - \dot{W}_{T1-HP}$
Turbine T1 (LP)	$\dot{W}_{T1-LP} = \dot{m}_{RC1}(h_{11} - h_{12})$	$\dot{I}_{T1-LP} = \dot{E}x_{11} - \dot{E}x_{12} - \dot{W}_{T1-LP}$
Turbine T2	$\dot{W}_{T2} = \dot{m}_{DC\&RC2}(h_{31} - h_{19})$	$\dot{I}_{T2} = \dot{E}x_{31} - \dot{E}x_{19} - \dot{W}_{T2}$
Turbine T3 (HP)	$\dot{W}_{T3-HP} = \dot{m}_{RC3}(h_{40} - h_{41})$	$\dot{I}_{T3-HP} = \dot{E}x_{40} - \dot{E}x_{41} - \dot{W}_{T3-HP}$
Turbine T3 (LP)	$\dot{W}_{T3-LP} = \dot{m}_{RC3}(h_{42} - h_{43})$	$\dot{I}_{T3-LP} = \dot{E}x_{42} - \dot{E}x_{43} - \dot{W}_{T3-LP}$
NG Expander (EXP)	$\dot{W}_{EXP} = \dot{m}_{LNG}(h_6 - h_7)$	$\dot{I}_{EXP} = \dot{E}x_6 - \dot{E}x_7 - \dot{W}_{EXP}$

Table B.2. Thermodynamic data of each state point of the polygeneration plant when operating with the selected working fluids and heat transfer fluids (Power cycle RC-1 – Methane; DC + power cycle RC-2 – CO₂; Power cycle RC-3 – Propane).

Nº	Fluid	\dot{m} , t/h	T, °C	p, MPa	h, kJ/kg	s, kJ/(kg·K)
1	LNG	180	-162	0.13	-912.68	-6.693
2	LNG	180	-158.6	7.20	-890.50	-6.644
3	LNG	180	-135	7.20	-807.98	-5.990
4	NG	180	-65	7.20	-437.55	-3.904
5	NG	180	-15	7.20	-189.79	-2.813
6	NG	180	5	7.20	-129.39	-2.588
7	NG	180	-47.8	3.00	-210.10	-2.524
8	NG	180	5	3.00	-78.24	-1.997
9	Methane	31.03	10	10.53	-153.95	-2.838
10	Methane	31.03	-62.1	3.20	-253.98	-2.754
11	Methane	31.03	10	3.20	-68.43	-1.994
12	Methane	31.03	-66.4	0.75	-210.42	-1.870
13	Methane	31.03	-112.9	0.75	-316.90	-2.454
14	Methane	31.03	-130	0.75	-795.53	-5.781
15	Methane	31.03	-122.9	10.53	-760.82	-5.723
16	Methane	31.03	-95.2	10.53	-654.34	-5.074
17	Seawater	1017	20	0.30	84.19	0.296
18	Seawater	1017	15	0.30	63.27	0.224
19	CO ₂	172.8	-0.4	0.85	-31.26	-0.503
20	CO ₂	172.8	1	0.68	-27.89	-0.450
21	CO ₂	172.8	-50	0.68	-413.85	-2.160
22	CO ₂	172.8	-49.5	1.88	-412.48	-2.158
23	CO ₂	172.8	-48.8	1.43	-411.33	-2.151
24	CO ₂	86.38	-48.8	1.43	-411.33	-2.151
25	CO ₂	86.38	-30	1.43	-69.96	-0.741
26	CO ₂	69.1	-48.8	1.43	-411.33	-2.151
27	CO ₂	69.1	-30	1.43	-69.96	-0.741
28	CO ₂	17.28	-48.8	1.43	-411.33	-2.151
29	CO ₂	17.28	-30	1.43	-69.96	-0.741
30	CO ₂	172.8	-30	1.43	-69.96	-0.741
31	CO ₂	172.8	30	1.43	-9.27	-0.517
32	NH ₃	21.93	-25	0.15	1430.62	5.983
33	NH ₃	21.93	-25	0.15	86.12	0.564
34	NH ₃	18.19	-10	0.29	1450.66	5.757
35	NH ₃	18.19	-10	0.29	153.95	0.829
36	Water	200.7	12	0.10	50.51	0.181
37	Water	200.7	5	0.10	21.12	0.076
38	Water	501.7	40	0.10	167.62	0.572
39	Water	501.7	35	0.10	146.72	0.505
40	Propane	102.6	300	18.15	1131.22	3.142
41	Propane	102.6	221.2	3.39	1011.31	3.185
42	Propane	102.6	300	3.39	1233.05	3.601
43	Propane	102.6	221.9	0.35	1045.98	3.669
44	Propane	102.6	17.3	0.35	609.95	2.552
45	Propane	102.6	-10	0.35	175.20	0.908
46	Propane	102.6	2.3	18.15	218.28	0.948
47	Propane	102.6	158.4	18.15	654.31	2.187
48	Seawater	519.5	20	0.30	84.19	0.296
49	Seawater	519.5	15	0.30	63.27	0.224
50	Seawater	1134	20	0.30	84.19	0.296
51	Seawater	1134	15	0.30	63.27	0.224

Appendix C. Supplementary data of the Combined Cryogenic Power and Cooling configurations developed in Chapter 4

C.1. Convective heat transfer correlations

The following is a description and the mathematical formulation of the different correlations utilized (classified by the heat transfer mechanism) to predict the film heat transfer coefficients utilized in the different models developed in this doctoral thesis.

Nomenclature:

D → Inner diameter of the tube, m.
 G → Total mass flux (liquid + vapor), $\text{kg}/(\text{m}^2 \cdot \text{s})$
 g → Gravity constant, m/s^2
 k → Thermal conductivity, $\text{W}/(\text{m} \cdot \text{K})$
 p_c → Critical pressure.
 Pr → Prandtl number
 p_r → Reduced pressure: p/p_c
 x → Vapor quality.

Greek letters

α → Convective heat transfer coefficient, $\text{W}/(\text{m}^2 \cdot \text{K})$
 ρ → Density, kg/m^3
 μ → Viscosity, $\text{Pa} \cdot \text{s}$
 σ → Surface tension, N/m

Subscripts

h → Hydraulic (diameter)
 i → Inner
 L → Saturated liquid.
 o → Outer
 V → Saturated vapour

Single-phase turbulent flow in circular tubes

The Dittus-Boelter equation is used to calculate the convective heat transfer coefficient for fully developed turbulent flows in circular tubes:

$$\alpha = 0.023 \cdot Re^{0.8} Pr^n$$

$n=0.4$ for the fluid being heated, and $n=0.3$ for the fluid being cooled [339].

Condensation in plain and horizontal tubes

According to Shah [262], the two-phase convective heat transfer coefficient (α_{TP}) depends on the following heat transfer regimes:

- Regime I: $\alpha_{TP} = \alpha_I$
- Regime II: $\alpha_{TP} = \alpha_I + \alpha_{Nu}$
- Regime III: $\alpha_{TP} = \alpha_{Nu}$

The heat transfer coefficients α_I and α_{Nu} , in $W/(m^2 \cdot K)$, are calculated as follows:

$$\alpha_I = h_{LO} \left(1 + \frac{3.8}{Z^{0.95}} \right) \left(\frac{\mu_L}{14\mu_L} \right)^{(0.0058+0.557 \cdot p_r)}$$

$$\alpha_{Nu} = 1.32 Re_{LO}^{-1/3} \left[\frac{\rho_L(\rho_L - \rho_G) g k_L^3}{\mu_L^2} \right]^{1/3}$$

where, α_{LO} and Re_{LO} are heat transfer coefficient and the Reynolds number both assuming liquid phase flowing alone in the tube, calculated as follows:

$$\alpha_{LO} = 0.023 Re_{LO}^{0.8} Pr^{0.4} k_L / D$$

$$Re_{LO} = \frac{G(1-x)D}{\mu_L}$$

For horizontal tubes, the conditions for each regime depends on the dimensionless vapor velocity (J_g) and are defined according to the following criteria:

- *Regime I* occur when $We_{GT} > 100$ and:

$$J_g \geq 0.98(Z + 0.263)^{-0.62}$$
- *Regime III* occurs when:

$$J_g \leq 0.95(1.254 + 2.27 \cdot Z^{1.249})^{-1}$$
- *Regime II* occurs when: neither of the above conditions is satisfied.

where J_g , the Shah's correlating parameter (Z) and the Weber number for all mass flowing as vapour (We_{GT}) are defined as:

$$J_g = \frac{x G}{[g D_i \rho_G(\rho_L - \rho_G)]^{0.5}}$$

$$Z = \left(\frac{1}{x} - 1\right)^{0.8} p_r^{0.4}$$

$$We_{GT} = \frac{G^2 D}{\rho_V \cdot \sigma}$$

Nucleate boiling

Jung et al. [263] proposed the following correlation to predict the boiling heat transfer coefficient for flammable refrigerants:

$$\alpha = 41.4 \frac{k_L}{D_b} \left[\frac{(\dot{Q}/A) D_b}{k_L T_{sat}} \right]^{C_2} (-\log_{10} p_r)^{-1.52} \times \left(1 - \frac{\rho_V}{\rho_L} \right)^{0.53}$$

where the exponent C_2 is defined as:

$$C_2 = 0.835(1 - p_r)^{1.33}$$

On the other hand, D_b denotes the bubble departure diameter (in m) which is calculated as follows:

$$D_b = 0.0146 \beta \left[\frac{2 \sigma}{g(\rho_L - \rho_V)} \right]$$

where, β is the contact angle of the bubbles (35°).

Condensation on tubes

Jung et al. [264] presented the following correlation to calculate the external condensation heat transfer coefficients for flammable refrigerants:

$$\alpha = 0.79 \left[\frac{\rho_L(\rho_L - \rho_V) \cdot g \cdot k_L^3 \cdot h_{fg}}{\mu_L \cdot \Delta T \cdot D_o} \right]^{0.25}$$

where ΔT ($T_{sat} - T_w$) is the wall subcooling (in K or °C) and h_{fg} is the specific enthalpy of vaporization (in kJ/kg).

LNG: Convective heat transfer at supercritical pressure

The correlation proposed by Bae and Kim [265] is used to calculate the heat transfer coefficient of LNG (assumed as pure methane) when its temperature is below the critical point. The correlation is as follows:

$$\alpha = 0.021 \cdot Re_b^{0.82} \cdot Pr_b^{0.5} \left(\frac{\rho_w}{\rho_b} \right)^{0.3} \left(\frac{\overline{Cp}}{Cp_b} \right)^n \times \frac{k_b}{D}$$

$$\overline{Cp} = \frac{h_w - h_b}{T_w - T_b}, \quad Re_b = \frac{G \cdot D}{\mu_b}, \quad Pr_b = \frac{Cp_b \cdot \mu_b}{k_b}$$

The subscript “b” denotes that parameters and properties are evaluated at the mass averaged temperature of the fluids, whilst the subscript “w” refers to the tube’s wall temperature. On the other hand, the exponent “n” is determined as follows:

- $n = 0.4$ If $T_b < T_w < T_c$ or $1.2 \cdot T_c < T_b < T_w$
- $n = 0.4 + 0.2 \left(\frac{T_w}{T_c} - 1 \right)$ If $T_b < T_c < T_w$
- $n = 0.4 + 0.2 \left(\frac{T_w}{T_c} - 1 \right) \left[1 - 5 \left(\frac{T_b}{T_c} - 1 \right) \right]$ If $T_c < T_b < 1.2 \cdot T_c$ and $T_b < T_w$

On the other hand, when both the pressure and the temperature of LNG/NG are above the critical values, the correlation of Liang et al. [266] is used to determine the convective heat transfer coefficient:

$$\alpha = 0.0068 \cdot Re^{0.94} Pr^{0.4} \times \frac{k}{D}$$

Flow across tube banks

The correlation of Zukauskas is utilized to determine the convective heat transfer coefficient for crossflow over tube banks and assuming an in-line arrangement:

- $Re < 100$ $Nu = 0.9 \cdot Re^{0.4} Pr^{0.36} (Pr/Pr_s)^{0.25}$
- $100 \leq Re < 1000$ $Nu = 0.52 \cdot Re^{0.5} Pr^{0.36} (Pr/Pr_s)^{0.25}$
- $1000 \leq Re < 2 \cdot 10^5$ $Nu = 0.27 \cdot Re^{0.63} Pr^{0.36} (Pr/Pr_s)^{0.25}$
- $2 \cdot 10^5 \leq Re \leq 2 \cdot 10^6$ $Nu = 0.033 \cdot Re^{0.8} Pr^{0.4} (Pr/Pr_s)^{0.25}$

Film coefficient in plate-and-frame heat exchangers

The correlation of Thonon is utilized:

$$\alpha = C_1 Re^m Pr^{1/3} \times \frac{k}{D_h}$$

where C_1 and m are functions of the Reynolds number and the Chevron angle.

C.2. Temperature profiles in heat exchangers

Figure C.1 depicts the temperature profile in each heat exchanger of the polygeneration plant presented in Figure 4.6.

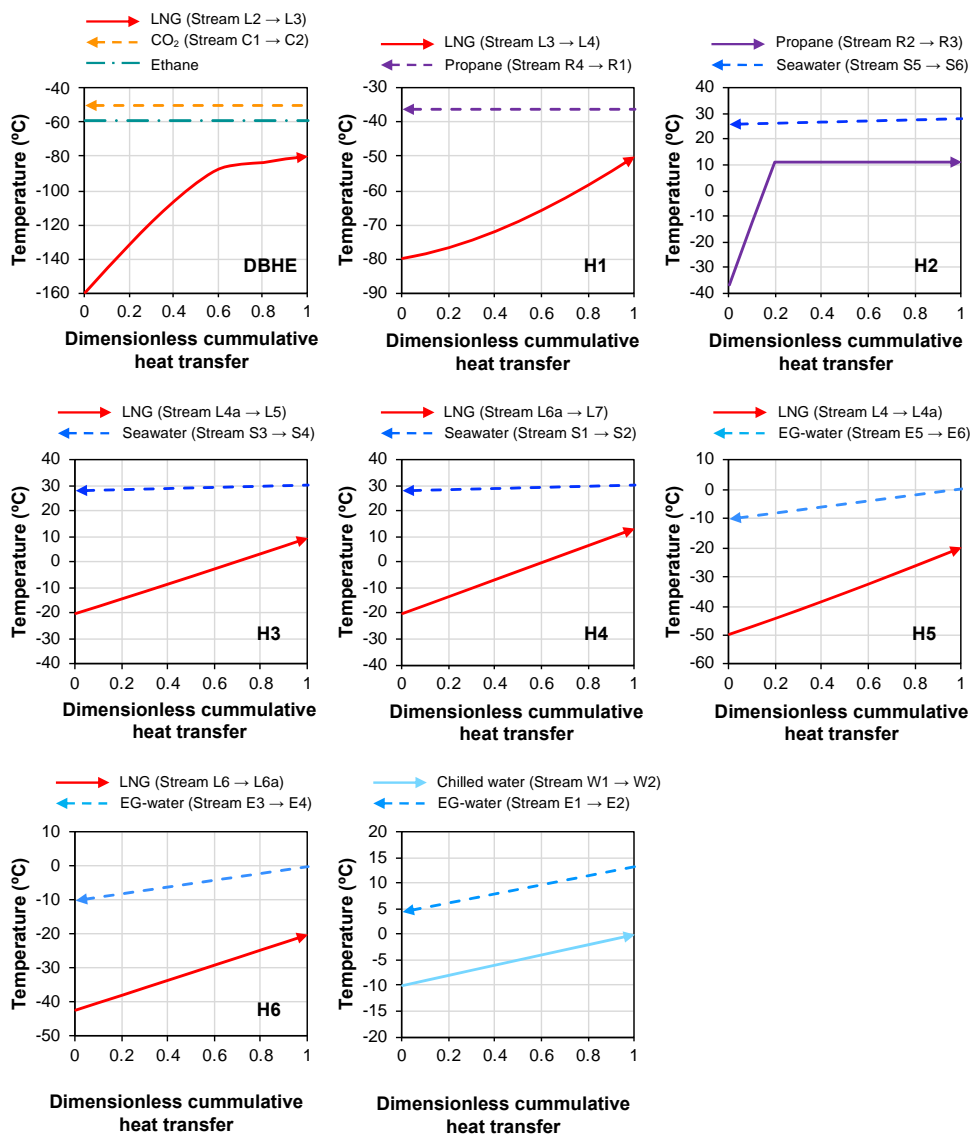


Figure C.1. Temperature profile in each heat exchanger of the polygeneration plant analysed in Chapter 4 of the thesis.

C.3. Heat transfer coefficients

Table C.1. Average convective and overall heat transfer coefficients calculated for each heat exchanger of the polygeneration plant analysed in [Chapter 4](#) (see [Figure 4.6](#)).

Heat exchanger	Hot stream		Cold stream		Overall heat transfer coefficient, W/(m ² ·K)
	Fluid	film heat transfer coefficient, W/(m ² ·K)	Fluid	Film heat transfer coefficient, W/(m ² ·K)	
DBHE	Ethane	2,159 ^a ; 2,362 ^b	LNG	2,776 ^a ; 7,625 ^b	1,067 ^a ; 1,628 ^b
H1	Propane	2,193	LNG	4,575	1,231
H2	HSW	4,982	Propane	6,019	1,950
H3	HSW	5,119	NG	1,078	779.7
H4	HSW	5,120	NG	749	591.7
H5	EG-Water	1,503	NG	1,436	657.9
H6	EG-Water	1,429	NG	723.7	445.4
H7	Chilled water	12,342	EG-Water	6,089	4,077

^a Section of the heat exchanger where LNG temperature is *below* the critical point.
^b Section of the heat exchanger where LNG temperature is *above* the critical point.
HSW: Heat source water (e.g., seawater, process water from cooling towers), assumed as regular water.

Appendix D. Supplementary material for Chapter 5

D.1. Freezing point and viscosity of aqueous ethylene glycol and propylene glycol solutions.

Figure D.1 shows the freezing point and the dynamic viscosities at different concentrations of aqueous ethylene glycol and propylene glycol solutions.

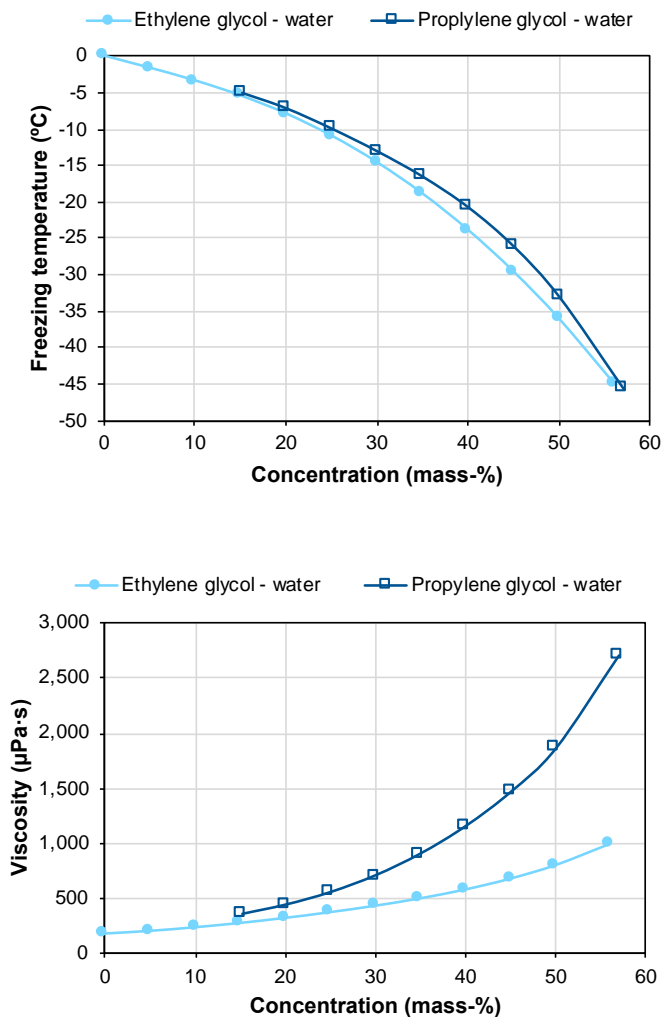


Figure D.1. Aqueous ethylene glycol and propylene glycol solutions. (a) Freezing point and (b) dynamic viscosity for a reference temperature of 273.15 K (0°C). Source of properties: Melinder [340].

D.2. Modelling of the ammonia compressor

The two-stage ammonia screw compressor utilized in the vapour-compression refrigeration cycle presented in Figure 5.10 is modelled through an isentropic efficiency whose mathematical expression has the following form:

$$\eta_{is} = \alpha - \beta \times CR = \alpha - \beta \times (p_{cond}/p_{evap}) \quad (D.1)$$

where, α and β are the coefficients to be determined, and CR denotes the compression ratio. Despite in the literature such type of polynomial expressions have been proposed to calculate the isentropic efficiency of compressors [325,341–344], it is required to develop one more suitable for the specific operating conditions (i.e., temperatures and compression ratios) and type of compressor utilized (or as similar as possible) in that part of the thesis.

To face the lack of the detailed manufacturer data which is required to determine accurately the coefficients of the equation above, the strategy has been to use a simplified modelling of a two-stage refrigeration cycle (see Figure D.2) and the basic catalogue data depicted in Table D.1 of the commercial model iZN70W/TUW (a two-stage ammonia semi-hermetic type screw compressor) and inverter drive manufactured by Kobe Steel, Ltd.

The system has been modelled in Engineering Equation Solver (EES). The energy balance in each component of the refrigeration cycle shown in Figure D.2 are depicted in Table D.2. The following modelling assumptions are made:

- Saturated state of the ammonia leaving the evaporator.
- Subcooling of 5 K of the ammonia leaving the condenser.
- Expansions in throttling devices are assumed isenthalpic.

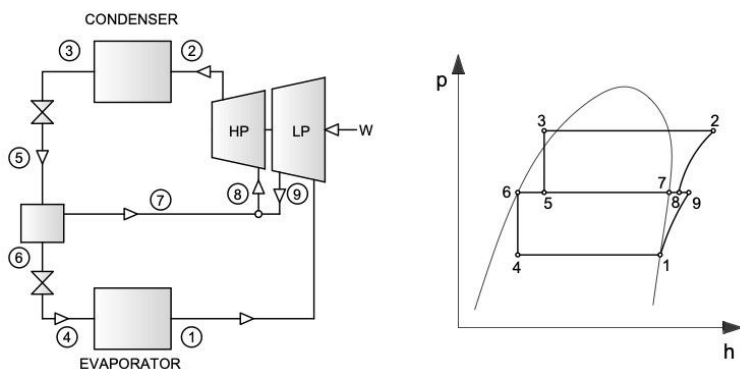


Figure D.2. Two-stage refrigeration cycle used to obtain an expression of the isentropic efficiency.

Table D.1. Catalogue data of the ammonia two-stage screw compressor (commercial model iZN70W/TUW) manufactured by Kobe Steel, Ltd.

CT (°C)	ET (°C)	PCD (kPa)	PEV (kPa)	CR	QEV (kW)	WC (kW)	EER (W/W)
35	-30	1350.8	119.43	11.31	81.7	40.1	2.04
	-35		93.098	14.51	70.4	40	1.76
	-40		71.692	18.84	57.3	39.1	1.47
	-45		54.489	24.79	45.0	38.1	1.18
	-50		40.836	33.08	34.3	36.8	0.93
40	30	1555.4	119.43	13.02	80.9	42.5	1.90
	-35		93.098	16.71	69.3	42.3	1.64
	-40		71.692	21.70	56.2	41.4	1.36
	-45		54.489	28.55	44.1	40.4	1.09
	-50		40.836	38.09	33.6	39.4	0.85

Nomenclature: CT: Condensing Temperature; ET: Evaporation temperature; PCD: Condensing pressure; PEV: Evaporating temperature; CR: Compression Ratio; QEV: Cooling effect, WC: Shaft power consumption; EER (QEV/WC): Energy Efficiency Ratio.

- Internal pressure losses are not considered.
- The power consumption indicated in the catalogue is assumed as the electricity consumed by the motor of the compressor.

The isentropic power and the shaft power required by the compressor are calculated from the following energy balances:

$$\dot{W}_{C,is} = \dot{m}_1(h_{9s} - h_1) + \dot{m}_2(h_{2s} - h_8) \quad (D.2)$$

$$\dot{W}_{C,shf} = \dot{W}_{motor} \times \eta_{motor} = \dot{W}_{C,is} \times \eta_{is} \quad (D.3)$$

The efficiency of the motor is a function of the load ratio (LR), which is calculated as follows:

$$LR = \frac{\dot{W}_{motor}}{\dot{W}_{motor,np}} \times 100\% \quad (D.4)$$

where, the subscript “ np ” denotes the nameplate capacity. According to diverse manufacturing data consulted, the efficiency of motors drops dramatically for load ratios below 10-30%. Thus, the generic relationship assumed between the motor’s efficiency and the load is illustrated in [Figure D.3](#) which corresponds to the following mathematical expressions:

Table D.2. Mass and energy balances and assumptions in each component of the two-stage refrigeration cycle illustrated in Figure D.2.

Component	Mass and energy balances
Evaporator	$\dot{m}_1 = \dot{m}_4$ $\dot{Q}_{ev} = \dot{m}_1(h_1 - h_4)$
Condenser	$\dot{m}_2 = \dot{m}_3$ $\dot{Q}_{cd} = \dot{m}_2(h_2 - h_3)$
Flash chamber	$\dot{m}_7 = \dot{m}_5 x_5$ $\dot{m}_6 = \dot{m}_5 - \dot{m}_7$
Throttling valve No.1	$\dot{m}_3 = \dot{m}_5$ $h_3 = h_5$
Throttling valve No.2	$\dot{m}_4 = \dot{m}_6$ $h_4 = h_6$
Mixing HP-LP	$\dot{m}_7 h_7 + \dot{m}_9 h_9 = \dot{m}_8 h_8$

$$\eta_{motor} = \begin{cases} LR < 10\%: 0.75 \times LR \\ LR \geq 10\%: -2.4403 \times LR^4 + 6.6769 \times LR^3 - 6.6273 \times LR^2 + 2.8309 \times LR + 0.5279 \end{cases} \quad (D.5)$$

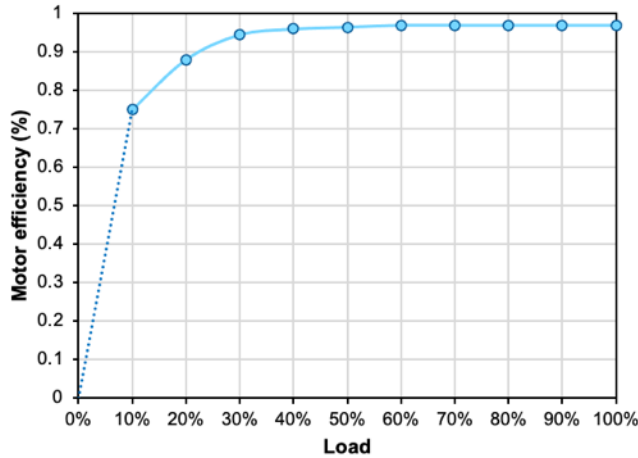


Figure D.3. Assumed motor efficiency as a function of the load.

The isentropic efficiency is defined as follows:

$$\eta_{is} = \frac{\dot{W}_{shaft}}{\dot{W}_{c,is}} \quad (D.6)$$

The isentropic efficiencies for the different compression ratios computed and the linear regression obtained are illustrated in Figure D.4.

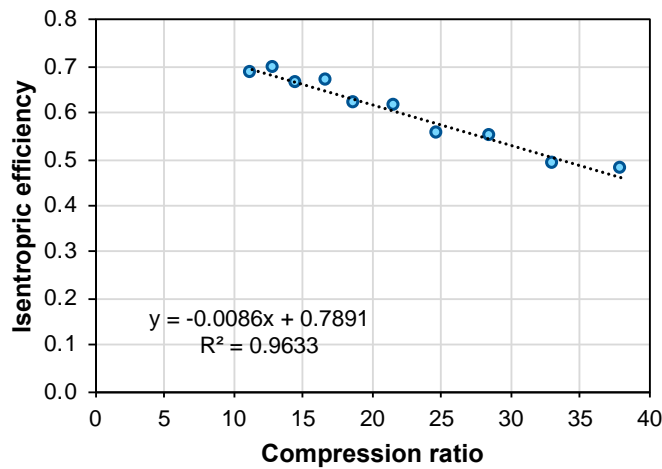


Figure D.4. Isentropic efficiencies of the two-stage ammonia compression calculated for the different compression ratios computed and the linear regression obtained.

According to the comparison shown in [Figure D.5](#) with others polynomial forms to calculate the isentropic efficiency of ammonia compressors proposed in the literature, the presented in this Appendix is the only suitable for the range of compression ratios at which the NH_3/CO_2 VCR machine presented in [Chapter 5](#) operates.

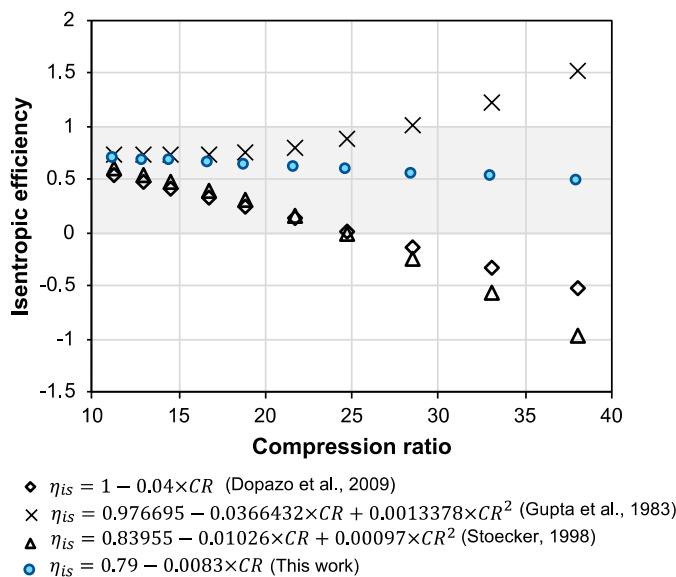


Figure D.5. Comparison of the isentropic efficiency utilized for the two-stage ammonia compressor with others used in the literature [\[325,342,344\]](#).

D.3. Modelling of the NH₃/CO₂ VCR machine

Table D.3 depicts the main mass and energy balances in each component of the NH₃/CO₂ refrigeration scheme shown in **Figure 5.10**. As for the compressor, **Figure D.6** shows the difference between the ideal and the shaft compression power, which are calculated as follows:

$$\dot{W}_{C,is} = \dot{m}_{A10}h_{A10s} - (\dot{m}_{A4}h_{A4} + \dot{m}_{A7}h_{A7} + \dot{m}_{A9}h_{A9}) \quad (D.7)$$

The shaft work required by the compressor is given by:

$$\dot{W}_{C,shf} = \dot{m}_{A10}h_{A10} - (\dot{m}_{A4}h_{A4} + \dot{m}_{A7}h_{A7} + \dot{m}_{A9}h_{A9}) \quad (D.8)$$

The isentropic efficiency of the compressor (whose expression was presented previously) is defined as the relation between them:

$$\eta_{C,is} = \frac{\dot{W}_{C,is}}{\dot{W}_{C,shf}} \quad (D.9)$$

Finally, the electric power consumed by the compressor is calculated as follows:

$$\dot{W}_{C,el} = \frac{\dot{W}_{C,shf}}{\eta_m} = \frac{\dot{W}_{C,is}}{\eta_{C,is} \times \eta_m} \quad (D.10)$$

Table D.3. Main mass and energy balances NH₃/CO₂ refrigeration machine. Numeration of state points corresponds to the schematic layout shown in **Figure 5.10**.

Component	Mass and energy balances
Ammonia evaporator / CO ₂ condenser	$\dot{m}_{A4} = \dot{m}_{A9}$ $\dot{Q}_{ev} = \dot{m}_{A4}(h_{A9} - h_{A4}) = \dot{m}_{CO_2}\Delta h_{CO_2}$
Ammonia condenser	$\dot{m}_{A1} = \dot{m}_{A10}$ $\dot{Q}_{cd} = \dot{m}_{A1}(h_{A10} - h_{A1})$
Throttling valve No.1	$\dot{m}_{A1} = \dot{m}_{A2}$ $h_{A1} = h_{A2}$
Throttling valve No.2	$\dot{m}_{A3} = \dot{m}_{A5}$ $h_{A3} = h_{A5}$
Throttling valve No.3	$\dot{m}_{A6} = \dot{m}_{A8}$ $h_{A6} = h_{A8}$
Liquid subcooler No. 1	$\dot{m}_{A4} = \dot{m}_{A2}x_{A2}$ $\dot{m}_{A2} = \dot{m}_{A3} + \dot{m}_{A4}$
Liquid subcooler No.2	$\dot{m}_{A7} = \dot{m}_{A5}x_{A5}$ $\dot{m}_{A5} = \dot{m}_{A6} - \dot{m}_{A7}$

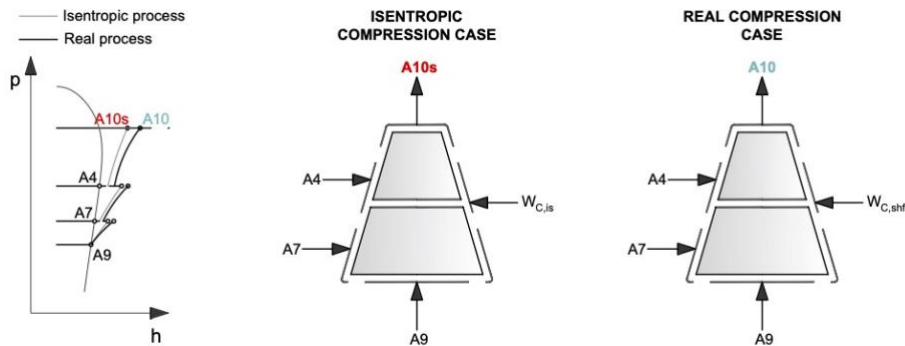


Figure D.6. Comparison between the isentropic compression and the real case.

where, the efficiency of the motor utilized is the shown in [Figure D.3](#). to obtain the expression for the isentropic efficiency.

From the modelling presented above, it has been developed a correlation to calculate the Energy Efficiency Ratio ($EER = \dot{Q}_R / \dot{W}_{C,el}$, in W/W). For a given fix temperature of the cold rooms (i.e., -18°C), it is assumed that the EER depends only on the temperature of the heat sink and the part load ratio ($PLR = \dot{Q}_R / \dot{Q}_{R,np}$) with the following format:

$$EER = f(T_o, PLR) = A \times T_o^3 + B \times T_o^2 + C \times T_o + D \quad (\text{D.11})$$

where the coefficients A , B , C and D are functions of the PLR , which is defined as the ratio of the thermal load to the nameplate capacity of the refrigeration machine. [Figure D.7](#) shows the variation of the EER with the heat sink temperature and the polynomial trendline (with the format given in [Eq. D.11](#) obtained for part load ratios ranging between 1 and 0.2. Then, [Table D.4](#) and [Figure D.8](#) shows the variation of the coefficients of [Eq. D.11](#) and their polynomial adjustment, respectively.

Finally, [Table D.5](#) shows the main thermodynamic data of the cycle for a baseline case.

Table D.4. Values of the coefficients of [Eq. D.11](#) calculated for different part-load ratios.

PLR	A	B	C	D
1	-0.000045	0.004823	-0.213519	5.653391
0.8	-0.000036	0.003954	-0.187336	5.407148
0.6	-0.000034	0.003567	-0.162100	4.909992
0.4	-0.000005	0.000941	-0.083454	3.852411
0.2	-0.000007	0.000730	-0.037746	1.926012

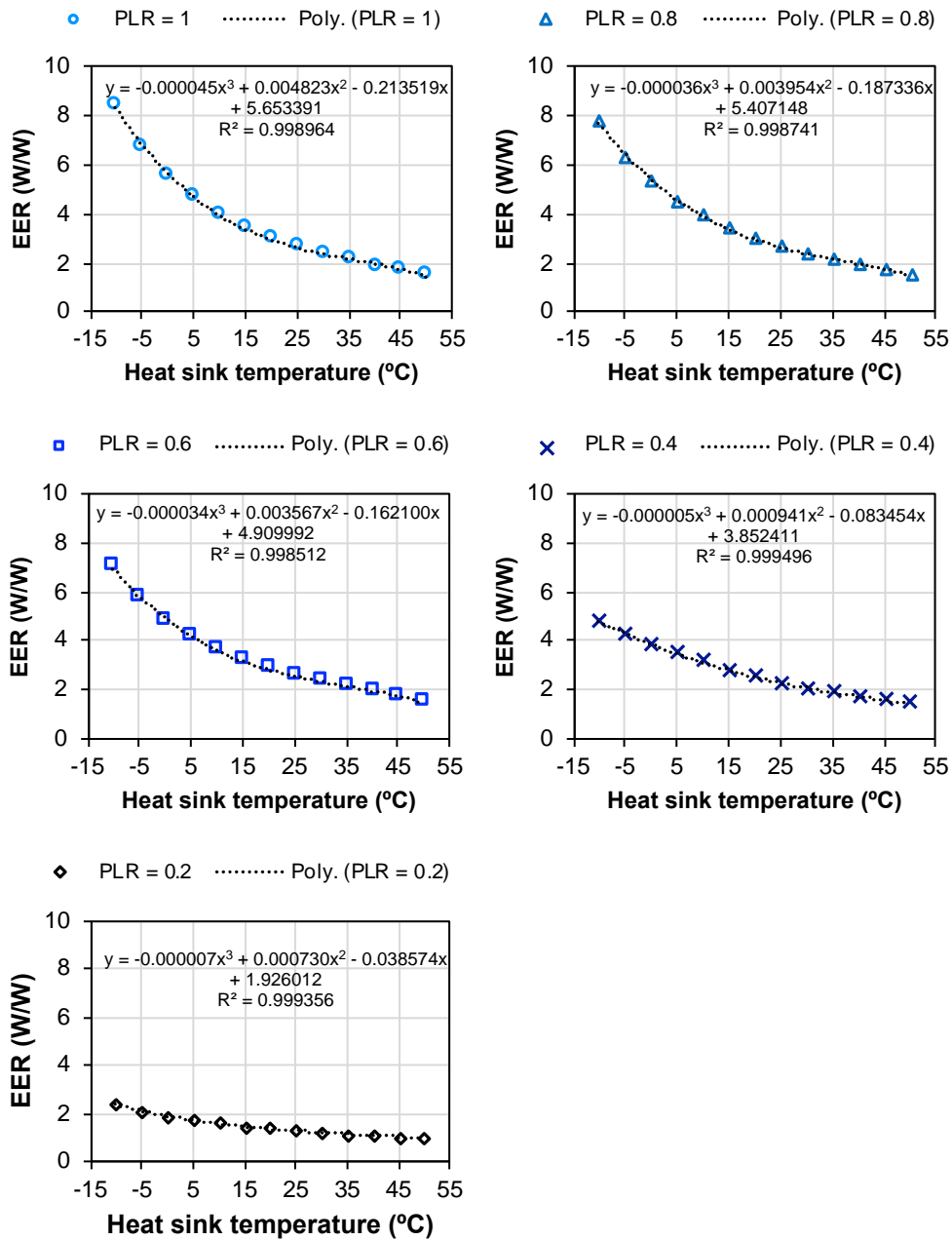


Figure D.7. Variation of the Energy Efficiency Ratio with the heat sink temperature and for different part-load ratios (PLRs).

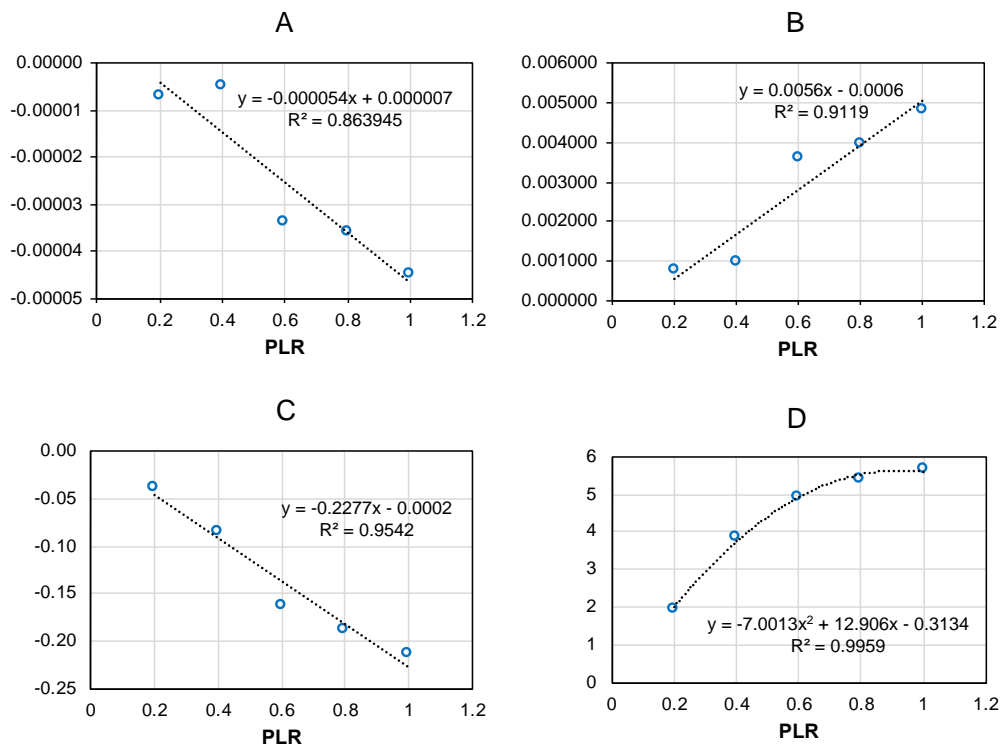


Figure D.8. Polynomial adjustment of the coefficients given in Eq. D.11 for part load ratios ranging between 1 and 0.2.

Table D.5. Thermodynamic data obtained from the simulation of the NH₃/CO₂ refrigeration cycle modelled. Baseline case: Cold room temperature: -18°C, Heat sink temperature: 32°C, Full load operation (PLR = 1). Nameplate refrigeration capacity: 45 kW (based on Newton R-3000 by Mayekawa). The intermediate pressures are those which optimize the refrigeration efficiency.

Stream	Flow rate, kg/h	Temperature, °C	Pressure, kPa	Vapor quality, %
A1	311.7	28.0	1,133.0	Subcooled
A2	311.7	6.9	552.4	8.1
A3	286.4	6.9	552.4	0
A4	25.24	6.9	552.4	1
A5	286.4	-13.2	254.6	7.1
A6	266.1	-13.2	254.6	0
A7	20.3	-13.2	254.6	1
A8	266.1	-32	108.2	6.2
A9	266.1	-32	108.2	1
A10	311.7	186	1,133.0	Superheated

Note: Energy Efficiency Ratio (EER) obtained for the baseline case: 2.29 W/W

UNIVERSITAT ROVIRA I VIRGILI
EXERGY RECOVERY FROM LNG-REGASIFICATION FOR POLYGENERATION OF ENERGY
Antonio Atienza Márquez



UNIVERSITAT
ROVIRA i VIRGILI